

# **Plastid Tubules in Higher Plants: An Analysis of Form and Function**

Mark T. Waters, BA (Oxon)



The University of  
**Nottingham**

A thesis submitted to the University of Nottingham  
for the degree of Doctor of Philosophy, September 2004

## ABSTRACT

Besides photosynthesis, plastids are responsible for starch storage, fatty acid biosynthesis and nitrate metabolism. Our understanding of plastids can be improved with observation by microscopy, but this has been hampered by the invisibility of many plastid types. By targeting green fluorescent protein (GFP) to the plastid in transgenic plants, the visualisation of plastids has become routinely possible. Using GFP, motile, tubular protrusions can be observed to emanate from the plastid envelope into the surrounding cytoplasm. These structures, called *stromules*, vary considerably in frequency and length between different plastid types, but their function is poorly understood.

During tomato fruit ripening, chloroplasts in the pericarp cells differentiate into chromoplasts. As chlorophyll degrades and carotenoids accumulate, plastid and stromule morphology change dramatically. Stromules become significantly more abundant upon chromoplast differentiation, but only in one cell type where plastids are large and sparsely distributed within the cell. Ectopic chloroplast components inhibit stromule formation, whereas preventing chloroplast development leads to increased numbers of stromules. Together, these findings imply that stromule function is closely related to the differentiation status, and thus role, of the plastid in question.

In tobacco seedlings, stromules in hypocotyl epidermal cells become longer as plastids become more widely distributed within the cell, implying a plastid density-dependent regulation of stromules. Co-expression of fluorescent proteins targeted to plastids, mitochondria and peroxisomes revealed a close spatio-temporal relationship between stromules and other organelles. Stromule and plastid fusion could not be induced under conditions which promote substantial fusion of mitochondria. Data are presented suggesting that organelles may be able to pass between cells, and an experiment was designed to test this possibility in the C<sub>4</sub> photosynthetic cells of maize.

Inhibitor studies have shown that stromule and plastid movement is dependent on the actin cytoskeleton and the ATPase activity of myosin. An *Arabidopsis* gene, *CHUP1*, is responsible for chloroplast relocation in response to light intensity and encodes a chloroplast-localised actin-binding protein. To assess whether this protein is involved in stromule movement, *CHUP1* was down-regulated with RNAi. Whilst plants with reduced *CHUP1* expression exhibited a *chup1* mutant phenotype, no significant effect on stromules was discovered. It was thus concluded that chloroplast relocation and stromule formation are two independent processes that employ different actin-dependent mechanisms.

It is proposed that stromules act primarily to increase the plastid surface area in response to a number of developmental and environmental factors.

## ACKNOWLEDGEMENTS

I would like to thank both my supervisor Kevin Pyke and my “advisor” Rupert Fray, who together have pushed and pulled me in varying directions throughout the past three years. Their guidance wasn’t always followed but it was still welcomed! I am also grateful for help and advice from various members of lab A38 – Zsuzsa Bodi, Arthur Coulton, Dan Forth, Ben Jaffé, Hong-Ying Li and James Newton. Many other members of the Division helped in all sorts of ways, from getting me out of a tight fix when some reagent had run out, to unloading undergraduate students – special thanks to Cathlene Eland in that respect! On a personal note, the working day on Sutton Bonington campus just wouldn’t have been the same without regular lunchtimes with the Crossword Crew (see below). We jibed, teased and laughed – poor Becky was a frequent target – but I’ll remember those times fondly. Thank, I thank you for happily sitting in the same boat as me: the fact that there was someone else struggling endlessly with tomato transformations with no one to help was comforting!

On the home front, I would especially like to thank Lucy for providing me with a comfortable, friendly place to live, for rescuing me from the clutches of Sutton Bonington village and introducing me to Planet Kegworth. Cathy, you’ve been the best source of encouragement and enthusiasm I’ve had over the past year and I am deeply grateful for everything, including the gruelling exercise regime! I also thank you for reminding me that there’s more to life than work. I must thank Fotini for introducing me to Greek culture and cuisine, and for keeping me sane and happy, especially during the early years. Lastly, I thank those whom I’ve always taken for granted, namely my parents John and Ann, who have given me the opportunity to get this far in life.

Finally, I acknowledge both financial and professional support from The Gatsby Charitable Foundation, which has assisted me immeasurably during this project.



“Lunchtime for Losers at Sutton Bonington”, by Daniel ‘Operation Okapi’ Zadik

# CONTENTS

ABSTRACT	ii
ACKNOWLEDGEMENTS	iii
CONTENTS	iv
LIST OF FIGURES AND TABLES	viii
ABBREVIATIONS	ix
I GENERAL INTRODUCTION	1
1.1 The origin and early evolution of plastids	1
1.2 The range of plastid forms in higher plants	4
1.2.1 Features common to all plastids	6
1.2.2 The proplastid	9
1.2.3 The chloroplast	11
1.2.3.1 Protein import, sorting and assembly	12
1.2.3.2 Thylakoid biogenesis	13
1.2.4 The amyloplast	14
1.2.5 The chromoplast	17
1.2.6 Other plastid types	20
1.3 Plastid morphology and dynamics	22
1.3.1 Plastid envelope motility	22
1.3.2 Diversity of stromules	26
1.3.3 Stromule movement and composition	28
1.3.4 Stromule functions	30
1.4 Green fluorescent protein (GFP)	31
1.4.1 Expression of GFP and its derivatives <i>in planta</i>	32
1.4.2 Applications of GFP	33
1.5 Aims of this work	35
2 MATERIALS AND METHODS	36
2.1 GENERAL MATERIALS	36
2.2 PLANT MATERIAL AND GROWTH CONDITIONS	36
2.2.1 Tomato ( <i>Lycopersicon esculentum</i> Mill. var. Ailsa Craig)	36
2.2.1.1 Crosses with fruit ripening mutants	38
2.2.1.2 Production of dark-grown fruit	40
2.2.2 Tobacco ( <i>Nicotiana tabacum</i> var. Petit Havana)	41
2.2.2.1 Generation of transgenic tobacco plants	41
2.2.2.2 Red and blue light growth conditions	43
2.2.2.3 Hypocotyl elongation experiment	44
2.2.2.4 Incubation of seedlings under anaerobic conditions	44
2.2.3 <i>Arabidopsis thaliana</i> (ecotype Columbia-0)	45
2.2.3.1 Generation of transgenic <i>Arabidopsis</i>	45
2.2.3.2 Screening for transgenic <i>Arabidopsis</i> primary transformants	46
2.2.3.3 Crossing <i>Arabidopsis</i>	47
2.2.3.4 Growth of <i>Arabidopsis</i> under high light conditions	47
2.2.4 Maize ( <i>Zea mays</i> var. Hi-II AXB)	48

2.2.4.1	Generation of transgenic maize	48
2.2.4.2	Selfing of maize	49
2.3	MICROSCOPY AND TISSUE SAMPLING	49
2.3.1	Tomato fruit pericarp	49
2.3.2	Tobacco hypocotyls	50
2.3.3	Leaf sections	51
2.3.4	Fluorescence recovery after photobleaching	51
2.4	IMAGE ANALYSIS	52
2.4.1	Tomato fruit pericarp	52
2.4.2	Tobacco hypocotyls	52
2.5	STATISTICAL ANALYSIS	52
2.6	MOLECULAR BIOLOGY	53
2.6.1	Generation of constructs	54
2.6.1.1	Plastid-targeted GFP in tomato and Arabidopsis	54
2.6.1.2	Plastid-targeted DsRED	54
2.6.1.3	Mitochondria-targeted GFP	55
2.6.1.4	Peroxisome-targeted ECFP	55
2.6.1.5	Silencing of CHUPI by RNAi	56
2.6.1.6	C-terminal fusion of CHUPI with sGFP	57
2.6.1.7	Plastid-targeted GFP for expression in maize	57
2.6.2	Electroporation of <i>A. tumefaciens</i>	58
2.6.2.1	Preparation of electro-competent cells	58
2.6.2.2	Introduction of plasmid DNA into <i>A. tumefaciens</i>	59
2.6.3	Plant genomic DNA extraction	59
2.6.4	Polymerase chain reaction of plant genomic sequences	60
2.6.4.1	Arabidopsis: Chapter 5	60
2.6.4.2	Maize: Chapter 6	61
2.6.5	Plant RNA extraction	61
2.6.6	Northern analysis	62
2.6.6.1	Electrophoresis and blotting of RNA to nylon membranes	62
2.6.6.2	Generation of DNA probes	64
2.6.6.3	Hybridisation of DNA probes to RNA immobilised on nylon membranes	65
2.6.6.4	Film exposure and development	66
2.6.6.5	Removal of bound probe from nylon membranes	67
2.6.7	Analysis of plant leaf proteins	67
2.6.7.1	Extraction and quantification of soluble leaf proteins	67
2.6.7.2	SDS-PAGE	68
2.6.7.3	Immunodetection of GFP	68
2.6.7.4	Film exposure and development	69
2.7	ISOLATION OF INTACT CHLOROPLASTS FROM LEAF TISSUE	69
3	STROMULE DEVELOPMENT DURING TOMATO FRUIT RIPENING	71
3.1	INTRODUCTION	71
3.1.1	Tomato fruit development	71
3.1.2	Plastid differentiation and pigment accumulation	76
3.1.3	Various aspects of tomato fruit development are affected by mutation	78
3.1.4	Scope of this Chapter	82

3.2 RESULTS	83
3.2.1 Two distinct plastid populations exist in the mesocarp of tomato fruit	83
3.2.2 Stromule frequency and length varies with plastid size and type	86
3.2.3 The <i>green flesh</i> mutation reduces stromule frequency in IM cells of ripe fruit	92
3.2.4 Inhibiting chloroplast development increases stromule frequency in a cell type-specific manner	95
3.2.5 The <i>rin</i> mutation dramatically decreases stromule abundance in tomato fruit	97
3.2.6 The <i>high pigment-1</i> mutation has no consistent effect on stromule abundance in tomato fruit	100
3.3 DISCUSSION	104
3.3.1 Mesocarp plastid dimorphism	104
3.3.2 Stromule formation depends on plastid differentiation and plastid size	105
3.3.3 Is plastid density important in determining stromule formation?	107
3.3.4 Conclusions	108
4 FACTORS INFLUENCING STROMULE BIOGENESIS IN TOBACCO HYPOCOTYL EPIDERMIS	110
4.1 INTRODUCTION	110
4.1.1 Seedling development	110
4.1.1.1 Photomorphogenesis is regulated by photoreceptor proteins	111
4.1.1.2 The long and short of it: cellular regulation of hypocotyl growth	115
4.1.2 Tobacco hypocotyls as a basis for studying stromules	116
4.1.3 Scope of the Chapter	116
4.2 RESULTS	118
4.2.1 Photomorphogenic and skotomorphogenic seedlings exhibit dramatic differences in plastid and stromule morphology	118
4.2.2 Blue and red light, provided at low intensity, increase stromule formation relative to white light	122
4.2.3 Light quality does not effect stromule formation when provided at equal intensity	125
4.2.4 Stromule length is negatively correlated with the density of plastids within the cell	128
4.2.5 Co-localisation of DsRED and aadA-GFP in stromules	131
4.2.5.1 DsRED and aadA-GFP show identical distributions in stromules	131
4.2.5.2 DsRED and aadA-GFP diffuse at different rates through stromules	135
4.2.6 Stromules are intimately associated with other organelles	136
4.2.6.1 Mitochondria	137
4.2.6.2 Peroxisomes	139
4.2.7 Low oxygen conditions promote fusion of mitochondria but not plastids	142
4.2.8 Mitochondria may pass through cell walls	145
4.3 DISCUSSION	148
4.3.1 Stromule formation is dependent upon plastid density within the cell	148
4.3.2 Stromules assist interactions between compartments within the cell	150
4.3.3 Can stromules fuse like mitochondria?	153
4.3.4 Protein movement through stromules depends on molecular size	157
4.3.5 Intercellular communication via organelles?	158
4.3.6 Conclusions	159
5 THE ROLE OF THE ACTIN-BINDING PROTEIN CHUPI IN STROMULE FORMATION	160
5.1 INTRODUCTION	160
5.1.1 The actin cytoskeleton is responsible for plastid movements	160
5.1.2 Chloroplast avoidance movement involves the actin-binding protein CHUPI	163
5.1.3 Scope of this Chapter	164
5.2 RESULTS	166

5.2.1 CHUPI binds actin through an $\alpha$ -actinin domain	166
5.2.2 Generation of lines with reduced <i>CHUPI</i> expression	169
5.2.2.1 Silencing of CHUPI by gene-specific post-transcriptional gene silencing	169
5.2.2.2 Isolation of insertion knock-out mutants of CHUPI	170
5.2.3 <i>CHUPI</i> is expressed strongly in wild type green tissue but not in roots	171
5.2.4 Subcellular localisation of CHUPI by fusion with GFP	173
5.2.5 Lines with reduced CHUPI activity exhibit a <i>chup1-1</i> mutant phenotype	176
5.2.6 Crossing of <i>recAgfp</i> lines and lines with reduced CHUPI activity	176
5.2.7 The effects of reduced CHUPI levels on chloroplast morphology	181
5.3 DISCUSSION	187
5.3.1 <i>CHUPI</i> _RNAi phenocopies the <i>chup1-1</i> mutant	187
5.3.2 CHUPI is probably not required for stromule formation and movement	187
5.3.3 Conclusions	191
6 STROMULE BIOGENESIS IN MAIZE CHLOROPLASTS	192
6.1 INTRODUCTION	192
6.1.1 $C_4$ photosynthesis	192
6.1.2 Metabolite movement during $C_4$ photosynthesis	196
6.1.3 Plasmodesmata in the maize leaf	197
6.1.4 Scope of the Chapter	199
6.2 RESULTS	201
6.2.1 Construct design and generation of transgenic plants	201
6.2.2 PCR screening of transformants	203
6.2.3 Northern analysis of transgenic lines	203
6.2.4 Confocal microscopy of strong transgene expressors	206
6.2.5 Immunoblot analysis reveals limited GFP accumulation	210
6.3 DISCUSSION	213
7 GENERAL DISCUSSION	219
7.1 Summary and main conclusions	219
7.2 Likely roles for stromules	222
7.3 Future prospects and challenges	224
REFERENCES	227
APPENDIX	242

# LIST OF FIGURES AND TABLES

Figure 1.1	Phylogeny of the embryophytes and their ancestral green algae	3
Figure 1.2	Interrelations between the different forms of plastid in higher plants	5
Figure 1.3	Variation in plastid and stromule morphology revealed by plastid-localised GFP	25
Figure 3.1	Tomato fruit pericarp and ripening stages	73
Figure 3.2	Confocal sections through the pericarp wall of a mature green fruit expressing <i>recA-gfp</i>	84
Figure 3.3	Changes in plastid and stromule morphology during ripening	85
Figure 3.4	Changes in stromule frequency and length in wild type tomato fruit during ripening	89
Figure 3.5	Stromule and chromoplast morphology in IM cells of B+7 wild type fruit	91
Figure 3.6	Plastid and stromule morphology in <i>gf</i> B+7 fruit	94
Figure 3.7	Plastid and stromule morphology in dark- and light-grown mature green fruit	96
Figure 3.8	Plastid and stromule morphology in <i>rin</i> fruit at B+40	99
Figure 3.9	The <i>hp-1</i> phenotype	102
Figure 3.10	Plastid and stromule morphology in <i>hp-1</i> fruit at MG and B+7	103
Figure 4.1	Constructs used to follow <i>in vivo</i> dynamics of organelles	119
Figure 4.2	Plastid morphology in hypocotyl epidermis depends on light	121
Figure 4.3	Plastid and seedling morphology under low intensity red and blue light	124
Figure 4.4	Plastid and seedling morphology under high intensity red and blue light	127
Figure 4.5	Stromule length is negatively correlated with plastid density	130
Figure 4.6	<i>aadA</i> -GFP and DsRED signals largely co-localise	133
Figure 4.7	FRAP analysis of movement of <i>aadA</i> -GFP and DsRED along stromules	134
Figure 4.8	Dynamics of plastids and mitochondria	138
Figure 4.9	Dynamics of plastids and peroxisomes	141
Figure 4.10	Reversible mitochondrial fusion brought about by oxygen deprivation	144
Figure 4.11	Putative intercellular passage of mitochondria	146
Figure 4.12	Model for the passing of mitochondria through cell walls in hypocotyl epidermis	147
Figure 5.1	Two types of force generating mechanism for organelle motility	162
Figure 5.2	<i>CHUPI</i> gene structure and PCR primers	167
Figure 5.3	Constructs generated to assess <i>CHUPI</i> function	167
Figure 5.4	Expression of <i>CHUPI</i> in wild type and <i>CHUPI</i> _RNAi lines	172
Figure 5.5	PCR screen for <i>CHUPI</i> T-DNA insertion mutants	172
Figure 5.6	Northern analysis of primary transformants expressing <i>CHUPI</i> -sgfp	174
Figure 5.7	Reduction of <i>CHUPI</i> activity leads to increased propensity to photodamage	175
Figure 5.8	Crossing of plastid-targeted GFP and <i>CHUPI</i> -compromised plants	178
Figure 5.9	PCR screen for confirmation of crosses and isolation of N605043 homozygotes	179
Figure 5.10	Expression of <i>CHUPI</i> in the F <sub>2</sub> generation following crossing	180
Figure 5.11	Leaf plastid morphology in wild type and <i>CHUPI</i> _RNAi plants	184
Figure 5.12	N605043 plants exhibit improper chloroplast accumulation under low light	185
Figure 5.13	Stromule formation and movement is unaffected in <i>CHUPI</i> _RNAi plants	186
Figure 6.1	Transverse section of a <i>Zea mays</i> leaf	194
Figure 6.2	The C <sub>4</sub> cycle requires intercellular metabolite shuttling between two cell types	195
Figure 6.3	Generation and screening of transgenic maize lines	202
Figure 6.4	Northern analysis of PCR-positive T <sub>1</sub> lines	205
Figure 6.5	Detection of GFP in transgenic maize leaf tissue by confocal microscopy	208
Figure 6.6	Motility and pleiomorphy of unidentified vesicles in transgenic leaf tissue	209
Figure 6.7	Protein extraction and western analysis from strong mGFP4 expressors	212
Table 1.1	Major classifications of chromoplasts	19
Table 2.1	Transgenic lines described in this work	37
Table 3.1	Major physiological and biochemical changes during tomato fruit ripening	74
Table 3.2	Stromule abundance, plastid size and plastid density in tomato fruit mesocarp cells	88
Table 5.1	Selected results from a BLAST-P search of the <i>CHUPI</i> amino acid sequence against known and predicted protein sequences in the <i>Arabidopsis</i> database	168

# ABBREVIATIONS

## I. UNITS OF MEASUREMENT

### A. Length

m	metre	cm	centimetre, $10^{-2}$ m
mm	millimetre, $10^{-3}$ m	$\mu\text{m}$	micrometre, $10^{-6}$ m
nm	nanometre, $10^{-9}$ m		

### B. Area

$\text{m}^2$	square metre	$\mu\text{m}^2$	square micrometre
--------------	--------------	-----------------	-------------------

### C. Mass

g	gram	mg	milligram, $10^{-3}$ g
$\mu\text{g}$	microgram, $10^{-6}$ g		

### D. Volume

l	litre	ml	millilitre, $10^{-3}$ l
$\mu\text{l}$	microlitre, $10^{-6}$ l		

### E. Concentration

M	molar, moles $\text{l}^{-1}$	mM	millimolar ( $10^{-3}$ M)
$\mu\text{M}$	micromolar, $10^{-6}$ M	$\text{g l}^{-1}$	grams per litre
$\text{mg l}^{-1}$	milligrams per litre, $10^{-3}$ $\text{g l}^{-1}$	$\mu\text{g ml}^{-1}$	micrograms per millilitre, $10^{-6}$ $\text{g l}^{-1}$

### F. Time

s	second	ms	millisecond, $10^{-3}$ s
min	minute	h	hour

### G. Other Units of Measurement

V	volt	kV	kilovolt, $10^3$ V
$\Omega$	ohm	$^{\circ}\text{C}$	degrees Celsius

## 2. OTHER ABBREVIATIONS

ACC	l-aminocyclopropane-l-carboxylic acid	IAA	indole-3-acetic acid
AMP	adenosine monophosphate	IM	inner mesocarp
Ar	argon	kb	kilobase pairs
ADP	adenosine diphosphate	kDa	kilodaltons
ATP	adenosine triphosphate	LED	light emitting diode
ATPase	ATP-hydrolysing protein	MG	mature green
B+1	one day post breaker	MOPS	3-(N-morpholino)propane-sulphonic acid
B+3	three days post breaker	mRNA	messenger RNA
B+7	seven days post breaker	NAD(P)H	nicotinamide adenine dinucleotide (phosphate)
bp	base pairs	NaOH	sodium hydroxide
CaMV	cauliflower mosaic virus	$\text{O}_2$	molecular oxygen
cDNA	complementary DNA	$\text{OD}_n$	optical density at $n$ nm
$\text{CO}_2$	carbon dioxide	OM	outer mesocarp
DNA	deoxyribonucleic acid	PAR	photosynthetically active radiation
dpa	days post anthesis	PCR	polymerase chain reaction
ECFP	enhanced cyan fluorescent protein	RNA	ribonucleic acid
EDTA	ethylenediaminetetraacetic acid	RNAi	interference RNA
ER	endoplasmic reticulum	Rubisco	ribulose 1,5-bisphosphate carboxylase/oxygenase
$F_n$	$n$ th generation after a cross	SDS	sodium dodecyl sulphate
FRAP	fluorescence return after photobleaching	SDS-PAGE	SDS-polyacrylamide gel electrophoresis
g	gravitational constant	s.f.	significant figures
GFP	green fluorescent protein	T-DNA	transfer DNA ( <i>Agrobacterium</i> -derived)
GTP	guanosine triphosphate	tris	tris(hydroxymethyl)methylamine
GTPase	GTP-hydrolysing protein	UTR	untranslated region
GUS	$\beta$ -glucuronidase	UV	ultraviolet
$\text{H}_2\text{S}$	dihydrogen sulphide	v/v	volume per volume
HeNe	helium-neon	w/v	weight per volume
HEPES	N-2-hydroxyethylpiperazine -N'-2-ethane-sulphonic acid		

# I GENERAL INTRODUCTION

## *1.1 The origin and early evolution of plastids*

The second law of thermodynamics dictates that all living organisms require an exogenous energy source for growth, development and reproduction. Whilst heterotrophic organisms obtain their energy and carbon from other organisms through nutrition, the ultimate source of this energy must be inorganic. Organisms that exploit such forms of energy and fix inorganic carbon are known as autotrophs. Although some chemoautotrophic bacteria fix inorganic carbon by using energy derived from the oxidation of chemical sources such as H<sub>2</sub>S, the vast majority of autotrophic life, and subsequently heterotrophic life, is based on the harnessing of energy from the sun. The ubiquitous process by which sunlight is converted into chemical energy, photosynthesis, arose approximately 3.6 billion years ago in a prokaryote (Niklas, 1997). The atmosphere of the early Earth was more reducing than that of the present, and oxygen did not reach high enough concentrations (1%-2% of present day levels) to support aerobic respiration until somewhere between 2.4 and 2.8 billion years ago (Knoll, 1992). It thus seems probable that the first photosynthetic bacteria were anoxygenic. However, eukaryotic photosynthesis liberates oxygen, and it is now widely accepted that photosynthesis in eukaryotes arose from an endosymbiotic event between an aerobic proto-eukaryote and an *oxygenic* photosynthetic prokaryote, most probably cyanobacterium-like in form (McFadden, 2001). Whilst the original photosynthetic prokaryote and its host are now inextricably associated, this symbiosis is the defining feature of all existing photosynthetic eukaryotes. To be precise, the fundamental photosynthetic events (i.e. the net fixation of carbon dioxide) occur in the evolutionary remnant of this prokaryote, the plastid.

The evolution of photosynthetic eukaryotes has followed a trend of increasing genetic and developmental complexity. Embryophytes, the land plants, are thought to have evolved from a fresh-water multicellular green alga of the order Charales about 470 million years ago, when various adaptations such as a waxy cuticle permitted survival in the desiccating terrestrial environment (Niklas, 1997; Karol *et al.*, 2001). The earliest embryophyte probably resembled a liverwort, with a free-living gametophyte and an ephemeral sporophyte, and without vascular tracheids. From this ancestral land plant evolved the monophyletic group of embryophytes observable today (Figure 1.1). Apart from a limited number of parasitic angiosperms, all of these organisms derive their energy from photosynthesis, and all contain a plastid compartment within their cells. Additionally, in line with the increase in morphological complexity and diversity from the liverwort-like ancestor to the angiosperms, the plastid compartment itself has also attained a variety of forms and functions during evolution, and yet has conserved a sufficient suite of characters that alludes to its prokaryotic ancestry.

Plastids in lower plants (green algae, liverworts, mosses, hornworts) contrast with those in higher (vascular) plants in various ways. Unicellular green algae like *Chlamydomonas reinhardtii* possess only one plastid, which occupies a large proportion of the cell volume. Many multicellular algae also contain single, spiral plastids that span the entire length of a cell e.g. *Spirogyra*, a common filamentous green alga of ponds and streams. Likewise, many hornworts possess only one chloroplast per cell (Vaughn *et al.*, 1992). In contrast, vascular plants possess from several to hundreds of plastids per cell, which is presumably an adaptation to coping with varying light conditions, because several, smaller chloroplasts can move within a cell to intercept or avoid light more efficiently than fewer, larger ones (Pyke, 1999; Jeong *et al.*, 2002). Secondly, the extent of plastid differentiation in the lower plants is restricted relative to higher plants, whose plastids perform a variety of functions and differentiate concomitantly with the cell type. Full chloroplast differentiation in angiosperms requires light, but most green algae synthe-

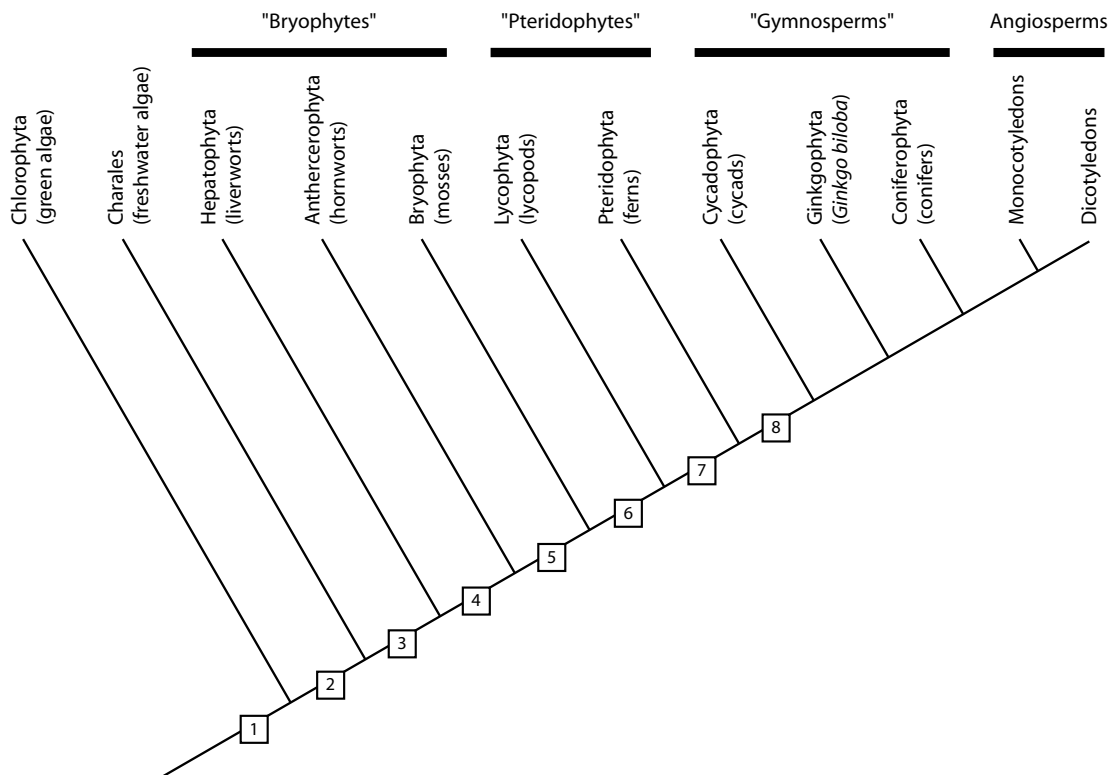


**Figure 1.1 Phylogeny of the embryophytes and their ancestral green algae**

Characters used to construct the phylogeny are as follows: 1. chlorophyll *a* + *b*, carotenoids, starch; 2. phragmoblast cell division, glycolate oxidase; 3. archegonium and antheridium; 4. indeterminate growth of sporophyte; 5. conducting tissue for water and sap; 6. lignified vascular tissue, sporophyte with multiple sporangia; 7. megaphyllous leaves; 8. seeds. "Bryophytes", "Pteridophytes" and "Gymnosperms" are historical classifications as shown but are paraphyletic groups and hence are not true taxa. The Ginkgophyta are today represented by a single species, *Ginkgo biloba*. Modified and adapted from Niklas (1997) and Karol *et al.* (2001).

se chlorophyll in the dark. In *Chlamydomonas*, although transcript levels for chlorophyll biosynthetic genes and Rubisco are attenuated when it is grown in the dark (Cahoon and Timko, 2000), the plastid still accumulates some chlorophyll and is competent to carry out photosynthesis upon transfer to the light. The ability to synthesise chlorophyll in the dark is also retained in mosses and some pterophytes such as *Selaginella* and *Isoetes*, but not in others such as the Equisitaceae (Kirk and Tilney-Bassett, 1978). Thirdly, the segregation of plastids between daughter cells during cell division varies amongst different taxa. In the hornwort *Anthoceros*, plastids are passed on to the daughter cell during mitosis in the form of chloroplasts (Vaughn *et al.*, 1992), which contrasts with *Isoetes* and higher vascular plants whose meristematic cells contain either one or several colourless proplastids respectively (Kirk and Tilney-Bassett, 1978). Such evidence upholds the established view that plastids are not created *de novo* but are part of a continuum of multiplying plastids transmitted from cell to cell. Given that plastids in these lower plants are generally chloroplastic in nature, even in the dark, it seems plausible that there has been little adaptation on the “default” plastid form of the ancestral green algae, and that plastid differentiation is generally limited to the chloroplast. The primary plastid function in these plants, therefore, appears to be photosynthesis.

## **1.2 The range of plastid forms in higher plants**

The vast majority of biochemical, ultrastructural and molecular-genetic studies on plastids have been performed on angiosperms. These plants are important agronomically, are easy to cultivate and offer a range of experimental advantages such as ease of genetic manipulation and availability of a wide range of mutants. In contrast with the non-vascular plants described earlier, plastids in angiosperms vary in size, shape, content and function. Plastids can perform several, interrelated roles simultaneously, and the various types are dynamically interconvertible (Figure 1.2).

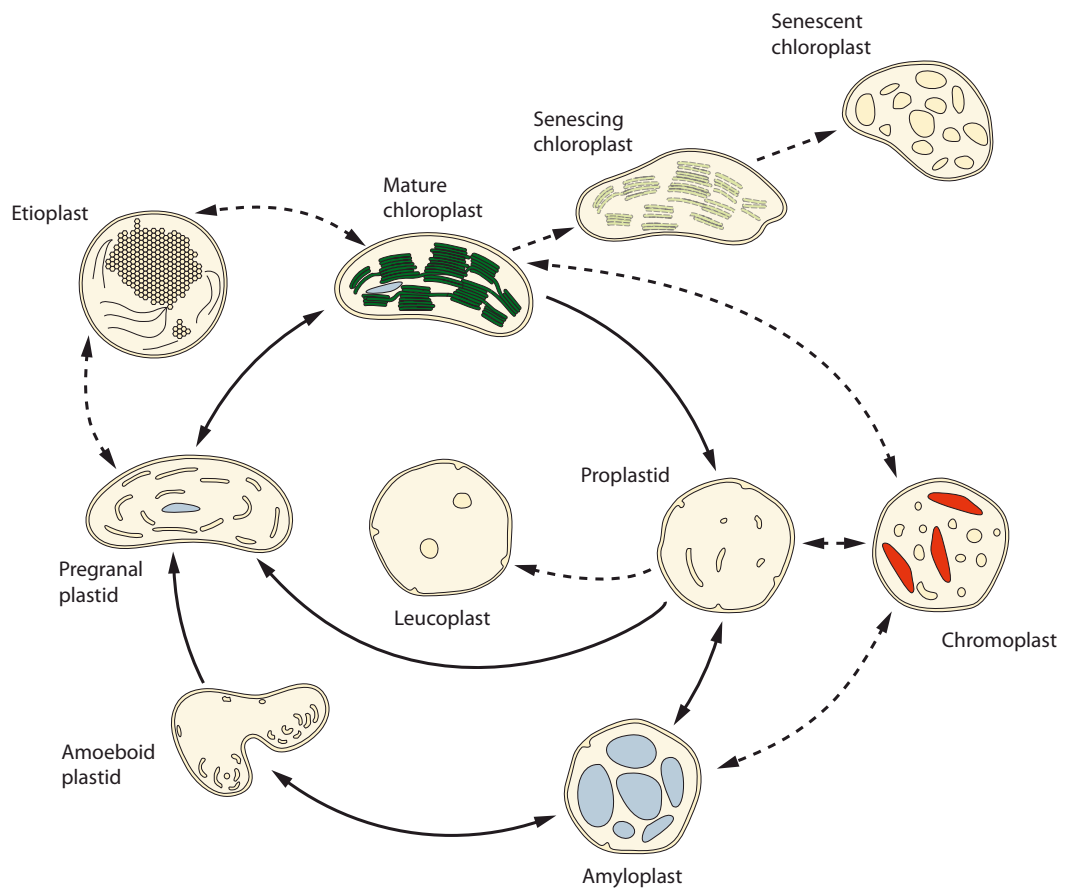


**Figure 1.2 Interrelations between the different forms of plastids in higher plants**

Solid lines indicate conversions which occur under normal plant developmental conditions; dashed lines specify conversions which are possible under a limited set of conditions or which are unusual. Note that this diagram is not exhaustive, as some plastid types do not neatly fall into one of these categories. Re-drawn and adapted from Buchanan *et al.* (2000).

Plastids are hence aptly named, with the term originating from the Greek *πλαστικός*, meaning “plastic, mouldable”. Traditionally plastids have been classified according to the obvious function of the plastid in question, generally based on their morphological appearance; a green plastid in leaf cells a chloroplast, a colourless one with starch grains an amyloplast etc. (Kirk and Tilney-Bassett, 1978). Such a classification is useful for describing the scope of plastid forms and how they are critical to plant development and reproductive success, but is an arbitrary and overly simplistic one since frequently a particular plastid expresses features of more than one type. A more flexible classification system might be based upon the physiological and biochemical properties of the plastid, or some other way of reflecting the range of forms a plastid can take that are intermediate between those somewhat rigid classifications. Nevertheless, distinct states of plastid differentiation do exist, each with specific though not necessarily unique properties.

### **1.2.1 Features common to all plastids**

Since all plastid varieties are interrelated, it follows that there are traits that are shared between them all – those that define a plastid. Like mitochondria, they possess a bounding double membrane, with a complex series of membrane-associated proteins which serve as an import apparatus for plastid-targeted proteins. Plastids import and export a wide range of metabolites and therefore possess selective transport proteins, mostly resident on the inner envelope membrane. Plastids also possess a genome (the plastome): whilst originally considered a circular chromosome, plastid DNA is now thought to consist of a variable mixture of branched and linear molecules complexed within membrane-bound nucleoids (Bendich, 2004). The plastome of higher plants encodes approximately 60-80 proteins, and is between 140 and 160 kb in size (Martin and Herrmann, 1998). The genome copy number is also variable but there can be in the region of 10,000 copies per leaf mesophyll cell (Maliga, 2002). During evolution, a large

proportion of the ancestral plastid genome has been transferred to the plant nucleus. It is estimated that the *Arabidopsis* nuclear genome contains some 4500 genes transferred from the original cyanobacterial endosymbiont over evolutionary history (Martin *et al.*, 2002). Notably, the number of protein-coding sequences residing on the plastome has decreased over evolutionary time (Martin and Herrmann, 1998), indicating that gene transfer may still be taking place. Indeed, DNA transfer from the nucleus seems to occur at a surprisingly high frequency, at an approximate rate of about one transposition event per 16,000 pollen grains (Huang *et al.*, 2003). The loss of several plastid genes has occurred in parallel in independent lineages (Martin *et al.*, 1998), suggesting that there has been strong selection pressure for the transfer of organellar genes to the nucleus. Numerous theories have been proposed to explain this phenomenon, but the most popular explanation is Muller's ratchet, or the avoidance of the accumulation of deleterious mutations (reviewed by Blanchard and Lynch, 2000). Accordingly, the vast majority of plastid proteins are encoded by genes located in the nucleus: although the *Arabidopsis* plastid genome encodes only 68 hypothetical proteins, some 1900-3000 proteins are predicted to be imported (Abdallah *et al.*, 2000; The Arabidopsis Genome Initiative, 2000). Thus from this numerical information alone it is clear that there is significant control over plastid development from the nucleus that has accumulated over evolutionary time. Much recent work has identified nuclear mutations that influence chloroplast development (León *et al.*, 1998), and it is well established that the plastid and nuclear genomes signal to each other to co-ordinate development during photomorphogenesis (Sullivan and Gray, 2002). Therefore, the diversity of plastid types and functions is largely brought about by the nucleus as a central part of cellular differentiation and development.

Despite the relatively basic spectrum of plastid form in lower plants, the molecular and morphological basis of plastid division spans all of the embryophytes. One of the most striking features of chloroplasts is their similarity to cyanobacteria, especially with re-

spect to size and the division process, which occurs through binary fission. There is a high degree of genetic conservation in the mechanism of division between eubacteria and chloroplasts. Bacterial *ftsZ* (*filamentous temperature sensitive*) mutants exhibit elongated, filamentous cells that fail to divide, and block at the earliest stage of cell division (Wang, Jones and Brun., 2001). The FtsZ protein shares homology with tubulin, and can polymerise *in vitro* in a GTP-dependent manner (Mukherjee and Lutkenhaus, 1998). At least two *ftsZ* nuclear gene families have been identified in *Arabidopsis*, and their genetic manipulation influences chloroplast size, number and morphology (Osteryoung *et al.*, 1998; Osteryoung and Pyke, 1998). In plants, as in bacteria, it has been demonstrated that FtsZ proteins form a ring around the midpoint of the chloroplast prior to division (Vitha *et al.*, 2001); the FtsZ ring structure may therefore be the contractile apparatus that, together with further interacting proteins, mediates the binary fission process. *ftsZ* homologues have been identified in a number of angiosperms – for example, *Lilium* (Mori *et al.*, 2001) and tobacco (Jeong, *et al.*, 2002) – as well as in the moss *Physcomitrella patens* (Kiessling *et al.*, 2000). Interestingly, plastids in some liverworts revert to the ancestral monoplastidic state during meiosis (Renzaglia *et al.*, 1994), as do root tip cells of *Isoetes* (Cleary *et al.*, 1992).

The plastid compartment has a number of biosynthetic and metabolic roles which are not specific to any one type of plastid (Neuhaus and Emes, 2000). Fatty acid biosynthesis – the early stages in the synthesis of membrane lipids, epicuticular waxes and the storage reserve triacylglycerides – is almost entirely limited to the plastid compartment (Ohlrogge and Jaworski, 1997). This is a metabolic pathway essential to cellular growth and maintenance, so is present in all plastid types, but is particularly prevalent in lipid storage plastids in oilseeds, and in the plastids of epidermal cells for epicuticular wax synthesis. The plastid is involved in the synthesis of the phytohormone abscisic acid (ABA) since it is a derivative of carotenoid biosynthesis, and in the initial stages of amino acid biosynthesis following fixation of inorganic nitrate in the cytosol. A fourth

major biochemical role of the plastid is carbohydrate metabolism. This involves mainly the metabolism of starch, synthesised either from imported hexose phosphates, or from excess 3-phosphoglyceric aldehyde (3-PGA) from the Calvin cycle.

Much of the terminology in defining plastid types has changed over the years, with some forms of plastid being grouped with another, others being renamed or even disregarded altogether (compare, for example, Thomson and Whatley, 1980, with Kirk and Tilney-Bassett, 1978). Here will be described the four main types for which some consensus has been reached; more obscure varieties will then be mentioned briefly.

### 1.2.2 The proplastid

The proplastid, previously called “eoplasts” (*eo-*: dawn, early), is basic to most pathways of plastid development and differentiation in higher plants. Proplastids are small, unpigmented plastids found in meristematic tissues, from which all plastids within a plant are ultimately derived. The entire plastid population within the plant is sourced from the plastids contained within the egg cell and the pollen, prior to gamete fertilization and zygote formation. In the majority of angiosperms, the pollen is devoid of functional plastids so that the plastid population is derived entirely from the few plastids within the egg cell (Corriveau and Coleman, 1988). Hence, in most species plastids are maternally inherited. During embryogenesis, proplastids derived from the egg cell divide as cell division occurs and the basic plan of the embryo is constructed. Upon establishment of clear meristematic regions at the shoot and root apices, proplastids proliferate in these regions as cells divide to ensure continuity of the plastid line within daughter cells (Chaley and Possingham, 1981). Although fundamental to plastid development, an understanding of proplastid biology is poor principally because of difficulties in observing, tracking and isolating such small, unpigmented organelles from dense tissues such as meristems. Much of the knowledge of proplastid behaviour during cell

division and development within the meristem comes from electron microscopy studies depicting proplastids dispersed throughout the cell and in various states of division (Chaley and Possingham, 1981; Robertson *et al.*, 1995). Estimations of proplastid population size in maize root meristem (Juniper and Clowes, 1965), spinach shoot meristem (Possingham and Rose, 1976) and *Arabidopsis* (Pyke and Leech, 1992) provides a consensus of between 10-20 proplastids per cell, although this number may change according to the stage of the cell cycle and the cellular position within the meristem. During this division stage, proplastids replicate their DNA, complexed within up to 10 nucleoid structures within the organelle (Miyamura *et al.*, 1990). Even at the earliest stages of cellular development, there are differences in proplastid morphology and DNA content between different layers of the shoot apical meristem (Fujie *et al.*, 1994), suggesting that even proplastids may show tissue-specific characteristics. Although proplastid segregation at cell division is of crucial importance to future cell viability, a distinct mechanism ensuring correct segregation of proplastids into daughter cells has not been elucidated. However, segregation of chloroplasts in cultured tobacco mesophyll protoplasts is achieved by their movement from the cell periphery to a perinuclear position prior to and following cell division, thus being inherited along with daughter nuclei (Sheahan *et al.*, 2004). Interestingly, giant proplastids, which are reduced in number in plastid division mutants, apparently are still able to ensure continuity of proplastids through cell lineages in meristems and mature tissues (Robertson *et al.*, 1995).

In terms of internal structure proplastids contain little definable structure other than traces of thylakoid-like membrane and sometimes starch grains. Proplastids in root meristems of *Salix* embryos contain a proteinaceous compound called phytoferritin, a storage form of iron, in their stroma (Maroder *et al.*, 2003). Several efforts have been made to assess levels of gene transcription by plastid DNA in proplastids. None of these studies has been able to measure activities at the individual cellular or tissue level within the meristem, which is technically very demanding. However, studies using pro-

plastids in spinach cotyledons (Harrak *et al.*, 1995), proplastids in cultured BY-2 cells (Sakai *et al.*, 1998) and meristematic tissues at the base of barley leaves (Baumgartner *et al.*, 1989) together show that the level of proplastid DNA transcription is very low. Furthermore, the development of the proplastid toward the chloroplast requires the expression of nuclear genes for ribosomal structures preceding those that are plastid encoded. The emphasis in these studies has been the initiation of the plastid differentiation pathway, but little is known of the essentially housekeeping metabolism that occurs during proplastid growth in meristematic cells.

### 1.2.3 The chloroplast

As the most widely studied plastid type, the chloroplast is the site of photosynthesis in the aerial parts of the plant. As opposed to all other types of plastid, mature chloroplasts are net energy producers (autotrophic), although developing chloroplasts in young tissue may act as a sink for resources. Chloroplasts are 4-6  $\mu\text{m}$  in diameter and typically are oblate-spheroid in shape. Most chloroplasts are found in the spongy mesophyll and palisade cells of the leaf, but they also occur in the outer cells of the stem and in bundle sheath cells surrounding the vasculature (Hibberd and Quick, 2002). They are present at variable density, but reach a maximum in leaf mesophyll cells where there are on average 120 chloroplasts, at least in *Arabidopsis* (Pyke and Leech, 1994). Numerous ultrastructural studies have revealed the presence of extensive, flattened sacs called grana that are stacked to form thylakoids (Kirk and Tilney-Bassett, 1978). These membranes are the site of electron transport, and the generation of a proton gradient across them drives ATP generation. Starch grains are a common feature of mature chloroplasts, and act as an insoluble form of photosynthate storage. Chloroplasts are defined by the presence of chlorophyll, but one must be careful in assigning photosynthesis as a primary role to all green plastids. Many trichomes possess green plastids, but they are very much smaller in size than mesophyll chloroplasts and present at a much lower density;

as an alternative primary function they may be implicated in the generation of compounds for secretion (McGaskill and Croteau, 1995; Turner *et al.*, 1999). The presence of chlorophyll in such tissues perhaps represents the need to generate sufficient photosynthate to sustain cellular activities, but not enough to provide net production of energy that can be mobilised to sink regions of the plant.

Chloroplasts normally develop from proplastids but can occasionally arise from other plastid types, such as during the re-greening of *Citrus* fruits when chromoplasts revert to chloroplasts (Thomson *et al.*, 1967). The mature chloroplast is a structurally complex entity with a large proteome consisting of contributions from two different genomes. Once a plastid has commenced the pathway towards chloroplast development, several inter-related activities take place during chloroplast biogenesis, each of which is essential for complete chloroplast functionality.

### 1.2.3.1 Protein import, sorting and assembly

The developing chloroplast must import between 1900-3000 proteins encoded by nuclear genes (Abdallah *et al.*, 2000; The Arabidopsis Genome Initiative, 2000). Proteins possessing an N-terminal transit peptide are transported in an unfolded state to the chloroplast envelope by cytosolic chaperones, where they are then recognised by the chloroplast protein import apparatus (Bauer *et al.*, 2001). Chloroplast protein import is an early, critical event that depends on a complex of several nuclear-encoded proteins (Jarvis and Soll, 2001). Various mutants disrupted in components of the import apparatus have been characterised, such as *ppil*, which exhibits a pale green phenotype due to improper chloroplast differentiation (Jarvis *et al.*, 1998). Furthermore, there is evidence that photosynthetic and non-photosynthetic proteins are imported through different protein import receptors, providing import specificity that may be important in directing plastid differentiation (Kubis *et al.*, 2003).

Imported proteins must subsequently be sorted between the various suborganellar locations available. These include the two envelope membranes, the stroma, the thylakoid membranes and the thylakoid lumen. This intraorganellar sorting is achieved by several parallel targeting pathways (Bauer *et al.*, 2001). Imported proteins attain functionality only when correctly assembled together with other subunits in the correct stoichiometry. Rubisco, for example, is a hexadecameric holoenzyme of eight large and eight small subunits encoded by the plastidial *rbcL* and nuclear *rbcS* genes respectively. Stoichiometry is maintained through modulation of translation initiation of *rbcL* mRNA: translation is either negatively regulated by the presence of excess RbcL subunits or, alternatively, it is activated by excess RbcS subunits (Rodermel, 2001).

#### 1.2.3.2 Thylakoid biogenesis

A chloroplast harvests light through chlorophyll and a variety of carotenoid-based accessory pigments. The biosynthesis of the chlorophylls is performed entirely in the chloroplast from the simple precursor glutamate (Beale, 1999). There is strong evidence that the presence of chlorophyll is necessary to stabilise the thylakoid membrane system and light-harvesting complex (León *et al.*, 1998), reflecting the recurring theme in chloroplast biogenesis that many processes are interdependent upon one another. On a morphological level, the formation of internal thylakoid membranes marks the process of chloroplast maturation. Thylakoid formation requires the reorganisation and biogenesis of internal membranes, together with the assembly of thylakoid-localised protein complexes. Thylakoid biogenesis is initiated by the development of long lamellae, which are later complemented by smaller, disc-shaped structures to form granal stacks. The mature chloroplast contains an interlocking network of granal thylakoid stacks connected by thylakoid lamellae, with a densely-packed stroma containing all of the soluble proteins involved in photosynthesis and other metabolic processes (reviewed by Staehelin, 2003). Thylakoid membranes are thought to be derived from invagina-

tions of the inner membrane, as maturing chloroplasts sometimes exhibit a continuum between the inner membrane and internal membrane structures (Vothknecht and Westhoff, 2001), although this continuum is not present in mature chloroplasts. It has been suggested that vesicle trafficking from the inner membrane to the thylakoids allows maintenance and regeneration of these structures in the mature chloroplast (Vothknecht and Westhoff, 2001). Furthermore, an ATP-dependent factor involved in vesicle fusion within pepper chromoplasts has been isolated and the gene cloned (Hugueney *et al.*, 1995). Such a “budding” mechanism of thylakoid biogenesis would explain how other hydrophobic membrane components (e.g. carotenoids, galactolipids), synthesised on the chloroplast envelope, are able to reach the thylakoid membranes themselves.

#### **1.2.4 The amyloplast**

During the course of evolution, the plastid has acquired the role of storing various compounds and sequestering them away from the metabolic activities of the cytosol. In contrast to the chloroplast, storage plastids are heterotrophic organelles that convert photosynthate derived from source tissues into a long-term storage molecule of high specific energy, which can be drawn upon as required during plant development. The major storage form for excess photosynthate is starch, an insoluble, complex, semi-crystalline polymer of glucose. All starch is synthesised in the plastid compartment, and is produced in two ways: either in leaf chloroplasts as a transient store of excess photosynthate, or in heterotrophic tissues synthesised from photosynthate unloaded from the phloem, providing a more long-term storage location. This latter class of starch is stored in a specialised colourless plastid, the amyloplast, which is of great economic and agricultural importance since some 75% of human energy intake is attributable to starch produced by plants (Duffus, 1984). Amyloplasts are present in the endosperm of many seeds, most notably those of the cereal crops, as well as in tubers of potato and

fruits such as bananas. In addition, amyloplasts are present in the columella cells in the root cap of most if not all plant species, where they are central to the perception of gravity (Kiss, 2000). However, these amyloplasts are highly specialised for a particular role, and probably represent only a superficial similarity to amyloplasts in storage tissues; indeed, it could be argued that their formation is regulated differently to that of other amyloplasts (see below).

Starch synthesis in amyloplasts occurs through the polymerisation of ADP-glucose, yielding highly branched amylopectin and relatively unbranched amylose, the latter composing 20-30% of the total (Smith *et al.*, 1997). The starch grain itself consists of a series of concentric rings of alternating semi-crystalline and amorphous zones, a structure resulting from regions of highly organised and poorly organised individual chains of amylopectin respectively (Smith *et al.*, 1997). In wheat and barley endosperm there are two major classes of starch grains: the A-type, of up to 45  $\mu\text{m}$  in diameter and the B-type, reaching up to 10  $\mu\text{m}$  in diameter and forming later in the developing endosperm, the ratio of which can significantly influence the quality and suitable post-harvest application of the starch (Langeveld *et al.*, 2000). In potato tubers, amyloplasts are usually dominated by a single large starch grain (Kirk and Tilney-Bassett, 1978) whereas in those in the columella cells of the root cap contain several starch grains (MacCleery and Kiss, 1999). The basis of this variability in grain number and morphology is poorly understood, but can be influenced by a number of developmental as well as environmental factors.

Amyloplasts generally develop from proplastids, but may also form from the dedifferentiation of chloroplasts (Thomson and Whatley, 1980). In red winter wheat, for example, plastids present in the coenocytic endosperm remain as proplastids with occasional tubular cristae, but only start to deposit starch once cellularisation is complete (Bechtel

and Wilson, 2003). Amyloplasts are also capable of redifferentiating into other plastid types, most famously in the re-greening of potato tubers where cell layers deep within the tuber undergo substantial chloroplast formation, albeit relatively slowly compared to meristematic proplastids (Ljubcic *et al.*, 1998).

In terms of the regulation of amyloplast differentiation, the majority of work has been performed on tobacco Bright-Yellow 2 (BY-2) cell suspension cultures, which can be induced to undergo changes in cell division and plastid metabolism by the addition of phytohormones to the culture medium. BY-2 cells grown in the dark possess proplastids, in line with the undifferentiated status of the cell. The presence of auxin (2,4-dichlorophenoxyacetic acid, 2,4-D) promotes the rapid proliferation of BY-2 cells, and plastids remain in the proplastid state. Upon replacement of 2,4-D with the cytokinin benzyladenine (BA), BY-2 cells no longer proliferate rapidly but shift behaviour and begin to accumulate starch and form amyloplasts (Sakai *et al.*, 1992; Sakai *et al.*, 1999). The number of plastids per cell remains approximately constant, but all plastids have been converted to large amyloplasts within 48 hours of transfer to BA-containing medium (Sakai *et al.*, 1992). This rapid change in plastid state is accompanied by changes in gene expression in both the plastid and nuclear genomes. For example, the plastomic Rubisco large subunit gene, *rbcL*, is dramatically down-regulated upon conversion of proplastids to amyloplasts, as are a number of other photosynthesis-related transcripts (Sakai *et al.*, 1992). Likewise, nuclear-localised starch synthesis genes such as ADP-glucose pyrophosphorylase small subunit (*AgpS*) are up-regulated by cytokinin and downregulated by auxin in this system (Miyazawa *et al.*, 1999). Similarly, the addition of 2,4-D to 2,4-D-depleted medium induces BY-2 cells to undergo the reverse process: cells begin to proliferate and amyloplasts apparently revert to proplastids within 12-18 hours of 2,4-D application, together with a concomitant decrease in *AgpS* mRNA levels (Miyazawa *et al.*, 2002). Thus, at least in the artificial environment of suspension cultures, the phytohormones auxin and cytokinin act antagonistically in directing plas-

tid differentiation. This is, however, a situation far removed from that *in planta*, and provides only a simplistic understanding of the cellular changes that occur during amyloplast biogenesis. Indeed, it appears quite opposite to what one might predict with regards to the amyloplasts in root cap columella cells. It has been shown that the auxin indole-3-acetic acid (IAA) is preferentially transported to these cells and is physiologically active there (Ottenschläger *et al.*, 2003; Swarup *et al.*, 2001). The studies on BY-2 cells imply that the plastids in root cap columella cells should not accumulate starch, and should remain as proplastids, thus suggesting that the genetic pathways that determine plastid status are more complex. In fact, it is of interest to understand how these plastids differentiate into amyloplasts whilst those in the adjacent quiescent centre of the root apex remain in the proplastid form. Moreover, it raises the general question of whether an amyloplast is anything more than a proplastid which contains the proteins required for substrate import and starch synthesis, a process which conceivably could be triggered in a number of different ways.

### 1.2.5 The chromoplast

During the process of higher plant evolution, plants developed symbiotic interactions with other life forms. Such interactions proved highly beneficial to plants in two particular areas of plant function, namely pollination of floral structures by insects and seed consumption and subsequent dispersal by animals. In both of these situations the display of coloured plant structures as an attractant was required and a specialised form of plastid, the chromoplast, evolved to carry out this function. The coloured pigments which accumulate in chromoplasts are mostly members of the carotenoid family starting with the  $C_{40}$  molecule phytoene and undergoing a variety of complex reactions to give rise to other carotenoids including carotenes, lycopene, lutein, violaxanthin and neoxanthin (Camara *et al.*, 1995, Bramley, 2002). Although many coloured plant structures rely entirely on chromoplasts for their pigmentation, a significant number of pet-

als and fruits contain pigmented chromoplasts often in addition to other pigments, usually in the vacuole (Kay *et al.*, 1981, Weston and Pyke, 1999). Early work on chromoplast biology was largely centered on light microscopy and documentation of different types of chromoplasts in different tissues and species. More modern studies using electron microscopy have led to the clarification of five classes of chromoplasts based upon the frequency of different substructures related to pigment storage within the chromoplast (Table 1.1; Thomson and Whatley 1980, Camara *et al.*, 1995). Of these, the globular chromoplast is thought to be the ancestral state: in algae, bryophytes, pterophytes and gymnosperms carotenoids often accumulate in lipid-associated granules within a chromoplast-like plastid (Camara *et al.*, 1995). Although such classification of chromoplast types may be convenient for documentation, the different classes are widely spread across different plant species and are present in a wide variety of organs including fruits, petals, anthers, sepals, arils and roots (Camara *et al.*, 1995). The highly heterogenous nature of chromoplasts within different organs and different species may simply reflect the extent to which differing profiles of carotenoids, flavonoids and other attractant pigments are stockpiled (Whatley and Whatley, 1987).

**Table 1.1** Major classifications of chromoplasts (compiled from Camara *et al.*, 1995)

Class	Defining features	Example
Globular	Pigment-containing plastoglobuli in stroma	<i>Lycopersicon esculentum</i> petal
Crystalline	Crystal deposits of lycopene and/or $\beta$ -carotene	<i>L. esculentum</i> fruit; <i>Daucus carota</i> root
Fibrillar-Tubular	Spindle-shaped, parallel bundles of fibrils	<i>Capsicum annum</i> fruit
Membranous	Concentric rings of membranes; few plastoglobuli	<i>Narcissus pseudonarcissus</i> corona
Reticulo-Tubular	Complex network of twisted fibrils	<i>Liriodendron tulipifera</i> (Yellow Poplar) petals

Chromoplasts usually differentiate from chloroplasts, a process typified by the ripening fruit of tomato (*Lycopersicon esculentum*). The transition from green chloroplast to pigmented chromoplast is a clearly defined developmental process with controlled disassembly of chloroplast components. The major observable changes which occur are the degradation of chlorophyll, the breakdown of thylakoid membrane complexes and the extensive synthesis and accumulation of carotenoid pigments, in particular lycopene and  $\beta$ -carotene (Marano *et al.*, 1993; Deruère *et al.*, 1994; Grierson and Kader, 1986). These processes are accompanied by expression of distinct nuclear genes, which are required for chromoplast differentiation and hence are labelled as chromoplast specific (Lawrence *et al.*, 1993; Lawrence *et al.*, 1997; Summer and Cline, 1999). These include phytoene synthase (Fraser *et al.*, 1994), 1-deoxy-D-xylulose-5-phosphate synthase (DXS) (Lois, 2000) and phytoene desaturase (Fraser *et al.*, 1994). In addition, a plastid terminal oxidase associated with phytoene desaturation is required for carotenoid synthesis, and is thus essential for proper development of chloroplasts as well as chromoplasts in tomato (Josse, 2000). In addition to enzymes involved in carotenoid metabolism, a distinct subset of newly expressed proteins have been identified in developing chromoplasts which appear to be required for the differentiation process to progress. Amongst these proteins are enzymes involved in response to oxidative stress (Livne and Gepstein, 1988; Römer *et al.*, 1992) and a group of proteins involved in carotenoid sequestration (Vishnevetsky *et al.*, 1999). One of these, fibrillin, appears to function as a structural protein in the biogenesis of fibril structures present in the fibrillar class of chromoplasts, in which carotenoids are sequestered internally and surrounded by a layer of polar lipids and coated with a layer of fibrillin (Deruère *et al.*, 1994). Although chromoplasts retain plastid DNA there is little evidence that plastid encoded genes are important in chromoplast function. Indeed plastid gene expression is reduced to a low level during chromoplast differentiation, apparently because of methylation of plastid DNA (Kobayashi *et al.*, 1990). Thus, the nuclear genome dominates this particular path of plastid differentiation.

### 1.2.6 Other plastid types

The literature describes various other forms of plastids which are very loosely defined. Thomson and Whatley (1980) refer to “amoeboid plastids” which they describe as an intermediate stage in the transition from proplastid (or, in their language, eoplast) to chloroplast, and from chloroplast to chromoplast, typified by a change from the spherical proplastid form to one lobed and flexible in appearance. With respect to the chloroplast to chromoplast transition, there is a case for an amoeboid stage, as shown in Chapter 3 – but whether this should be classified as a type of plastid with a distinct function is doubtful, especially considering that the resulting chromoplast is also highly variable in shape. These authors also refer to the “proteinoplast”, a form of plastid in which membrane-bound inclusions stain positively for protein, and which may be amorphous or crystalline. However, these plastids do not seem to form any coherent class, and are found in a variety of cell types – proteinaceous inclusion bodies are found in many types of plastid without their becoming specific protein storage organelles.

A frequently encountered term in plastid developmental biology is the etioplast (French *étioler*, to bleach), used to describe a plastid in etiolated leaves that has been blocked along the stage of chloroplast development. Etioplasts accumulate large quantities of a colourless chlorophyll precursor called protochlorophyllide, which accumulates in a prominent, semi-crystalline membranous structure called the prolamellar body. This structure is the result of continued generation of lipids that, in the presence of proteins whose synthesis are induced by light, would normally form the thylakoid membranes (Sundqvist and Dahlin, 1997). As such, the etioplast may fulfil the role of a plastid “primed” to become a chloroplast since the development of thylakoids and photosynthetic apparatus occurs very rapidly upon exposure of etioplasts to light. The first visible changes, consisting of a disordering of the prolamellar body, occurs within five minutes of exposure to light, and primary thylakoid lamellae are formed within just two hours (Kirk and Tilney-Bassett, 1978). Nevertheless, whilst useful for studying the process of

thylakoid biogenesis and light perception, the etioplast is somewhat an artificial plastid that has little relevance to plastid development in general.

Other plastid terms include the leucoplast, elaioplast and gerontoplast (or senescent plastid). Of all the plastid types, the gerontoplast is unique because it represents a truly terminal state of plastid development, representing the remnant of a chloroplast from which all nutrients have been reclaimed during leaf senescence and which will be sacrificed along with the rest of the leaf tissue. The gerontoplast is responsible for the yellow and orange colours of senescing leaves, revealed once the chlorophyll has degraded; little or no new synthesis takes place during their formation. The term “leucoplast” describes colourless plastids present in tissue types like trichomes which generate secretory compounds such as monoterpenes (Turner *et al.*, 1999). This definition should probably be extended to other kinds of colourless plastids such as those in the root or in epidermal cells of onion bulbs, for example, which do not appear to have a term of consensus in the literature. Finally, the elaioplast is a plastid that has been modified as an oil storage organelle, and may be involved in the production and/or storage of aromatic compounds; these are usually found in oilseeds and in the epidermal cells of the monocot families Liliaceae and Orchidaceae (Kirk and Tilney-Bassett, 1978).

The plastid compartment has evolved greatly from the ancestral photosynthetic organelle, yet retains a great deal of the features observed in extant cyanobacteria. Non-pigmented plastids in angiosperms may represent an improvement in efficiency relative to lower plants and algae, because removal of the photosynthetic apparatus in tissues where it would be ineffective would be a cost-saving adaptation. The variety of plastid types observed in the angiosperms illustrates the diversity of roles that this organelle has assumed, and how it has been recruited by angiosperms as a multiply adaptive structure since the initial endosymbiotic event.

### **1.3 Plastid morphology and dynamics**

Much of our knowledge regarding cellular dynamics results from meticulous observation through microscopes and the real-time visualisation of cellular behaviour in living tissue. Several distinct microscopy techniques have been developed since the days of the Dutchman Antoni van Leeuwenhoek (1632-1723), who first used microscopy to examine motile micro-organisms, and of the English physicist Robert Hooke (1635-1702), who described the cellular structure of dead cork bark and hence discovered the cell (Mazzerello, 1999). Microscopy today allows extremely high resolution of events *in vivo*, even allowing the tracking and subcellular localisation of proteins within specific cell types (Oparka *et al.*, 1996; Swarup *et al.*, 2001). Since the discovery of chloroplasts, microscopy has been used extensively to investigate the structure and function of plastids. Schimper (1885) described an array of plastid types in angiosperms and organised them according to their colour. His comprehensive work has formed the basis of our current classification of the plastids, and has laid the foundation for microscopy as a method for analysing the diverse aspects of plastid development, differentiation and division.

#### **1.3.1 Plastid envelope motility**

Besides pigmentation, different plastid types vary dramatically in size and shape, both within and between species. These differences result from long-term shifts in plastid morphology due to differentiation, but there is also plenty to be learnt from observing the behaviour of plastids over a much shorter timescale. Organelles exhibit vectorial movement in plant cells (Williamson, 1993), and plastids in particular are able to move in response to changes in light intensity (Kagawa and Wada, 2002). However, a distinction ought to be made between this 'holistic' organelle movement within cells and the autonomous, pleiomorphic movement of individual organelles, even though the molecular basis (at least in terms of motor proteins bringing about the locomotion) may be

similar. This latter aspect of plastid motility is of particular interest to understanding plastid functionality. One notable feature that has consistently emerged from watching plastids *in vivo* is that plastids are not static, independent organelles as is often assumed, but are instead highly dynamic entities that sometimes connect with one another: membranous conduits emanating from the plastid surface extend and retract into the cytoplasm, and form a bridge connecting individual plastids. These protrusions, now known as *stromules*, are tubular extensions of the plastid envelope that contain stroma, and permit the transport of molecules along their length. The use of green fluorescent protein (GFP, see §1.4 and Figure 1.3) to highlight plastids has provided the means with which to observe these structures regularly, but references to plastid protrusions and dynamics can be found in the literature that spans the past one hundred years or so (reviewed by Gray *et al.*, 2001).

Prior to the use of GFP, one of the most convincing testimonies of plastid motility was reported by Sam Wildman and colleagues at the University of California. Using a combination of phase contrast microscopy and cinephotomicrography, Wildman *et al.* (1962) described how chloroplasts in living spinach palisade cells consist of two visually distinct sub-regions: an inner, non-motile chlorophyll-bearing structure, and a surrounding colourless “jacket of material” which constantly varies in shape. They further described how “long protuberances extend from the jackets into the surrounding cytoplasm”. Wildman (1967) later reported that isolated chloroplasts lacking their envelope lose their motility, whereas those with an intact envelope retain it: some images clearly showed intact chloroplasts with stromules. As part of the general study into cellular cytoplasmic streaming, the authors (Wildman *et al.*, 1962; Wildman, 1967) reported that the protuberances could segment into smaller, free-flowing structures visually indistinguishable from mitochondria – prompting the authors to suggest that these two organelle types are interconvertible. Whilst such a proposition might be now dismissed given

the current understanding of the biogenesis of plastids and mitochondria, the observation that stromules might fragment is something that should not.

Electron microscopy has also been extensively employed to investigate changes in plastid ultrastructure but this method obviously prevents any assessment of plastid motility, and is prone to fixation artefacts. Nonetheless, several examples exist in which fixed samples exhibit tubular protrusions from the plastid surface (Gray *et al.*, 2001). In order to preserve the cells in a condition as close as possible to their natural state, Bourett *et al.* (1999) used high pressure freezing to describe the ultrastructure of stromules in rice leaf tissue. They described protuberances of up to 4.1  $\mu\text{m}$  in length that are contiguous with the stroma, and confirm this through immunolocalisation of the large subunit of Rubisco to both the main body of the chloroplast and the protuberances. They also presented one instance of two chloroplasts apparently interconnected by such a protuberance.

However, it was not until the advent of GFP and confocal laser scanning microscopy that stromules could be investigated more systematically in living tissue. The first use of this approach was reported by Köhler *et al.* (1997a), who expressed plastid-targeted GFP in tobacco and petunia, and provided the first evidence that stromules were more extensive – both in length and abundance – in some tissue types than others. They described tubules of between 0.35 and 0.85  $\mu\text{m}$  in diameter and up to 15  $\mu\text{m}$  in length; furthermore, they demonstrated the transfer of GFP from one plastid to another along an interconnecting stromule by the use of selective photobleaching followed by monitoring the subsequent return of fluorescence (Köhler *et al.*, 1997a). This work led to the final acceptance of plastid protuberances in living tissue, and a variety of similar investigations have shown that stromules are a feature in all species so far examined using GFP, but that they are highly variable in form and abundance (Figure 1.3).

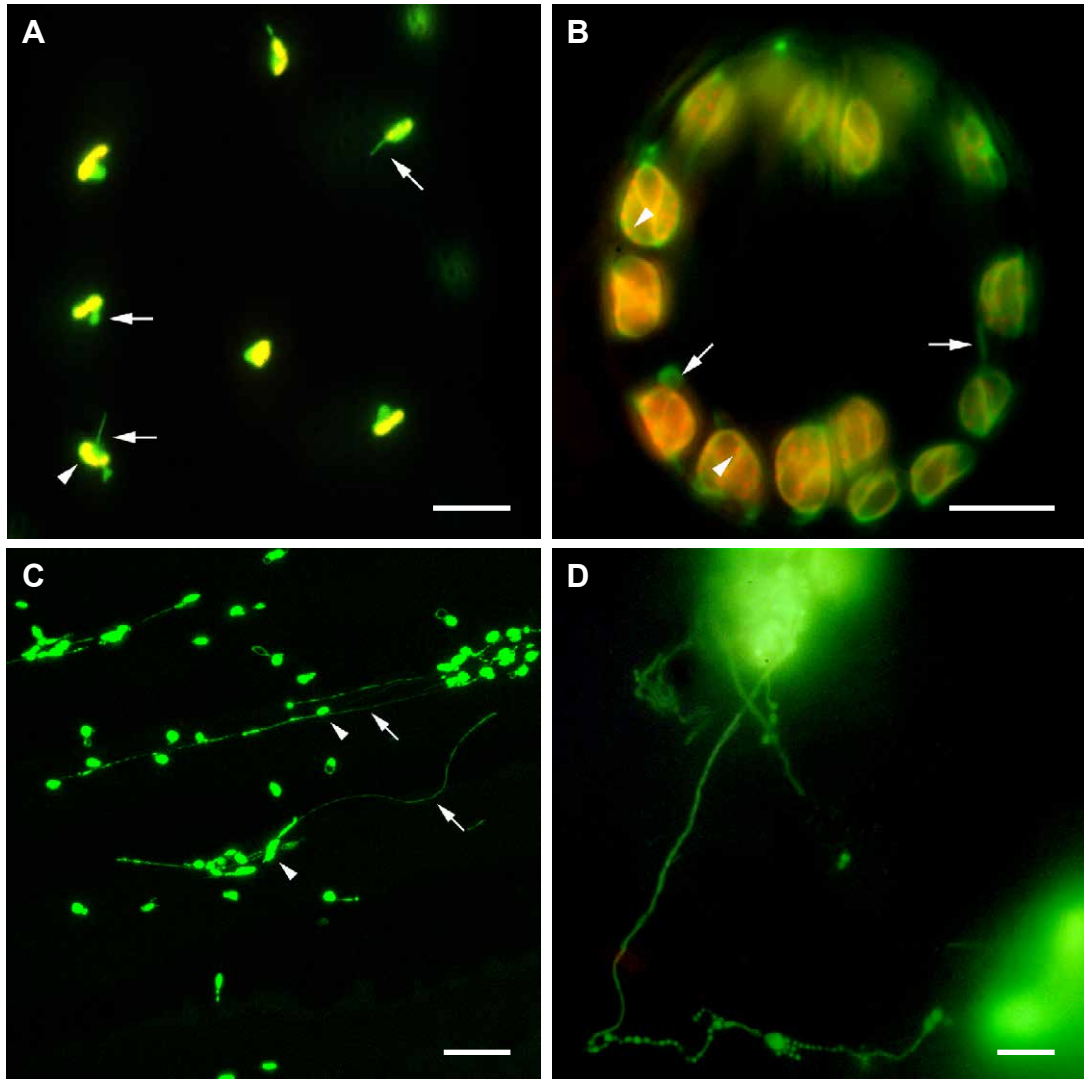


**Figure 1.3 Variation in plastid and stromule morphology revealed by plastid-localised GFP**

(A) Epifluorescence micrograph of plastids in a Type V trichome of tomato. Chlorophyll autofluorescence is red, but when combined with GFP fluorescence appears yellow. The plastid body (arrowhead) contains a central chlorophyllous region (yellow) surrounded by a motile, stroma-containing region (green). Note that stromules (arrows) contain no chlorophyll. (B) Epifluorescence micrograph of chloroplasts in a pair of stomatal guard cells in the abaxial leaf epidermis of tomato. These chloroplasts are large and contain starch grains, as can be seen from their patterned appearance. Putative thylakoid granal stacks can be discerned from punctate regions of red chlorophyll autofluorescence (arrowheads). Limited stromules and plastid envelope protrusions can be seen (arrows). (C) Confocal maximum projection of differentiating chloroplasts in the hypocotyl epidermal cells of tobacco. Only GFP fluorescence is depicted. Note the very long stromules (arrows) and relatively well-defined plastid bodies (arrowheads). (D) Epifluorescence micrograph of a long stromule with a beaded, vesicular superstructure that appears to interconnect two chromoplasts in a ripe tomato fruit pericarp cell. Scale bars: A, B, D, 5  $\mu\text{m}$ ; C, 20  $\mu\text{m}$ .

### 1.3.2 Diversity of stromules

Stromules have been observed in a number of higher plant taxa, including both monocotyledonous (Langeveld *et al.*, 2000; Arimura *et al.*, 2001) and dicotyledonous (Köhler *et al.*, 1997a; Hibberd *et al.*, 1998; Pyke and Howells, 2002) plants, but patterns of stromule distribution amongst different plastid types are becoming clear. In general, stromules are rarer (that is, fewer plastids produce stromules) and less extensive (stromules are shorter or less developed in shape) on chloroplasts than on other plastid types. The most extensive overview of stromule abundance in different tissues thus far published is that of Köhler and Hanson (2000), using transgenic tobacco carrying a constitutive plastid-targeted GFP construct. In this report, the authors define a stromule as a protrusion of less than 0.8  $\mu\text{m}$  in diameter, whilst the rest of the plastid is defined as the “plastid body”. Chloroplasts in mesophyll and stomatal guard cells, which are amongst the largest (5-7  $\mu\text{m}$  in length) and most regularly-shaped plastids in the plant, showed very few stromules, with most plastids in a cell exhibiting none. In contrast, the achlorophyllous plastids in petal epidermal cells and roots appeared much less regular in shape and were generally smaller and highly variable in size (1.8-3  $\mu\text{m}$  in diameter). Almost all plastids in these cells exhibited stromules, and root plastids of the meristematic zone frequently formed a circle around a non-fluorescent area reminiscent of the nucleus, with stromules pointing towards the cell periphery (Köhler and Hanson, 2000).

Stromule frequency and scope is, broadly speaking, negatively correlated with chloroplastic features. Nearly every leucoplast in onion bulb epidermal cells exhibits stromules (Gray *et al.*, 2001). Köhler and Hanson (2000) presented images of plastid morphology from leaf explants that had been placed under callus-inductive conditions. Plastids from green leaf tissue adjacent to the dividing callus tissue showed few stromules, whereas plastids from pale green and colourless tissue showed increasing degrees

of elongation and irregularity in shape. Stromules were correspondingly much more abundant and extensive. However, it might be argued that these changes in plastid morphology are merely a reflection of cellular differentiation. It is thus important to determine whether stromule formation is specific to the cell type in question, or whether it is more a result of the plastid state of differentiation.

Stromules have been seen to form highly intricate networks, with plastid bodies apparently interconnected by stromules. When tobacco cells were incubated under liquid suspension culture, their plastids exhibited “octopus- or millipede”-like morphologies, with plastid bodies frequently clustered around the nucleus (Köhler and Hanson, 2000); however, photobleaching experiments concluded that the majority of these plastids were not interconnected. Partial plastid networks have also been described in the ripe fruit of tomato that are not present in the unripe (green) fruit (Pyke and Howells, 2002). Particularly extensive stromule formations that spread throughout the cell and that appear to link most plastids have been observed in tobacco epidermis (Arimura *et al.*, 2001), which contrasts with reports of plastid morphology in epidermal cells of tomato where stromules are relatively rare (Pyke and Howells, 2002). Occasional “nodules” or vesicle-like entities with no obvious attachment to a plastid or stromule were also reported by Arimura *et al.* (2001), reminiscent of Wildman’s (1962) supposition that stromules may sever and form mitochondrion-like structures. A point to note, however, regarding the epidermal plastid “networks” reported by Arimura *et al.* (2001) is that plastids were visualised using transient expression of GFP, delivered via particle bombardment of detached leaf tissue. It is quite possible that plastid morphology could change dramatically over the time course of a particle bombardment procedure, thus not accurately representing a genuine *in planta* characteristic. However, together with the general tendency for stromules to be rare in green tissue, results such as these do demonstrate that plastid morphology is highly variable and may be under the control of a large number of contributing environmental and developmental factors.

### 1.3.3 Stromule movement and composition

Several reports describe how stromules move about substantially within the cytoplasm of the cell (Köhler *et al.*, 1997a; Langeveld *et al.*, 2000; Shiina *et al.*, 2000; Arimura *et al.*, 2001; Pyke and Howells, 2002). Their movements are invariably described as extending, shrinking and waving around the cytoplasm, occasionally branching and forming ring-like structures. The actin cytoskeleton has been implicated in the movement of chloroplasts (Kagawa and Wada, 2002) and of other organelles (Williamson, 1993) within the plant cell, and has been shown to be intricately associated with the chloroplast through immunofluorescent labelling (Kandasamy and Meagher, 1999). The movement of stromules appears to be based on the same acto-myosin mechanism, as inferred from the use of inhibitors on tobacco and onion cells expressing plastid-targeted GFP (J. A. Sullivan and J. C. Gray, unpublished; cited in Gray *et al.*, 2001). The microtubule inhibitors oryzalin and amiprophosmethyl had no effect on stromules, whereas latrunculin B (an inhibitor of actin polymerisation) and 2,3-butanedione 2-monoxime (a general inhibitor of myosin ATPase activity) efficiently prevented their movement (J. A. Sullivan and J. C. Gray, unpublished; cited in Gray *et al.*, 2001). However, no mention was made of the effect on stromule formation, or whether they disappeared altogether. It is noteworthy that these reports partially contradict results from Kwok and Hanson (2003), who concluded that actin microfilaments promote stromule and plastid movement, whereas microtubules actually prevent it: oryzalin treatment increased plastid motility, suggesting a release of inhibition of movement. The authors suggest that a normally dense network of microtubules restrict plastid and stromule movement, and when removed by drug treatment this restriction is partially removed. Further evidence for the promotive influence of actin was provided by the visualisation of the actin cytoskeleton in tobacco hypocotyl epidermis with a fusion between GFP and an actin-binding protein, talin (Kwok and Hanson, 2004b). In this study, stromules were observed to associate with actin microfilaments, with rearrangements of the microfilaments correlating with stromule movements and shifts in stromule morphology. The authors thus suggest

that it is the movement of microfilaments that is chiefly responsible for stromule motility, and not the movement of stromules along a fixed cytoskeletal element. However, the effects of myosin inhibitors on stromule movement suggest that the latter scenario does take place, and may do so in parallel with microfilament movements. Thus, the basis for stromule movement is somewhat controversial, and seems to be regulated by at least two independent mechanisms.

Both inner and outer envelope membranes are present in stromules, as inferred by the localisation of GFP to each membrane in turn by the appropriate protein targeting domains (J. A. Sullivan and J. C. Gray, unpublished; cited in Gray *et al.*, 2001). Movement of both membranes along the external actin cytoskeleton would presumably require some form of contact between the two membranes, but extensive contact is not thought to exist except transiently during protein translocation (Keegstra and Froelich, 1999). Because of this, there may be some form of internal motility system to plastids. In this respect, an FtsZ-based “plastoskeleton” has been inferred from the overexpression of an FtsZ-GFP fusion protein in *Physcomitrella patens* (Kiessling *et al.*, 2000; Reski, 2002). Plastids showed a filamentous, reticulate scaffold of FtsZ apparently just below the plastid envelope (Kiessling *et al.*, 2000), although there is no conclusive evidence as yet that plastids maintain their shape in a way analogous to the eukaryotic cell. FtsZ, with homology to tubulin, may constitute an internal motility mechanism. However, it has been suggested that the plastoskeleton inferred by Kiessling *et al.* (2000) is actually an artefact as a result of FtsZ overexpression, since immunodetection of FtsZ proteins in wild type cells did not reveal such structures (Vitha *et al.*, 2001). Moreover, there is no electron micrographic evidence for a plastoskeleton underlying the plastid envelope.

At present, all the available evidence suggests there is no compartmentation between stromules and the rest of the stroma. Stromules have generally been labelled with

stroma-targeted, non-endogenous proteins such as GFP, and the stromule and plastid body appear homogeneous (e.g. Pyke and Howells, 2002), but this may not reflect the distribution of endogenous plastid proteins. Fusions of plastid-resident proteins of a range of sizes (Rubisco and aspartate amino transferase) with GFP also label the plastid body and stromules equally (Kwok and Hanson, 2004a), suggesting that there is no selective entry of proteins into stromules. Highlighting of the plastid envelope with a GFP fusion to a full-length acyl-coenzyme A synthetase also showed an even distribution across stromules and the plastid body (Schnurr *et al.*, 2002). Therefore, the current view is that stromule membranes are entirely contiguous with, and identical in topology to, the rest of the plastid envelope. Likewise, the stroma and its soluble contents are equally distributed between the stromule and the plastid body; only membrane-bound entities like thylakoids are excluded from stromules (Gray *et al.*, 2001).

#### **1.3.4 Stromule functions**

The precise role of stromules in plastid functioning is unknown, although various hypotheses have been put forward. The observation that GFP can be transported along stromules (Köhler *et al.*, 1997a; Köhler *et al.*, 2000) suggests that they might be important in the transfer of macromolecules, such as imported proteins, and metabolites either between plastid bodies or from peripheral locations in the cell towards the plastid body. The transfer of molecules between individual plastid bodies is probably not a primary role of stromules however, since the majority of stromules do not appear to join plastids together (Köhler *et al.*, 2000; Gray *et al.*, 2001). However, nucleic acids may travel along stromules: the microinjection of individual plastids with a plasmid encoding GFP led to the spread of fluorescence throughout the plastids within a cell (Knoiblauch *et al.*, 1999), perhaps due to the movement of any combination of DNA, RNA or protein. Further indirect evidence for nucleic acid transfer between plastids comes

from the fusion of protoplasts from two different species, which resulted in recombination between the two chloroplast genomes (Baldev *et al.*, 1998).

It has also been proposed that stromules stretching towards the cell periphery may aid in the transduction of photoelectric signals perceived at the cell surface to the organelle membrane system itself (Tirlapur *et al.*, 1999). Furthermore, metabolic interactions with mitochondria and peroxisomes could be maximised through physical contact with stromules, especially if these organelles and stromules co-exist on the same actin microfilaments (Gray *et al.*, 2001). Nevertheless, the most likely role for stromules is to provide further surface area for processes such as protein import and metabolite exchange, whilst minimising the plastid volume required to produce them (Gray *et al.*, 2001). It appears that plastids at a high density (such as in mesophyll cells) produce relatively fewer stromules than those more widely distributed throughout the cell (such as root or trichome cells). In the latter types of cells, the increased surface area of the plastid compartment in contact with the cytoplasm could help compensate for the lower plastid density, presumably maintained as such for reasons of economy. However, any apparent negative correlation of stromule frequency with plastid density is difficult to distinguish from the negative correlation with chloroplast features, as the two factors often arise simultaneously. If the irregularity of stromule abundance is a reflection of their functions, it follows that an understanding of what governs stromule variability will be key to elucidating such functions.

#### **1.4 Green fluorescent protein (GFP)**

*Aequorea victoria* is a hydrozoan jellyfish that exhibits bioluminescence at several foci along the margin of the jellyfish umbrella. Within the cytoplasm of the cells at these points are bioluminescent granules, which contain a  $\text{Ca}^{2+}$ -activated photoprotein, aequorin, and an accessory protein, GFP. In this system, blue light emitted by aequorin

is absorbed by GFP and re-emitted as green light (Morise *et al.*, 1974). GFP is highly stable and is resistant to proteases, 6M guanidine-HCl and 8M urea; in addition, the protein is stable in neutral buffers up to 65 °C and maintains fluorescence at pH between 5.5 and 12 (Haseloff, 1999). Wild type GFP is maximally excited at 400 nm, and emits light with a peak of 509 nm (Haseloff, 1999). Fluorescence results from a covalently attached chromophore that is formed co-translationally from the oxidation and cyclisation of three residues (Prasher *et al.*, 1992). When expressed in anaerobically-grown *Escherichia coli*, GFP fails to fluoresce, but this property will develop once oxygen is supplied to the culture (Heim *et al.*, 1994). Molecular oxygen appears to be the only co-factor necessary for GFP maturation (Heim *et al.*, 1994), which is key to the successful expression of GFP in a number of heterologous systems.

#### **1.4.1 Expression of GFP and its derivatives in *planta***

Initial attempts to express the wild type GFP in plants were largely unsuccessful because of improper processing of the *gfp* mRNA (Haseloff *et al.*, 1997). In *Arabidopsis*, an 84-nucleotide section was deleted from the mRNA, most probably due to recognition of a cryptic splice site (Haseloff *et al.*, 1997). Site-directed mutagenesis removed the cryptic splice site within the cDNA, which produced a transcript with modified codon usage. This modified gene, termed *mgfp4*, produced bright fluorescence in stably transformed plants when driven by the CaMV 35S promoter (Haseloff *et al.*, 1997). Since this first modification of *gfp* for expression in plants, a number of derivatives have been developed. In particular, there now exist several spectrally shifted GFP variants with differing excitation and emission characteristics resulting from altered codon usage and amino acid substitutions that confer improved folding properties (Haseloff, 1999). The most widely used GFP variants are CFP (cyan fluorescent protein) and YFP (yellow fluorescent protein), which exhibit blue- and red-shifted emissions respectively. Overlap of emission spectra can be negated by confocal microscopy, thus allowing more than one

fluorescent protein to be imaged simultaneously. Since the discovery of GFP, genes encoding fluorescent proteins have been cloned from non-bioluminescent anthozoan corals. These include DsRED, an orange-red fluorescent protein from the coral *Discosoma* spp. (Matz *et al.*, 1999), and Kaede, a photoconvertible protein from *Trachyphyllia geoffroyi* that can be induced to change its emission characteristics from green to red following excitation by UV light (Ando *et al.*, 2002). These proteins share a high degree of homology with GFP, and the evolution of different colours has occurred independently 15 times during the radiation of the cnidarians (Shagin *et al.*, 2004).

#### 1.4.2 Applications of GFP

GFP is a vital marker that allows high resolution imaging of *in vivo* events. Although markers such as  $\beta$ -glucuronidase (GUS) have been widely used to follow gene expression patterns (Wilson *et al.*, 2001; Hammond *et al.*, 2003) and protein localisation (von Arnim and Deng, 1994), the procedure is labour-intensive, destructive and is not suitable for rapidly screening segregating populations. In addition, GUS is of little use in following the time course of gene expression. GFP has thus become a ubiquitous tool for molecular and cell biology in a number of organisms. In plants, GFP has been used as screenable markers for genetic transformation (Kahn and Maliga, 1999), as an assay for viral suppression of gene silencing (Voinnet *et al.*, 1998) and to analyse the spatio-temporal patterns of gene expression (Swarup *et al.*, 2001). Furthermore, GFP expression can be limited to particular cell types to study the behaviour of specific cell types within the plant (Boisnard-Lorig *et al.*, 2001). This has been achieved by transformation of *Arabidopsis* with a construct encoding the yeast transcriptional activator GAL4 driven by a weak promoter, coupled with a GAL4-responsive GFP gene. Upon transformation, the construct lands randomly within the genome. Integration near to tissue-specific enhancers leads to GAL4 transcription and translation, and the subsequent expression of GFP. Thus, this system has provided a series of lines with tissue-specific

GFP expression because of transactivation by GAL4 (Haseloff and Siemering, 1998). Moreover, the transactivation system is an elegant tool for directing the ectopic expression of genes in particular cell types. A chosen gene can be cloned behind the GAL4 promoter and used to transform *Arabidopsis*. When crossed into a GAL4 transactivation background that exhibits a GFP expression pattern of interest, expression of the chosen gene will occur specifically in the same cells that express GFP (Haseloff and Siemering, 1998, R. Swarup 2004, unpublished results).

Perhaps the most powerful application of GFP is the ability to localise proteins to specific sub-cellular locations within the cell. This can be used for two broad purposes: firstly, to determine the location of a novel protein by constructing a translational fusion with GFP. This approach has been used in a high-throughput screen for the location of unknown expressed proteins by fusing a cDNA library to GFP and expressing them transiently in *Nicotiana benthamiana* using a viral vector (Escobar *et al.*, 2003). Secondly, by taking advantage of organellar protein sorting, GFP can be targeted deliberately and specifically to regions of the cell for the study of cellular dynamics (Hanson and Köhler, 2001). This presents a basis for studying a number of cellular processes: for instance, by targeting GFP to the endoplasmic reticulum and following its movement to the apoplast, an *in vivo*, non-invasive assay for defects in the secretory pathway has been developed (Batoko *et al.*, 2000).

In this study, various fluorescent proteins are targeted to the plastid, mitochondrion and peroxisome compartments to study their behaviour in the living cell. Since these organelles are typically colourless, fluorescent proteins provide a remarkably facile way of observing their movements and dynamic changes. Furthermore, the unequivocal identification of each organelle is possible, because confocal microscopy allows the discrimination between the differentially localised fluorescent proteins.

## ***1.5 Aims of this work***

The overall aim of this work is to further our general understanding of stromule biology. As a relatively recent subject of research, there remain several unknowns regarding the nature and functions of stromules. Using a variety of experimental approaches, this work intends to answer three broad questions:

1. What factors determine the variability in stromule abundance observed from cell to cell?
2. What can be inferred about stromule functions from such variability, and the interactions of stromules with other organelles?
3. How do stromules form and move?

These questions will be addressed in four ways. Firstly, a detailed inspection of the changes in stromule biogenesis during tomato fruit ripening will place emphasis on the effects of plastid differentiation on this process (Chapter 3). In Chapter 4, the effects of light quality and quantity on stromule formation in tobacco hypocotyls will be assessed, together with an evaluation of stromule interactions with other organelles. Thirdly, Chapter 5 focuses on the role of a specific *Arabidopsis* chloroplast actin-binding protein on stromule formation and chloroplast morphology. Finally, Chapter 6 describes efforts to investigate the possibility of cell-cell communication via stromules in the C<sub>4</sub> photosynthetic system of maize.

## 2 MATERIALS AND METHODS

### 2.1 GENERAL MATERIALS

Unless otherwise mentioned, all laboratory chemicals were obtained from Sigma (Sigma-Aldrich Company Ltd., Poole, Dorset, UK). Microbiological media were sourced from Oxoid (Basingstoke, Hamps., UK). Synthetic oligonucleotides were designed manually and ordered from Sigma-Genosys (Sigma-Genosys Ltd, Haverhill, Suffolk, UK). All radiochemicals were obtained from Amersham Biosciences (Amersham plc, Little Chalfont, Bucks, UK).

### 2.2 PLANT MATERIAL AND GROWTH CONDITIONS

Several different transgenic lines, of four different plant species, were generated during the course of this work. Their nomenclature, the construct they carry and the selectable marker used in their isolation are outlined in Table 2.1.

#### 2.2.1 Tomato (*Lycopersicon esculentum* Mill. var. *Ailsa Craig*)

Tomato seeds were sown in a 6:1 mixture of compost and perlite, and germinated under glasshouse conditions (minimum 16 h day regime, 22-26 °C). Plants were allowed to grow to full maturity in 25 cm pots to maximise fruit yield, and fruit was sampled from the first or second truss. Plants were watered daily and fed twice weekly with Sangral 1:1:1 NPK fertiliser (William-Sinclair Holdings plc., Lincoln, UK) once fruit had started to set. Transgenic tomato plants of wild type background, containing a construct

**Table 2.1** Transgenic lines described in this work

Line	Description	Construct(s)	Selectable Marker(s)	Reference
<b>Tomato (Ailsa Craig)</b>				
a17	Plastid-targeted GFP	pBIN/ <i>recAgfp</i>	<i>nptII</i>	Pyke and Howells (2002) Köhler et al. (1997)
<i>rin</i> (a17)	<i>ripening inhibitor</i> crossed with a17	pBIN/ <i>recAgfp</i>	<i>nptII</i>	This work
<i>gf</i> (a17)	<i>green flesh</i> crossed with a17	pBIN/ <i>recAgfp</i>	<i>nptII</i>	This work
<i>hp</i> (a17)	<i>high pigment-1</i> crossed with a17	pBIN/ <i>recAgfp</i>	<i>nptII</i>	This work
<b>Tobacco (Petit Havana)</b>				
rbcS-DsRED	Plastid-targeted DsRED	pBC/ <i>rbcS</i> -DsRED	<i>nptII</i>	This work
MSK57	Transplastomic GFP	FLARE16-S2	<i>aadA</i>	Kahn and Maliga (1999)
atp-GFP	Mitochondria-targeted GFP	pBIN4/3	<i>nptII</i>	Logan and Leaver (2000)
ECFP-SKL	Peroxisome-targeted ECFP	PGR/ECFP-SKL	<i>nptII</i>	This work
MPA12	<i>rbcS</i> -DsRED x atp-GFP (dual label: plastids & mitochondria)	pBC/ <i>rbcS</i> -DsRED pBIN4/3	<i>nptII</i>	This work
PP2	<i>rbcS</i> -DsRED x ECFP-SKL (dual label: plastids & peroxisomes)	pBC/ <i>rbcS</i> -DsRED pGR/ECFP-SKL	<i>nptII</i>	This work
MSK57xDsRED	<i>rbcS</i> -DsRED x MSK57	pBC/ <i>rbcS</i> -DsRED FLARE16-S2	<i>nptII</i> , <i>aadA</i>	This work
<b>Arabidopsis (Col-0)</b>				
Col.	Wild type Columbia	None	None	
<i>CHUP1</i> _RNAi/#	<i>CHUP1</i> knockdown by RNAi	pB7/ <i>CHUP1</i> _RNAi	<i>bar</i>	This work
<i>CHUP1</i> -GFP	C-terminal fusion of <i>CHUP1</i> with sGFP	pGW/ <i>CHUP1</i> -GFP	<i>nptII</i> , <i>hpt</i>	This work
N605043	T-DNA insert in At3g25690 SALK_I05043.36.90.x	pROK2	<i>nptII</i>	Alonso et al. (2003)
<i>recAgfp</i> /#	Plastid-targeted GFP	pBIN/ <i>recAgfp</i>	<i>nptII</i>	This work
<b>Maize (Hi-II AXB)</b>				
ZM ####.###	Plastid-targeted GFP	pAHC25/ <i>recAgfp</i>	<i>bar</i>	This work

# represents alphanumeric characters, denoting a series of independent primary transgenic events. *nptII*: neomycin phosphotransferase II, conferring kanamycin resistance; *hpt*: hygromycin phosphotransferase, conferring resistance to hygromycin; *bar*: bialaphos acetyltransferase, conferring resistance to glufosinate ammonium-containing herbicides (e.g. BASTA) and phosphinothricin; *aadA*: adenylyltransferase, conferring resistance to spectinomycin/streptomycin.

targeting GFP to the plastid (Figure 3.1 C), were generated as described previously (Pyke and Howells, 2002; Bird *et al.*, 1988). Details of the construct used in this line are provided in §2.6.

### 2.2.1.1 Crosses with fruit ripening mutants

Tomato lines homozygous for the mutations *ripening inhibitor* (*rin*, semi-dominant), *green flesh* (*gf*, recessive) and *high pigment-1* (*hp-1*, recessive) were crossed with the transgenic line a17 expressing plastid-targeted GFP. The mutant lines have been rendered near-isogenic with the Ailsa Craig background by repeated back-crossing (Darby *et al.*, 1977). Plants of the F<sub>2</sub> generation were screened for both GFP expression and the mutant phenotype as described below.

Crossing was performed as follows. A recipient flower was selected that had begun to open but was not yet shedding pollen, as determined by gentle tapping. One point of a pair of fine forceps was inserted into the corolla tube, with the other point grasping the outside of the corolla between the petals and the calyx. The corolla was removed with a single sharp tug of the forceps, which also removed the stamens fused to the inner surface of the corolla. This left an emasculated flower with a prominent gynoecium, surrounded by the calyx. Donor pollen was collected from a fully open, shedding flower by placing a 1.5 ml microcentrifuge tube beneath the corolla and tapping the flower gently. Pollen was then transferred from the tube to the stigma of the recipient flower using a sterile pipette tip. The flower was labelled appropriately and inspected one week later to confirm fruit set.

#### 2.2.1.1.1 *green flesh*

Pollen from a17 plants was used to pollinate emasculated flowers of a homozygous *gf* plant. The F<sub>1</sub> population was screened for GFP expression by use of an epifluorescence stereomicroscope, with a positive GFP signal indicating a successful cross. Forty F<sub>2</sub> seeds were sown in soil and the cotyledons screened for GFP expression. Seedlings identified as positive for GFP expression were potted on and grown to maturity in the glasshouse, in order to identify *gf* individuals. Seed from these plants was harvested and experimental analysis was performed on F<sub>3</sub> individuals.

#### 2.2.1.1.2 *ripening inhibitor*

Pollen from mature *rin* plants was used to pollinate emasculated flowers of an a17 plant. The *rin* locus is tightly linked to a genetically distinct locus, *macrocalyx* (*mc*) (Vrebalov *et al.*, 2002). The F<sub>1</sub> generation, heterozygous for *rin*, showed an intermediate *rin* and *mc* phenotype, indicating that the cross was successful. The F<sub>2</sub> generation seeds were surface sterilised by washing in 10% bleach for 10 minutes, then 70% ethanol for 10 minutes, followed by three rinses with sterile distilled water, and were then germinated on MSR3 media (4.2 g l<sup>-1</sup> MS salts, 3% sucrose, 1 mg l<sup>-1</sup> thiamine, 0.5 mg l<sup>-1</sup> nicotinic acid, 0.5 mg l<sup>-1</sup> pyroxidine, 7% agar) supplemented with 50 mg l<sup>-1</sup> kanamycin. Transgenic individuals were identified by means of their normal root growth, and forty such seedlings were transferred to soil in the glasshouse. Wild type plants could be distinguished before fruit set due to the tightly linked *mc* phenotype; all plants with enlarged sepals and petals were potted on as potential heterozygotes or homozygotes. These plants were grown to maturity and homozygotes for *rin* were identified according to the fruit phenotype. The F<sub>3</sub> seed from each homozygous individual was then harvested and maintained as separate lines. Experimental analysis was performed on F<sub>3</sub> individuals.

### 2.2.1.1.3 *high pigment-1*

Pollen from a17 plants was used to pollinate emasculated flowers of a homozygous *hp-1* plant. The F<sub>1</sub> population was screened for GFP expression as described for the *gf* cross. The F<sub>2</sub> seedlings were first screened for the *hp-1* phenotype according to the procedure outlined by Yen *et al.* (1997). *hp-1* exhibits an exaggerated photomorphogenic phenotype, with a shorter hypocotyl and increased anthocyanin production. This is most severe under red light but can also be detected during de-etiolation, as described here. Approximately forty seeds were surface sterilised and sown on MSR3 media in plastic pots. The seeds were germinated in the dark at 24 °C by wrapping the pots in two layers of aluminium foil and incubated for 7 days. The foil was then removed and the seedlings allowed to de-etiolate for two further days in a growth room at 24°C under a 16 h light/8 h dark cycle, 180 µmol m<sup>-2</sup> sec<sup>-1</sup>. Seedlings were scored as either normal (+/+ or *hp*/+; light-coloured, elongated hypocotyls) or mutant (*hp/hp*; short, purple hypocotyls; Figure 3.9). Seeds of the wild type (a17) and *hp* mutant parent lines were treated identically and used as negative and positive controls respectively to ensure correct identification of the *hp* mutant phenotype. Mutant seedlings were then screened further for GFP expression as before, and those expressing GFP were transferred to soil and grown to maturity in the glasshouse. The F<sub>3</sub> seed from each homozygous individual was then harvested and maintained as separate lines. Experimental analysis was performed on F<sub>3</sub> individuals.

### 2.2.1.2 Production of dark-grown fruit

To obtain dark-grown fruit expressing the plastid-targeted GFP construct (wild type background), the first or second truss from an a17 plant was covered with an A5-sized, brown paper envelope containing four sheets of A4 paper. This was then covered in one layer of aluminium foil and secured over the developing truss with masking tape, and tapped by hand every so often to promote pollination. Fruit were examined by micros-

copy at a stage equivalent to mature green, as judged by the fruit on an untreated truss of a plant of similar age.

### 2.2.2 Tobacco (*Nicotiana tabacum* var. Petit Havana)

Tobacco was grown under identical glasshouse conditions as tomato. After nuclear transformation, primary transformants were rescued from tissue culture, potted on in soil, and allowed to flower to produce seed for subsequent experiments. Plants expressing more than one transgene for dual labelling experiments (e.g. plastid-targeted DsRED and mitochondria-targeted GFP) were generated by crossing primary transformants and screening the F<sub>1</sub> generation by microscopy. The F<sub>1</sub> individuals with the best expression signals were selfed, and the F<sub>2</sub> generation was used for experiments. Seeds were surface sterilised as described for tomato, and germinated on MSR3 media in sterile, 8 cm-high plastic pots. Prior to transfer to the growth room, seeds sown on MSR3 were stratified at 4 °C for two nights. Growth room conditions were 24 °C with a 16 h light/8 h dark cycle, with lighting provided at 180  $\mu\text{mol m}^{-2} \text{sec}^{-1}$  by cool white fluorescent tubes, except for specific experimental conditions as described below. Treatments requiring seedling growth in the dark were identical except that the pot was wrapped in two layers of aluminium foil.

#### 2.2.2.1 Generation of transgenic tobacco plants

Wild type *N. tabacum* 'Petit Havana' seeds were germinated on MSR3 media in 8 cm-high plastic pots, and allowed to grow until 8-10 leaves had appeared after approximately 6 weeks. The night before the transformation procedure, a single colony of the *Agrobacterium tumefaciens* strain carrying the plasmid for transformation (see §2.6) was used to inoculate 100 ml of APM media (5.0 g l<sup>-1</sup> yeast extract, 0.5 g l<sup>-1</sup> acid-hydrolysed casein, 8.0 g l<sup>-1</sup> mannitol, 2.0 g l<sup>-1</sup> ammonium sulphate, 0.2 g l<sup>-1</sup> magnesium

chloride and 5.0 g l<sup>-1</sup> sodium chloride, adjusted to pH 6.6 with dilute hydrochloric acid), supplemented with the appropriate antibiotic(s) and 25 µg ml<sup>-1</sup> rifampicin. The culture was allowed to grow until it reached an OD<sub>600</sub> of 0.6, at which point the bacteria were pelleted in sterile 50 ml centrifuge tubes (Bibby Sterilin Ltd., Staffs., UK) and resuspended in liquid MSR3 media to an OD<sub>600</sub> of 0.1-0.2.

Meanwhile, the larger tobacco leaves were excised under aseptic conditions and cut into segments approximately 1 cm square. These explants were then incubated with the resuspended bacteria in the centrifuge tube, taking care not to damage the leaf tissue with forceps. The tube was inverted from time to time to ensure thorough mixing of the bacteria and explants, and after 15 min the explants were dabbed dry on sterile filter paper to remove excess bacteria, and then placed individually on solidified 3C5ZR media (MSR3 supplemented with 0.5 µM IAA and 0.5 µM zeatin), adaxial side uppermost. The plates were sealed with Parafilm M (Pechinery Plastic Packaging, Chicago, IL, USA) and placed in the growth room in an inverted orientation for 24 h. The explants were then transferred to fresh 3C5ZR plates containing 50 µg.ml<sup>-1</sup> kanamycin as a selective agent and 0.4 µg.ml<sup>-1</sup> Augmentin (SmithKline Beecham, Herts., UK) to kill the bacteria, then re-sealed and placed back in the growth room for three weeks.

Callus growth at the edges of the explants was subcultured onto fresh 3C5ZR media with selection every three weeks. Once the callus started to shoot, the callus was transferred to selective 3C5ZR media in 8 cm-high pots. Large shoots were excised at the base with a sharp scalpel and placed in MSR3 media, also supplemented with 50 µg.ml<sup>-1</sup> kanamycin, and allowed to root. Those shoots with a vigorous root system, which usually appeared within two weeks, were transferred to soil as putative primary transformants. Such plantlets were covered for one week with a plastic bag to acclimatise the plant to the new growth conditions.

### 2.2.2.2 Red and blue light growth conditions

Two different methods were used for growing seedlings under red and blue light, which gave greatly different fluence rates and different results. These two methods are termed “low fluence rate” and “high fluence rate”.

#### 2.2.2.2.1 Low fluence rate

Seeds of line MSK57xDsRED were surface sterilised, sown and stratified as above. Red and blue light was provided by two purpose-built light boxes containing fluorescent tubes filtered by Deep Orange No. 58 or Deep Blue No. 20 cinemoid film (Strand Lighting, Hammersmith, London, UK), and a fan to dissipate heat. The red source peaked at 640 nm, whilst the blue source output peaked at 440 nm (Gilbert, 1990). The fluence rates were determined to be 1.8 and 0.9  $\mu\text{mol m}^{-2} \text{sec}^{-1}$  for the red and blue light boxes respectively, and 180  $\mu\text{mol m}^{-2} \text{sec}^{-1}$  for white light. The light boxes were kept in a dark growth room held at a constant 24 °C. Following stratification, the pots were placed in each light box for 10 days, with light supplied continuously. Pots were wrapped in two layers of aluminium foil before being examined immediately by confocal microscopy.

#### 2.2.2.2.2 High fluence rate

Seeds of line MSK57xDsRED were surface sterilised, sown and stratified as above. Relatively high red and blue fluences were provided by narrow bandwidth LED arrays with peak light output at 670 nm and 450 nm respectively, according to Franklin *et al.* (2003). The equipment was housed at the University of Leicester, Department of Biology, and provided with the courtesy of Prof Garry Whitelam. The red, blue and white light sources were all standardised to 60  $\mu\text{mol.m}^{-2}.\text{sec}^{-1}$ , thus ensuring only light quality varied between treatments. Red and blue light arrays were located in their own dedicated growth rooms, and white light was provided in a growth cabinet. The temperature was

maintained at 24 °C. Following stratification, the pots were placed under each light source for 10 days, and light was supplied continuously. The pots were wrapped in two layers of aluminium foil for transport to the confocal microscope, where they were imaged immediately.

### 2.2.2.3 *Hypocotyl elongation experiment*

Seeds of line MSK57xDsRED were surface sterilised, sown and stratified as above. Seeds were sown in four separate pots and, following stratification, were exposed to light in the growth room for four hours to ensure germination, and then were wrapped in two layers of foil to induce hypocotyl elongation. The foil was removed after 5, 6, 7 or 9 days and each pot was then exposed to light for 1 further day. Each pot thus contained seedlings that were 6, 7, 8 or 10 days post germination. The hypocotyls of 10 seedlings from each treatment were measured to the nearest 0.5 mm with a ruler, and representatives were digitally photographed.

### 2.2.2.4 *Incubation of seedlings under anaerobic conditions*

Seeds of line MPA12 were surface sterilised, sown and stratified as above. Pots were exposed to light in the growth room for four hours to ensure germination, and then wrapped in two layers of foil to induce hypocotyl elongation. After 7 days, the pots were unwrapped and exposed to light for one further day. During this day of light, the seedlings were treated with an atmosphere containing less than 1% oxygen as follows. Twelve holes of approximately 8 mm in diameter were formed in evenly distributed positions in the pot lid with a hot glass rod to melt the plastic. The pot was then placed inside a 3.5 l airtight chamber designed for cultivation of anaerophilic micro-organisms (Oxoid Ltd., Basingstoke, Hamps., UK; Cat. #HP0031), in which was placed a fresh anaerobic atmosphere generation pouch (Oxoid, Cat. #AN0035) and an anaerobic indica-

tor (Oxoid, Cat. #BR0055) to confirm that the conditions within the jar were anaerobic (Figure 4.10 E). The chamber was quickly sealed and placed in the growth room for 4-6 hours before being opened and the seedlings imaged immediately by confocal microscopy. Control (non-treated) seedlings were also placed in the chamber except the pot lid remained airtight. For recovery under normal atmosphere, the treated pot was allowed to equilibrate with the air for a few minutes, and was then re-sealed with a new lid without holes to minimise dehydration of the seedlings.

### 2.2.3 *Arabidopsis thaliana* (ecotype Columbia-0)

*Arabidopsis* was grown under identical glasshouse conditions as tomato, except with a lower temperature range of 21-25 °C. Ambient glasshouse light intensity ranged from 200 – 400  $\mu\text{mol m}^{-2} \text{sec}^{-1}$  depending on cloud coverage. Seeds of line N605043 were obtained from the Nottingham Arabidopsis Stock Centre, Nottingham, UK (accessed through <http://arabidopsis.info>).

#### 2.2.3.1 Generation of transgenic *Arabidopsis*

Wild type *Arabidopsis* was transformed by the floral dip method (Clough and Bent, 1998). Plants were prepared by growing three plants in an 8 cm diameter pot until the inflorescences were no taller than 10 cm. More inflorescences could be induced by removing the dominant inflorescences at an early stage. Just prior to transformation, any siliques that had already formed were removed. Constructs for transformation into *Arabidopsis* were introduced into *Agrobacterium* strain C58 (see §2.6.2). For each construct, a starter culture was initiated by inoculating 5 ml of APM, supplemented with the appropriate antibiotic(s) and 25  $\mu\text{g.ml}^{-1}$  rifampicin, with a single colony of *Agrobacterium*, and was grown overnight. The next morning, 1 ml of this starter culture was used to inoculate 100 ml of APM including antibiotics, and the OD<sub>600</sub> of this culture was

monitored regularly until it had reached ~0.8. At this point, 5 g (0.5% w/v) sucrose and 50  $\mu$ l (0.05 % v/v) Silwet L-77 (OSi Specialities, Inc., Danbury, CT, USA) was added to the culture and mixed thoroughly. The culture was poured into a wide plastic pot and the inflorescences of prepared plants were submerged in the culture for 5 s with gentle agitation. A plastic sleeve was placed over the plant and folded back to maintain humidity within the sleeve. After 24 h, the sleeve was opened, and the plants were allowed to grow as normal for a further 3-4 weeks until the siliques were dry and the seed ready for collection.

### 2.2.3.2 Screening for transgenic *Arabidopsis* primary transformants

For constructs conferring kanamycin resistance, transformants were selected on MSR3 media containing 50  $\mu$ g.ml<sup>-1</sup> kanamycin. Approximately 1000 seeds were surface sterilised by treatment with 50% bleach for 5 min followed by three rinses with sterile distilled water. They were then resuspended in 70% ethanol, poured onto sterile filter paper, and allowed to dry. Seeds were then scraped off the filter paper with a sterile spatula and onto 10 cm square plates (Bibby Sterilin) containing the selective MSR3 media. The seeds were stratified at 4 °C for two days and then transferred to a growth room with the same conditions as described in §2.2.2. After 10 days, seedlings with dark green cotyledons and an extended root system were identified as kanamycin resistant and transferred to soil in the glasshouse. The plants were left in an incubator for 4-5 days to acclimatise. Once they had grown sufficiently, leaf tissue was sampled for confirmation of transformation by PCR (see §2.6.4.1).

For constructs carrying the *bar* gene, primary transformants were sown on compost and allowed to grow for 10 days. The seedlings were then sprayed liberally with a solution of Complete Weedkiller herbicide (Wilkinson, Notts, UK) containing 150 mg l<sup>-1</sup> glufosinate ammonium as the active ingredient. Two days later, the spray was re-applied.

Seedlings that were resistant to the herbicide remained green, and were potted on to fresh compost. Transgene integration was then confirmed by PCR (see §2.6.4.1).

### 2.2.3.3 *Crossing Arabidopsis*

Plants grown in long day conditions for approximately four weeks were used for crossing, and pollen recipient plants were prepared as follows. Several inflorescences per plant were stripped of any siliques that had already formed or any flowers which had already opened. The largest unopened buds were chosen for dissection, and all younger ones, including the inflorescence meristem, were removed with ultra-fine forceps. Typically, this left an inflorescence axis with three to four unopened floral buds. Under a dissecting microscope and using ultra-fine forceps, the floral organs were removed starting with the sepals, then petals and finally the stamens with non-dehisced anthers, leaving just the central carpel. Pollen from the donor plant was obtained by removing stamens from recently opened flowers, which were then brushed against the recipient stigmatic surface to transfer pollen. Several (6-8) flowers were pollinated for each cross, and the inflorescence labelled accordingly with plastic tape. The plants were covered with a plastic sleeve and inspected after 5 days. A green, elongated silique was indicative of a successful cross. After about two weeks, the dry siliques were harvested and the seeds sown on agar plates as described in §2.2.3.2. Successful crossing was confirmed by PCR and GFP screening.

### 2.2.3.4 *Growth of Arabidopsis under high light conditions*

A light rig was constructed consisting of a metal frame approximately 1.5 m wide by 1.2 m high and 0.8 m deep. From this, three housings containing 400W OSRAM Powerstar bulbs (HQ1-BT; OSRAM Ltd, Slough, UK) providing white light were suspended from the frame by metal chains. An optimal distance from the lights to the plants was empiri-

cally determined such that leaf bleaching would occur slowly (i.e. over 24 h) for wild type plants, and this distance was established as 450 mm directly below the filament of the bulbs. At this distance, the photosynthetically active radiation was measured as  $1200 \mu\text{mol m}^{-2} \text{sec}^{-1}$ . Plants of each genotype were placed at this distance for a total of 48 h, and each plant was photographed every 12 h. The pots were placed in a tray containing water such that the soil was constantly moist. Temperature was monitored with a maximum/minimum thermometer, and was maintained at between 23 and 26 °C by the use of a fan combined with air conditioning in the glasshouse corridor.

#### **2.2.4 Maize (*Zea mays* var. Hi-II AXB)**

Maize was grown under identical glasshouse conditions as tomato, except at the higher temperature of 26 °C. Kernels were germinated in a 6:1 mixture of low nutrient compost and vermiculite and transferred to individual 10 cm diameter pots with high nutrient compost after ten days. After approximately four weeks, the plants were transferred to 25 cm diameter pots where they remained until maturity. Plants were watered daily and fed once a week with Sangral 1:1:1 NPK fertiliser (William-Sinclair Holdings plc., Lincoln, UK).

##### *2.2.4.1 Generation of transgenic maize*

Transgenic lines of maize were provided as a service by Zhanyuan Zhang (Plant Transformation Core Facility, University of Missouri-Columbia, Columbia, MO, USA). The technique used was biolistic transformation of embryogenic callus. Information regarding the service is available at:

[http://www.psu.missouri.edu/muptcf/maize\\_service.htm](http://www.psu.missouri.edu/muptcf/maize_service.htm)

Primary transformants were out-crossed with wild type Hi-II AXB to introduce hybrid vigour, and the resulting seed (termed T<sub>1</sub>) was supplied. This T<sub>1</sub> seed was thus predicted to be segregating 1:1 for heterozygotes and azygotes. A total of ten independent transgenic events were analysed.

#### 2.2.4.2 *Selfing of maize*

Developing ears were covered with semi-transparent, waxed paper envelopes which were cut and attached to one another to create a single sleeve of approximately 20 cm by 7 cm. Once the first silks were visible, the ear was cut back to about 1 cm below the tips of the husk ears and re-covered with the sleeve. The next day, the silks had re-grown resembling a short brush. Pollen was collected from the tassels of the same plant by covering the male inflorescence with a large paper bag and tapping to dislodge pollen. The top of the sleeve covering the ear was cut off and the pollen poured gently down the sleeve and onto the silks. The cut end of the sleeve was then folded back onto itself and secured with a paper clip. Once the silks had died back, the sleeve was removed and the ear allowed to ripen.

## 2.3 MICROSCOPY AND TISSUE SAMPLING

### 2.3.1 Tomato fruit pericarp

Fruit tissue from tomato plants was harvested and imaged immediately. Fruit pericarp was sliced in a longitudinal (i.e. apical-basal) direction using a sharp scalpel blade. Tissue was selected from regions of pericarp approximately equidistant from the stylar and penduncular poles of the fruit, and thin sections mounted on a glass slide in 10% glycerol. Using confocal microscopy, the upper 20-40 µm of individual pericarp cells were imaged as a Z-series and the component images (taken 1 µm apart) were merged to

form a maximum intensity projection. Such images display the upper surface of the approximately spherical cell, with the plastids situated between the vacuole and the plasma membrane. Confocal microscopy was performed with a Leica TCS2 confocal scanhead attached to a Leica DMRE upright microscope. GFP and chlorophyll were excited using the 488 nm line from the Ar laser, and emission signals were collected in separate channels, at wavelengths between 495 and 526 nm for GFP fluorescence, and between 631 and 729 nm for chlorophyll fluorescence. Transmitted light was also collected in a separate channel. The GFP signal and chlorophyll autofluorescence were false-coloured green and red respectively. Images shown are maximum intensity projections of optical slices produced by the LCS software provided. Epifluorescence microscopy was performed on a Nikon Optiphot microscope (Nikon UK Ltd, Surrey, UK) with a DM 510 fluorescence filter block, and images were acquired using a DXM-1200 digital camera (Nikon). Further image manipulation, including level adjustment and channel merging, was performed using Adobe Photoshop 7 (Adobe Systems Inc., San Jose, CA, USA).

### **2.3.2 Tobacco hypocotyls**

Tobacco hypocotyls were imaged by dissecting the hypocotyl from the seedling before mounting. The upper 15-20  $\mu\text{m}$  of the central region (i.e. midway between the root and cotyledonary tips) of the hypocotyl, encompassing the epidermis, was imaged. Confocal microscopy was performed using the Leica TCS SP2 as before. Enhanced cyan fluorescent protein (ECFP) was excited using the Ar laser at 458 nm, and emission collected between 495 and 577 nm. DsRED was excited using the HeNe laser at 543 nm, and emission collected between 578 and 643 nm. Unless otherwise specified, images shown are maximum intensity projections of optical slices produced by the LCS software provided.

### 2.3.3 Leaf sections

In order to view living cells, leaf tissue was cut into 5 mm square sections and placed directly onto a microscope slide, mounted in 10% glycerol. Often it was useful to place two coverslips either side of the mounted tissue to aid positioning of another coverslip over the thick sample. The orientation of the tissue depended on the cell layer of interest; spongy mesophyll cells could be most easily viewed by placing the leaf section abaxial side uppermost, whereas placing the adaxial side uppermost allowed imaging of palisade mesophyll cells. Images were then collected using the Leica TCS SP2 confocal microscope and a 63x oil immersion objective..

### 2.3.4 Fluorescence recovery after photobleaching

FRAP experiments were performed using the Leica TCS SP2 confocal microscope described above. GFP and DsRED were excited and emission collected using the same excitation and emission wavelengths, except that bleaching was performed using the Ar laser alone. Two pre-bleach images were collected of a suitable stromule at 4X zoom and 20% laser power. A rectangular region of interest (ROI) was set at a point midway along the length of the stromule, establishing the location for bleaching. Bleaching was performed by two 100% laser power scans zoomed in on the ROI. Recovery images were taken at 2.0 s intervals, for twenty images, using the pre-bleach settings. Two further ROIs were set: one adjacent to the bleached region of stromule as a measure of fluorescence loss, and another on an unconnected plastid as a control for general photobleaching. The images were analysed with the LCS software provided and the data exported to Microsoft Excel, where the fluorescence values for each ROI were normalised by dividing by the pre-bleach value for the respective ROI.

## 2.4 IMAGE ANALYSIS

### 2.4.1 Tomato fruit pericarp

Fruit were examined at four developmental stages: mature green (MG), one day post-breaker (B+1), three days post-breaker (B+3) and ripe (B+7). The maximum intensity projections from the confocal microscope were imported into LUCIA G quantitative image analysis software (Nikon) and quantified in various ways as follows. A 400 by 400 pixel square “quadrat” (equivalent to 156  $\mu\text{m}$  by 156  $\mu\text{m}$ ) was positioned over the centre of the imaged cell, and the proportion of plastids with stromules within the quadrat was recorded. A stromule was defined as any visible projection emanating from the surface of the plastid of less than 1  $\mu\text{m}$  in diameter. From this information, an estimate of plastid density could be obtained (i.e. number of plastids within the quadrat). In addition, stromule length was determined from up to 15 stromules from each image, and plastid plan surface area (estimated with a best fit 5-point ellipse) was determined as a mean of at least five plastids within the quadrat.

### 2.4.2 Tobacco hypocotyls

For tobacco seedlings the same methodology was employed as described for tomato, except that the quadrat was equivalent to 93  $\mu\text{m}$  by 93  $\mu\text{m}$  due to the higher magnification of the image. The quadrat covered several cells, and the term “plastid index” equates to the number of plastids counted within the quadrat. Stromules were measured only on those plastids where the plastid body could be reasonably defined.

## 2.5 STATISTICAL ANALYSIS

For each of the tomato fruit developmental stages considered, the mesocarp was divided into inner and outer regions based on the plastid dimorphism observed between

them. At least 10 cells were measured from each developmental stage and region of the mesocarp considered (i.e. at least 20 cells per stage), sampling from at least four different fruit per stage. Each cell was considered an independent data point. For measuring the relationship between stromule length and plastid density in tobacco hypocotyl epidermis, 10 images per treatment were analysed, and each image was treated as an independent data point for stromule length and plastid index. Image analysis data were entered into MINITAB 13 statistical software (Minitab Inc., PA, USA). The proportion of plastids with stromules was transformed with the angular transformation ( $\text{asin}\sqrt{X}$ , where  $X$  is the proportion) to stabilise variance, creating a linear variable termed “stromule index”, which allows more valid comparison between treatments when displayed graphically. Stromule lengths were found to be right skewed and thus were transformed by converting to natural logarithms before statistical analysis was performed. To assess differences between plastid parameters, Mann-Whitney rank sum tests were utilised as this test requires the satisfaction of fewer assumptions.

## **2.6 MOLECULAR BIOLOGY**

Molecular cloning was carried out according to standard techniques (Sambrook and Russell, 2001). Plasmid manipulation was performed using *Escherichia coli* strain DH5 $\alpha$ . Restriction endonucleases, T4 DNA ligases and other enzymes were sourced from various manufacturers (Promega Corp., Madison, WI, USA; New England Biolabs, Beverly, MA, USA; and MBI Fermentas, Hanover, MD, USA). Restriction fragments were isolated from agarose gels using the QIAQuick gel extraction kit (QIAGEN GmbH, Hilden, Germany) according to the manufacturer’s instructions. Recombinant colonies were screened by restriction digestion and/or PCR-based methods. Plasmid DNA was isolated either by a standard alkaline lysis method (Sambrook and Russell, 2001), or by use of a QIAFilter midiprep kit (QIAGEN) according to the manufacturer’s instructions.

Recombinant plasmids were sequenced to verify construct integrity prior to introduction into *Agrobacterium tumefaciens* for plant transformation.

## 2.6.1 Generation of constructs

### 2.6.1.1 Plastid-targeted GFP in tomato and Arabidopsis

The construct was a gift from Prof. Maureen R. Hanson (Dept. Molecular Biology and Genetics, Cornell University, Ithaca, USA). It consists of the *Arabidopsis* recA transit sequence fused upstream of the mGFP4 coding region, driven by a double CaMV 35S promoter and terminated by the nopaline synthase terminator sequence (Köhler *et al.* 1997; Figure 3.1 C). The construct is here termed pBIN/recA-gfp. The expression cassette is within a pBIN19-based binary vector, supplied in *A. tumefaciens* strain C58C1.

### 2.6.1.2 Plastid-targeted DsRED

In order to highlight plastids and associated stromules, a red fluorescent protein (DsRED) derived from the anthozoan coral *Discosoma* spp. (Matz *et al.*, 1999) was used, and targeted to the plastid by fusing to the chloroplast transit peptide of the *Petunia* rbcS subunit of Rubisco. A 693 bp fragment encoding the DsRED cDNA was amplified from pDsRed (Clontech, Palo Alto, CA, USA) via PCR. The forward primer was 5'-CTT GCA TGC GGT CTT CCA AGA ATG TTA TC-3' (*SphI* site underlined); the reverse primer was 5'-AAA GCA TGC T CTA GAG TCG CGG CCG CTA AAG-3' (*SphI* and *XbaI* sites underlined). The PCR conditions were as follows: initial denaturation 95 °C 2 min; denaturation 95 °C 1 min, primer annealing 46 °C 30 s, extension 72 °C 1 min, for 35 cycles; and a final 10 min extension step at 72 °C, using a proprietary mixture of proof-reading and non-proofreading DNA polymerases, DyNAzyme (Finnzymes, Espoo, Finland). The PCR product was cut consecutively with *SphI* and *XbaI*, and directionally

cloned into pBSrbcS, directly downstream of the 177 bp rbcS transit sequence, giving rise to the rbcS transit sequence and dsRED in a translational fusion. The resulting 870 bp rbcS-dsRED cassette was isolated with *Xba*I and *Kpn*I and directionally cloned into the multiple cloning site (MCS) of pBC35, a pBIN19-derived binary vector with the CaMV 35S promoter and terminator sequences flanking the MCS. Finally the construct, termed pBC/rbcS-dsRED (Figure 4.1 A), was introduced into *A. tumefaciens* LBA4044.

### 2.6.1.3 Mitochondria-targeted GFP

The mitochondria-targeted GFP construct, pBIN4/3, was a kind gift from Dr D. C. Logan (Logan and Leaver, 2000). It consists of a cDNA encoding the mitochondrial pre-sequence from *Nicotiana plumbaginifolia*  $\beta$ -ATPase (nucleotides 387-666) and the *mgfp5* gene ligated together, and placed into pBIN121 downstream of the CaMV 35S promoter (Figure 4.1 B). The construct was supplied in *A. tumefaciens* strain C58C1.

### 2.6.1.4 Peroxisome-targeted ECFP

The sequence encoding ECFP (enhanced cyan fluorescent protein) was amplified by PCR from pBINH2::ECFP, a gift from J. Hasseloff, University of Cambridge, UK. The forward primer was 5'-TTA GGA TCC TTC ATG TGC AAG GGC GAG GAG CTG-3' (*Bam*HI site underlined), and the reverse primer was 5'-TTC GAG CTC TTA GAG CTT AGA TTT GTA TAG TTC ATC CAT GCC GAG AGT-3' (relocated stop codon and additional nine nucleotides encoding S-K-L are underlined). The PCR conditions were as follows: initial denaturation 95 °C 2 min; denaturation 95 °C 30 s, primer annealing 48 °C 30 s, extension 72 °C 1 min, for 32 cycles; and a final 10 min extension step to promote A-tailing at 72 °C. DyNAzyme was used for improved amplification fidelity. The resulting 730 bp product was cloned into pGEM-T Easy (Promega), prior to being ligated into the *Bam*HI-*Sph*I backbone of pDH51. This produced a vector with the

CaMV 35S promoter and terminator sequences flanking ECFP-SKL (Figure 4.1 C). The whole cassette was then ligated into the *Eco*R1 site of pGREEN0029, generating the final binary vector, pGR/ECFP-SKL. Finally, the plasmid was mobilised into *A. tumefaciens* strain LBA4044 by electroporation in conjunction with pSOUP, a secondary plasmid required for replication of pGREEN plasmids in *Agrobacterium* (Hellens *et al.*, 2000).

#### 2.6.1.5 Silencing of *CHUP1* by RNAi

A 521 bp exon fragment of *CHUP1* was amplified from *Arabidopsis thaliana* (ecotype Columbia-0) genomic DNA by PCR. The forward primer was 5'-CACC TGC ATG TTT ACG GTA TGA GTT-3'; the reverse primer was 5'-CTT GTT GTT GTG TTC TGA TTC-3'. The PCR reaction parameters were: initial denaturation 95 °C 2 min; denaturation 95 °C 1 min, primer annealing 58 °C 30 s, extension 72 °C 2 min, for 32 cycles; and a final 5 min extension step at 72 °C. The proofreading DNA polymerase *Pfu* (Promega) was used for improved fidelity. The 521 bp fragment was gel purified and ligated into pENTR/D-TOPO using the pENTR Directional TOPO cloning kit (Invitrogen Corp., CA, USA) to create the Gateway Entry vector pENTR/CHUP500i. This Entry vector was used in a LR reaction with the Destination vector pB7GWIWG2 (Karimi *et al.*, 2002). This binary vector contains two pairs of *attR* recombination sites in an inverted repeat formation, separated by an *A. thaliana* genomic intron. Following recombination with pENTR/CHUP500i, the 521 bp exon fragment was incorporated into pB7GWIWG2 between the *attR1* and *attR2* recombination sites of each repeat. This resulted in a construct driven by the CaMV 35S promoter consisting of an inverted repeat of 521 bp of *CHUP1* DNA, with each repeat separated by an intron (Figure 5.3 A). This plasmid was designated pB7/CHUP\_RNAi. Upon transcription *in planta*, subsequent intron splicing produces double-stranded RNA which, via post-transcriptional gene silencing, should silence the endogenous *CHUP1* gene. Finally, the construct was mobilised into *A. tumefaciens* strain C58 for plant transformation.

### 2.6.1.6 C-terminal fusion of CHUP1 with sGFP

The entire *CHUP1* coding region, starting from the translation initiation site and including introns, was amplified from *Arabidopsis thaliana* (ecotype Columbia) genomic DNA by PCR. The forward primer was 5'-CACC ATG TTT GTC GGG ATA GGG TTT-3'. The reverse primer was 5'-AAC ACC GTT TAC AGA TTC TTC TTC ATT G-3', replacing the endogenous stop codon with one coding for glycine (underlined). A "touchdown" protocol was performed in order to optimise the PCR reaction parameters and minimise non-specific amplification (Sambrook and Russell, 2001), using the proofreading DNA polymerase *Pfu* (Promega). The program details were: initial denaturation 95 °C 2 min; denaturation 95 °C 45 s, primer annealing 66 °C 30 s, decreasing by 2 °C per cycle, extension 72 °C 12 min, for 7 cycles until the annealing temperature reached 54 °C. The remaining 28 cycles were carried out thus: denaturation 95 °C 45 s, primer annealing 54 °C 30 s, extension 72 °C 12 min. A final extension step of 72 °C 10 min was then performed. The resultant 3.7 kb fragment was gel purified and ligated into pENTR/D-TOPO using the pENTR Directional TOPO cloning kit (Invitrogen) to create the Gateway Entry vector pENTR/C-CHUP. This Entry vector was used in a LR reaction with the Destination vector pGWB5 (a pBI101-based binary vector; a gift from T. Nakagawa, Shimane University, Japan) to produce a translational fusion with GFP at the C-terminus (Figure 5.2 B). This construct, termed pGW/CHUP-GFP, provided constitutive expression of the transgene by means of the CaMV 35S promoter and nopaline synthase terminator (Figure 5.2 B). Finally, the construct was mobilised into *A. tumefaciens* strain C58 for plant transformation.

### 2.6.1.7 Plastid-targeted GFP for expression in maize

The vector pAHC25 was designed for constitutive expression of a transgene in monocots by use of the maize ubiquitin promoter and 5' UTR of the ubiquitin gene (Christensen and Quail, 1996). In order to replace the original  $\beta$ -glucuronidase (GUS) coding se-

quence with that for mGFP4, pAHC25 was digested with *SacI* (immediately upstream of the *nos* terminator) and *SmaI* (at the 5' end of the GUS coding sequence), leaving the ubiquitin promoter, 5' UTR and *nos* terminator sequences intact. The plastid-targeted GFP sequence was derived from the same construct used by Köhler *et al.* (1997): in this construct, the *recA-mgfp4* coding sequence is flanked by a double 35S promoter and the *nos* terminator sequences. *recA-mgfp4* was isolated as follows. First, the vector was linearised at the *BamHI* site immediately upstream of *recA*. The 3' recessed termini were filled with the Klenow fragment of DNA polymerase I, producing a blunt end. Next, the linearised, blunt vector was digested at the *SacI* site that links the 3' end of *mgfp4* to the *nos* terminator, releasing the *recA-mgfp4* fragment with a 5' blunt end and a 3' *SalI* overhang. This fragment was then directionally cloned into the *SmaI/SacI*-prepared pAHC25, producing pAHC25/*recA-gfp* (Figure 6.3 A).

## 2.6.2 Electroporation of *A. tumefaciens*

The same procedure, based on a modification of Wen-jun and Forde (1989), was used irrespective of the strain of *Agrobacterium*.

### 2.6.2.1 Preparation of electro-competent cells

A single colony of wild type (i.e. carrying no binary vector) *A. tumefaciens* was used to inoculate a starter culture of 20 ml of APM media containing 25 µg.ml<sup>-1</sup> rifampicin (see §2.2.2.1), and was incubated in the dark with shaking at 29 °C overnight. The next day, 2 ml of this culture was added to 50 ml of fresh APM and the OD<sub>600</sub> monitored over the day. Once at OD<sub>600</sub> of 0.5-0.7, the culture was chilled on ice, transferred into a 250 ml polypropylene centrifuge bottle (Nalgene, Herts, UK) and pelleted in a pre-cooled Sorvall GSA rotor (Kendro, Herts, UK) at 4 °C and 1000xg for 5 minutes. The pellet was washed and re-pelleted successively in 1, 0.5, 0.02 and 0.02 culture volumes of ice-cold,

filter-sterilised 10 % (v/v) glycerol, with identical centrifuge steps in between. After the final wash, the bacteria were again pelleted and resuspended in 0.01 volume of ice-cold 10% glycerol. Aliquots of 40  $\mu$ l were dispensed into sterile 1.5 ml microcentrifuge tubes, flash-frozen in liquid nitrogen, and stored at  $-70^{\circ}\text{C}$ .

#### 2.6.2.2 Introduction of plasmid DNA into *A. tumefaciens*

Aliquots of bacteria were defrosted on ice and added to a pre-chilled 2 mm electroporation cuvette (EquiBio, Thermo Electron Corp., MA, USA). Between 50-100 ng of plasmid DNA (up to 5  $\mu$ l) was added, and the cuvette and its contents were held on ice for 20 min. During this time, 1 ml of APM media was chilled on ice. The bacteria were then electroporated using a MicroPulser electroporator (Bio-Rad UK, Herts, UK) with the built-in settings for *Agrobacterium* (2.5 kV, 200  $\Omega$ , 0.2 cm cuvette gap, pulse length 3.8 ms). Immediately after electroporation, 800  $\mu$ l of chilled APM was added to the cuvette, which was capped and then placed in a horizontal position in a shaking incubator at  $29^{\circ}\text{C}$  for 3 hours. APM agar plates (APM plus 10 g l<sup>-1</sup> bacteriological agar) were prepared with antibiotics as appropriate for each construct. The electroporated bacteria were spread onto the plates in 20, 50 and 200  $\mu$ l quantities, and incubated at  $29^{\circ}\text{C}$  for three days. Colonies were picked and cultured for plasmid extraction by alkaline lysis, and transformation was verified by PCR and/or restriction digestion.

#### 2.6.3 Plant genomic DNA extraction

Plant genomic DNA was isolated using the Sigma GenElute Plant Genomic DNA Mini-prep Kit (Sigma-Aldrich; product code G2N70) according to the manufacturer's instructions. In the case of *Arabidopsis*, 2-3 whole leaves were excised, placed in a sterile 2 ml microcentrifuge tube and frozen in liquid nitrogen. The leaf tissue was then ground in the tube itself using a plastic rod with a bevelled tip, in the continual presence of liquid

nitrogen. Once the tissue was ground to a fine powder, the nitrogen was allowed to evaporate and the lysis solutions provided with the kit were added directly to the tube, and the DNA extraction procedure was continued. For maize, young leaf tissue (typically the third leaf) was frozen in liquid nitrogen and ground in a pre-chilled pestle and mortar. Up to 100 mg of the fine powder was transferred to a sterile 2 ml microcentrifuge tube, to which the lysis solutions were added.

At the end of the extraction procedure, the DNA was eluted in 60  $\mu$ l of TE buffer containing approximately 5  $\mu$ g of DNA. Integrity and approximate yields of the DNA were determined by running 5  $\mu$ l on a 0.8% agarose-TBE gel.

## 2.6.4 Polymerase chain reaction of plant genomic sequences

### 2.6.4.1 Arabidopsis: Chapter 5

For screening SALK insert line SALK\_105043.36.90.x, two complementary PCRs were performed: one amplifying across the insertion site, and a second using a primer site from within the left border of the T-DNA and another downstream within the *CHUP1* gene. Primer sequences and relative binding sites are indicated in Figure 5.1. PCR conditions, identical for both pairs of primers, were: initial denaturation 94 °C 4 min; denaturation 94 °C 1 min, primer annealing 56 °C 45 s, extension 72 °C 1 min, for 30 cycles; and a final 10 min extension step at 72 °C.

To verify that BASTA-resistant *CHUP1*\_RNAi primary transformants carried the transgene, PCR was performed using a forward primer homologous to the 3' end of the *CHUP1* repeat and a reverse primer homologous to the CaMV 35S terminator sequence used in the construct (Figure 5.2). The forward primer was 5'-CTT GTT GTT GTG TTC TGA TTC-3', and the reverse primer was 5'-TTA TCT GGG AAC TAC TCA CAC-3'. PCR

conditions were: initial denaturation 94 °C 4 min; denaturation 94 °C 1 min, primer annealing 58 °C 45 s, extension 72 °C 1 min 30 s, for 30 cycles; and a final 10 min extension step at 72 °C. This reaction produced a band of the expected size of approximately 700 bp.

#### 2.6.4.2 Maize: Chapter 6

The full-length mGFP4 coding sequence was amplified from transgenic genomic samples. The forward primer was 5'-CCG TCG ACA GTA AAG GAG AAG AAC TTT TCA CTG-3', and the reverse primer was 5'-CCG TCG ACT TTG TAT AGT TCA TCC ATG CC-3'. PCR conditions were: initial denaturation 94 °C 4 min; denaturation 94 °C 45 s, primer annealing 55 °C 45 s, extension 72 °C 1 min, for 30 cycles; and a final 10 min extension step at 72 °C.

A 444 bp fragment of the maize *RbcS1* gene was amplified from genomic samples using the forward primer 5'-TGT GGA AGC TGC CCA TGT GC-3' and the reverse primer 5'-TAG CAG GTA TAG AGG TAG CCA ATG C-3' according to Chiter *et al.* (2000). PCR conditions were: initial denaturation 95 °C 5 min; denaturation 94 °C 1 min, primer annealing 60 °C 1 min, extension 72 °C 1 min, for 35 cycles; and a final 10 min extension step at 72 °C.

### 2.6.5 Plant RNA extraction

Total plant RNA was isolated using the QIAGEN RNeasy Plant Mini Kit (QIAGEN, Cat. # 74904) according to the manufacturer's instructions. *Arabidopsis* leaf and inflorescence tissue was excised and placed in a sterile 2 ml microcentrifuge tube before being placed immediately into liquid nitrogen. Root tissue was obtained by removing the soil ball from the pot and knocking off excess soil whilst minimising damage to the roots. The

soil adhering to the roots was rinsed off under the tap, and the roots dabbed dry on tissue paper. Root tissue was cut off, folded, placed in a sterile 2 ml microcentrifuge tube and then flash-frozen in liquid nitrogen. All tissue types were emptied into a pre-chilled pestle and mortar and ground to a fine powder; 100 mg of this tissue was placed in a 1.5 ml microcentrifuge tube, and the RNeasy protocol followed from this point onwards. Maize tissue was treated in much the same way, except that the leaf tissue was selected from young expanding leaves (typically the fifth to seventh leaf), wrapped in foil and placed straight into liquid nitrogen. The tissue was ground, weighed and transferred into a 1.5ml microcentrifuge tube as described for *Arabidopsis*.

Purified RNA was eluted in water and quantified by measuring the absorbance at 260 nm ( $A_{260}$ ) in a spectrophotometer, using a quartz cuvette. Dilutions of 5 in 1000 were analysed, and RNA concentrations were calculated using the relationship that an  $A_{260}$  of 1 unit corresponds to 40  $\mu\text{g}$  of RNA per ml of water. RNA integrity was confirmed by denaturing gel electrophoresis (see §2.6.6).

## 2.6.6 Northern analysis

### 2.6.6.1 Electrophoresis and blotting of RNA to nylon membranes

RNA was separated by formaldehyde agarose gel electrophoresis. A 1.2% agarose gel was prepared containing 1x Running Buffer (20 mM 3-[N-morpholino]propanesulfonic acid (MOPS), 5 mM sodium acetate, 1 mM EDTA). To this, 1.8 ml of 37% formaldehyde and 1  $\mu\text{l}$  of a 10  $\text{mg}\cdot\text{ml}^{-1}$  ethidium bromide stock solution were added per 100 ml of molten gel. The gel was poured and allowed to equilibrate for 30 min with 1x Running Buffer. RNA samples were prepared by adding the appropriate amount of 5x RNA Loading Buffer (per 10 ml: 10 mg bromophenol blue, 80  $\mu\text{l}$  0.5 M EDTA pH 8.0, 720  $\mu\text{l}$  37% formaldehyde, 2 ml glycerol, 3084  $\mu\text{l}$  formamide, 4 ml 10x Running Buffer, then RNase-

free water to 10 ml) to 5 – 10 µg of total RNA. The samples were heated on a hot block at 65 °C for 3 min and then placed on ice. Once cool, the samples were loaded onto the gel along with 3 µg of RNA ladder (Invitrogen). The gel was run at 5-7 V/cm in 1x Running Buffer until the blue dye had migrated 10-15 cm.

After electrophoresis, the gel was viewed using a UV transilluminator alongside a UV-fluorescent ruler for estimation of band migration distance. The gel was then placed in several gel volumes of 0.05 N NaOH and agitated for 10 min using an orbital shaker to partially hydrolyse the RNA. The NaOH was removed and replaced with 20x standard saline citrate (SSC; 175.3 g NaCl, 88.2 g sodium citrate per litre; final concentrations 3.0 M Na<sup>+</sup>/Cl<sup>-</sup>, 0.3 M citrate), and the gel was shaken for 40 min to equilibrate the gel with the blotting buffer.

To immobilise the RNA to a membrane, an upward flow capillary blot was constructed according to Sambrook and Russell (2001). Briefly, 20x SSC was poured in a glass tray over which a glass plate support was placed. A wick made from Whatman 3MM filter paper (Whatman plc, Kent, UK) was thoroughly soaked in 20x SSC and laid over the glass plate with the tips extending into the buffer reservoir. On this, two pieces of gel-sized Whatman paper were overlaid, and the gel placed on these in an inverted position. The edges of the gel were delineated with plastic wrap such that the plastic wrap extended over the glass tray, leaving the centre of the gel (and all lanes containing RNA) exposed. A gel-sized charged nylon membrane (Hybond N+, Amersham Biosciences) was also soaked in 20x SSC and placed over the gel, ensuring that there were no air bubbles between the gel and the membrane. One at a time, three more pre-soaked pieces of Whatman paper were placed on top of the membrane, which were then covered with paper towels to a height of about 10 cm. Finally, a glass plate and a 1 kg mass were placed on top of the towels to compress the apparatus. Blotting was allowed to

proceed for 12 h and the membrane was then washed in 2x SSC for 5 min. RNA was then fixed on the membrane by UV-crosslinking in a Stratalinker (Stratagene, La Jolla, CA, USA), and was either allowed to air dry or prepared for hybridisation.

#### 2.6.6.2 Generation of DNA probes

Complementary sequences for probes were generated by amplifying by PCR from cloned or genomic sources, as described below. PCR products were gel purified and their concentration estimated by running an aliquot on a TBE agarose gel. Between 5 and 25 ng of DNA was added to a labelling reaction using the Rediprime II random prime labelling kit (Amersham Biosciences) according to the manufacturer's instructions. Once ready, the 50 µl probe reaction was added directly to the hybridisation tube containing the blot and prehybridisation buffer.

##### 2.6.6.2.1 *Arabidopsis*: Chapter 5

For detection of *CHUP1* transcripts, a 600 bp fragment of exon 4 of *CHUP1* was amplified by PCR from genomic DNA. The forward primer was 5'-CACC TGA GGG TTT GAA TTC CGT TGC-3' and the reverse primer was 5'-TCG GTT CTC GAT TTC CCC TAA-3'. The PCR conditions were: initial denaturation 95 °C 2 min; denaturation 95 °C 1 min, primer annealing 60 °C 30 s, extension 72 °C 2 min, for 30 cycles; and a final 10 min extension step at 72 °C. A single band of the expected size was produced, and used directly as a probe.

For detection of transcripts from the *UBQ10* gene, a 700 bp fragment was PCR-amplified from genomic DNA and cloned into pENTR/D-TOPO. The forward primer was 5'-CACC AGA GTT CTG ACA CCA TTG ATA-3' and the reverse primer was 5'-GCA TAA CAG AGA CGA GAT TTA GAA-3'. The PCR conditions were: initial denaturation 95

°C 2 min; denaturation 95 °C 1 min, primer annealing 60 °C 30 s, extension 72 °C 2 min, for 30 cycles; and a final 10 min extension step at 72 °C. The PCR produced three major bands, of which the largest (700 bp) was gel purified, cloned and sequenced. The resulting clone (pENTR/UBQ10) was used as a “clean” source of a single *UBQ10* coding sequence. Template for probe labelling was obtained from pENTR/UBQ10 by PCR amplification using standard M13-20 primers, which span the cloning site of pENTR/D-TOPO.

A 600 bp fragment of the *sgfp* gene was amplified by PCR from pGWB5. The forward primer was 5'-ACC TAC GGC AAG CTG ACC CTG-3' and the reverse primer was 5'-TTG TAC AGC TCG TCC ATG CCG-3'. The PCR conditions were: initial denaturation 94 °C 2 min; denaturation 94 °C 45 s, primer annealing 62 °C 30 s, extension 72 °C 1 min, for 30 cycles; and a final 10 min extension step at 72 °C.

#### 2.6.6.2.2 Maize: Chapter 6

The mGFP4 and *RbcS1* sequences were identical to those described in §2.6.4.2, and were amplified by PCR with the same conditions, except that mGFP4 was amplified from the plasmid pBIN*recAgfp*.

#### 2.6.6.3 Hybridisation of DNA probes to RNA immobilised on nylon membranes

The membrane containing fixed RNA was rolled up and placed inside a hybridisation tube, to which 10 ml or 20 of prehybridisation buffer (0.5 M phosphate buffer pH 7.2, 7% SDS, 10 mM EDTA) was added, depending on the size of the membrane. Large membranes were rolled together with a nylon mesh to improve probe access. The membrane was then incubated in an oven with constant rotation at 65 °C for at least two

hours. The prepared probe was then added directly to the prehybridisation buffer and the tube was returned to the hybridisation oven for a further 12 h at 65 °C.

Following hybridisation, the membrane was rinsed briefly in 2x SSC, 0.1% (w/v) SDS at room temperature and then washed several times with increasing stringency. The first wash was performed for 20 min in an excess of 2x SSC, 0.1% (w/v) SDS at room temperature. A medium stringency wash was then performed in 1x SSC, 0.1% (w/v) SDS for 15 min at 65 °C. The blot was then monitored for non-specific probe activity with a Geiger-Müller counter and washed once more in the same solution until this activity was appreciably removed. Finally, and if necessary, a high stringency wash was performed in 0.1x SSC, 0.1% (w/v) SDS at 65 °C for 5 min. Without being allowed to dry out, the membrane was then wrapped in plastic and heat sealed before proceeding to autoradiography.

#### *2.6.6.4 Film exposure and development*

The plastic-wrapped filter was placed in an autoradiography cassette. Under a red safe-light, a sheet of X-OMAT film (Kodak, Herts., UK) was placed in the cassette overlying the hybridised filter. Depending on the strength of the radioactive signal, the cassette was stored at - 70 °C for between 4 and 48 h.

To develop the film, the autoradiography cassette was first allowed to thaw. In a photographic dark room, the film was removed and washed in developer solution for 3 min with gentle shaking. The film was then briefly rinsed under running water before being placed in fixer solution for a further 3 min. Once developed the film was rinsed thoroughly with water and allowed to air dry. Autoradiographs were then digitised by scanning, and prepared for presentation using Adobe Photoshop 7.

### 2.6.6.5 Removal of bound probe from nylon membranes

To prepare a membrane for re-probing, old probe was stripped from the membrane by placing it in a plastic dish and adding 500 ml of 0.5% (w/v) SDS heated to 95-100 °C. The dish was placed on an orbital shaker and the solution allowed to cool to room temperature. The membrane was then monitored for radioactivity and the procedure repeated if necessary until the signal was below 5 counts per second. The membrane was then competent for another round of prehybridisation/hybridisation.

## 2.6.7 Analysis of plant leaf proteins

### 2.6.7.1 Extraction and quantification of soluble leaf proteins

Approximately 1 g of young, expanding maize leaves was harvested and weighed before being wrapped in foil and frozen in liquid nitrogen. The tissue was ground to a fine powder in a pestle and mortar in liquid nitrogen, and once the nitrogen had evaporated, was transferred to a 50 ml centrifuge tube containing 1.5 ml of Protein Extraction Buffer (18% [w/v] sucrose, 10 mM MgCl<sub>2</sub>, 0.1 M Tris-HCl pH 8.0, 0.28% β-mercaptoethanol) per 0.5 g of leaf tissue. The mixture was vortexed vigorously for 10 s and then filtered through one layer of Miracloth into a fresh 50 ml centrifuge tube. The extract was then split equally into microcentrifuge tubes and centrifuged at >13,000 x g for 10 min. The supernatant, containing leaf total soluble proteins was recovered and stored at - 70 °C.

Proteins were quantified using the Bio-Rad Protein Assay (Bio-Rad) according to the manufacturer's instructions. The assay is based on the absorbance change of an acidified solution of Coomassie® Brilliant Blue G-250 dye upon addition of protein. A calibration curve was produced using bovine serum albumin standards.

### 2.6.7.2 SDS-PAGE

Proteins were separated on a 10% ProSieve 50 (Cambrex Bio Science, Nottingham, UK) acrylamide resolving gel, with a 5% stacking gel. Equal quantities of protein were combined with 0.5 volumes of 3x Protein Loading Buffer (per 10 ml: 1.8 ml 1 M Tris-HCl pH6.8, 1.5 ml  $\beta$ -mercaptoethanol, 3 ml 20% [w/v] SDS, 10 mg bromophenol blue, 3 ml glycerol, distilled water to 10 ml), boiled for 2 min and then placed on ice. The samples were loaded onto duplicate gels, and electrophoresed in Tris/Glycine/SDS Buffer (25 mM Tris, 50 mM glycine, 1% [w/v] SDS) using a MiniProtean III (Bio-Rad) apparatus. Protein size standards were provided by MultiMark protein ladder (Invitrogen). In order to verify equal loading of protein samples, one gel was stained with Coomassie® Brilliant Blue (2.5 g l<sup>-1</sup> Coomassie® Brilliant Blue, 30% ethanol, 10% glacial acetic acid) for 1 h and then destained for 2-3 h with regular changes of destaining solution (30% ethanol, 10% glacial acetic acid). The second gel was used for protein transfer onto a nitrocellulose membrane (Schleicher & Schuell, Dassel, Germany), using a Bio-Rad Trans-blot semi-dry transfer cell (Bio-Rad).

### 2.6.7.3 Immunodetection of GFP

Western blotting was performed with the WesternBreeze kit (Invitrogen) according to the manufacturer's instructions. Briefly, the nitrocellulose membrane was washed in a blocking solution for 30 min to which was added the primary antibody (rabbit anti-GFP, Molecular Probes, Eugene, OR, USA) to a final concentration of 0.4  $\mu\text{g}\cdot\text{ml}^{-1}$ . The membrane was incubated with the primary antibody for an hour, washed, and then exposed to an alkaline phosphatase-conjugated anti-rabbit secondary antibody for a further hour. After several further wash steps to remove unbound secondary antibody, a chemiluminescent substrate was added to the membrane, and the membrane prepared for autoluminography.

#### 2.6.7.4 Film exposure and development

Films were exposed to the membrane for an empirically determined time. In a dark room under safelight, the membrane was placed in an autoradiography cassette with a sheet of X-OMAT film (Kodak) for 30 s. The membrane was then moved to another region of the film, and the cassette shut for another 2 min. The process was repeated twice more for 5 min and 15 min of exposure time. Films were then developed as described in §2.6.6.4, producing a range of exposures which could be selected based on the strength of the signals of interest relative to background.

## 2.7 ISOLATION OF INTACT CHLOROPLASTS FROM LEAF TISSUE

The same procedure was employed for both maize and tomato. All centrifugation steps were carried out at 4 °C, and all equipment was pre-chilled in a cold room or on ice.

Young, expanding leaf tissue was collected early in the morning to minimise chloroplast starch content. A continuous Percoll (Amersham Biosciences) gradient was made by mixing 5 ml Percoll with 5 ml of Gradient Buffer (100 mM HEPES-KOH pH 7.5, 0.66 M sorbitol, 2 mM MgCl<sub>2</sub>, 2 mM MnCl<sub>2</sub>, 4 mM EDTA, 10 mM Na-ascorbate, 2% (w/v) bovine serum albumin) in an 11.5 ml polyallomer centrifuge tube (Kontron Ultracrimp; Kontron Instruments, Munich, Germany). The gradient was established by spinning the tubes at 52,000 x g in a swing-out rotor in an ultracentrifuge (Centrikon T-1065 and TST28-38 rotor; Kontron) for 40 min. Once formed, the gradients were kept on ice until the crude chloroplast extract was ready. Between 6 and 10 g of fresh leaf tissue was chopped into 100 ml of ice-cold GR Buffer (50 mM HEPES-KOH pH 7.5, 0.33 M sorbitol, 1 mM MgCl<sub>2</sub>, 1 mM MnCl<sub>2</sub>, 2 mM EDTA, 5 mM Na-ascorbate, 1% (w/v) bovine serum albumin) in a pre-chilled blender (Waring, Torrington, CT, USA). The tissue was ground using four short (2 second) pulses at low speed. The crude extract was filtered through one layer of Miracloth (Merck Biosciences, Nottingham, UK), pre-wet with GR

buffer, using a funnel. The extract was squeezed gently and filtered into two 50 ml centrifuge tubes (Bibby Sterilin). The chloroplasts were then spun down at 3000 x g for 8 min using an Eppendorf 5810R and F34 rotor (Eppendorf UK Ltd, Cambridge, UK). The supernatant was decanted and the pellet resuspended in 1.5 ml of ice-cold GR buffer with a fine-haired paintbrush. The chloroplast suspension was layered onto the prepared Percoll gradients using a wide-bore Pasteur pipette. The gradients were spun at 6,500 x g for 15 min, yielding two bands: the upper band contained broken chloroplasts, and the lower band consisted of intact chloroplasts (Figure 6.7 B). The upper band was removed and discarded and, using a Pasteur pipette, the lower band was transferred to a fresh 50 ml centrifuge tube and diluted with three volumes of IB Buffer (50 mM HEPES-KOH pH 8.0, 0.33 M sorbitol). The suspension was spun once more in the Eppendorf centrifuge at 2,600 x g for 8 min. The supernatant was aspirated and 1 ml of fresh IB buffer was added to resuspend the pellet again. This suspension was transferred to a cold 1.5 ml microcentrifuge tube and centrifuged at 2,600 x g for 8 min using the Eppendorf F45 rotor. Finally, the supernatant was removed and the pellet resuspended in 50-100  $\mu$ l of SDS Buffer (6% [w/v] sucrose, 2% [w/v] SDS, 0.28% [v/v]  $\beta$ -mercaptoethanol) and placed on a hot-block (90-100 °C) for 5 min to dissolve the pellet. The tube was then placed on ice, ready for protein quantification and SDS-PAGE.

# 3 STROMULE DEVELOPMENT DURING TOMATO FRUIT RIPENING

## 3.1 INTRODUCTION

### 3.1.1 Tomato fruit development

The ripening fruit of *Lycopersicon esculentum* L. has long been the subject of research. The fruit – the seed-bearing organ that develops following flower fertilisation – varies considerably in form between species, so no single example will suffice as a model for studying all aspects of fruit development. Nevertheless, the tomato is an important food crop and undergoes a number of processes typical of a wide variety of fruits, and is thus a good choice for exemplifying fruit development in general. The tomato fruit is classified as a berry since the thick, juicy pericarp completely encloses the locules (enlarged carpels) that contain the seeds. Much work on tomato fruit has focussed on the holistic role of ethylene in the regulation of ripening (Theologis, 1992; Alexander and Grierson, 2002), and has led to a detailed picture of the molecular genetics of ripening. In addition, the implication of carotenoids, and lycopene in particular, as important components of human dietary intake has led to close elucidation of the regulatory pathways of carotenoid biosynthesis in tomato fruit (Bramley, 2002). Furthermore, the tomato also represents an excellent system for investigating plastid differentiation and development since chloroplasts undergo the transition to chromoplasts in a well characterised manner (Bathgate *et al.*, 1985; Cheung *et al.*, 1993). The availability of a range of tomato mutants has been instrumental in elucidating the mechanistic details of these developmental processes, amongst others.

Fruit set in tomato is initiated following the successful fertilisation of the ovule. In the flower, the ovary wall, which surrounds the ovules, consists of undifferentiated paren-

chyma cells, vascular tissue and inner and outer epidermis (Gillaspy *et al.*, 1993). Upon flower fertilisation, the ovary wall undergoes a highly co-ordinated set of cell division and expansion events giving rise to the pericarp. Cell division in the ovary wall takes place over 7-10 days following fertilisation by which time the fruit has attained an approximate size of 0.8 cm. Subsequent fruit growth is achieved by cell expansion over 6-7 weeks (Gillaspy *et al.*, 1993). Complex signals from the fertilised gametophyte and subsequently from the developing embryo determine the rate of cell division in the pericarp, an inference supported by the positive correlation between the number of fertilised ovules and the final size and weight of the fruit (Gillaspy *et al.*, 1993). A fully expanded but green fruit is termed mature green, with immature green usually used to describe fruit of 50% or less in final size (Lincoln and Fischer, 1988). The mature green stage can last several days before the first hint of yellow colour is detectable, a brief event called breaker (B), which occurs by about 40 days post anthesis (dpa). The ripening process then proceeds rapidly, and by 7 days post breaker (B+7) chlorophyll is absent, and the fruit is red and acceptably soft; however, further lycopene accumulation and softening occurs beyond this age (Fraser *et al.*, 1994).

The pericarp consists of three distinct layers: the exocarp (including the outer epidermis), the mesocarp, a multi-celled middle layer, and the endocarp, a single celled-layer that lines the locules (Gillaspy *et al.*, 1993; Figure 3.1 A). An apical-basal vascular system pervades the mesocarp, distributed in a regular manner rather like the lines of longitude on a globe. In the mature fruit, the pericarp cells are large (up to 0.5 mm in diameter) and highly vacuolated, and their morphological similarity to leaf palisade cells reflects the ontogenical modification of the leaf structure to form the carpel (Gillaspy *et al.*, 1993). The massive increase in cell size that occurs in the pericarp from fertilisation onwards is accompanied by the induction of plastid division.

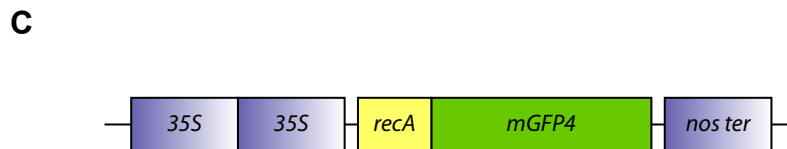
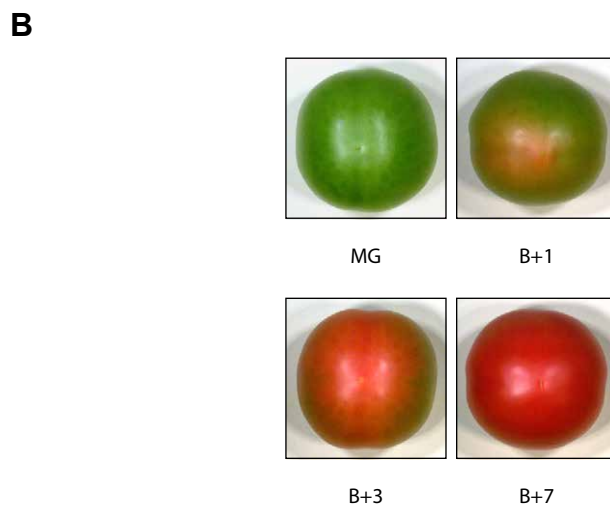
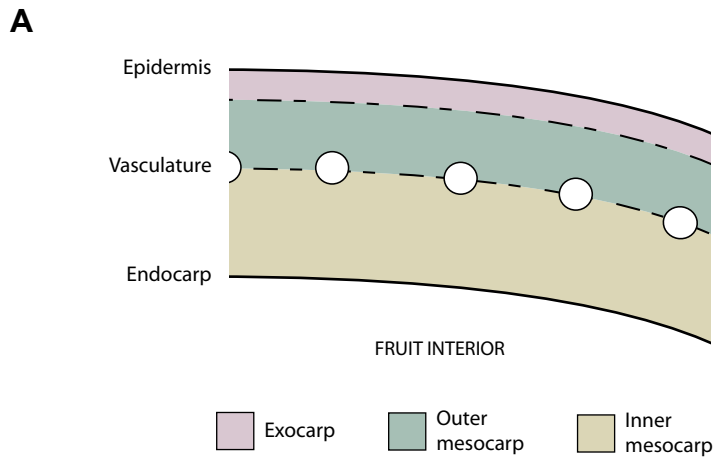


**Figure 3.1 Tomato fruit pericarp and ripening stages**

(A) Part of a longitudinal section through a full-sized tomato fruit pericarp. The pericarp is the fleshy wall of the fruit. The epidermis and endocarp are both single cell layers, and are depicted by solid lines. Dashed lines indicate approximate boundaries between the different layers; the mesocarp is divided into two sub-regions based on plastid morphology and cell size (here termed outer and inner mesocarp). The two sub-regions are approximately delineated at the level where the vasculature pervades the mesocarp. (B) Representative fruit from each of the four stages of ripening considered. Note the slight colour change that is visible in B+1, indicating the start of chromoplast differentiation. (C) The plastid-targeted GFP construct expressed in line a17. 35S: CaMV 35S promoter; *recA*: N-terminal chloroplast transit peptide from *Arabidopsis recA* protein; *nos ter*: nopaline synthase terminator sequence.

Recent work on plastid division in tomato fruit has concluded that the majority of plastid division occurs at the green stage of fruit development (Cookson *et al.*, 2003), which is consistent with the general view that plastid division is linked to cell expansion (Pyke, 1997). Chromoplasts *per se* are certainly capable of undergoing binary fission (Camara *et al.*, 1995), but this does not seem to be a major contributor to the plastid population in tomato. The chloroplasts in green fruit pericarp cells are photosynthetically competent, but unlike leaves fruit tissue does not show a net carbon uptake and thus the developing fruit can be regarded as a sink tissue (Ho and Hewitt, 1986). Mature green fruit contain high levels of starch which is mostly synthesised from hexose phosphates (Büker *et al.*, 1998) derived from apoplastic sucrose unloaded from the phloem (Damon *et al.*, 1988). Starch levels reach a peak at approximately 25 dpa (Robinson *et al.*, 1988), although absolute starch levels vary between cultivars and proximal-distal position of the fruit on the truss (Ho and Hewitt, 1986). During ripening, this starch is progressively broken down and mobilised into soluble sugars (mostly glucose and fructose, which together constitute 47% of the dry matter of a ripe fruit) and organic acids (mostly citric acid and malic acid), which together make a major contribution to the taste of the fruit (Grierson and Kader, 1986). This rapid accumulation of reducing sugars is reflected by the strong correlation between the starch content of green fruit and the final soluble sugar content of ripe fruit among various cultivars (Ho and Hewitt, 1986).

**Table 3.1** Major physiological and biochemical changes during tomato fruit ripening. (Adapted from Bryant and Cuming, 1999)

- 
- Increased ethylene biosynthesis
  - Changes in gene expression
  - Increased respiratory activity (the “climacteric”)
  - Loss of thylakoids and photosynthetic enzymes
  - Degradation of chlorophyll
  - Synthesis of carotenoids, especially lycopene
  - Changes in organic acid metabolism
  - Increases in activity of polysaccharide-hydrolysing enzymes, especially polygalacturonase
  - Depolymerisation of cell wall uronides
  - Softening
  - Increased susceptibility to pathogen attack
-

The ripening process in tomato fruit consists of a number of physiological and biochemical changes (Table 3.1). Concomitant with the shifts in sugar profile are the ripening-related changes in fruit texture and colour, which are mediated by the autocatalytic production of the plant hormone ethylene (Grierson *et al.*, 1981; Grierson and Kader, 1986). The tomato is classified as a climacteric fruit, since the initiation of ripening is associated with an increase in respiration and a burst of ethylene release. The inhibition of ethylene production through antisense-silencing of ACC oxidase (which catalyses the final step in ethylene biosynthesis) significantly retards fruit ripening and extends shelf-life (Oeller *et al.*, 1991). The tomato mutant *Never-ripe* (*Nr*) has an ethylene-insensitive, non-ripening phenotype characterised by orange fruit at maturity that soften very slowly (Grierson and Kader, 1986). *NR* encodes one of the five ethylene receptor genes in tomato and is homologous to the *Arabidopsis* ethylene receptor *ETR1* (Wilkinson *et al.*, 1995). A mutation in the N-terminal ethylene-binding domain (Wilkinson *et al.*, 1995) renders the *Nr* mutant receptor incapable of binding ethylene, explaining why *Nr* fruits fail to ripen upon exposure to exogenous ethylene. In *Arabidopsis*, loss of function of any one of the five members of the ethylene receptor family does not bestow insensitivity to ethylene, but mutations in the ethylene binding domain of any one receptor does (Hua and Meyerowitz, 1998). Furthermore, quadruple mutants in which four ethylene receptors are knocked out exhibit a constitutive ethylene response phenotype (Hua and Meyerowitz, 1998). These observations suggest a “negative inhibition” model for ethylene perception, in which a pentameric ethylene receptor normally blocks ripening, and this block is relieved upon the binding of ethylene. The dominant-negative nature of the *Nr* mutation, and the inability of the protein to bind to ethylene, suggests that the same model holds in tomato. This hypothesis was confirmed when the specific antisense inhibition of the mutant *Nr* gene rescued the aberrant ripening phenotype (Hackett *et al.*, 2000). Consistent with the *Arabidopsis* model, *NR* is not strictly required for ripening, presumably because other members of the ethylene receptor gene family act redundantly (Hackett *et al.*, 2000). The *Nr* phenotype results from the

mutant protein occupying a position in the ethylene receptor complex, blocking the receptor's ability to transduce the ethylene signal and thus preventing the release of the suppression of ripening. When the mutant Nr protein is absent, other members of the family can take its place and form a functional ethylene receptor (Hua and Meyerowitz, 1998).

Since mutations such as *Never ripe* appear to regulate the ripening process on a global scale, the production and perception of ethylene is considered an early event in the ripening process which induces novel gene expression. Ripening used to be considered a senescent process, but it is distinct from leaf senescence because metabolites are not relocated and recovered but instead are converted to sugars and organic acids and remain *in situ*. Proteins involved in carotenoid biosynthesis and cell wall softening (e.g. polygalacturonases) are up-regulated; in addition, photosynthesis-related genes such as *rbcS* are specifically down-regulated as ripening commences (Gillaspy *et al.*, 1993). A number of novel cDNAs have been described that are ripening related, some of whose protein products are directed to the developing chromoplast (Lawrence *et al.*, 1997). The development of tomato fruit is thus a regulated, active process; one of the central downstream events of ethylene signal transduction is the accumulation of carotenoids and the simultaneous differentiation of chloroplasts into chromoplasts.

### 3.1.2 Plastid differentiation and pigment accumulation

One of the most obvious changes during tomato fruit ripening is the colour change in the pericarp, which is a direct result of the degradation of chlorophyll and the build up of carotenoid pigments in the plastid. The chromoplast becomes a hyper-accumulator of carotenoids: there is a 53-fold increase in total carotenes from immature green to fully ripe fruit (Fraser *et al.*, 1994). Approximately 38 per cent of this rise is due to the accretion of the red pigment lycopene, which increases nearly 300-fold over the same

time period (Fraser *et al.*, 1994). Lycopene forms crystals in membrane-bound inclusions in the chromoplast that are presumably the remnants of the thylakoid membranes from the degenerating chloroplast (Harris and Spurr, 1969b; Cheung *et al.*, 1993).  $\beta$ -carotene is also a major pigment in tomato chromoplasts: small crystals of the pigment form in the plastid stroma and are particularly prevalent in the mutant *high beta* (Harris and Spurr, 1969a; Camara *et al.*, 1995). Such dramatic changes in plastid biochemistry are the downstream events resulting from the initiation of ripening, and are brought about by the induction of novel gene expression. The formation of carotenoids is mediated by the activity of phytoene synthase, which catalyses the production of phytoene, the colourless precursor of all carotenoids. The fruit-expressed phytoene synthase, *PSY1*, is specifically up-regulated in a ripening specific fashion (Fraser *et al.*, 1994), and is mutated in the tomato mutant *yellow flesh* (Fray and Grierson, 1993). In this mutant, the fruit lose chlorophyll and go on to ripen normally (i.e. they soften) but remain yellow since no carotenoids are synthesised. A similar expression pattern is observed for *Pds*, which encodes the next enzyme in the biosynthetic chain, phytoene desaturase (Fraser *et al.*, 1994). Whilst ripening induces the up-regulation of these genes, expression of the gene for lycopene  $\beta$ -cyclase falls, thus reducing the amount of lycopene diverted towards  $\beta$ -carotene synthesis and allowing the preferential accumulation of lycopene (Pecker *et al.*, 1996). As such, the transcriptional regulation of nuclear gene expression is the principal mechanism of regulating carotenoid biosynthesis in tomato fruit. This is paralleled by simultaneous reductions in photosynthetic gene expression, from both nuclear and plastid genomes (Camara *et al.*, 1995). Plastid gene expression is generally decreased in the chromoplast relative to the chloroplast; however, changes in plastid gene expression are not brought about by a general dismantling of the plastid transcriptional apparatus, since some plastid genes (e.g. *psbA*) are expressed for longer and at higher levels during tomato fruit ripening than others (e.g. *rbcL*; Camara *et al.*, 1995). Nevertheless, the chromoplast does not perform high levels

of protein synthesis, an inference supported by the disappearance of plastoribosomes in mature chromoplasts (Camara *et al.*, 1995).

Despite the decreased levels of *in organello* protein synthesis, large quantities of nuclear-encoded proteins are synthesised in the cytosol and imported into the chromoplast to support the differentiation process. The protein profiles of tomato fruit chloroplasts and chromoplasts differ quite considerably (Bathgate *et al.*, 1985); obvious candidates for such chromoplast specific proteins include carotenogenic enzymes, as well as proteins involved in the degradation of the photosynthetic apparatus. The profiles of *in vitro* translation products of mRNA isolated from four stages of ripening between mature green and ripe fruit differ quite considerably, and specific proteins are capable of import into isolated pea chloroplasts (Lawrence *et al.*, 1993). Chromoplasts isolated from bell pepper (*Capsicum annuum*) retain the ability to import *in vitro* translated proteins, and also contain levels of protein import machinery comparable to chloroplasts (Summer and Kline, 1999). These chromoplasts are also able to target proteins to the internal plastid membrane system using the two of the three pathways found in chloroplasts, as the thylakoid-localised chloroplast protein OE17 also localised to a membrane-bound lumenal compartment in chromoplasts (Summer and Kline, 1999). However, these chromoplasts are unable to integrate the major light-harvesting chlorophyll a/b-binding protein (LHCP) into internal membranes, suggesting that chromoplast differentiation is at least partially achieved by restricting certain protein import mechanisms (Summer and Kline, 1999).

### 3.1.3 Various aspects of tomato fruit development are affected by mutation

Besides *Never ripe*, several other mutations have been characterised that affect ripening in tomato fruit, and fall in to two broad categories: those that affect the global ripening process (such as *Never ripe*), and those that influence a particular feature of fruit devel-

opment. The mutation *ripening inhibitor (rin)* is an example of the former. The *rin* locus confers a non-ripening phenotype to fruit, which develop normally until breaker whereupon they very gradually lose chlorophyll and turn yellow, but do not accumulate lycopene and show reduced carotenoid levels in general (Tigchelaar *et al.*, 1978). The *rin* locus is tightly linked to the *macrocalyx (mc)* locus, and is accompanied by greatly enlarged sepals and a loss of inflorescence determinacy. Genetic separation of these two loci has not been reported. *rin* fruit do not undergo a respiratory climacteric, and exhibit only trace levels of polygalacturonase activity (Tigchelaar *et al.*, 1978). The cloning of *RIN* and the complementation of *rin/mc* individuals has revealed that *RIN* is a MADS-box transcription factor that specifically mediates ripening, whereas the *MC* locus is responsible for the loss of inflorescence determinacy and enlarged sepal phenotype (Vrebalov *et al.*, 2002). The *rin/mc* phenotype results from a 2.6. kb deletion of the region between these two loci, leading to a transcriptional fusion of the two coding regions and the consequent inactivation of both genes (Vrebalov *et al.*, 2002), which also explains why the two mutant phenotypes are inseparable. Its identification as a transcription factor and its global effect on ripening means that *RIN* is considered a master regulator of the ripening process, upstream of ethylene and *NR* in the regulatory cascade; in addition, *RIN* expression is not significantly up-regulated in response to ethylene, which is unusual for ripening related genes (Vrebalov *et al.*, 2002). However, it is possible to rescue partially the mutant by the exogenous application of ethylene (Lincoln and Fischer, 1988). In *rin* fruit, only some ethylene-inducible genes are up-regulated following gassing with ethylene, and even these genes are expressed at lower levels relative to the wild type response (Lincoln and Fischer, 1988). There is a corresponding slight increase in softness and lycopene accumulation in ethylene-treated *rin* fruits, but they do not closely resemble wild type ripe fruit (Tigchelaar *et al.*, 1978). Given this fundamental arrest of proper fruit development, the *rin* mutant should serve as a useful tool for deciphering the general effects of a block on the ripening process on plastid and stromule morphology.

There are several fruit colour mutants of tomato, most of which are specific blocks in the carotenoid pathway like *yellow flesh* (for a review, see Bramley, 2002). The mutant *green flesh* (*gf*) is distinct in that rather than exhibiting an aberration in the accumulation of a pigment, it is deficient in the removal of chlorophyll from the developing chromoplast (Cheung *et al.*, 1993) as well as its degradation in senescing leaves (Akhtar *et al.*, 1999). As discussed above, chlorophyll and the associated photosynthetic apparatus are gradually removed upon the commencement of ripening, but in *gf* this process takes very much longer: by B+7 both carotenoids and chlorophyll are present in the pericarp, resulting in a dirty-red fruit colour. Electron micrographs clearly show that thylakoid structures are maintained in *gf* ripe fruit, and photosynthetic proteins such as both subunits of Rubisco and LHCP II, and their corresponding transcript levels remain elevated relative to wild type in *gf* ripe fruit (Cheung *et al.*, 1993). A similar phenotype is apparent in leaves, which fail to senesce properly and do not lose chlorophyll before they eventually wither and abscise (Akhtar *et al.*, 1999). The molecular identity of *GF* is unknown, but it appears to be involved in mediating the proper action of phaeophorbide *a* oxygenase, which is a component of the chlorophyll breakdown pathway (Akhtar *et al.*, 1999). As a basis for studying plastid morphology, the *gf* mutant is invaluable: since stromules are generally rare on chloroplasts (Gray *et al.*, 2001), a direct test of any inhibitory effect of chloroplast status on stromule formation can be addressed in this mutant background.

Although not strictly a ripening mutant, ripe fruit of the *high pigment-1* (*hp-1*) mutant are a deeper red relative to wild type, and leaves are also a darker green (Cookson *et al.*, 2003). Since both the ripe fruit and leaves of *hp-1* individuals possess a 1.8-fold increase in total carotenoids (Bramley, 1997; Cookson *et al.*, 2003), the *hp-1* mutation is non-fruit specific. *hp-1* influences fruit appearance through an indirect effect on plastid density, plastid number and plastid size, resulting in an increased total chromoplast area per cell and therefore higher levels of carotenoids (Cookson *et al.*, 2003). Homozygous

*hp-1* seedlings also demonstrate an exaggerated photomorphogenic response with increased anthocyanin content and decreased hypocotyl elongation, but do not exhibit disturbances in phytochrome levels, stability or spectral responsiveness (Peters *et al.*, 1992). Furthermore, seedlings homozygous for the most severe allele, *hp-1<sup>w</sup>*, express high levels of *RBCS*, *CHS* and *CAB* in the dark (Peters *et al.*, 1998), a phenotype that is reminiscent of constitutively photomorphogenic and light signalling mutants (Chapter 4). *HP-1* thus appears to act as a negative regulator in the phytochrome signal transduction pathway. This notion was confirmed by the identification of *HP-1* as the tomato homologue of DDB1 (UV-damaged DNA-binding protein 1; Liebermann *et al.*, 2004). In *Arabidopsis*, there are two DDB1 homologues (DDB1A and DDB1B), whereas tomato only appears to possess one (Schroeder *et al.*, 2002; Liebermann *et al.*, 2004). In *Arabidopsis*, DDB1A is postulated to interact with DET1 (DE-ETIOLATED 1) in the nucleus as a modifier of chromatin structure (Schroeder *et al.*, 2002). *det1* mutants are photomorphogenic in the dark, with pleiotropic effects on plant development throughout the life cycle that are enhanced when DDB1A function is knocked out (Schroeder *et al.*, 2002). The tomato mutant *hp-2*, phenotypically similar but non-allelic to *hp-1*, is deficient in the homologue of *DET1* (Mustilli *et al.*, 1999), consistent with *hp-1* and *hp-2* interacting genetically and biochemically in directing light-regulated plant development.

The basis of *hp-1* on plastid number is unclear, but may be a result of increased sensitivity to cytokinin, which promotes chloroplast division in moss (Kasten *et al.*, 1997; Cookson *et al.*, 2003). The *hp-1* mutant will allow an assessment of the effect of increased plastid density on stromule biogenesis. It is conceivable that stromules increase plastid surface area when plastid density is particularly low: if this is the case, then the *hp-1* mutant should exhibit differences in stromule abundance relative to wild type.

### **3.1.4 Scope of this Chapter**

The tomato fruit is an ideal basis for investigating stromule behaviour in relation to plastid differentiation, and is supported by the existence of various mutations affecting both the ripening process and specific aspects of plastid development. Only the basic changes in plastid morphology in tomato fruit have been described so far (Pyke and Howells, 2002) which leave many questions to be answered. This Chapter will describe a more thorough examination of the changes in plastid morphology in pericarp cells and stromule occurrence during tomato fruit ripening. In addition, it will address the effects of manipulating various aspects of fruit development in order to dissect the factors that influence stromule formation.

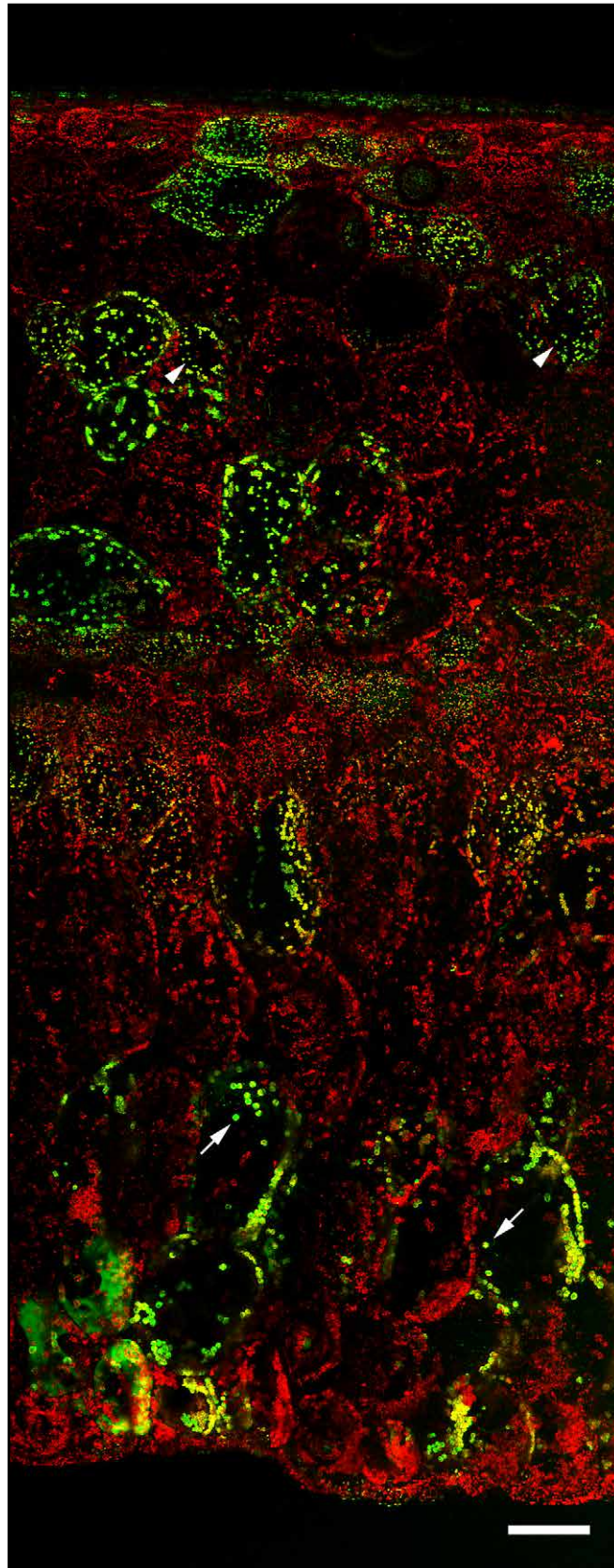
## 3.2 RESULTS

### 3.2.1 Two distinct plastid populations exist in the mesocarp of tomato fruit

Developing tomato fruit can be classified according to size and colour. The four stages considered here cover the transition from chloroplast to chromoplast in a mature (i.e. full-sized) fruit. At mature green (MG), fruit enlargement has ceased. Breaker (B) marks the initiation of ripening when the first colour change becomes apparent; all subsequent stages are defined as days post breaker (i.e. B+1, B+3, B+7; Figure 3.1 B). By B+7 an Ailsa Craig tomato fruit is ripe, with almost maximal levels of carotenoids and little or no remnant chlorophyll (Fraser et al., 1994). Inspection of whole pericarp sections from mature green (MG) fruit expressing a plastid stroma-targeted GFP construct, *re-cAgfp* (Figure 3.1 C), reveals that the vasculature appears to delineate two distinct cell types within the mesocarp itself (Figure 3.2). In MG fruit, the mesocarp cells outermost to the vasculature (outer mesocarp, or OM cells) possess small, numerous chloroplasts, whereas those towards the interior of the fruit (inner mesocarp, or IM cells) contain large, starch-filled plastids that are fewer in number (as indicated by staining with potassium iodide/iodine solution, data not shown; Figure 3.2 and Figure 3.3). This plastid dimorphism is maintained throughout the fruit ripening process such that the plastids in mesocarp cells from different locations are present at greatly different densities and exhibit major differences in size and morphology (Figure 3.3; Table 3.2). In ripe fruit (B+7), the chromoplasts in OM and IM cells are highly distinct. In OM cells, chromoplasts often take on an oblong, needle-like appearance (Figure 3.3 G), whereas IM-cell chromoplasts are much larger and ovoid in shape (Figure 3.3 H). The different cell populations and stages of fruit ripening are also associated with dramatic shifts in stromule morphology. In MG fruit, stromules in IM cells tend to be much longer and conspicuous than those in OM cells (Figure 3.3, insets).

**Figure 3.2 Confocal sections through the pericarp wall of a mature green fruit expressing *recA-gfp***

Four maximum projections of a confocal series along the z-axis were assembled to produce this composite image. The exterior of the fruit is at the top. Red represents chlorophyll autofluorescence and green is GFP fluorescence. Overlap of the two signals produces yellow. The regions of the pericarp depicted in Figure 3.1 are shown on the right; in this case, the vasculature is running from left to right across this longitudinal (apical-basal) section through the pericarp. Note the large globular plastids in the inner mesocarp cells (arrowed) compared with the smaller plastids in the outer mesocarp (arrowheads). The patchiness of colour (red to yellow to green) reflects cell-to-cell variation in GFP expression. Scale bar: 200  $\mu\text{m}$ .



Epidermis

Exocarp

Outer  
mesocarp

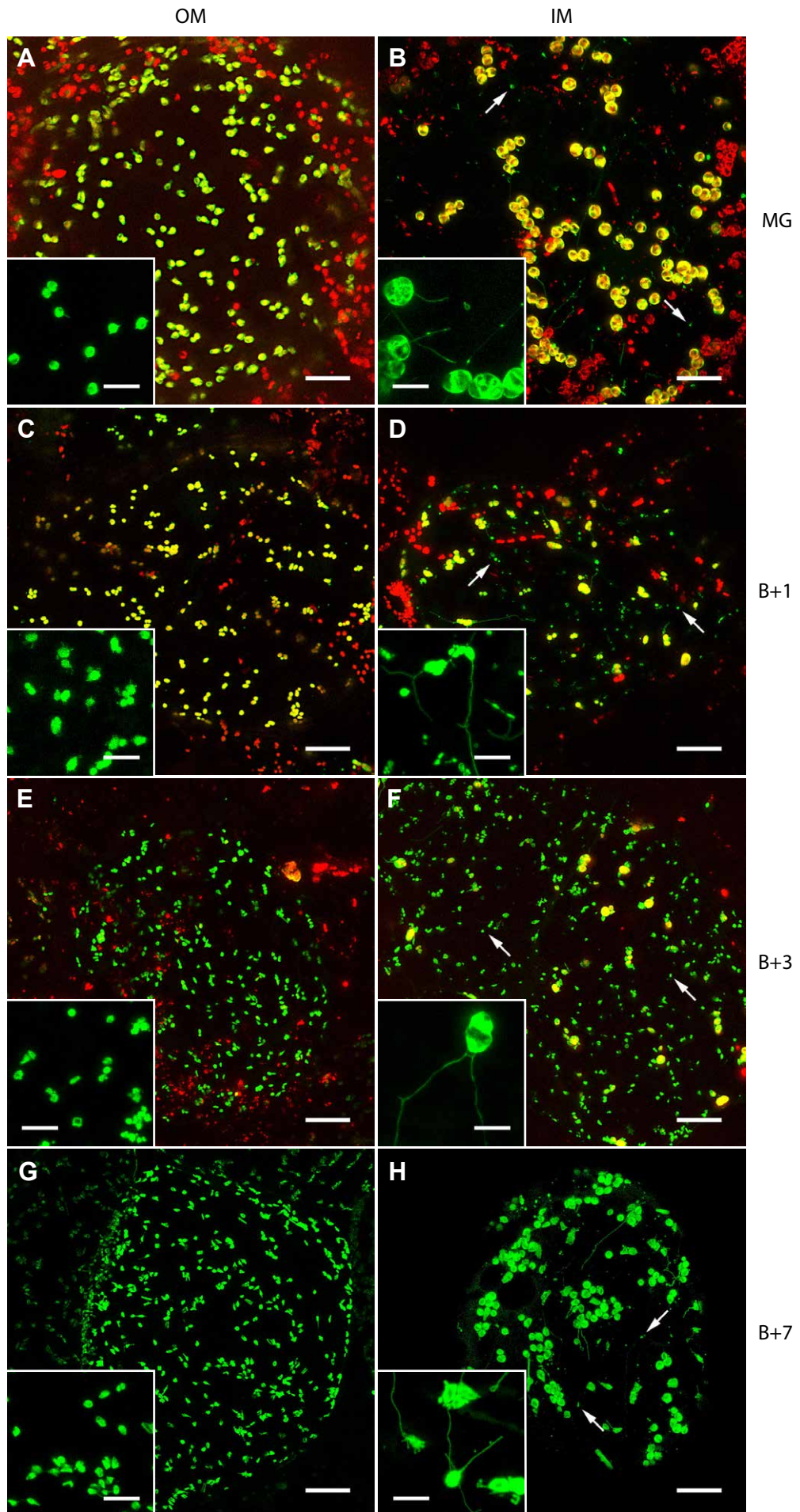
Vasculature

Inner  
mesocarp

Endocarp

### **Figure 3.3 Changes in plastid and stromule morphology during ripening**

Confocal maximum projections of individual cells from the outer mesocarp (OM) and inner mesocarp (IM) at various stages of ripening (MG, mature green; B+1, B+3, B+7, one, three and seven day(s) post-breaker respectively). Insets show higher magnifications of representative cells. With the exception of (G), (H) and the insets, all images show a combination of GFP and chlorophyll autofluorescence signals false-coloured green and red respectively, with yellow representing overlap. Note the consistent difference in plastid size between OM and IM cells at each stage, and the IM-cell specific plastid-derived vesicles which show GFP signal only (B, D, F, H, arrows). Scale bars: main images, 40  $\mu\text{m}$ ; insets, 10  $\mu\text{m}$ .



Stromules in MG OM cells are often stubby and do not protrude far into the cytoplasm, with a mean length of 5.6  $\mu\text{m}$  (Table 3.2). These are reminiscent of stromules found on chloroplasts in tissues such as mesophyll cells and trichomes (Figure 1.3). However, stromules in IM cells of MG fruit can be extremely long, with a mean length of 13.5  $\mu\text{m}$  (Table 3.2). These OM-IM cell differences are maintained at all stages, but the distinction is most pronounced once ripening commences (Figure 3.3, insets). Stromules are longest in IM cells from B+7 fruit, and there is often more than one stromule per chloroplast in this cell type (Figure 3.3 H). In addition, IM cells frequently show variably-sized vesicles that are not directly associated with plastids or stromules, and which contain GFP but not chlorophyll (Figure 3.3). These vesicles may be formed following the collapse of long stromules, since OM cells (with short stromules) do not possess them. It should also be noted that IM cell plastids from MG, B+1 and B+3 fruit show considerable intracellular variability in size (Table 3.2, Figure 3.3). This may be due to rapid mobilisation of starch reserves that commences just prior to breaker and proceeds through ripening (Büker *et al.*, 1998). Furthermore, the changes in plastid morphology may be compounded by incomplete thylakoid degradation and varying degrees of plastid differentiation. Such metabolic and developmental events are presumably not simultaneous throughout the fruit or even within a cell, leaving a heterogeneous population of plastids of different sizes and differentiation status.

### 3.2.2 Stromule frequency and length varies with plastid size and type

To investigate further how stromule abundance changes during ripening, the stromule frequency (i.e. the proportion of plastids with stromules) and stromule length in both OM and IM cells were measured at each of the four stages of wild type fruit development. Stromule frequency is expressed as “stromule index” for quantification (see §2.5). In addition, other parameters such as plastid size and plastids per unit area (a measure

of plastid density within the cell; hereafter termed “plastid index”) were determined (Table 3.2).

The stromule index is significantly lower in OM cells than in IM cells at all stages post-breaker (Mann-Whitney rank sum test,  $P > 0.05$ ; Figure 3.4 A), except in the case of MG fruit where there is no significant difference. The pattern of stromule index as ripening progresses differs between each of the two cell types. In OM cells, stromule index remains approximately constant throughout fruit development with only small changes. However, in IM cells there is a large and significant increase in stromule frequency upon the initiation of ripening i.e. between MG and B+1, where the proportion of plastids with stromules rises from 7% to 32% respectively (Mann-Whitney,  $P < 0.001$ ; Figure 3.4 A and Table 3.2). After the B+1 stage, stromule frequency in IM cells remains high and approximately constant with no significant change. From these data, it can be inferred that there is a dramatic increase in stromule frequency during the differentiation of chloroplasts to chromoplasts, but that this change is IM cell-specific.

Stromule length also varies between both cell types during fruit development. In OM cells, stromule length remains constant across all fruit stages, although there appears to be a transitory and significant increase at B+3 (Mann-Whitney,  $P < 0.001$ ; Figure 3.4 B). This may be due to plastids in fruit of this stage being intermediate between chloroplast and chromoplast, leading to discrepancies in plastid morphology that are typical of neither the mature chloroplast nor chromoplast. However, in IM cells stromule length is consistently and significantly higher than in the corresponding OM cells at all stages of fruit development considered (Figure 3.4 B). Furthermore, there is an increase in stromule length upon the transition from MG to B+1, and still a further increase between B+1 and B+7 (Mann-Whitney,  $P < 0.001$  and  $P = 0.02$  respectively; Figure 3.4 B).

**Table 3.2** Stromule abundance, plastid size and plastid density in tomato fruit mesocarp cells

Genotype	Stage	Cell type	N <sup>a</sup>	Mean stromule frequency (%) <sup>b</sup>	Mean stromule length (µm) <sup>c</sup>	Max. stromule length (µm) <sup>d</sup>	Mean plastid plan area (µm <sup>2</sup> ) <sup>e</sup>	Plastid index (plastids per 10,000 µm <sup>2</sup> ) <sup>f</sup>
Wild type (WT)	MG	OM	23	12	5.6 ± 0.3	28	24.0 ± 1.2	27.2 ± 2.6
		IM	24	7	13.5 ± 1.2	70	49.0 ± 3.2	17.2 ± 1.3
	B+1	OM	12	8	4.8 ± 0.5	22	20.2 ± 1.3	29.8 ± 2.4
		IM	15	32	31.7 ± 3.2	180	38.1 ± 2.6	11.6 ± 1.5
	B+3	OM	15	12	11.1 ± 1.2	52	22.8 ± 1.3	20.7 ± 2.6
		IM	15	32	37.6 ± 3.8	220	42.9 ± 2.8	10.7 ± 1.6
	B+7	OM	18	5	5.8 ± 0.6	36	19.6 ± 1.1	32.9 ± 2.9
IM		21	39	32.6 ± 1.9	180	40.7 ± 1.8	12.7 ± 1.4	
WT [dark grown]	MG	OM	10	25	4.7 ± 0.5	20	17.4 ± 0.9	18.6 ± 1.1
		IM	10	12	11.3 ± 1.8	50	52.0 ± 4.3	11.7 ± 1.3
green flesh	B+7	OM	17	8	6.2 ± 0.8	59	21.0 ± 1.1	30.6 ± 2.6
		IM	22	27	39.2 ± 2.9	200	54.9 ± 3.6	7.0 ± 2.8
ripening inhibitor	~B+40	OM	11	15	2.4 ± 0.1	5.1	10.4 ± 0.2	45.4 ± 7.1
		IM	10	19	2.7 ± 0.1	4.9	12.9 ± 0.3	41.1 ± 7.2
high pigment-1	MG	OM	19	15	5.5 ± 0.3	19	21.5 ± 1.0	76 ± 3.5
		IM	15	23	23.7 ± 1.9	160	69.0 ± 4.3	36 ± 2.9
B+7	B+7	OM	14	5	3.3 ± 0.2	8.9	23.7 ± 0.9	82 ± 4.1
		IM	12	31	23.0 ± 1.8	97	58.7 ± 2.6	24 ± 1.8

<sup>a</sup> number of cells used to calculate stromule index<sup>b</sup> mean proportion of plastids with stromules from N cells<sup>c</sup> mean ± 1 SE of measurements from at least 5 stromules from each of N cells<sup>d</sup> maximum stromule length across all N cells (2 s.f.)<sup>e</sup> mean ± 1 SE of measurements from 5 plastids from each of N cells<sup>f</sup> mean ± 1 SE of measurements from N cells

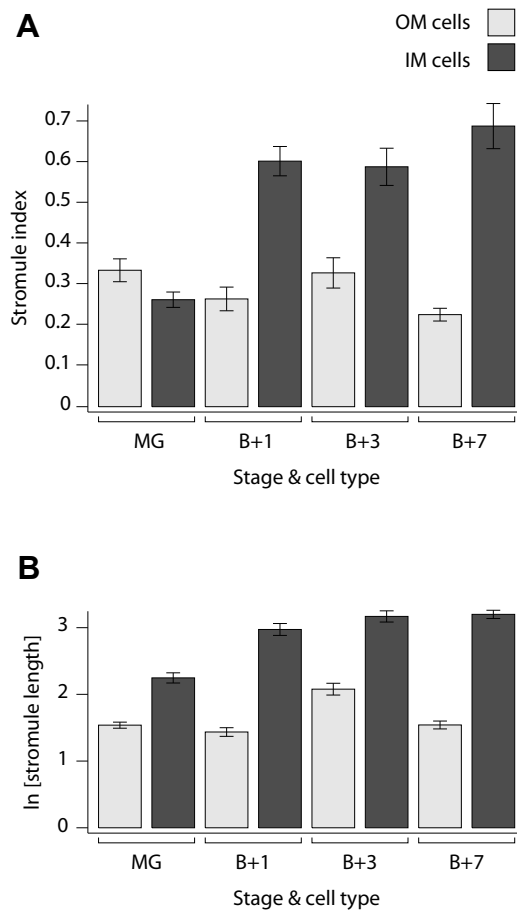


**Figure 3.4 Changes in stromule frequency and length in wild type tomato fruit during ripening**

(A) Stromule index (a measure of stromule frequency; see §2.5). (B) Stromule length plotted on a logarithmic scale. Bar heights show means, and error bars signify  $\pm 1$  SE.

This suggests that the transition from chloroplast to chromoplast correlates with increased stromule length but only in IM cells.

By B+7, the most dramatic suite of stromule morphologies emerges, from simple long tubules, to multiply-branched protrusions and heavily vesiculated stromules that assume a beads-on-a-string like structure (Figure 3.5). GFP thus reveals that chromoplasts in IM cells of ripe tomato fruit are extremely variable in morphology, with apparently flexible envelope membranes that can contribute to structures ranging from complicated convolutions (Figure 3.5 E) to elongated, branched stromules spanning large cytoplasmic distances (Figure 3.5 C). In IM cells of B+7 fruit, many chromoplasts thus appear to be interconnected by stromules; the proportion seems to be greater in fruit of this stage than of earlier stages, although definitive proof of interconnection would require the use of fluorescence recovery after photobleaching (FRAP) techniques.

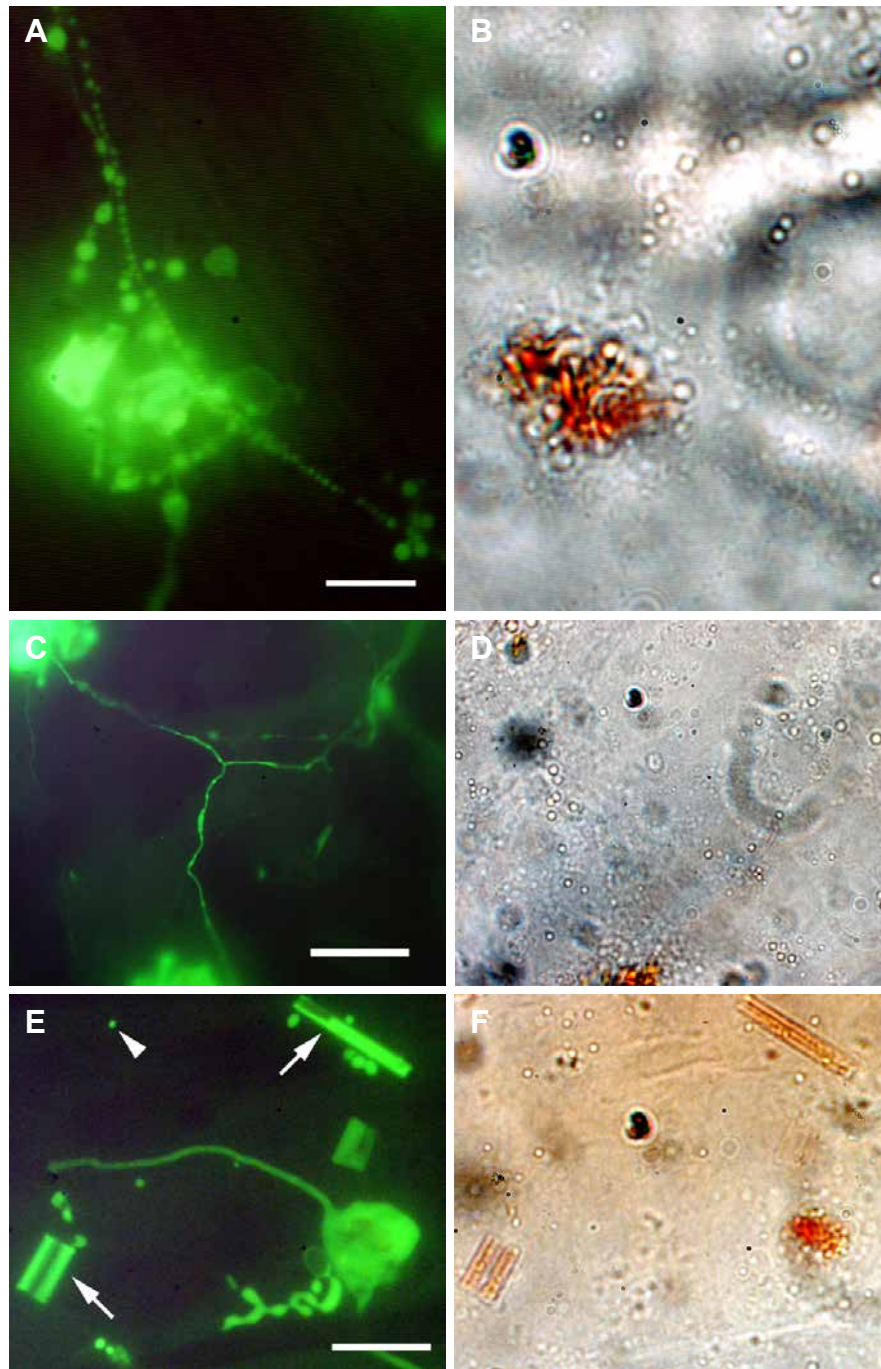


**Figure 3.5 Stromule and chromoplast morphology in IM cells of B+7 wild type fruit**

High magnification epifluorescence (A, C, E) and the corresponding brightfield (B, D, F) images of chromoplasts and their associated stromules. (A), (B) A single chromoplast projects multiple, long stromules with a vesiculated, beaded superstructure; these "beads" do not appear to move along stromules in any vectorial movement, but instead remain fixed in position relative to one another. (C), (D) A trilete-structured stromules appears to connect at least two chromoplast bodies. (E), (F) Chromoplasts can be poorly defined entities: lycopene crystals are enclosed by GFP-containing membrane (arrows), whilst a more typical chromoplast with associated stromule and membrane distortions is present at the lower-right of the image. Also visible are apparently separate GFP-containing vesicles (arrowhead). Scale bars: (A) 10  $\mu\text{m}$ ; (C, E) 5  $\mu\text{m}$ .

### 3.2.3 The *green flesh* mutation reduces stromule frequency in IM cells of ripe fruit

Since chloroplasts generally produce fewer and shorter stromules than non-green plastid types (Gray *et al.*, 2001; Köhler and Hanson, 2000), it seemed plausible that experimentally maintaining a chloroplast-like plastid status might inhibit stromule formation in ripe fruit mesocarp cells. To test whether the presence of chloroplast components such as thylakoid membranes and chlorophyll leads to a decrease in stromules on chromoplasts, the plastid-targeted GFP construct was crossed into the *green flesh* (*gf*) mutant background. In wild type fruit, chlorophyll and the associated photosynthetic apparatus are gradually removed from the chloroplast upon the commencement of ripening, but in *gf* this process takes very much longer so that by B+7 both carotenoids and chlorophyll are present in the pericarp plastids, resulting in a dirty-red fruit colour (Figure 3.6 C, E). Plastids in such fruit thus possess properties associated with both chloroplasts and chromoplasts (Cheung *et al.*, 1993).

Compared with wild type B+7 fruit, stromules in *gf* fruit appear superficially similar to wild type. They are rare in OM cells, but relatively common and extensive in IM cells, even though confocal imaging reveals the presence of both chlorophyll and lycopene (Figure 3.6 A, B). However, quantitative measurements revealed that the mutation has mixed effects on both stromule frequency and length. Stromules are more rare in IM cells of *gf* B+7 fruit than in wild type (27% vs. 39% of plastids possess stromules respectively; Table 3.2 and Figure 3.6 F), and this difference, although small, is significant ( $P = 0.02$ , Mann-Whitney). The effect on stromule frequency in OM cells is apparently the opposite (Figure 3.6 F), but this difference does not reach the 5% significance level ( $P = 0.15$ ). In terms of stromule length, there are no significant differences between *gf* and wild type in either OM or IM cells (Figure 3.6 G). Furthermore, parameters such as mean and maximum stromule length remain much the same in *gf* as in wild type (Table

3.2). However, whilst plastid density and size in OM cells are essentially the same in both genotypes, plastid density in IM cells is significantly lower in *gf* than it is in wild type (Table 3.2). This may be compensated for by the increased size of *gf* plastids in IM cells, and may be a feature of the *gf* mutation on chromoplast development. It is notable that both the physical appearance of plastids and stromules, as well as the frequencies and lengths of stromules from *gf* fruit, are comparable to those obtained from ripening wild type fruit (compare, for example, Figure 3.3 D with Figure 3.6 B): in both of these situations plastid differentiation is incomplete, with morphologies intermediate between chloroplast and chromoplast. Collectively, these findings suggest that maintaining the chloroplast state reduces the tendency for stromule formation.

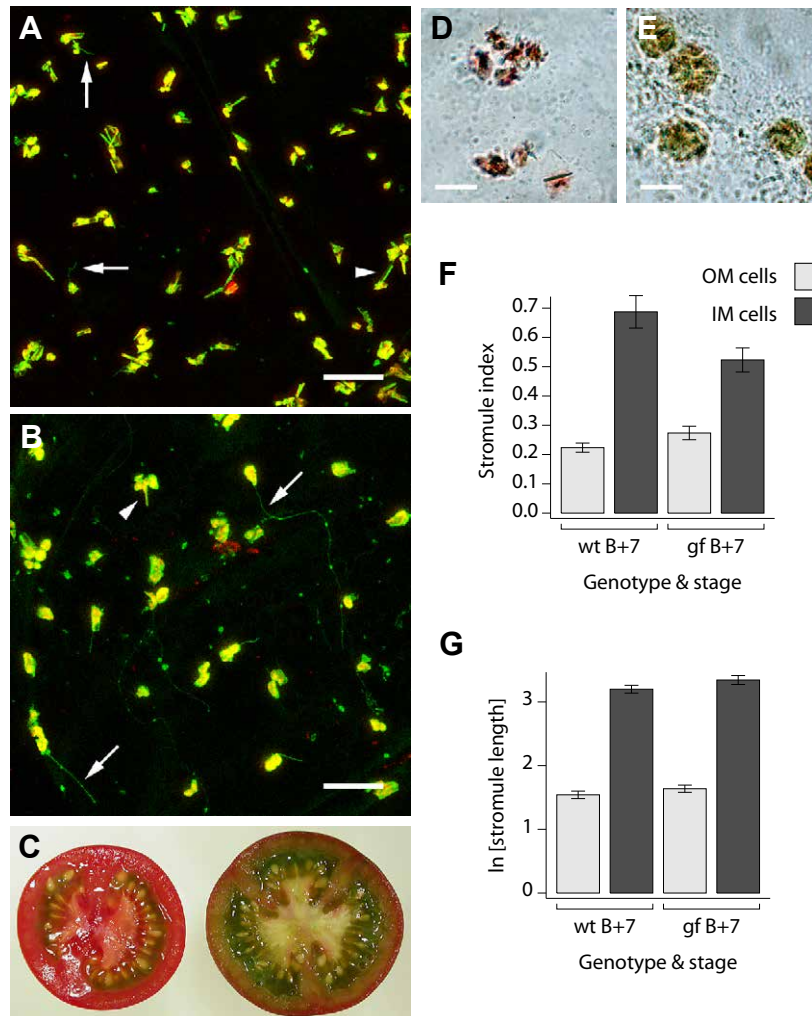


### Figure 3.6 Plastid and stromule morphology in *gf* B+7 fruit

Confocal images of representative (A) OM cells and (B) IM cells from B+7 *gf* fruit. GFP and chlorophyll autofluorescence signals are false-coloured green and red respectively, with yellow representing overlap. Note that stromules (arrows) and lycopene crystal deformations (arrowheads) are different in width and regularity in shape. (C) Wild type (left) and *gf* B+7 fruit sections. Note the brown-red colour of the *gf* pericarp. Brightfield images of (D) wild type and (E) *gf* plastids show the differences in pigmentation responsible for the fruit colour. Note the presence of both lycopene crystals and chlorophyll in *gf* plastids. (F) Stromule index and (G) stromule length in wild type (wt) and *gf* B+7 fruit. Bar heights represent the mean  $\pm$  1 SE. Scale bars: (A, B): 40  $\mu$ m; (D, E): 10  $\mu$ m.

### 3.2.4 Inhibiting chloroplast development increases stromule frequency in a cell type-specific manner

To address the impact of the absence of chloroplast components on stromule formation, the effects of inhibiting chloroplast differentiation were investigated. It is well known that chloroplast differentiation requires light in higher plants (Sundqvist *et al.*, 1980). Upon flower fertilisation, the cells in the ovary wall undergo multiple divisions prior to expanding (Gillaspy *et al.*, 1993), and this is accompanied by concomitant plastid division and chloroplast differentiation. Preventing light from reaching the post-fertilisation flower therefore prevents chloroplasts from developing, and results in a white fruit which is otherwise morphologically normal when compared with light-grown fruit at the equivalent mature green stage (Figure 3.7 C). Fruit grown in this way will develop as normal and ripen fully, suggesting that the light signal is not required for chloroplast differentiation (Figure 3.7 D). A large induction in stromule frequency relative to light-grown fruit was observed in OM cells of dark-grown fruit when inspected casually (Figure 3.7 A), but this difference was not so apparent in IM cells in which the plastids retained their large, starchy appearance (albeit without chlorophyll), and with few, relatively long stromules (Figure 3.7 B). Quantitative analysis of the images confirmed this general conclusion: within OM cells, stromule frequency was significantly higher in dark-grown than light-grown fruit ( $P=0.007$ , Mann-Whitney), but not different in IM cells ( $P=0.07$ ; Figure 3.7 E). Stromule length in IM cells did not vary significantly between the two treatments ( $P=0.39$ ) and, surprisingly, there was no significant difference in stromule lengths in OM cells between dark and light-grown fruit ( $P=0.22$ ; Figure 3.7 F). From these data it appears that stromules are more common on plastids that have not become chloroplasts, but that this apparent link can be modulated by other factors, since IM cell plastids in MG fruit retain their morphological characteristics whether they are chloroplastic or not.

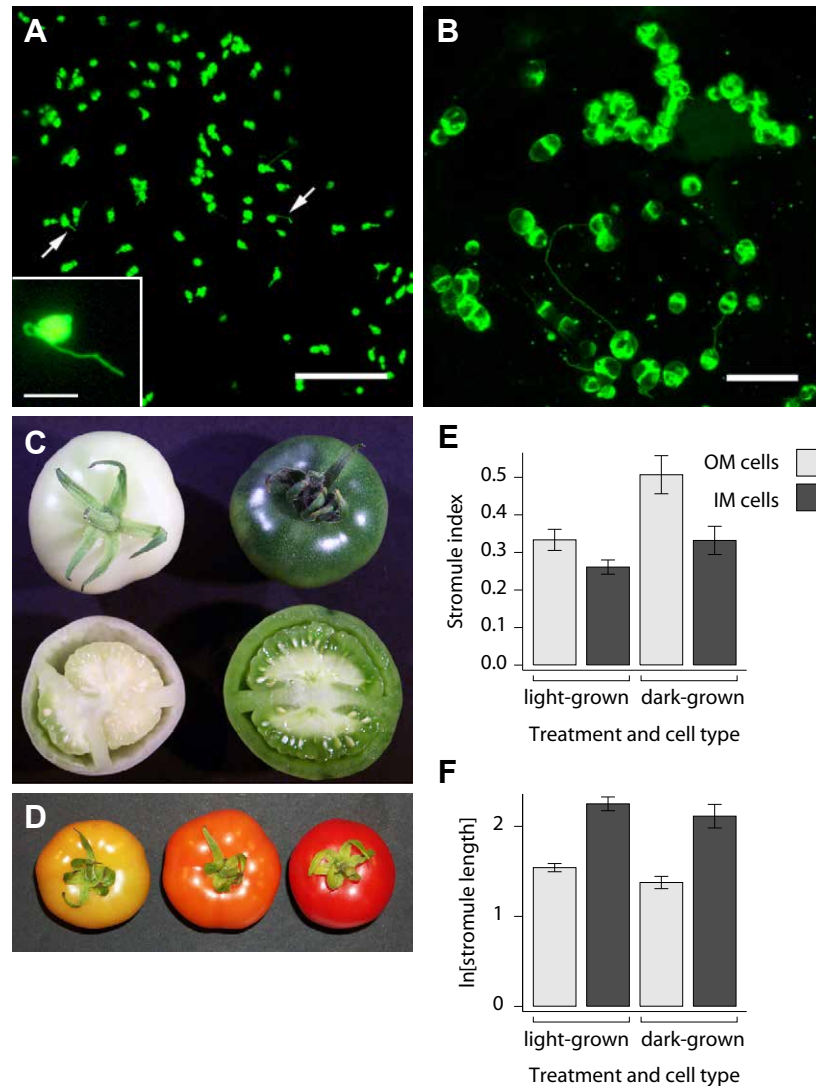


**Figure 3.7 Plastid and stromule morphology in dark- and light-grown mature green fruit**

(A) Confocal maximum projection of an OM cell from dark-grown fruit; stromules are arrowed. Inset: epifluorescence micrograph of a representative plastid from this tissue, showing a lack of chlorophyll autofluorescence. (B) Confocal maximum projection of an IM cell from dark-grown fruit. Note the prominent starch grains causing patchiness of GFP fluorescence. (C) Representative image of dark-grown and light-grown fruit at approximately similar (MG) stages of development. (D) Dark-grown fruit ripen normally. Approximate stages (left to right): B+3, B+5, B+9. (E) Stromule index and (F) stromule length in dark- and light-grown fruit. Bar heights represent the mean  $\pm$  1 S.E. Scale bars: 40  $\mu$ m (inset 5  $\mu$ m).

### 3.2.5 The *rin* mutation dramatically decreases stromule abundance in tomato fruit

The *gfp* transgene was introduced into the *rin* mutant background by crossing. Plastid morphology is indistinguishable from that of wild type during the green stages of fruit development before breaker is reached, with the mesocarp plastid dimorphism readily apparent in MG fruit (data not shown). By 40 days post-“breaker”, *rin* fruit are hard and yellow (Figure 3.8 C), since most chlorophyll has been lost but the major carotenogenic pathways have not been activated, as is evident from the yellow appearance of the plastids (Figure 3.8 D). Much of the plastid dimorphism has been lost by this stage: in both IM and OM cells, plastid size and density are similar to one another, but dramatically different from wild type when compared to either MG or B+7 fruit (Table 3.2). The plastids in yellow *rin* fruit are small and numerous in comparison to wild type mesocarp cells, and are relatively regular in shape. The plastids appear to be arrested in development just beyond the point at which the chloroplasts begin to differentiate – that is, chlorophyll is lost but no other aspects of normal chromoplast formation take place. Moreover, the plastids in yellow *rin* fruit often appear in a state of division, or to have recently carried out division (Figure 3.8 A, B); this is supported by the data indicating the greatly increased plastid density and reduced plastid size (Table 3.2).

The loss of plastid dimorphism across the mesocarp is also reflected in the stromule architecture in *rin* fruit: long, extensive stromules are entirely absent and are replaced by rather limited protrusions that are sometimes vesicular in nature (Figure 3.8 A, B). When analysed quantitatively, the OM-IM differences in stromule frequency largely disappear, as there is no significant difference between these two cell types in B+40 *rin* fruit ( $P=0.22$ , Mann-Whitney). Furthermore, relative to wild type B+7 fruit, stromules are less common in IM cells but more so in OM cells of *rin* fruit (Figure 3.8 E). As is clear from the images, stromules are much shorter in *rin* B+40 fruit than in wild type B+7 fruit

in both IM and OM cells, but there is still a small and significant difference in stromule length between OM and IM cells within the mutant fruit ( $P=0.01$ , Mann-Whitney; Figure 3.8 F and Table 3.2). This suggests that there remains some aspect of plastid dimorphism even at this late stage of fruit development, although it is much reduced relative to wild type fruit. These data indicate that the *rin* mutation has a major impact on stromule morphogenesis. Since the stromules are frequently observed extending and retracting into the cytoplasm (data not shown), it is unlikely that the results are artefacts of inactivity associated with senescing cells. The fact that the stromules are motile and formed quite readily indicates that the basic machinery for stromule formation and movement are not compromised in this mutant. Therefore, the dramatic effects on stromule behaviour are an indirect result of a block on plastid development.

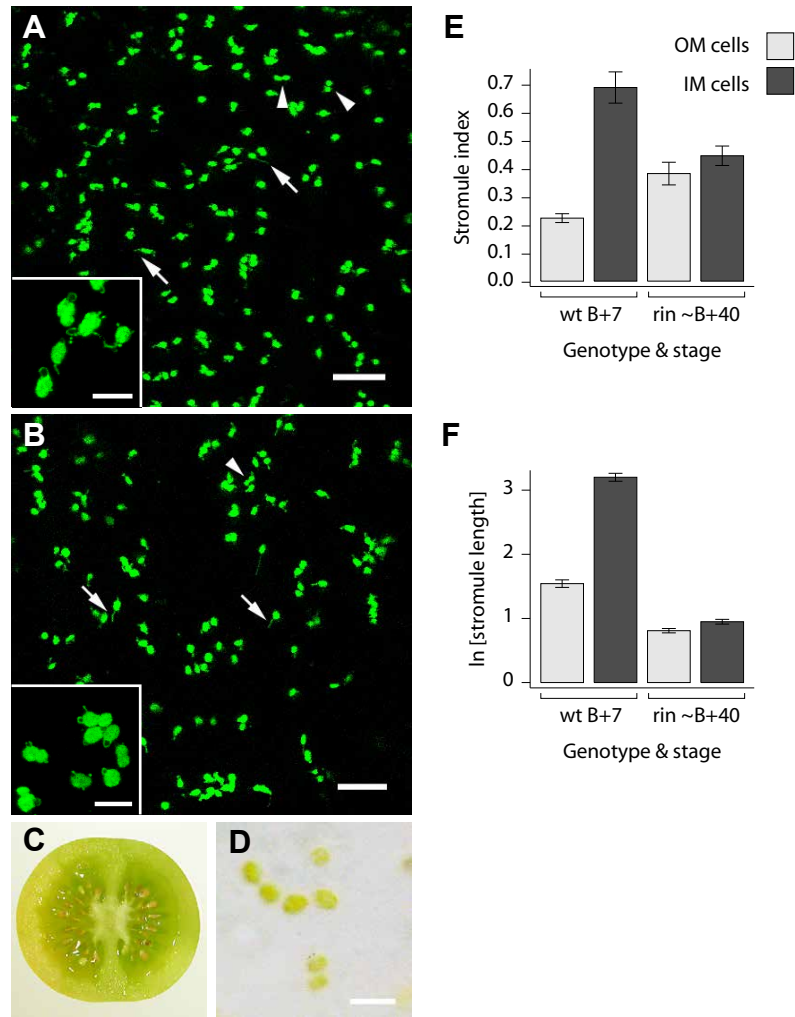


**Figure 3.8 Plastid and stromule morphology in *rin* fruit at B+40**

Confocal maximum projections of (A) OM and (B) IM cells from full yellow B+40 *rin* fruit. Note the conspicuously small plastids and short stromule protrusions (arrows). Some plastids appear to have divided recently (arrowheads). Insets show loops and short protrusions typical in this mutant. (C) Cross-section of a representative *rin* fruit and (D) brightfield image of typical plastids. (E) Stromule index and (F) stromule length in *rin* B+40 fruit compared to wild type B+7 fruit. Bar heights represent the mean  $\pm$  1 S.E. Scale bars: (A), (B): 20  $\mu$ m (insets 10  $\mu$ m); (D): 10  $\mu$ m.

### 3.2.6 The *high pigment-1* mutation has no consistent effect on stromule abundance in tomato fruit

The *hp-1* fruit pigmentation phenotype was not dramatic when compared to wild type, with a slightly deeper pigmentation in ripe fruit but not in MG fruit (Figure 3.9 A). To confirm that the fruit were from homozygous *hp-1* mutants, the seeds were harvested and screened based on the exaggerated photomorphogenic phenotype of *hp-1* (Figure 3.9 B). One hundred percent (18/18) of the seeds sown exhibited short, purple hypocotyls, implying that the crossed line was breeding true with respect to *hp-1*.

Plastid and stromule morphology was analysed in OM and IM cells at both MG and B+7 stages of fruit development in *hp-1*. Plastid dimorphism across the mesocarp was evident in the mutant (Figure 3.10 A-D). The plastids appeared morphologically identical to wild type, except that a much greater proportion of OM cell chromoplasts possessed the needle-like lycopene crystal deformations, which were often several micrometres in length (Figure 3.10 C). The *hp-1* mutation is reported to exhibit a greater density of plastids in pericarp tissue (Cookson *et al.*, 2003). However, there was no significant difference in plastid index between the wild type and *hp-1* at either MG or B+7 in both OM and IM cells (M-W,  $P > 0.05$ ; Figure 3.10 E). There appeared to be a slight decrease in plastid index within IM cells in both genotypes between MG and B+7, suggesting that the mesocarp cells expanded slightly during ripening (Figure 3.10 E). There was, nonetheless, a significant difference in plastid plan area between wild type and *hp-1*: plastids in IM cells of *hp-1* were larger on average (M-W,  $P < 0.05$ ), but not in OM cells where there was no appreciable difference (Figure 3.10 F). Thus, while it appears that the density of plastids is no different in the mutant, plastid size is greater but only in one population of plastids.

Like in wild type fruit, the *hp-1* mutant shows no significant difference in stromule frequency between OM and IM cells at MG but a large distinction at B+7 (Figure 3.10G). There is no difference in stromule frequency in OM cells between the two genotypes, and, whilst there is a significant increase in stromule frequency in IM cells of *hp-1* fruit at MG relative to wild type (M-W,  $P < 0.01$ ), this is reversed by B+7 (Figure 3.10 G). Thus, the effect of the *hp-1* mutation on stromule frequency is inconsistent across fruit development. In terms of stromule length, the typical difference between OM and IM cells is apparent in *hp-1*, but again there is no consistent difference between the two genotypes. Stromules in OM cells are approximately the same length at MG, but at B+7 they are much shorter in *hp-1* (Figure 3.10 H). This may be due to the increased deposition of lycopene crystals, which in itself may be a phenotype of *hp-1*, thus reducing the amount of membrane available for stromule formation (see Discussion). In IM cells, stromule length is greater in *hp-1* than wild type at MG, but this difference is again reversed by B+7 (Figure 3.10 H). Likewise, this increase at MG may be a direct result of increased plastid size and increased membrane availability.

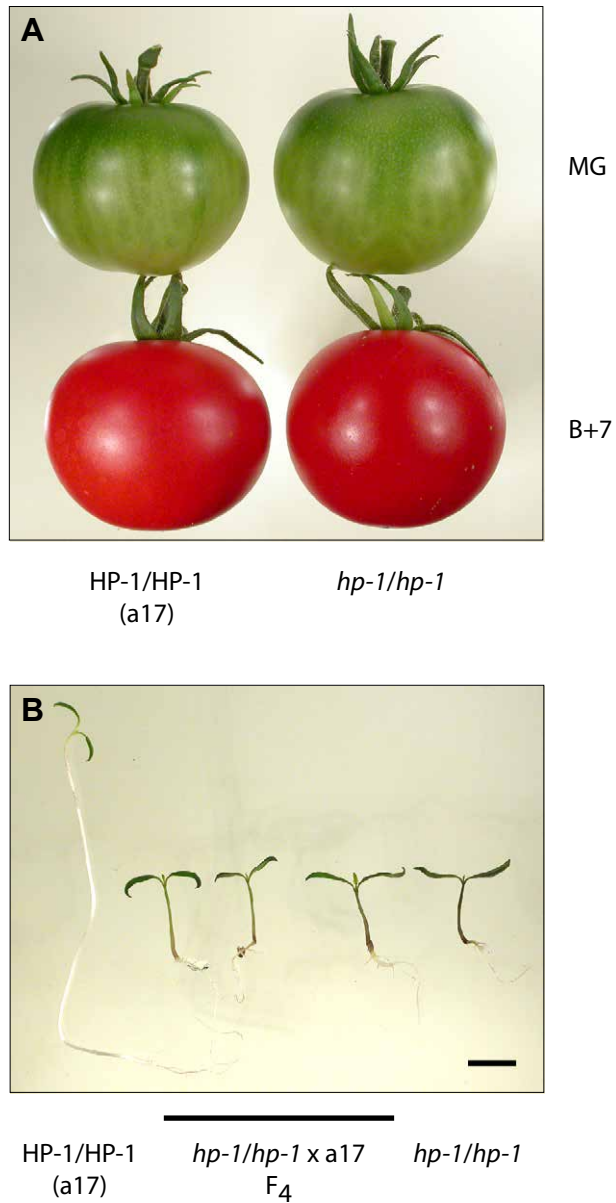
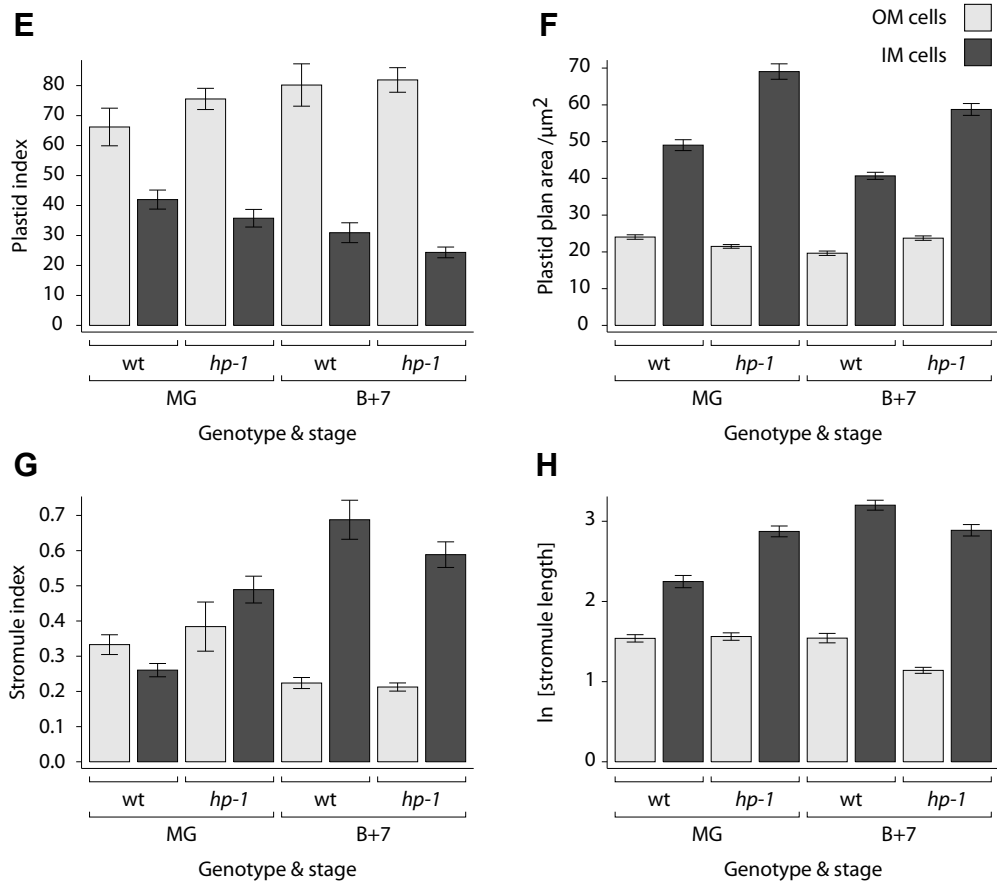
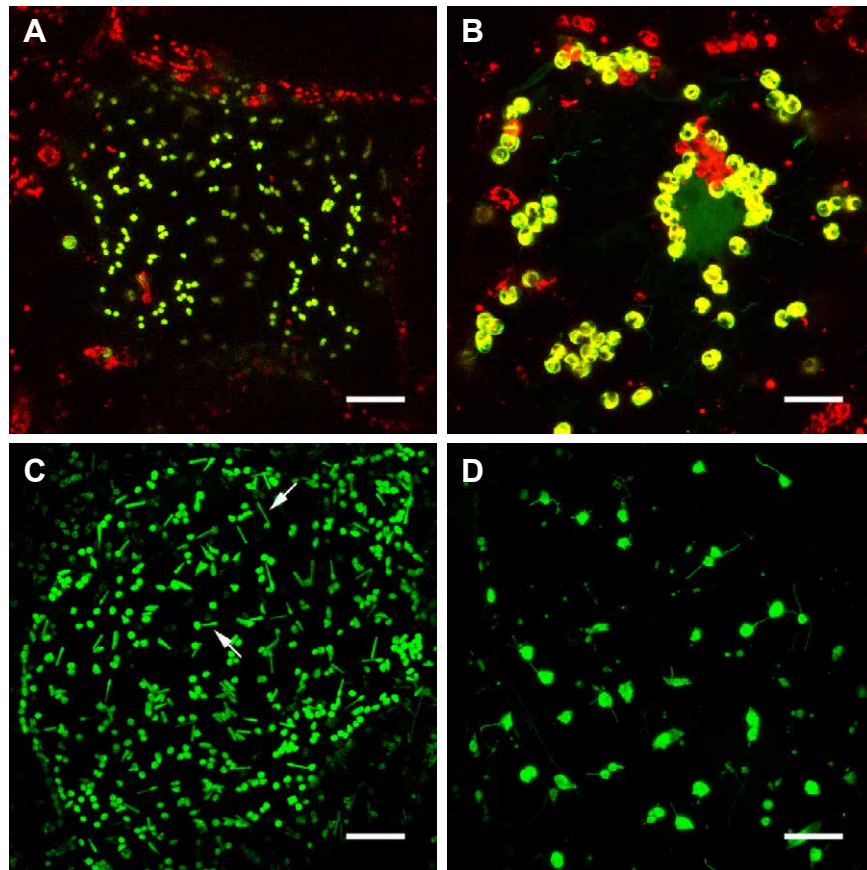


**Figure 3.9 The *hp-1* phenotype**

(A) Fruit. Note the subtly deeper red of *hp-1* B+7 fruit compared to the wild type (in this case, the a17 parental line). (B) Exaggerated photomorphogenic phenotype of *hp-1* seedlings. Seeds were germinated on nutrient agar media in sterile plastic pots, and wrapped in two layers of foil for 7 days. After this time, the foil was removed and the seedlings allowed to de-etiolate for 2-3 days. Wild type (a17) seedlings exhibited a long, pale hypocotyl (left). Hypocotyls of *hp-1* mutant seedlings were much shorter and accumulated substantial amounts of anthocyanin (right). Three representative seedlings from the F<sub>4</sub> generation of a cross between a17 and *hp-1* are shown, indicating the inheritance of the *hp-1* phenotype. Scale bar: 2 cm.

**Figure 3.10 Plastid and stromule morphology in *hp-1* fruit at MG and B+7**

Confocal maximum projections of (A, C) OM and (B, D) IM cells from MG (A, B) and B+7 (C, D) *hp-1* fruit. Note the clear OM-IM plastid dimorphism, and the abundance of lycopene crystal distortions in chromoplasts in (C), arrowed. (A) and (B) show a combination of chlorophyll autofluorescence and GFP signals. (E-H) Quantification of plastid morphology in *hp-1* fruit at MG and B+7 in comparison to wild type. (E) Plastid index, a measure of number of plastids per unit area; (F) plastid plan area; (G) stromule index; (H) stromule length. Bars represent  $\pm 1$  S.E. Scale bars: 40  $\mu\text{m}$ .



### 3.3 DISCUSSION

Previous studies into the distribution of stromules between different plastid and cell types have shown that they are highly variable for reasons which are unclear (Köhler and Hanson, 2000; Pyke and Howells, 2002). The data described here show that plastid differentiation and plastid size can independently influence the frequency and extent of stromules, thus providing insight into some of the developmental factors that regulate their formation.

#### 3.3.1 Mesocarp plastid dimorphism

Tomato fruit mesocarp contains two morphologically distinct populations of plastids, which differ in plastid size and number. A difference in tomato fruit pigmentation across the pericarp has been reported before: Lois *et al.*, (2000) reported that the most intense pigmentation resides in the peripheral regions of the pericarp, which coincides with the OM cells and their densely packed plastids. Two types of tomato fruit chromoplast have been documented previously (Rosso, 1967; Harris and Spurr, 1969b), which resemble closely the needle-like OM and ovoid IM chromoplasts described here. Moreover, Öztig (1962) noted that the chromoplast shape varies with position of the cell in the fruit. These two types of chromoplast are derived from progenitor chloroplasts that also exhibit dimorphism; however, the plastids present in IM cells of MG fruit may be better considered as amyloplasts, for the following reasons. Firstly, both the presence of starch in these plastids of dark-grown fruit and the subsequent normal fruit ripening indicate that fruit photosynthesis is not essential for starch production or for fruit development. Secondly, tomato fruit are sink organs and no net photosynthesis occurs in mature green fruits (Ho and Hewitt, 1986). IM plastids of MG fruit are thus atypical of chloroplasts in general, and therefore their morphology and associated stromules do not closely resemble those of other chloroplasts. Amyloplast stromules (Langeveld *et al.*, 2000) and protrusions containing starch grains (Bechtel and Wilson, 2003) have

been reported in wheat endosperm, and estimates of the length of amyloplast stromules in this tissue range from 2-30  $\mu\text{m}$  (Langeveld *et al.*, 2000), comparable to the IM cell plastid stromules from MG fruit.

The increase in stromule abundance during chromoplast differentiation only occurs in IM cells, suggesting that attainment of the chromoplast state *per se* is not sufficient for increased stromule abundance. This presents two aspects to be explained, namely why there exists such a dramatic difference in plastid morphology between OM and IM cells, and why the increase in stromule abundance is specific to IM cells. The plastid dimorphism originates from the early stages of fruit development, when starch distribution is non-uniform throughout the pericarp (Ho and Hewitt, 1986). It is unclear why the starch-storing plastids in IM cells should be less densely packed than non-storing ones of OM cells. Amyloplasts in wheat endosperm can be 10  $\mu\text{m}$  or more in diameter (Langeveld *et al.*, 2000), probably as a result of the starch granule expansion. Rapid starch granule deposition in IM cell plastids may restrict plastid division while the cell continues to expand during fruit growth: a similar observation in wheat endosperm prompted Bechtel and Wilson (2003) to speculate that amyloplasts may divide by some form of budding. This decreased plastid number/increased plastid size then persists through to the chromoplast stage, resulting in the large ovoid chromoplasts typical of IM cells. In OM cells however, where bulky starch granules do not restrict plastid division, the plastids are smaller and attain a higher number within the cell, and maintain this state as chromoplasts in ripe fruit.

### 3.3.2 Stromule formation depends on plastid differentiation and plastid size

Besides the dramatic changes that occur upon chromoplast differentiation, the negative impact of chloroplast components on stromule formation further demonstrates that plastid differentiation is a major contributor to the process. Stromules are less common

in IM cells of B+7 *gf* fruit than in wild type because the plastids in these cells are still chloroplast-like in nature, and thus express some morphological features typical of chloroplasts. The *gf* mutation had no effect in OM cells, reflecting the relative constancy of plastid morphology in this tissue in wild type fruit. Similarly, the *rin* mutation shows how blocking plastid differentiation affects stromule formation. By B+40 the plastid dimorphism in the mesocarp has largely disappeared, implying that substantial plastid division must have occurred post-breaker, especially in the IM cells. Stromules are also remarkably similar between the two cell types, with absolute differences being small. These observations suggest that the nature of plastid stromules is much more closely related to the differentiation status of the plastid in question rather than the cell type. By blocking chromoplast development, the morphology associated with chromoplasts and the two plastid populations are lost.

In general, smaller plastids produce the shortest stromules (Table 3.2), presumably due to limited amounts of membrane available to be incorporated into them. Perhaps a more accurate assertion would be that plastid size places an upper limit on the length of a stromule. However, whilst mesophyll chloroplasts are amongst the largest plastids in a plant, they produce relatively short stromules (Gray *et al.*, 2001), indicating that there must be other factors that control stromule formation. Little is known about the molecular regulation of plastid and organelle morphology in plants, but changes in membrane elasticity and amenability to distortion may be one contributing factor to stromule formation. Members of the FtsZ family of proteins have been implicated in regulating chloroplast shape (Kiessling *et al.*, 2000). FtsZ proteins are involved in chloroplast division in both higher and lower plants, and share structural and functional similarity to tubulins (Osteryoung and McAndrew, 2001). Overexpression of an FtsZ-GFP fusion protein in *Physcomitrella patens* showed a filamentous, reticulate scaffold of FtsZ apparently just below the plastid envelope (Kiessling *et al.*, 2000), suggesting that plastids maintain their shape by means of a proteinaceous “plastosome”,

although this may be an artefact of FtsZ overexpression (Vitha *et al.*, 2001). Nevertheless, it has been confirmed that the actin cytoskeleton is at least partially responsible for stromule movement (Kwok and Hanson, 2003), so it is conceivable that the ability of actin microfilaments to distort the plastid membrane is related to its elasticity as determined by some plastidial structural component. Changes in stromule length and frequency may be a result of changes in plastid membrane amenability to deformation, increased plastid-cytoskeletal activity or a combination of both. In addition, the increase in chromoplast membrane availability may be enhanced by the break-up of thylakoid membranes and their incorporation into stromules. Accordingly, OM cells of wild type may fruit possess fewer and shorter stromules than IM cells because of a fundamental, developmentally early difference in plastid size and hence membrane availability. Upon ripening, the large IM plastids lose some chloroplast/amyloplast structural features and the plastid envelope attains a form more amenable to stromule biogenesis. Consequently, plastids at the transitional stages of chloroplast-chromoplast differentiation have intermediate forms.

### 3.3.3 Is plastid density important in determining stromule formation?

It is notable that long stromules are associated with plastids that are further apart, whereas short stromules are present in cells with a high density of plastids (Table 3.2). A test of the effects of plastid density on stromule formation was attempted with the *hp-1* mutant, but no significant difference in plastid density was observed between the mutant and wild type, although there was a difference in plastid size in IM cells (Figure 3.10). This increase in plastid size, but not plastid density, may be the primary cause of the increased pigmentation reported for this mutant (Cookson *et al.*, 2003). Furthermore, the particularly large plastids in IM cells of MG *hp-1* fruit may account for the marginal differences in stromule length relative to wild type. However, no consistent or dramatic effect of *hp-1* on stromule abundance could be detected. The *hp-1* mutant

thus did not provide any insight into the effects of plastid density, perhaps because the impact of the mutation on plastid density was insufficient to reveal such a link.

How might stromules benefit plastid activities in mesocarp cells? In IM cells, the increase in stromule membranes would improve metabolic contact between the plastid and the cytosol. In OM cells, the higher density of plastids would not require this. In MG fruit, stromules may be important in starch generation, by acting as a surface for import of hexose phosphates from the cytosol. Once the fruit begins to ripen, stromules might provide greater import area for novel proteins involved in carotenoid biosynthesis and chromoplast differentiation (Camara *et al.*, 1995). The data presented in Table 3.2 allow an estimation of the relative contribution of stromules to plastid surface area and volume (for calculations, see Appendix). In the case of an average IM cell chromoplast at B+7, a single stromule of 33  $\mu\text{m}$  in length occupies just 9.6% of the plastid volume, but constitutes some 36% of the total plastid surface area (assuming that the plastid body is a sphere and the stromule a uniform cylinder of 0.9  $\mu\text{m}$  in diameter). Using the mean values for the proportion of plastids with stromules, a similar estimate can be made of the impact of stromules on total, cellular plastid surface area. In an average IM cell at B+7, 18% of the total plastid surface area but only 4% of the total plastid volume is attributable to stromules. Thus, stromules do not only improve surface area at minimal expense to volume on a plastid-by-plastid basis, but also for the entire cell, provided sufficient plastids possess them.

### 3.3.4 Conclusions

Evidently, plastid differentiation influences stromule biogenesis. However, this effect is not universal since plastid size, and perhaps membrane flexibility, are also important factors. The possible influence of the density of plastids within the cell could not reliably be established using tomato fruit pericarp as a system, and this will be investigated

by other means in Chapter 4. The extremes in stromule size and frequency in the inner mesocarp of ripe fruit suggests that this tissue would be a good source from which to isolate stromules, and this presents a promising avenue for future research. Additionally, the existence of two distinct populations of chromoplast in the ripe fruit may be associated with the accumulation of differing profiles of carotenoids. If this be the case, tissue-specific regulation of carotenoid biosynthesis genes may improve the nutritional benefit of tomato fruit.

# 4 FACTORS INFLUENCING STROMULE BIOGENESIS IN TOBACCO HYPOCOTYL EPIDERMIS

## 4.1 INTRODUCTION

### 4.1.1 Seedling development

Tobacco and *Arabidopsis* are both examples of epigeal seedlings, in which the cotyledons penetrate the soil upon germination to reach the light and become photosynthetic, providing a source of energy for seedling establishment. To achieve this, the seedling must sense light and implement a developmental programme appropriate to the conditions. Germinating seedlings have two alternative paths of development based on the detection of light. When grown in the light, a seedling produces a short hypocotyl, the cotyledons expand and chloroplasts develop. In addition, root growth is promoted and the shoot apical meristem activated in preparation for post-seedling development. This mode of development is called photomorphogenesis, and in the case of tobacco the hypocotyl reaches about 2-3 mm in length before leaf development is initiated. In the absence of light, a seedling undergoes skotomorphogenesis, where endosperm resources are prioritised towards obtaining light and post-seedling development is inhibited. The key features of skotomorphogenesis are a greatly elongated hypocotyl (which may reach over 40 mm long in tobacco), reduced root development and a failure of the cotyledons to green and enlarge. Cotyledonary plastids assume the etioplast state, primed for conversion to chloroplasts upon exposure to light. De-etiolation occurs when light is encountered: the cotyledons green, hypocotyl elongation stops and the seedling embarks on further development. The decision to follow one path of development over the other is of critical adaptive significance: skotomorphogenesis is essential in order for a buried seedling to clear the soil, but competition for light and other resources means a rapid transition to autotrophic growth is equally important to survival.

#### 4.1.1.1 Photomorphogenesis is regulated by photoreceptor proteins

Plants are able to detect different wavelengths of light through the action of specific classes of photoreceptors. These proteins form three groups according to the wavelength of light they perceive: the phytochromes respond to red and far-red light (600-750 nm), whereas the cryptochromes and phototropins respond to the blue/UV-A region of the spectrum between 320-500 nm (Sullivan and Deng, 2003). In terms of directing developmental responses to changes in light quality and quantity, the phytochromes and cryptochromes are the important receptors (Smith, 2000; Lin, 2002), whilst phototropins control directional growth (phototropisms) and chloroplast avoidance movement (Briggs and Christie, 2002; Wada *et al.*, 2003). Photomorphogenesis is thus brought about by the detection of red and/or blue light by co-ordination between the phytochromes and cryptochromes, followed by signal transduction to the cell nucleus, triggering dramatic changes in expression of about 2500 genes in *Arabidopsis* (Tepperman *et al.*, 2001).

##### 4.1.1.1.1 Phytochromes

Phytochromes, for which there is a small family of five genes in *Arabidopsis* (*phyA-E*), are 125 kDa chromoproteins that form homodimers *in vivo*. The different phytochromes have overlapping but distinct roles in plant development. For example, phyA and phyB predominantly act during seedling establishment, whilst phyE regulates plant architecture during later stages of development for purposes such as shade avoidance (Smith, 2000). Each polypeptide contains a tetrapyrrole chromophore called phytychromobilin that is covalently attached to the N-terminus of the protein. The chromophore is responsible for light absorption and directing the conformational changes in phytochrome structure that occur upon activation (Smith, 2000). All phytochromes exist in two interconvertible forms: Pr, the biologically inactive form that absorbs red light, and Pfr, the active form that absorbs far-red. Upon absorption of red light by the

chromophore, Pr is converted to Pfr, triggering a biochemical response. Phytochrome-GFP fusions show that upon activation, phytochrome translocates from the cytoplasm into the nucleus where it forms a punctate pattern of fluorescence which may represent 'multimolecular transcriptome complexes' acting on the promoters of photoresponsive genes (Quail, 2002).

Using a yeast two-hybrid screen, Ni *et al.* (1998) identified a nuclear-localised phytochrome-interacting factor, PIF3, a member of the basic helix-loop-helix (bHLH) family of transcriptional activators. In *Arabidopsis* plants antisense for *PIF3*, normal photosensiveness is compromised, with transcript levels for chlorophyll *a/b* binding protein (*CAB*) and chalcone synthase (*CHS*) much reduced relative to wild type (Ni *et al.*, 1998). Further work showed that phyB binds to PIF3 in a reversible, far-red-dependent manner (Ni *et al.*, 1999). Moreover, PIF3 binds in a sequence-specific fashion to a G-box DNA sequence found in the promoters of many photoresponsive genes including *CIRCADIAN CLOCK-ASSOCIATED PROTEIN1* (*CCA1*) and *LATE ELONGATED HYPOCOTYL* (*LHY*) (Martínez-García *et al.*, 2000). The binding of phyB to PIF3 can occur while PIF3 is bound to the G-box *in vitro*, but only following photoactivation of phyB (Martínez-García *et al.*, 2000). Although it is yet to be shown that binding of active phytochrome to PIF3 specifically promotes transcription of *CCA1* and *LHY*, the rapid and transient induction of these genes following exposure of seedlings to red light strongly suggests that this is the case (Martínez-García *et al.*, 2000). Most significantly, *CCA1* encodes a MYB-class transcription factor that positively regulates the expression of *CAB* genes (required for chloroplast biogenesis), indicating that PIF3 is a major entry point for phytochrome signal transduction in bringing about photomorphogenesis (Quail, 2002). Recently it has been shown that PIF3 is rapidly degraded in the nucleus upon transfer to the light, suggesting it acts transiently as the major phytochrome-based switch from skotomorphogenic to photomorphogenic development (Bauer *et al.*, 2004).

#### 4.1.1.1.2 Cryptochromes

The cryptochromes are flavoproteins of 70-80 kDa in size. They absorb light through two chromophores attached to an amino-terminal domain which shows homology to DNA photolyases, light-activated DNA repair enzymes found in a wide variety of prokaryotic and eukaryotic microbes (Lin, 2002). In *Arabidopsis* there are two cryptochrome genes, *CRY1* and *CRY2*, encoding proteins with similar amino termini but distinct carboxy termini (Lin, 2002). Unlike phytochromes, cryptochromes are constitutively nuclear (Kleiner *et al.*, 1999; Más *et al.*, 2000). Cryptochromes have been implicated in regulating the degree of hypocotyl elongation in a dose-dependent manner: *Arabidopsis* *CRY1* and *CRY2* were isolated in screens for impaired inhibition of hypocotyl elongation in blue light, and overexpression of both *CRY1* and *CRY2* leads to a short hypocotyl phenotype in blue light (reviewed in Lin, 2002).

The exact nature of cryptochrome signalling action is unknown, but photoactivation by blue light may involve a redox reaction either within the flavoprotein itself or between protein partners (Lin, 2002). Although there have been various reports of cryptochromes interacting directly with phytochromes both physically and in a genetic sense (Más *et al.*, 2000; Neff and Chory, 1998), cryptochromes are thought to act primarily by triggering the post-translational degradation of inhibitors of photomorphogenesis. A collection of eleven *Arabidopsis* loci, designated *COP/DET/FUS*, has been identified as responsible for regulating photomorphogenesis. Mutants in these genes show photomorphogenic development in the dark that closely mimics wild type development in the light, and the recessive, pleiotropic nature of such mutations indicates that the genes act to negatively regulate photomorphogenesis in the dark (Wei and Deng, 1996). Eight of these eleven genes encode proteins that form a nuclear complex called the COP9 signalosome, which possesses structural and biochemical similarity to part of the 26S proteasome responsible for the degradation of ubiquitylated proteins (Sullivan *et al.*, 2003). Another member of the class - COP1 (constitutively photomorphogenic1) -

has a light-regulated nucleocytoplasmic partitioning whereby it is nuclear-enriched in the dark but shuttles to the cytoplasm in the light (von Arnim and Deng, 1994). COP1 is postulated to be an E3 ubiquitin-protein ligase, which targets specific proteins for degradation by ubiquitylation (Osterlund *et al.*, 2000). Another protein required for light-regulated development is HY5, a basic leucine zipper transcription factor that also binds to the G-box in light-responsive promoters and interacts with COP1 *in vivo* (Osterlund *et al.*, 1999). It is thought that COP1 labels HY5 for degradation, probably by the COP9 signalosome, preventing it from promoting the transcription of downstream genes (Osterlund *et al.*, 1999, 2000). Thus, in the light, translocation of COP1 to the cytoplasm, and/or its degradation in the nucleus, allows HY5 to accumulate, leading to the transcription of downstream genes and the onset of photomorphogenesis. Significantly, it has recently been demonstrated that CRY1 physically interacts with COP1 in a light-dependent manner (Wang, Ma *et al.*, 2001; Yang *et al.*, 2001). Moreover, the constitutive photomorphogenic phenotype of *cop1* mutants is epistatic to the *cry1* mutant; that is, *COP1* acts downstream of *CRY1* (Ang and Deng, 1994). Thus, although the mechanism for COP1 translocation or degradation in response to light has yet to be elucidated, CRY1 is a prime candidate for mediating this change and releasing the repression of photomorphogenesis by the COP9 signalosome. It should also be noted that successful photomorphogenesis of *cry1;cry2* double mutants in white light indicates that phytochromes, in addition to cryptochromes, also act through the *COP/DET/FUS* pathway.

The control of seedling development is thus subject to both positive (promotory) and negative (repressive) factors. For example, the activation of *CCA1* and *LHY* expression by PIF3 is promoted by the conversion of Pr to Pfr by red light; in this sense, molecular processes leading to photomorphogenesis are “switched on”. However, the removal of the COP1 and the COP9 signalosome by CRY1 suggests that certain aspects of photomorphogenesis are actively repressed until a light signal is received. This reflects the

fact that a concerted photomorphogenic response takes place on several molecular and physiological levels; whilst the phytochromes and cryptochromes both detect and respond to light, their diversity allows plastic development in the face of variation in quality, quantity, duration and direction of light.

#### 4.1.1.2 The long and short of it: cellular regulation of hypocotyl growth

Ultimately, the effects of light on seedling development must be translated into physiological changes, including substantial hypocotyl growth. Hypocotyl cells are formed in the embryo and do not undergo division during seedling growth, implying that all hypocotyl elongation is due to cell expansion, at least in *Arabidopsis* (Gendreau *et al.*, 1997). Extensive cell wall modification must occur to allow for this expansion, involving both the loosening of pre-existing structures and the laying down of new components. A rapid uptake of water into the vacuole is necessary to produce turgor pressure to drive this expansion. The *det3* mutant, defective in hypocotyl elongation in the dark, encodes a vacuolar H<sup>+</sup>/ATPase subunit that may be important in regulating the vacuolar uptake of water (Schumacher *et al.*, 1999). Whilst the vacuole produces the force, the cytoskeleton is responsible for regulating the direction of cellular expansion. The association of the cellulose synthase complex with cortical microtubules means that microtubule alignment determines the direction of cellulose microfibril deposition and thus cell elongation (Lloyd and Chan, 2004). Moreover, actin microfilaments must align with the direction of cell growth since they are responsible for the transport of Golgi-derived vesicles to the apoplast for cell wall synthesis.

There are also cellular differences between light- and dark-grown hypocotyls. Light-grown hypocotyl epidermal cells exhibit an acropetal differentiation pattern and grow in a uniform manner. However, dark-grown epidermal cells do not differentiate and instead grow non-uniformly: a zone of rapid cell elongation moves in an acropetal di-

rection as skotomorphogenesis proceeds (Gendreau *et al.*, 1997). Furthermore, epidermal cells from dark-grown *Arabidopsis* hypocotyls perform another round of DNA endoreduplication relative to light-grown seedlings, reflecting that increased cell size correlates with DNA content in many organisms (Gendreau *et al.*, 1997). *det1* mutants, which are constitutively photomorphogenic in the dark, resemble light-grown wild type seedlings in this respect, indicating that this endoreduplication/epidermal differentiation is a developmental feature independent of other aspects of photomorphogenesis such as photosynthetic competency (Gendreau *et al.*, 1997; Nemhauser and Chory, 2002).

#### **4.1.2 Tobacco hypocotyls as a basis for studying stromules**

Tobacco hypocotyl epidermis is a readily accessible and easily obtainable tissue for microscopy. The two alternatives for seedling development provide a means to assess how factors such as plastid differentiation, cell expansion, light quality and light quantity affect stromule formation in this cell type. Tobacco is highly amenable to genetic manipulation and crossing, so producing lines containing multiple transgenes becomes a feasible experimental approach. Furthermore, this tissue has been the main subject of research in this field so far (Kwok and Hanson 2003; 2004a; 2004b). These advantages, together with the rapid growth of seedlings providing quick experimental turn-around, mean tobacco hypocotyl epidermis is an excellent system for studying stromule activity.

#### **4.1.3 Scope of the Chapter**

This Chapter describes a series of experiments that answer a broad range of related questions about stromules. Firstly, it aims to define how plastid and stromule morphology differs between photo- and skotomorphogenic seedlings. Secondly, it assesses the effects of light quality on stromule formation, and investigates how the density of plas-

tids within the cell is a significant factor in the process. Finally, this Chapter investigates the dynamic interactions between stromules and other organelles within the plant cell as a means of demonstrating a functional relationship between the two.

It should be noted that the following definitions regarding seedling development are used:

- *Photomorphogenic*: a seedling grown in the presence of light since germination (but not necessarily in continuous light);
- *Skotomorphogenic*: a seedling grown entirely in the dark since germination;
- *De-etiolated*: a skotomorphogenic seedling that has been exposed to light and has been allowed to green.

Examples of such seedlings are shown in Figure 4.2 D.

## 4.2 RESULTS

### 4.2.1 Photomorphogenic and skotomorphogenic seedlings exhibit dramatic differences in plastid and stromule morphology

Since plastid differentiation status is important in determining the extent of stromule formation, the existence of a similar effect in tobacco hypocotyl epidermis was investigated. Seeds of line MSK57xDsRED were used in these experiments. This line expresses both DsRED and GFP in the plastid, and is the F<sub>2</sub> generation of a cross between a primary transformant containing the *rbcS*-DsRED transgene and a stably transformed transplastomic line expressing *aadA*-GFP (Table 2.1; Figure 4.1). Seeds were germinated on media and incubated in a growth room either in the light (180  $\mu\text{mol m}^{-2} \text{sec}^{-1}$ ) or in complete darkness for seven days. Whilst both proteins produced a strong fluorescent signal in light-grown seedlings, often DsRED exhibited better fluorescence in the dark-grown seedlings. Thus, these seedlings provided two independent means of visualising stromules, and it was possible to select the stronger of the two signals for imaging.

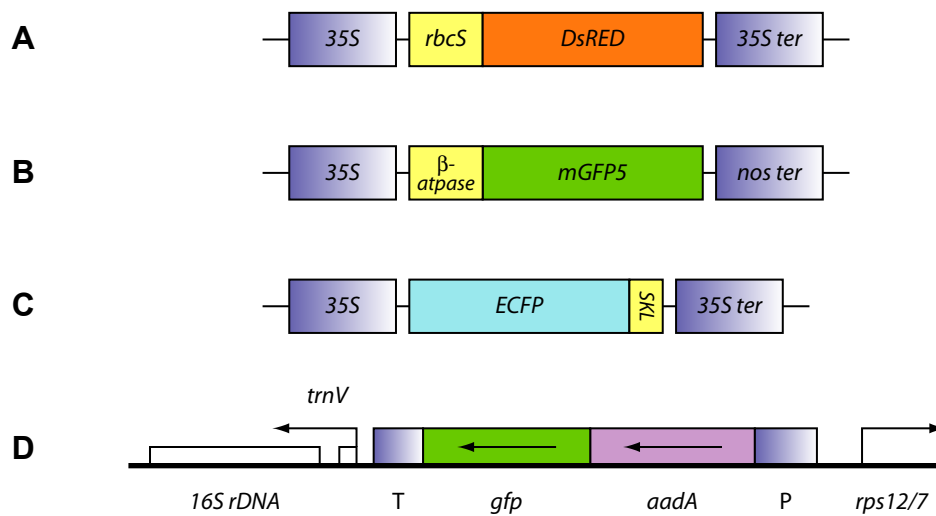


**Figure 4.1 Constructs used to follow in vivo dynamics of organelles**

Constructs A-C were used to transform the nuclear genome of tobacco. (A) Plastid-targeted DsRED. The N-terminal plastid transit peptide is derived from *Petunia* RbcS (Rubisco small subunit). (B) Mitochondria-targeted mGFP5. Targeting specificity is provided by an N-terminal portion of the *Nicotiana plumbaginifolia*  $\beta$ -ATPase. (C) Peroxisome-targeted ECFP. The tripeptide S-K-L at the C-terminus confers targeting to the peroxisome. (D) FLARE16-S2, present on the plastid genome of MKSK57. The promoter (P) is derived from the strong plastidial ribosomal RNA operon (Prn). The promoter includes the rbcL gene leader sequence immediately prior to the aadA-gfp fusion which, together with the 3' UTR from the *PsbA* gene as a terminator (T), enhances mRNA stability. The construct inserted into the tobacco plastid genome at the trnV/rps12/7 intergenic region; these regions were thus included in the plastid transformation vector to assist homologous recombination. (D) is adapted from Kahn and Maliga (1999). 35S: CaMV 35S promoter; 35S ter: CaMV 35S terminator sequence; nos ter: nopaline synthase terminator sequence.

In light-grown seedlings, plastids of the hypocotyl epidermal cells accumulate chlorophyll (as determined by chlorophyll autofluorescence; data not shown) and these chloroplasts are relatively regular in shape, adopting an oblate-spheroid form typical of leaf epidermal plastids (Figure 4.2 A). The chloroplasts form only very short, stubby stromules, which are generally quite rare, as is typical of this plastid type. In the dark however, the plastids are achlorophyllous and leucoplast-like in nature, lose their regular shape and size, and instead assume a variety of elongated, pleiomorphic forms with loops and outgrowths of the plastid membrane (Figure 4.2 B). In these cells, stromule morphology is radically different when compared to those from light-grown seedlings. The stromules are typified by extreme length (greater than 30  $\mu\text{m}$  is not exceptional) and increased regularity, with the majority of plastids exhibiting a stromule-like protrusion of some form (Figure 4.2 B). An additional and notable difference in the hypocotyl epidermal cells of light- and dark-grown seedlings is the packing density of the plastids. Faint autofluorescence of the cell walls shows that hypocotyl epidermal cells in light-grown seedlings are short relative to their width, with the cells arranged in parallel files (Figure 4.2 A). In such cells, the plastids are packed close together, with most plastids no further than 10  $\mu\text{m}$  away from its nearest neighbour. In dark-grown seedlings, the same cells are greatly elongated as is evident from the lack of transverse cell walls (Figure 4.2 B), and correspondingly the plastids are much more sparsely distributed. Occasionally, the plastids in this tissue form aggregates where several plastids assemble in a small region of the cell, but it is frequent to find plastids more than 20  $\mu\text{m}$  removed from their nearest neighbour (Figure 4.2 B).

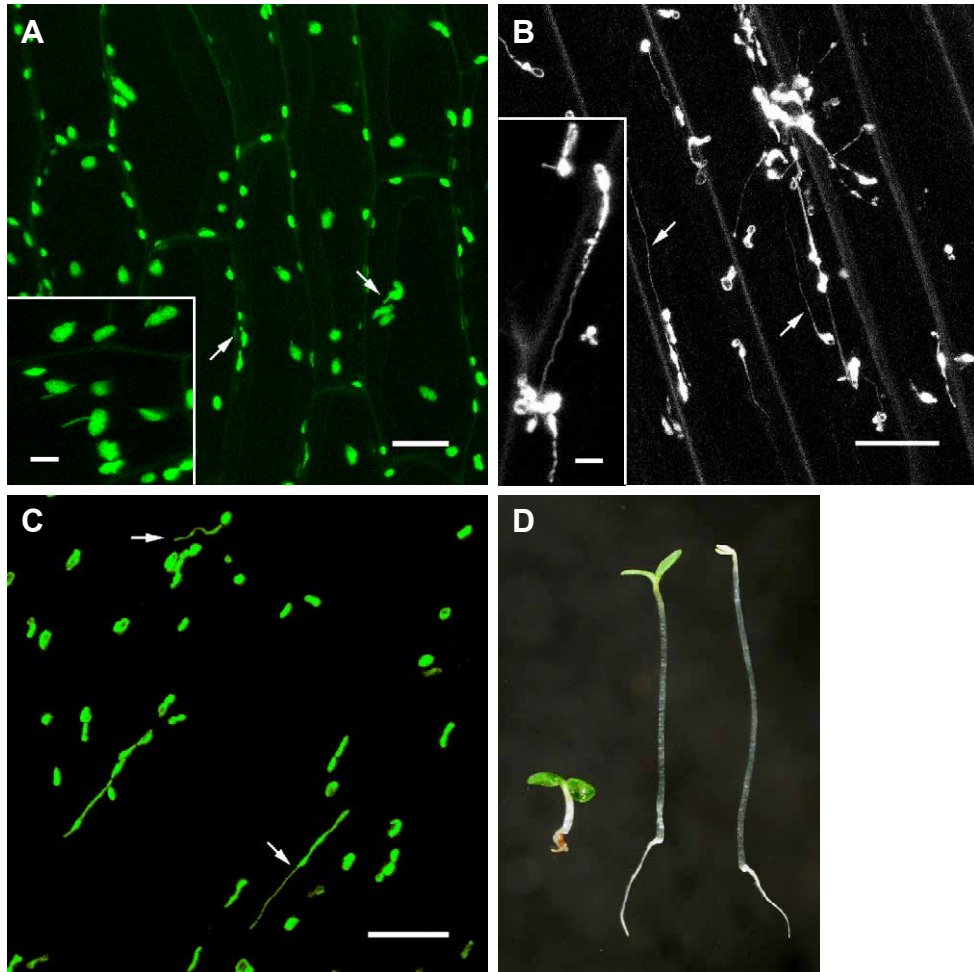


**Figure 4.2 Plastid morphology in hypocotyl epidermis depends on light**

(A) Plastids from photomorphogenic seedlings are regular in shape and have short, rare stromules (arrowed). The *aadA-gfp* signal is shown, false-coloured green. (B) Etiolated (skotomorphogenic) seedlings possess distorted, pleiomorphic plastids with long and abundant stromules (arrowed). The DsRED signal is shown here, and represented in grayscale for improved contrast. Note the faintly autofluorescent parallel cell walls, and the relative dispersal of plastids within the cells compared to photomorphogenic seedlings. (C) Dark-grown seedlings exposed to light for one day (de-etiolated seedlings) also possess long stromules and irregularly-shaped plastids, intermediate between (A) and (B). (D) Seedling morphology at seven days post-germination: left, photomorphogenic, middle, de-etiolated, right, skotomorphogenic. Scale bars: main images, 20  $\mu\text{m}$ ; insets, 5  $\mu\text{m}$ .

To examine whether this light-dark difference could be rescued by a relatively brief period of light, etiolated seedlings were exposed to white light for 24 h immediately prior to microscopy. This was sufficient time to cause the cotyledons to green partially (Figure 4.2 D); moreover, it improved the expression of *aadA*-GFP. However, it did not result in the elimination of long stromules or the formation of regularly shaped plastids like those observed in photomorphogenic seedlings (Figure 4.2 C). In terms of plastid form and plastid density, these de-etiolated seedlings appeared to be intermediate between photo- and skotomorphogenic seedlings. This suggests that the hypocotyl epidermal cells of these seedlings contained incompletely differentiated chloroplasts, perhaps explaining the intermediate stromule length and frequency observed.

The effect of light on seedling development is an intensely studied phenomenon. The two alternative modes of seedling development (photomorphogenesis and skotomorphogenesis) exhibit starkly contrasting characteristics, the most notable differences being in cotyledon development and hypocotyl elongation. The observed changes in plastid morphology between light-grown and dark-grown seedlings suggest that whilst plastid differentiation status is important in determining stromule abundance, this may not be the sole factor since seedling development in the light and dark differs by more than simply plastid differentiation. To investigate this issue further, the effects of light quality (i.e. wavelength) on stromule formation were first considered.

#### **4.2.2 Blue and red light, provided at low intensity, increase stromule formation relative to white light**

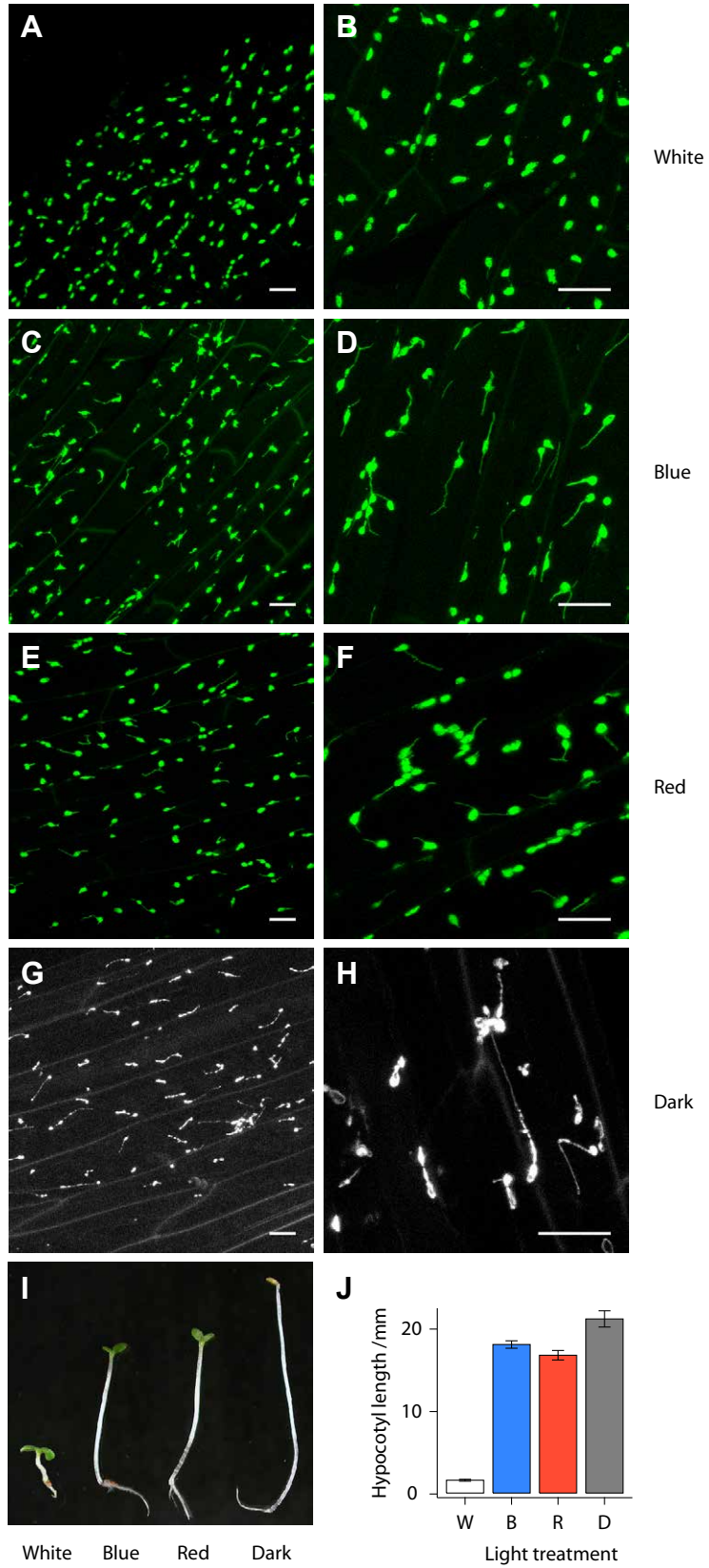
Both red and blue light are capable of directing photomorphogenesis, but they are detected by distinct families of photoreceptors (Sullivan and Deng, 2003). The movement of chloroplasts in response to high and low light intensities is brought about specifically by blue light, mediated by the phototropins; red light is unable to produce this effect

(Wada *et al.*, 2003). This suggests that plastids are capable of responding to different wavelengths of light in differing manners. Furthermore, the fact that chloroplasts possess a certain degree of autonomy in their movement responses to blue light (Wada *et al.*, 2003) indicates that the mechanisms for movement may be accessible by every plastid in an independent manner, which is an unambiguous mark of stromules. Given also that blue light-mediated chloroplast movement is mediated by the actin cytoskeleton, it is reasonable to infer that there may be common features between this process and stromule formation. Likewise, a feasible hypothesis may be that blue light induces a specific change in plastid morphology that red light does not. In order to test this notion, MSK57xDsRED seeds were germinated on nutrient agar and grown for ten days in the presence of continuous red, blue or white light, or in complete darkness, before being examined by microscopy.

As shown in Figure 4.3, growth of seedlings in both red and blue light produced epidermal plastid and stromule morphologies intermediate between white light and darkness. The plastid bodies appeared similar in shape to those from white light-grown seedlings, which, together with the ability to detect chlorophyll autofluorescence in these plastids (data not shown), indicates that these plastids had also become chloroplastic in nature. Readily visible stromules of about 10-20  $\mu\text{m}$  in length were present on most plastids from seedlings grown in red or blue light, which was similar to the observations from dark grown seedlings (Figure 4.3). Furthermore, the relative dispersal of plastids throughout the cells of red and blue light-grown seedlings was intermediate between those of white light-grown and dark-grown seedlings. Saliiently, it was not possible to discern any difference in stromules between seedlings grown in red or blue light: the similarities in plastid morphology were consistently observed across several seedlings and experimental repetitions.

**Figure 4.3 Plastid and seedling morphology under low intensity red and blue light**

MSK57xDsRED seedlings were grown under white (A, B) blue (C, D) or red (E, F) light, or complete darkness for ten days (G, H). Representative images are shown with low (A, C, E, G) or high (B, D, F, H) magnification. The DsRED signal was used for the dark-grown seedlings and is represented in grayscale; all others show *aadA*-GFP fluorescence. Note that stromule length and abundance is very much higher under red and blue light at these intensities than under white light (see text). (I) Morphology of seedlings grown under each light treatment. (J) Hypocotyl lengths of seedlings grown under each light treatment were measured to the nearest mm. Error bars: mean  $\pm$ 1 S.E.,  $n = 10$ . Scale bars: 20  $\mu$ m.



It was noted that although the seedlings grown in red and blue light were essentially photomorphogenic (i.e. the cotyledons had expanded and turned green, and the hypocotyl epidermal plastids accumulated chlorophyll and attained the regular, oblate-spheroid shape associated with chloroplasts), inhibition of hypocotyl elongation was not complete under these conditions (Figure 4.3 I, J). Indeed, the hypocotyl response was closer to that of dark-grown seedlings than to that of white light-grown seedlings. Since the primary symptom of seedlings exposed to low light intensity is hypocotyl elongation (a process normally inhibited by blue light), this suggested that the light intensity of the red and blue sources was insufficient to mimic the normal photomorphogenic response. In addition to the fact that there were no differences in stromules between red and blue light, it also hinted that the degree of hypocotyl elongation, rather than light quality, explained the differences in stromule abundance and length between red/blue light and white light. Measurements of the red and blue light sources used in this experiment (produced by filtering light through plastic film; see §2.2.2.2.1) revealed that they emitted a much lower light intensity compared to white, with PAR readings of 1.8, 0.8 and 180  $\mu\text{mol m}^{-2} \text{sec}^{-1}$  respectively. It was therefore decided to control for light intensity between the different light treatments, and thus produce similar degrees of hypocotyl elongation, in order to clarify this situation.

#### **4.2.3 Light quality does not effect stromule formation when provided at equal intensity**

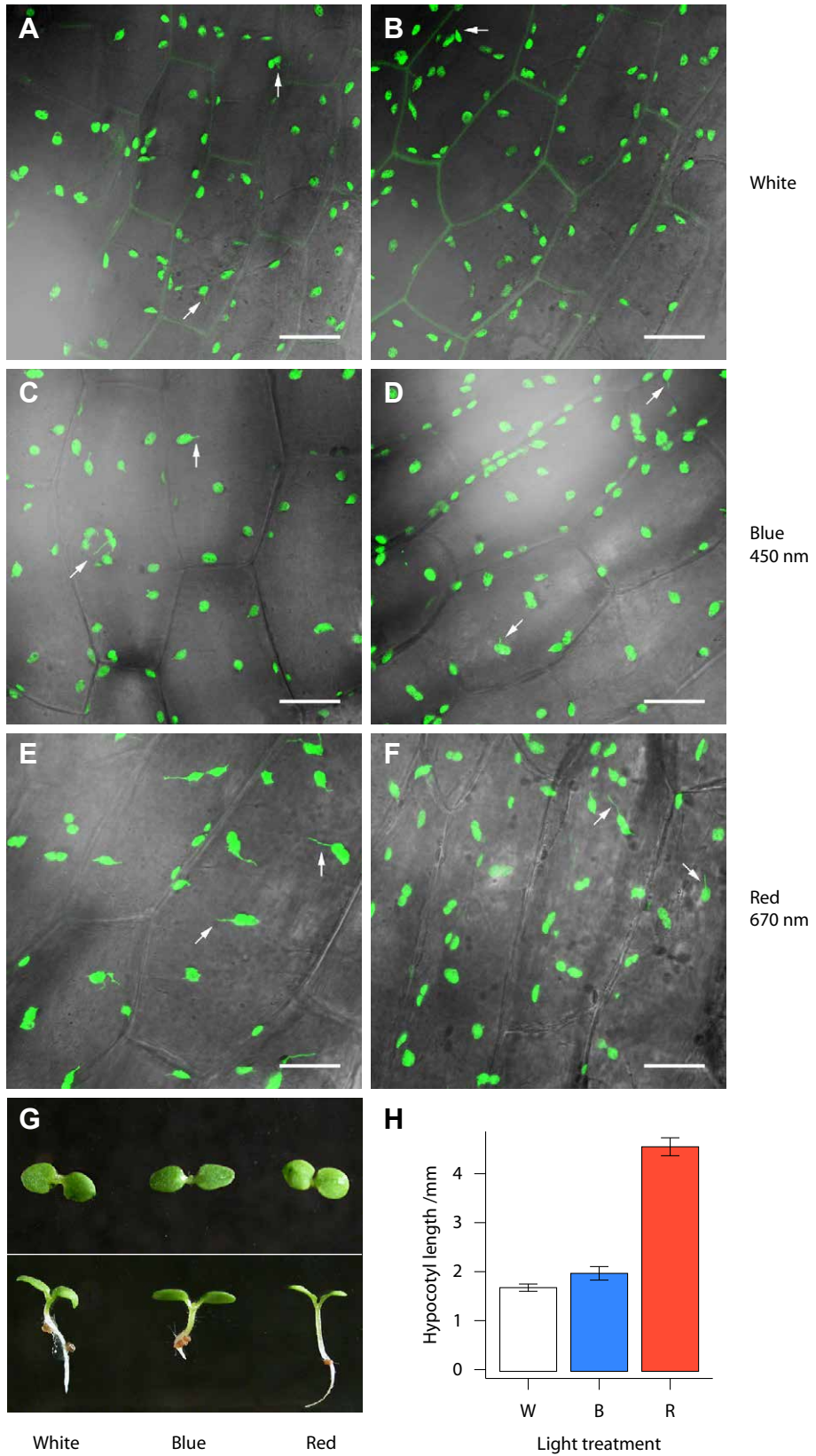
Using light-emitting diode (LED) arrays, relatively high intensity light sources of well-defined, narrow spectra can be produced (Franklin *et al.*, 2003). In this experiment, MSK57xDsRED seeds were germinated on nutrient agar under continuous red, blue or white light as before, except that all light was supplied at 60  $\mu\text{mol m}^{-2} \text{sec}^{-1}$ , produced by LEDs (for red and blue) or cool fluorescent tubes (for white). The blue LEDs emitted at a peak of 450 nm, whereas the red LEDs emitted at a peak of 670nm. Thus, this more

controlled experimental design produced stricter conditions for examining the potential effects of light wavelength on stromule development.

Seedlings grown under red, blue and white light of identical intensities underwent photomorphogenesis to a much more similar degree than did those under different intensities (Figure 4.4 G, H; c.f. Figure 4.3 I, J). Although red light caused a significantly greater amount of hypocotyl elongation than either blue or white, the absolute difference was small, especially when compared to the hypocotyl elongation induced by total darkness (Figure 4.3 J). When examined by confocal microscopy, the differences in plastid morphology that were previously observed between red/blue light and white light disappeared. Plastid bodies were, as before, regular and chloroplast-like in appearance, and stromules were largely indistinguishable between light treatments. The typical 2-5  $\mu\text{m}$  protrusions from chloroplasts were found in all light treatments, in stark contrast to the red and blue results from low light intensities (Figure 4.4; c.f. Figure 4.3). Superficially, red light-grown seedlings produced stromules slightly longer than the other two treatments (Figure 4.4 E, F), but this difference was not statistically significant. Superimposing the GFP image on top of the transmitted light image allowed the depiction of cell walls and a corresponding estimation of relative plastid dispersal. Again, this also was similar between the three light treatments, except that slightly elongated hypocotyls grown under red light led to moderately more elongated epidermal cells. Nevertheless, the important observation is that by controlling the light intensity, the preliminary differences in stromule abundance between seedlings grown under different light regimes were abolished.

#### **Figure 4.4 Plastid and seedling morphology under high intensity red and blue light**

MSK57xDsRED seedlings were grown under white (A, B) blue (C, D) or red (E, F) light of equal intensity ( $60 \mu\text{mol.m}^{-2}.\text{sec}^{-2}$ ) for ten days. Representative images are maximum projections of a confocal series along the z-axis (aadA-GFP signal), overlaid upon the transmitted light image to show the cell boundaries. Note that under all treatments the plastids are regular in form with rare, short stromules (arrowed). The degree of cell elongation is also apparent, with most plastids relatively close together. (G) The degree of hypocotyl elongation is much lower under higher intensity red and blue light than that shown in Figure 4.3. Note that red light has still produced twice as much hypocotyl elongation than either white or blue. (H) Quantification of seedling hypocotyl elongation. Error bars: mean  $\pm$  1 S.E.,  $n = 12$ . Scale bars: 20  $\mu\text{m}$ .



Together, these data thus suggested that hypocotyl elongation (brought about mainly by reduced light intensity) was an important factor in explaining why low intensity red and blue light induced greater stromule formation relative to white light, and that light quality *per se* was not. Therefore, an experiment was devised to investigate whether stromule length is directly related to the degree of hypocotyl elongation.

#### **4.2.4 Stromule length is negatively correlated with the density of plastids within the cell**

During skotomorphogenesis, hypocotyl elongation is brought about almost entirely by cell elongation rather than cytokinesis (Gendreau *et al.*, 1997). Making use of this fact, an experiment was designed to manipulate hypocotyl elongation, thus inducing different hypocotyl epidermal cell volumes. The intention was to assess how plastid density in epidermal cells changed with hypocotyl elongation, and how this influenced stromule morphology.

MSK57xDsRED seeds were sown on nutrient agar, stratified and grown for 5, 6, 7 or 9 days in complete darkness. After each of these periods, the seedlings were exposed to a further day of light in order to improve the expression of the fluorescent proteins (see Discussion), and to prevent further hypocotyl elongation. Differing periods of growth in the dark led to a five-fold range of hypocotyl lengths (Figure 4.5 A-D [insets], E). It was assumed that this also led to a similar range of cell sizes; substantial cell elongation was evident from the scarcity of transverse cell walls in images from the more elongated seedlings (Figure 4.5 A-D). All treatments produced hypocotyls that were at least twice as elongated as those from seedlings grown in continuous white light (Figure 4.5 E; c.f. Figure 4.4 H; note also the differences in cell size). The periods of dark growth followed by brief de-etiolation led to plastids with an elongated appearance and irregular shape, with abundant stromules (Figure 4.5 A-D). Note that this is consistent with the stromule

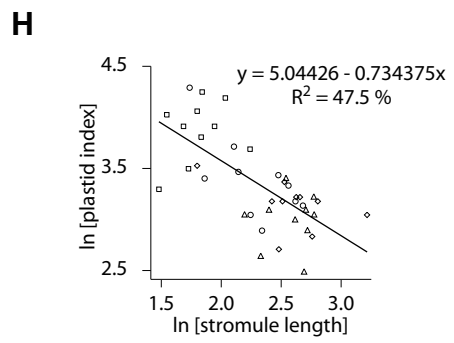
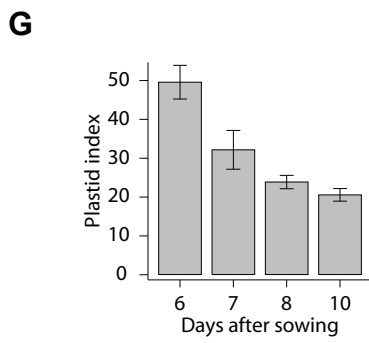
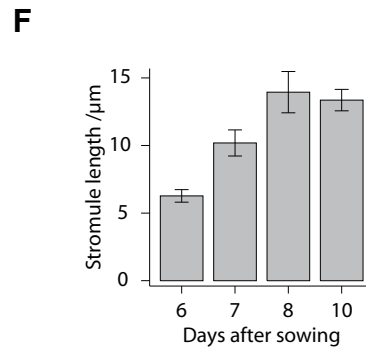
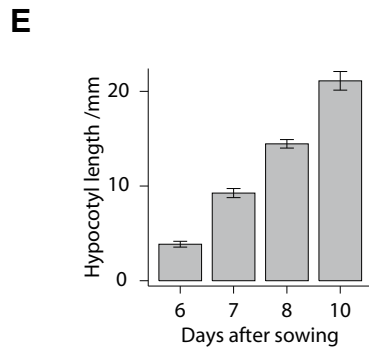
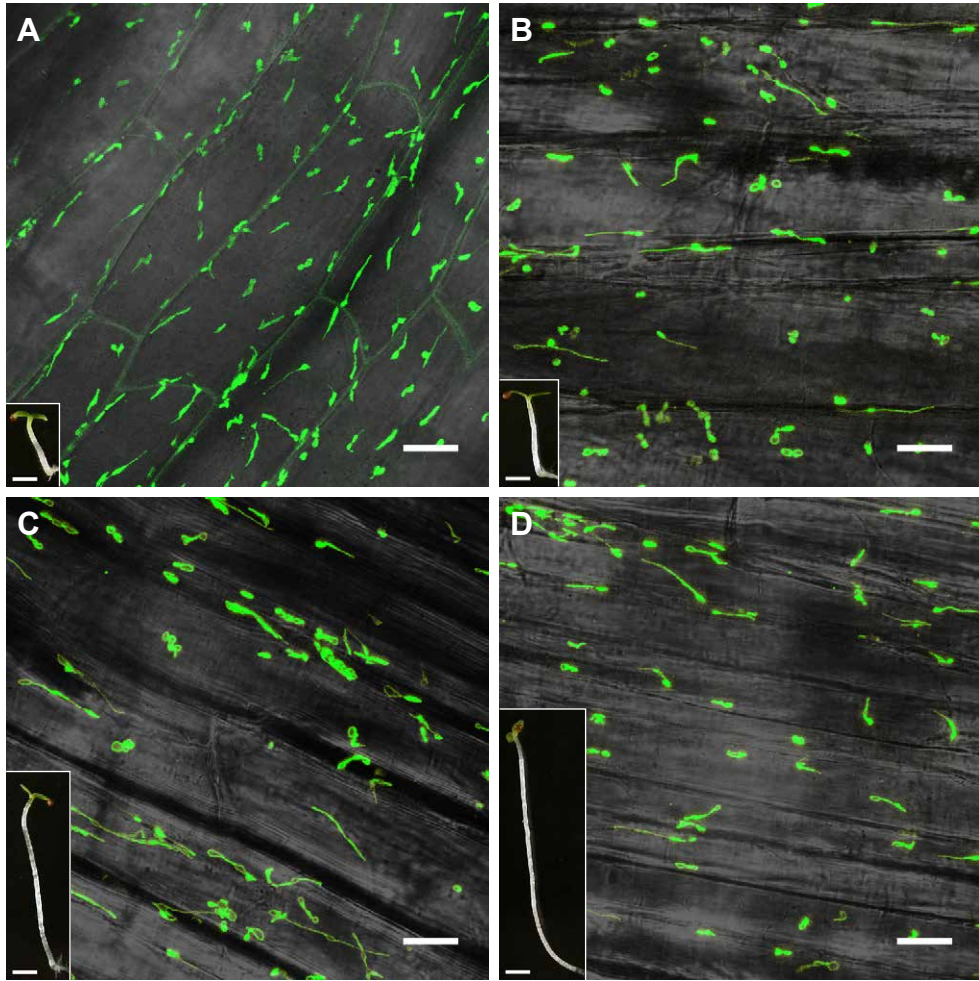
morphology of seven day-old dark-grown seedlings that had been de-etiolated for 24 h (Figure 4.2 C, D).

Inspection of epidermal cells from the central region of the hypocotyl (i.e. midway along the apical-basal axis) revealed that stromule length tended to increase with hypocotyl length. Whilst stromules in 6-day old seedlings were frequently short and rarely more than 10  $\mu\text{m}$  long, stromules from 8- and 10-day old seedlings often reached 20-30  $\mu\text{m}$  in length (Figure 4.5 A-D). When subjected to quantitative analysis of ten images per treatment, the increase in stromule length with hypocotyl length became more apparent (Figure 4.5 F). Notably, there was on average a 2.3-fold increase in stromule length between 6- and 8-day old seedlings, but no increase thereafter. At the same time, estimates of plastid density (i.e. plastids per unit area) showed that, as the hypocotyl elongates and the epidermal cells expand, the plastid density decreases by an average of 50% between 6- and 8-day old seedlings (Figure 4.5 G). Again, plastid density does not change significantly between 8- and 10-day old seedlings. The implication of these data is that increasing the inter-plastid distance in these cells correlates with an increased length of stromules. To test this, plastid density was plotted against the mean stromule length for each of ten images taken from each of the four treatments. Taking natural logarithms of these values produced a highly significant negative correlation between the two factors (Figure 4.5 H;  $P < 0.001$ ,  $R^2 = 47.5\%$ ).

Taken together with the results of light quality and quantity, these data suggest that the relative density of plastids correlates well with their tendency to produce long stromules. Furthermore, the data indicate that the initial differences observed between white light and red/blue light (Figure 4.3) were most likely due to the dispersal of plastids in the cell rather than to effects of light quality.

#### **Figure 4.5 Stromule length is negatively correlated with plastid density**

MSK57xDsRED seeds were sown on nutrient agar and allowed to germinate in the dark for 5, 6, 7 or 9 days in order to induce hypocotyl elongation, followed by one day of light treatment to induce de-etiolation. (A-D) Stromules in hypocotyl epidermis (A) 6 days, (B) 7 days, (C) 8 days and (D) 10 days after sowing. Images are maximum projections of a confocal series along the z-axis (aadA-GFP signal), superimposed on a transmitted light image to highlight cell walls. Note that stromules are mostly orientated parallel to the lateral cell walls, running in parallel across each image. Note also that plastid count per unit area generally decreases and stromule length increases as the hypocotyl extends. Insets show representative seedlings for each treatment. Scale bars: 20  $\mu\text{m}$  (insets 2 mm). (E) Hypocotyl length increases with duration of dark treatment. Bars indicate means  $\pm$  1 S.E.,  $n = 10$  seedlings. (F) Stromule length increases with duration of dark treatment. Bars indicate means  $\pm$  1 S.E.,  $n = 10$  images; up to 15 stromules were measured per image. (G) Plastid index, a direct measure of number of plastids per unit area, decreases with hypocotyl elongation. Bars indicate means  $\pm$  1 S.E.,  $n = 10$  images. (H) Stromule length is negatively correlated with plastid index, and hence plastid density. Note the logged scale. Squares, 6 days; circles, 7 days; diamonds, 8 days; triangles, 10 days. Each point represents the mean stromule length plotted against the stromule index for each image (10 images per treatment).



#### 4.2.5 Co-localisation of DsRED and aadA-GFP in stromules

The expression of two different fluorescent proteins in the plastid of MSK57xDsRED plants was advantageous because it allowed the selection of the stronger signal during microscopy. However, it also gave the opportunity to pose two questions related to the movement of proteins through stromules. Firstly, it remains unknown whether there is any size exclusion limit for entry into stromules, nor is it known whether proteins are selected for transport into stromules. Secondly, if diffusion is the main mechanism for transport of proteins through stromules, then larger molecules should move more slowly than smaller ones. DsRED is a 30 kDa protein which forms a 119 kDa tetramer *in vivo* and possibly even octamers at high protein concentrations (Matz *et al.*, 1999; Baird *et al.*, 2000). The aadA-GFP fusion produced by the FLARE16-S2 transplastomic construct is ~58 kDa in size (Kahn and Maliga, 1999). This difference in size meant that it was possible to test the relative ability of the stromules to transport molecules of different sizes. Since the two fluorescent proteins can be readily separated by their emission characteristics, they can be used to study their relative movement within *the same stromules* simultaneously.

##### 4.2.5.1 DsRED and aadA-GFP show identical distributions in stromules

Optimisation of excitation and emission wavelengths for each fluorescent protein ensured that only very little bleed-through between channels occurred. This was verified by using the DsRED channel's settings on MSK57 seedlings, and the GFP channel's settings on rbcS-DsRED seedlings separately (data not shown). A very small amount of fluorescence in the green channel could be detected from DsRed when excited by the 543 nm laser line, since immature DsRED exhibits a weak green fluorescence (Baird *et al.*, 2000); however, this was always small relative to true GFP fluorescence when excited at 488 nm. As such, the data collected in the green and red channels were a good reflection of the pattern of aadA-GFP and DsRED expression respectively.

Inspection of stromules with a variety of lengths and diameters consistently revealed no difference in aadA-GFP and DsRED localisation in stromules. Although cell-to-cell expression of each protein could vary relative to one another, there were no instances where only one signal could be detected in a stromule (Figure 4.6), which might be expected if larger proteins were excluded. Moreover, there was no evidence of increased incorporation of one protein over the other in a stromule relative to the fluorescence of the plastid body. In other words, a strong DsRED signal in the plastid body was always associated with a strong stromule signal, and likewise for aadA-GFP. Thus, there was no evidence of selective entry into stromules, at least with these two (non-endogenous) proteins, suggesting that they are equally capable of moving into stromules.

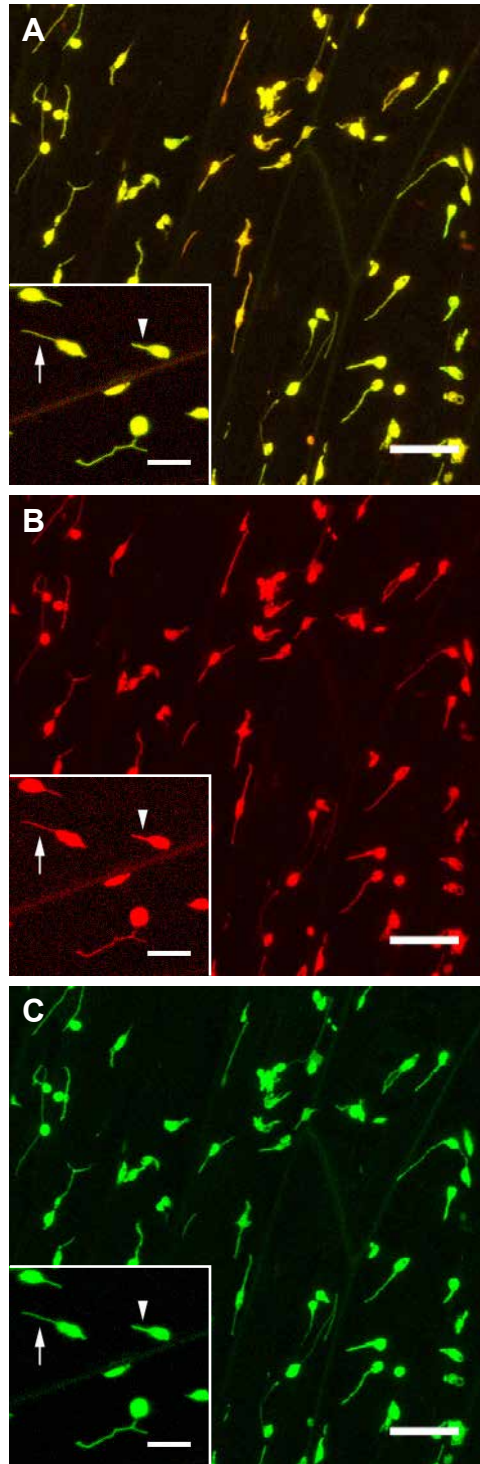


**Figure 4.6 aadA-GFP and DsRED signals largely co-localise**

MSK57xDsRED seedlings were grown for ten days under low intensity blue light to produce strong fluorescent signals for both aadA-GFP and DsRED, and to induce numerous stromules. (A) Overlay of both DsRED (B) and aadA-GFP (C) signals. Note the complete overlap (yellow). Insets: Thick (arrowheads) and thin (arrows) stromules both contain DsRED and aadA-GFP. Scale bars: main images 20  $\mu\text{m}$ , insets 10  $\mu\text{m}$ .

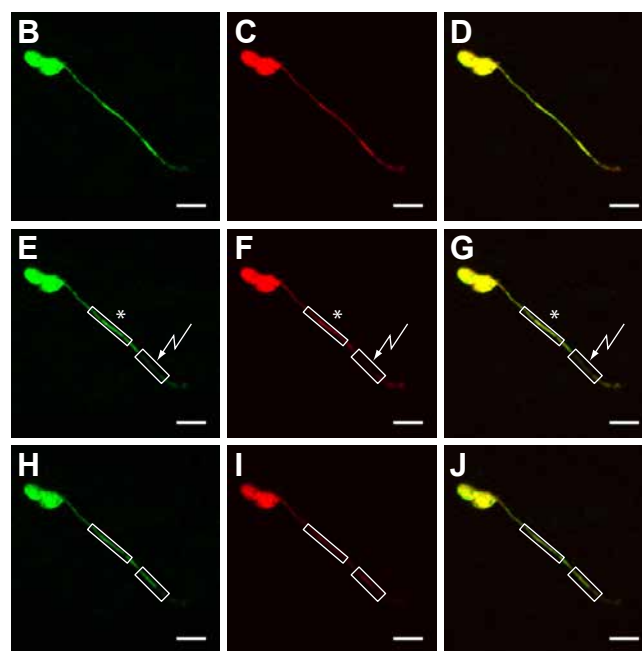
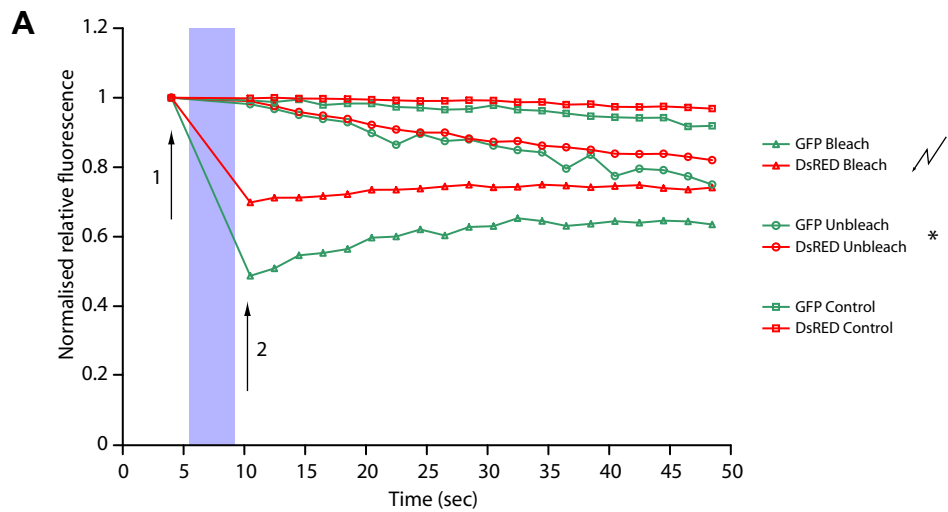


**Figure 4.7 FRAP analysis of movement of aadA-GFP and DsRED along stromules**

MSK57xDsRED seedlings were grown for ten days under low intensity blue light to produce strong fluorescent signals for both aadA-GFP and DsRED, and to induce numerous stromules. A small region of a single stromule (arrowed box, E-G) was photobleached with high laser power and the recovery of fluorescence followed for 40 s. Loss of fluorescence from an adjacent area (asterisked box, E-G) was also determined, as was the fluorescence of another, unconnected plastid body as a control (not visible). (A) Time course of fluorescence values for each of the two proteins at each of three regions of interest (ROI). Fluorescence values are normalised by representing them as a proportion of the pre-bleach value. Arrows indicate the values immediately before (1) and after (2) bleaching. The blue bar depicts the time during which bleaching took place. (B-D) Pre-bleach images (i.e. Arrow 1). (E-G) immediate post-bleach images (i.e. Arrow 2). Note the loss of fluorescence in the bleached area relative to B-D. (H-J) recovery images at the end of the time course. Note the return of fluorescence to the bleached region and the slight loss from the asterisked (unbleached) region relative to E-G. (B, E, H) aadA-GFP; (C, F, I) DsRED; (D, G, J) overlay. Scale bar: 5  $\mu\text{m}$ .

#### 4.2.5.2 DsRED and aadA-GFP diffuse at different rates through stromules

To consider whether larger proteins move more slowly through stromules, as would be predicted if diffusion were the main determinant of protein movement, FRAP analysis was performed. When a fluorescent protein is excited with very high laser power, the fluorophore is destroyed, a process known as photobleaching. A region of a stromule was photobleached with two scans of maximum laser power and the return of fluorescence from each protein was measured in the same region (arrowed rectangle, Figure 4.7 E-J). In addition, an adjacent region of the stromule was measured for the corresponding loss of fluorescence as aadA-GFP and DsRED diffused from that area into the bleached part of the stromule (asterisked rectangle, Figure 4.7 E-J). Thus, the recovery of fluorescence over time in the photobleached region occurs at the expense of the loss of fluorescence from adjacent areas. A typical FRAP result is shown in Figure 4.7 A. At each time point, the fluorescence signal from each region and protein was normalised by dividing by its initial fluorescence at  $t=0$  s, thus eliminating differences in relative brightness between the two fluorescent proteins. The first post-bleach image was collected at  $t=10$  s. The degree of fluorescence recovery can be determined by the absolute change in fluorescence over the time course of the experiment: this equates to the rate of recovery and the speed at which photobleached molecules are replaced by ones capable of fluorescence. Furthermore, this should be mirrored by the loss of fluorescence from adjacent, unbleached areas.

The immediate decrease in fluorescence in the bleached region indicates that aadA-GFP was bleached more strongly than DsRED (Figure 4.7). This is probably because the maximum laser power was provided at 488 nm, a wavelength that does not excite DsRED efficiently. Return of fluorescence into the bleached region was slightly more rapid for GFP than for DsRED. Over 40 s, aadA-GFP recovers approximately 15% of its original fluorescence value, whereas for DsRED the value is 5% or less (Figure 4.7 A). In

addition, there is a corresponding greater loss of aadA-GFP fluorescence than that of DsRED in the adjacent unbleached regions, although the difference is small (Figure 4.7 A). These data imply that larger proteins move more slowly through stromules and, by inference, that this movement occurs via diffusion rather than by some form of active transport.

#### 4.2.6 Stromules are intimately associated with other organelles

The increase in plastid surface area provided by stromules suggests that they may mediate interactions between different cellular compartments. Compartmentalisation gives eukaryotic cells a mechanism for optimising biochemical processes. Restricting the movement of metabolites and proteins within smaller, membrane-bound compartments means that metabolites can be separated and specifically concentrated, whilst pH can be optimised and compounds sequestered. These benefits translate into improved rates of reactions and the ultimate specialisation of organelles for particular processes. However, no organelle exists in isolation, as the performance of a cell depends upon the integration of functions performed by individual organelles. The plastid, for example, generates ATP and carbon backbones for biosynthesis, which are required throughout the cell. The bounding semi-permeable membranes that surround organelles restrict the exchange of compounds by diffusion, a problem which is overcome in two broad ways. Firstly, membrane-resident carrier proteins assist the transport of metabolites, proteins and ions. Secondly, organelles move through the cytoplasm in an ATP-dependent manner to improve mixing and minimise diffusion distances, a process known as cytoplasmic streaming (Williamson *et al.*, 1993). Plastids (Kandasamy and Meagher, 1999; Kwok and Hanson, 2003), mitochondria (Van Gestel *et al.*, 2002), Golgi stacks (Boevink *et al.*, 1998; Nebenführ *et al.*, 1999) and peroxisomes (Mathur *et al.*, 2002; Jedd and Chua, 2002) all move in this way on the actin cytoskeleton in plant cells.

Stromules increase the surface area of plastids, especially in large cells where individual plastids are relatively distant from one another. In such cells, close association between organelles would become important in order to minimise diffusion distances. Stromules could thus become central to mediating such close contact, since the potential for interactions increases with the available membrane surface area. To investigate whether such interactions take place on stromule membranes, and thus to test whether this is a feasible role for stromules as an aid to plastid activities, plastids were highlighted in conjunction with either mitochondria or peroxisomes using different fluorescent proteins as vital markers, and observed in hypocotyl epidermis.

#### 4.2.6.1 Mitochondria

A construct consisting of a translational fusion between the N-terminus of the *Nicotiana plumbaginifolia*  $\beta$ -ATPase and mGFP5 (atp-GFP) was used to target GFP to the mitochondria (Figure 4.1; Logan and Leaver, 2000). When expressed in tobacco, this construct efficiently labelled numerous, highly motile organelles dispersed throughout the cytoplasm in hypocotyl epidermis (Figure 4.8). These organelles, assumed to be mitochondria, ranged from 0.5 - 1  $\mu\text{m}$  in length, typically adopting a sausage-like or spherical appearance, and streamed rapidly throughout the cell. These observations are entirely consistent with previous descriptions of the *in vivo* behaviour of plant mitochondria (Van Gestel *et al.*, 1999, Logan and Leaver, 2000).

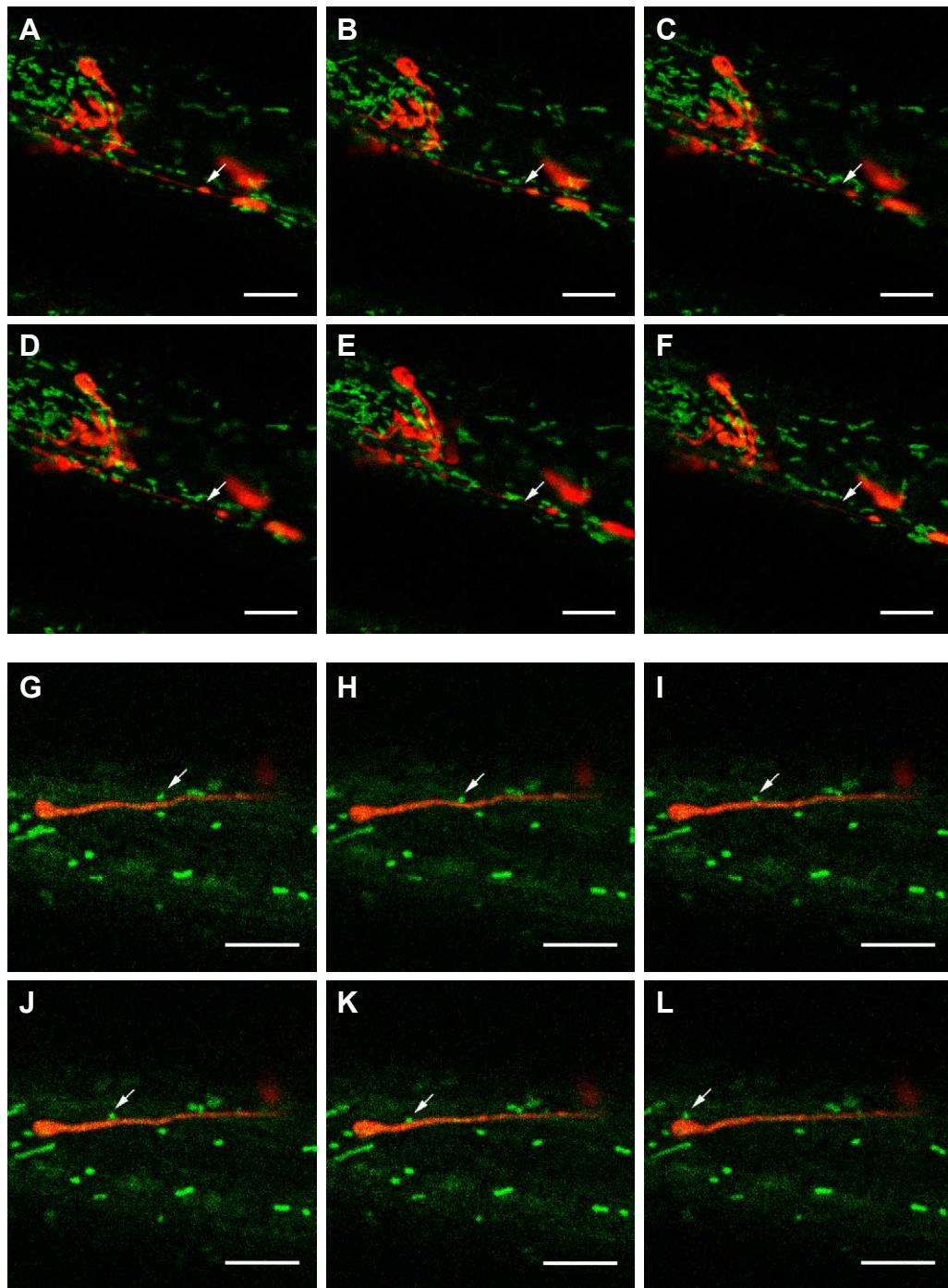


**Figure 4.8 Dynamics of plastids and mitochondria**

In each image, plastids are false coloured red (DsRED fluorescence) and mitochondria green (mGFP5 fluorescence), with overlap appearing yellow. (A-F) Selected images from a time-lapse series showing relative movement of plastids and mitochondria; the arrow initially points to a large vesicle attached to plastid body by a stromule in (A) but remains fixed in subsequent images to illustrate movement. Note the close association between plastid bodies and mitochondria, as well as along the stromule. Each image is 17 seconds apart. (G-L) Movement of a mitochondrion (arrowed) along a stromule and plastid body. Note that both are motile, but that the other mitochondria are relatively static. Each image is 5.3 seconds apart. Scale bars: 8  $\mu\text{m}$ .

Plants expressing atp-GFP were crossed with plants expressing plastid-targeted DsRED (*rbcS*-DsRED). The F<sub>1</sub> individual expressing both constructs the most strongly was selfed, yielding the F<sub>2</sub> generation MPA12 (Table 2.1). Seedlings of this generation were used to investigate the interrelations between plastids and mitochondria. Mitochondria in elongated hypocotyl epidermal cells were frequently associated with plastid bodies and stromules but were also highly abundant in other regions of the cell (Figure 4.8 A-F). Notably, mitochondria were often aligned with, and adjacent to, stromules of varying lengths. However, these associations were frequently transient with both organelles shifting relative positions over a matter of seconds (Figure 4.8 A-F). Closer inspection of stromule-mitochondria dynamics revealed an intimate association between the two, with both organelles possibly occupying the same actin microfilament. In Figure 4.8 G-L, a single mitochondrion can be seen traversing the same path as a stromule, at all times maintaining close contact with it. The other mitochondria in the image series are static, revealing that organelle movement is rather staccato and irregular. These findings indicate that stromules provide a substantial further surface that mediates plastid-mitochondrion contact in a dynamic manner.

#### 4.2.6.2 Peroxisomes

Enhanced cyan-fluorescent protein (ECFP), a blue-shifted variant of GFP, was targeted to the peroxisomal compartment by means of a C-terminal tripeptide (Figure 4.1). Primary transformants made with this construct were crossed with *rbcS*-DsRED lines and strong double expressors were selected in the F<sub>1</sub> and selfed; experiments were performed on F<sub>2</sub> seedlings from the line designated PP2 (Table 2.1).

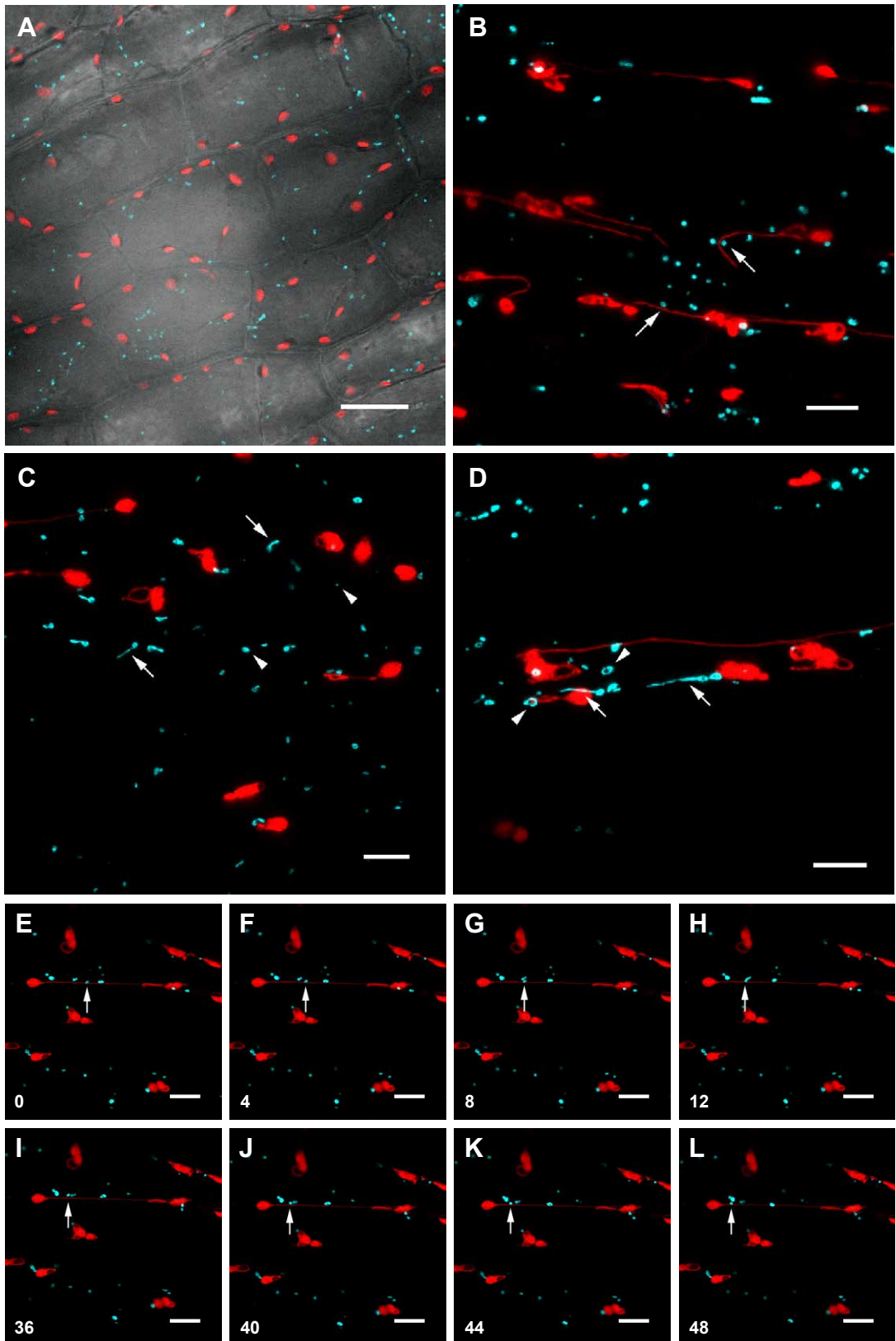
Peroxisomes in tobacco hypocotyl epidermal cells are motile and distributed evenly throughout the cytoplasm, but are generally larger and less numerous than mitochondria (Figure 4.9 A). Like mitochondria, peroxisomes are closely associated with strom-

ules and plastid bodies in de-etiolated seedlings, although not exclusively so (Figure 4.9 B). Peroxisomes are variable in shape and size: whilst generally spherical in appearance, they range from ~200 nm to 1.5  $\mu\text{m}$  in diameter (Figure 4.9 C), and occasionally they produce stromule-like protrusions many times longer than the diameter of the peroxisome “body” (Figure 4.9 D). Notably, these protrusions are aligned in the same direction as the plastid stromules and the general direction of cytoplasmic streaming. Considering in addition the loop-like forms peroxisomes adopt (Figure 4.9 D), these observations indicate that this is a very plastic organelle reminiscent of the flexibility of plastid morphology.

In order to assess whether peroxisomes interact with stromules in a dynamic manner like mitochondria, time-lapse imaging was performed on a stromule connecting two plastid bodies with numerous associated peroxisomes. Vectorial transport of a single peroxisome along the length of the stromule is clearly visible, albeit discontinuously and with variable speed (Figure 4.9 E-L). Several peroxisomes that also appear to align with the stromule are apparently static, further indicating that organelle movement is irregular. Additionally, these data imply that stromules improve plastid-peroxisome contact in a transient manner; slow, discontinuous movement presumably augments this contact time.

### **Figure 4.9 Dynamics of plastids and peroxisomes**

In each image, plastids are false coloured red (DsRED fluorescence) and peroxisomes cyan (ECFP fluorescence), with overlap appearing white. (A) Distribution of plastids and peroxisomes in hypocotyl epidermis of an 8 day-old white light-grown seedling. Superimposition on transmitted light image shows the cell walls. (B) Plastids and peroxisomes in hypocotyl epidermis of an 8-day old de-etiolated seedling. Note the close association of some peroxisomes with stromules (arrows) as well as plastid bodies. (C) Variation in peroxisomal size (arrowheads) and shape (arrows). (D) Peroxisomes sometimes form stromule-like structures (arrows) and lariat shapes (arrowheads). (E-L) Time-lapse series indicating peroxisomal motility along stromules (arrow). Numbers indicate time in seconds from the beginning of the series. Between 12 s and 36 s the peroxisome was relatively static; movement recommenced at 36 s. (A-D) Maximum projections along z-axis; (E-L) single plane confocal images captured over time. Scale bars: (A), 20  $\mu\text{m}$ ; (B-D), 8  $\mu\text{m}$ ; (E-L), 5  $\mu\text{m}$ .



#### 4.2.7 Low oxygen conditions promote fusion of mitochondria but not plastids

Although comparatively rare, stromules can join individual plastid bodies. Unless such interconnecting stromules are derived from incompletely divided plastids, the plastid envelope must be able to fuse with membranes from other plastids in order to create the conduit. Although poorly investigated in plants, extremes in mitochondrial size due to fusion have been reported following oxygen deprivation in both cultured suspension cells of tobacco (Van Gestel and Verbelen, 2002) and in leaf mesophyll cells of *Arabidopsis* (Ramonell *et al.*, 2001). In tobacco suspension cells, mitochondria were shown to fuse and form a reticulate network of megamitochondria upon oxygen starvation by plating at high cell density, but normal mitochondrial morphology would return when oxygen concentrations increased (Van Gestel and Verbelen, 2002). This rapid, inducible and reversible mitochondrial fusion suggests that plastids and stromules, also with a double bounding membrane, might be able to fuse in a similar manner. To investigate this possibility, MPA12 seedlings were exposed to low oxygen conditions for 4-6 h and examined by confocal microscopy.

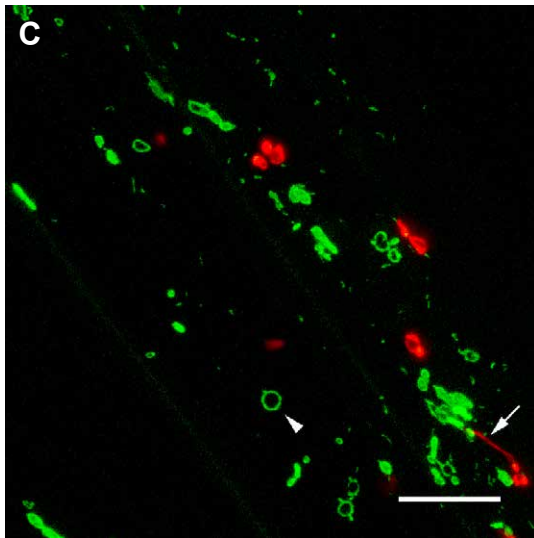
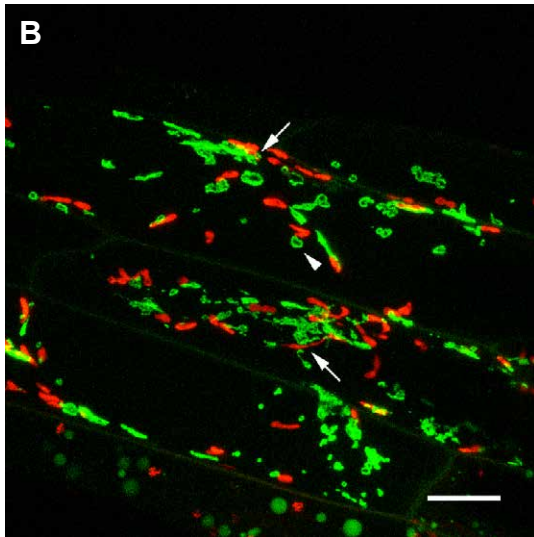
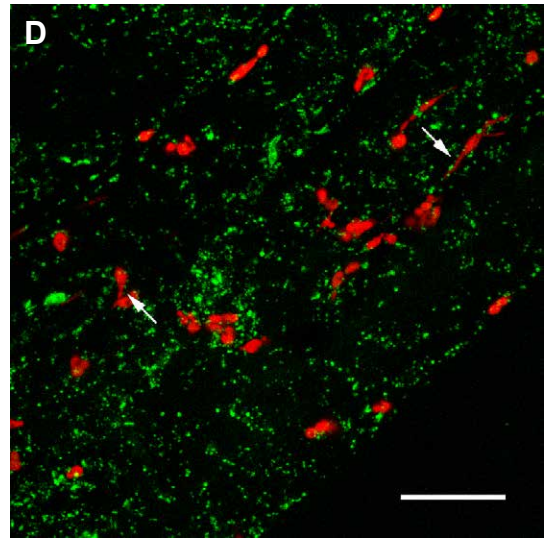
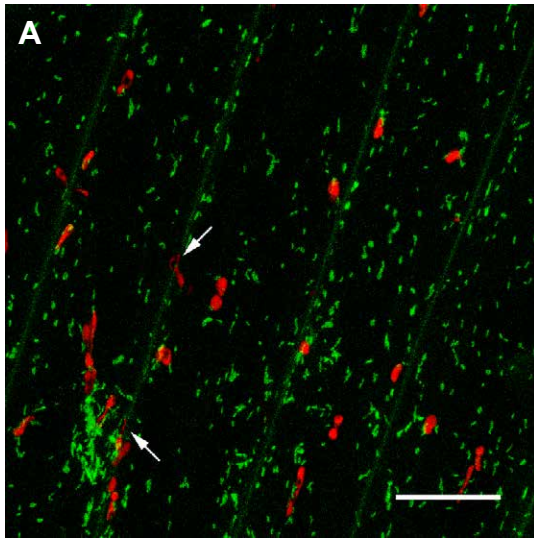
Oxygen deprivation was carried out by placing an unsealed pot of seedlings in an anaerobic jar (Figure 4.10 E; see §2.2.2.4). Under normal atmospheric conditions (i.e. in a sealed pot), mitochondria are small and motile, and are numerous and evenly distributed throughout the cytoplasm of the hypocotyl epidermal cells (Figure 4.10 A). After 4-6 h of oxygen starvation, the mitochondria undergo substantial fusion forming large entities frequently bigger than plastids (Figure 4.10 B, C). These structures are much less motile than the unfused counterparts, and commonly form agglomerates with plastids in an unevenly distributed way (Figure 4.10 B). Megamitochondrial morphology was highly variable: whilst plate-like, irregularly shaped structures were the most common (Figure 4.10 B), lariat-like forms were also frequently observed (Figure 4.10 C). However, the complex reticulate network described by Van Gestel and Verbelen (2002)

was never observed in these cells, perhaps because the greatly increased epidermal cell size and more dispersed mitochondria force the splitting of any such network. The mitochondrial fusion was readily reversible upon return of oxygen to the seedlings (Figure 4.10 D); however, mitochondrial motility was much reduced relative to non-treated seedlings.

Most notably, there were no clear differences in plastid morphology and stromule abundance between treated and untreated seedlings. Plastids showed no evidence of fusion or shape change, and whilst stromules were present in oxygen-deprived cells, they were no more common (Figure 4.10 B, C). Thus, whilst mitochondria are highly sensitive to changes in oxygen conditions, plastids appear to show no response, and the mechanism remains enigmatic for the possible fusion of plastid membranes to form stromules.

#### **Figure 4.10 Reversible mitochondrial fusion brought about by oxygen deprivation**

In each image, plastids are false coloured red (DsRED fluorescence) and mitochondria green (mGFP5 fluorescence), with overlap appearing yellow. Stromules are arrowed. (A) Under normal atmospheric conditions, mitochondria are small and numerous. The slightly elongated appearance of the mitochondria is partially due to their motility. (B, C) Mitochondria in oxygen-deprived cells fuse to form large, immotile megamitochondria. Note their tendency to agglomerate and form loops and lariat-like forms (arrowheads). (D) Six hours after return of oxygen, the mitochondrial fusion has reversed although some large mitochondria remain. The spherical shape of the unfused mitochondria reflects their relative immotility compared to (A). (E) Anaerobic apparatus used in the experiment. Note the pot of seedlings with air holes in the lid. Indicated are the sachet that absorbs oxygen and releases carbon dioxide (★), and the anaerobic indicator (⊗). Scale bars: 20 μm.



### 4.2.8 Mitochondria may pass through cell walls

In one experiment treating MPA12 seedlings with low oxygen conditions, an extremely long, tubular “mitochondrion” was observed which appeared to pass from one epidermal cell to another one in an adjacent cell file (Figure 4.11). Confocal sectioning along the  $z$ -axis showed that the “mitochondrion” was approximately 1  $\mu\text{m}$  thick and over 80  $\mu\text{m}$  long, and adopted an “m” shape that appeared to follow the contours of the cell (Figure 4.11 A-D). Notably, the mitochondrion converged on a single point which coincided with faint autofluorescence of the cell wall (Figure 4.11 D). Furthermore, when superimposed on the transmitted light image, the maximum projection image shows that the crossing point coincides with a region of light diffraction, typical of plant cell walls (Figure 4.11 E). The “m” shape was confirmed with a series of rotational projections around the  $y$ -axis (Figure 4.11 G-L); this shape is compatible with the notion that the mitochondrion follows the elliptical shape of the epidermal cells and crosses at a plasmodesmatal junction (Figure 4.12). This intriguing and unprecedented observation implies that there could be some form of intercellular communication occurring via mitochondria, or that organelles may be shared between cells.

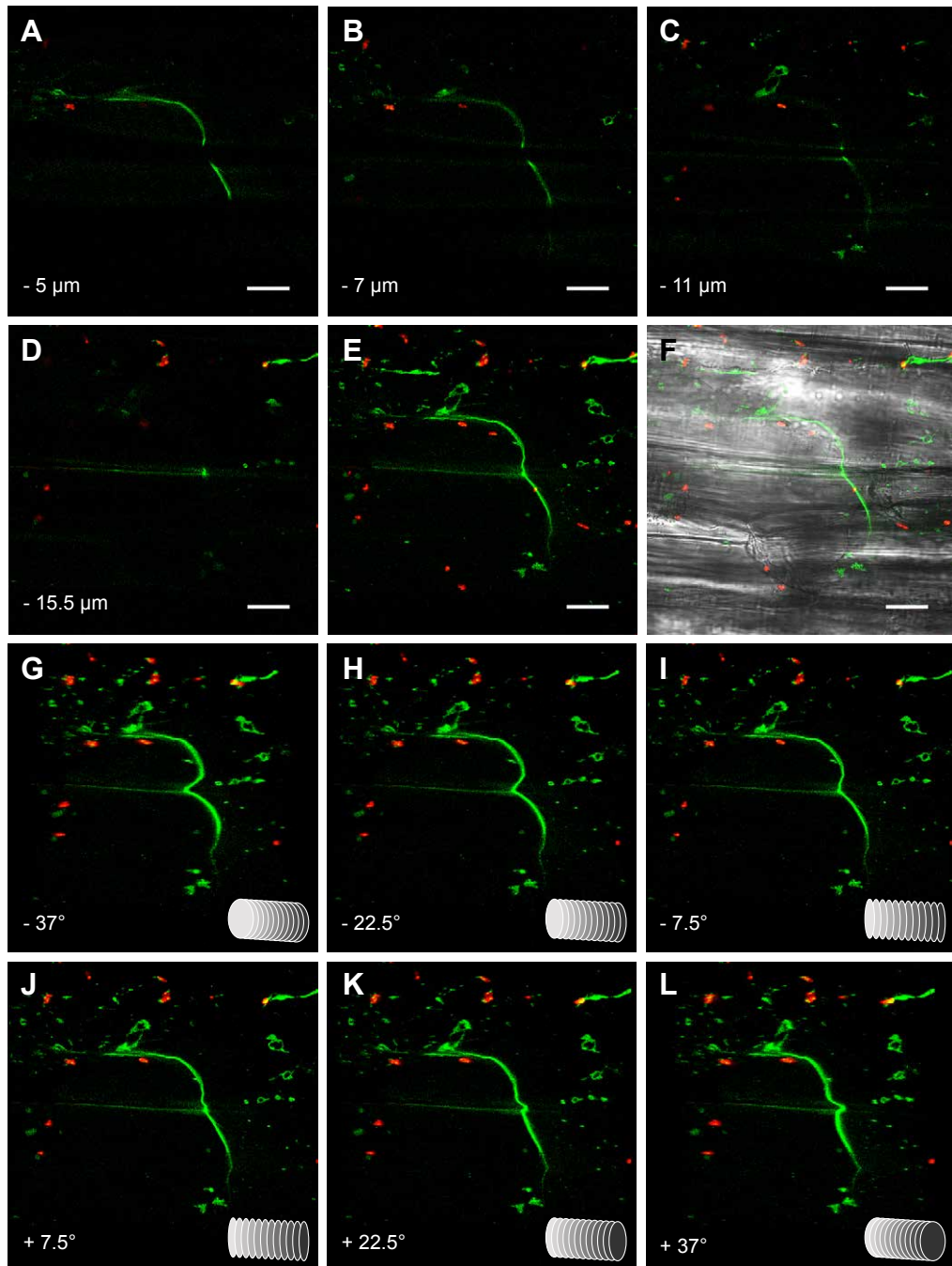


**Figure 4.11 Putative intercellular passage of mitochondria**

In each image, plastids are false coloured red (DsRED fluorescence) and mitochondria green (mGFP5 fluorescence), with overlap appearing yellow. (A-D) Individual sections along the z-axis. Distances below the upper origin are indicated; the maximum projection image (E) represents approximately 20  $\mu\text{m}$  in depth. (F) The maximum projection image superimposed on the transmitted light image to show cell walls. The cells are running in parallel files from left to right in the image. (G-H) Individual images from a series of a rotation of the maximum projection image about the y-axis, illustrating the depth of the sample. Indicated are the angles of view relative to directly downwards ( $0^\circ$  would be same view as that shown in E). For reference, the lower right of each image shows the relative rotation of an imaginary cylinder when viewed from each respective angle. Note how the mitochondrion adopts an "m" shape. Scale bars: 20  $\mu\text{m}$ .

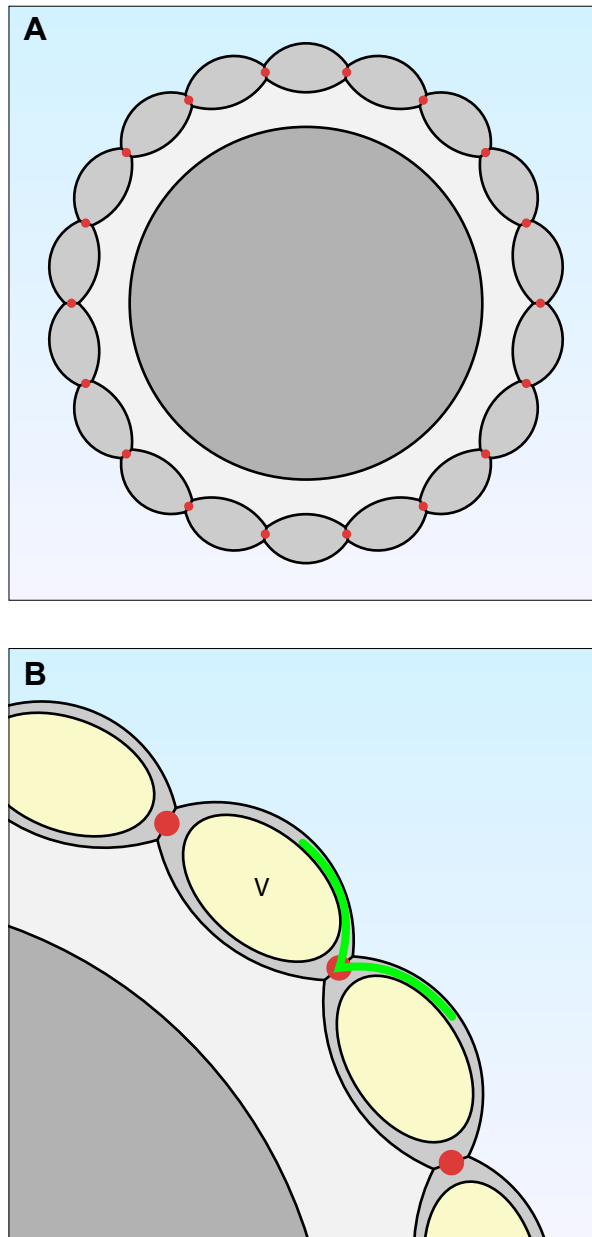


**Figure 4.12 Model for the passing of mitochondria through cell walls in hypocotyl epidermis**

(A) A simplified diagram of a transverse section of a tobacco hypocotyl. The outermost cells, the epidermis, adopt an elliptical shape and form parallel cell files, presumably interconnected by plasmodesmata (red circles). (B) Close-up of the epidermis. Epidermal cells contain a central vacuole (V) that provides turgor and pushes the cytoplasm and its contents towards the periphery of the cell. The mitochondrion in question (green) is thus forced to follow the contours of the cell wall and the vacuole, dips to cross the cell boundary at a plasmodesma, and then rises again in the next cell. The mitochondrion thus adopts a shallow "m" shape.

## 4.3 DISCUSSION

### 4.3.1 Stromule formation is dependent upon plastid density within the cell

The differences in plastid morphology between skotomorphogenic, photomorphogenic and de-etiolated seedlings confirm that plastid differentiation status is an important determinant in stromule formation (Figure 4.2). Nevertheless, dramatic differences in seedling development complicate this conclusion: as the hypocotyl length increases, so does the epidermal cell volume and, correspondingly, the average distance between each plastid. One of the major contributing factors to stromule formation in this tissue appears to be the relative distribution of plastids within the cell. Several lines of evidence favour this interpretation.

Firstly, brief de-etiolation does not remove long stromules, suggesting that plastid differentiation status alone is insufficient to explain their abundance. However, to assess properly the effects of plastid differentiation during de-etiolation, seedlings would need to be given longer periods of de-etiolation and examined to see if a) the number of plastids per cell increases and b) stromules disappear as chloroplasts differentiate more fully. Secondly, and related to the first point, although low fluences of red and blue light were sufficient to direct chloroplast differentiation in both the hypocotyl and the cotyledons, stromules were much more abundant under these conditions than in seedlings grown under moderate light intensity that inhibited hypocotyl elongation (Figure 4.3, 4.4). Finally, experimentally manipulating the degree of hypocotyl elongation uncovered a negative correlation between stromule length and plastid density (Figure 4.5).

The rapid increase in epidermal cell volume during skotomorphogenesis leads to decreased plastid density, but this appears to reach a minimum value despite further cell elongation (Figure 4.5 G). Similarly, mean stromule length tails off with increasing cell

elongation (Figure 4.5 F), implying that plastid density and stromule length have lower and upper limits respectively. Rapid hypocotyl elongation may prevent plastid division from occurring fast enough to maintain a high density of plastids, but some degree of division presumably occurs since too sparse a distribution of plastids would be detrimental to the cell. To compensate for this, stromules would provide the necessary increase in plastid surface area as inter-plastid distance increases. Whilst plastid density in dividing and expanding mesophyll cells remains approximately constant where maximal light interception is important (Pyke, 1997), it is presumably more efficient (and quicker) for a hypocotyl epidermal cell to increase stromule abundance rather than maintain a high density of plastids. Increased plastid surface area in these cells might be of particular importance since expanding cells require rapid synthesis and supply of fatty acids for incorporation into phospholipids. Galactolipids are synthesised on the plastid envelope and exported to the ER, possibly via plastid-ER contact sites (Kelly and Dörmann, 2004). Interestingly, a plastidial acyl-coenzyme A synthetase, which activates fatty acids for export from plastids, has been localised to the plastid envelope including stromules (Schnurr *et al.*, 2002). Similarly, it may be significant that stromules are aligned with the cell wall, thus supplying fatty acids close to their point of need; however, this may be an indirect effect of the orientation of the actin cytoskeleton and cytoplasmic streaming in general (Kwok and Hanson, 2004b). Furthermore, the frequent and long stromules aid interactions with other organelles (see below).

Is it surprising that light quality had little effect on stromule abundance, once light intensity was matched? Both blue and red light are effective in directing chloroplast differentiation since the signalling cascades of both families of photoreceptors converge on the activation of G-box-containing promoters. A small but significant increase in hypocotyl elongation in red light relative to blue or white light probably reflects the fact that blue light is generally the stronger inhibitor of this response. This is evident from the phenotype of the *cry1* mutant versus that of *phyA* or *phyB* mutants in blue light

(Neff and Chory, 1998), and from the dose-dependent effect of CRY1 (Lin, 2002). Nevertheless, the postulated effect of blue light on stromule formation (due to similarities in the chloroplast avoidance response mechanisms) was not observed. This may be evidence that the regulatory networks underpinning chloroplast avoidance movement and stromule formation are different, or that growth under continuous blue light of moderate intensity does not trigger changes in plastid and stromule motility. Responses of stromules to red or blue light may differ following transfer of dark-grown seedlings into light of these wavelengths, which would assess whether plastids are more “blind” to one type of light than to another (see General Discussion).

#### **4.3.2 Stromules assist interactions between compartments within the cell**

Dual labelling of plastids in conjunction with mitochondria or peroxisomes revealed a function for stromules: they provide improved surface area for inter-organellar contact. This is a specific and significant role for these structures in large cells with low plastid density and, whilst there was no evidence for preferential clustering of organelles around plastids and stromules under these experimental conditions, mitochondria and peroxisomes associated very closely with stromules and sometimes in high numbers.

The primary role for mitochondria in heterotrophic cells such as those in etiolated hypocotyls is to generate and supply ATP. Plastids, with their extensive biosynthetic pathways, require ATP for the production of fatty acids that are then exported for use throughout the cell (Ohlrogge and Jarworski, 1997). Whilst mitochondria can synthesise their own fatty acids, this pathway is primarily used for the generation of short-chained molecules such as lipoic acid, indicating that mitochondria presumably use plastid-derived, 18-C fatty acids for membrane biogenesis (Wada *et al.*, 1997). Mitochondria also export citrate and acetate, potential precursors for the production of acyl-CoA in the plastid, which is the start point for all fatty acid biosynthesis (Fischer and Weber,

2002). Thus, there is extensive and bi-directional metabolic flow between these two organelles that could be optimised by close physical contact.

Peroxisomes are single membrane-bound organelles with a generally oxidative type of metabolism. They are metabolically plastic, as they perform different roles in different cell types and under different environmental conditions (Reumann, 2000). In leaves, the peroxisome takes part in the photorespiratory cycle, a process shared with the plastid and mitochondrion (Douce and Neuburger, 1999). These “leaf peroxisomes” are thus chiefly responsible for the oxidation of glycolate and scavenging of lost carbon, but in non-photosynthetic cells peroxisomes perform several other functions. The glyoxysome, a specialised peroxisome found in oilseeds, contains enzymes involved in the oxidation of fatty acids in the glyoxylate cycle. In other cell types, the function of peroxisomes is unknown, and these are simply referred to as “unspecialised peroxisomes” (Reumann, 2000). In addition to oxidative processes as part of a larger metabolic cycle, peroxisomes are involved in the generation and degeneration of hydrogen peroxide and superoxide radicals (Corpas *et al.*, 2001). The peroxisome, with high levels of catalase and superoxide dismutase, may act as a scavenger of active oxygen species (Corpas *et al.*, 2001). These derivatives of oxidative metabolism are recognised by the cell as stress signals, and the peroxisome plays an important part in regulating the redox status of the cell in response to such stimuli (del Río *et al.*, 1996).

The underlying reason for the relationship between peroxisomes and plastids in tobacco hypocotyl epidermis is not obvious. Whilst there is a direct metabolic link between plastids and peroxisomes in the photorespiratory cycle, this process is probably insignificant in etiolated seedlings and in the non-photosynthetic cells of the epidermis. The glyoxylate cycle, however, is of prime importance in the  $\beta$ -oxidation of fatty acids in seed storage reserves. The tobacco seed contains approximately 40% oil on a dry

weight basis, stored in the endosperm (Giannelos *et al.*, 2002). The glyoxylate cycle converts acetyl-CoA into succinate for feeding into the TCA cycle, thus mobilising storage reserves for the synthesis of structural carbohydrates such as cellulose (Eastmond and Graham, 2001). Enhanced peroxisomal activity and motility in germinating tobacco seeds would thus be expected, except that the majority of glyoxylate cycle activity presumably occurs in the endosperm where storage reserves are being broken down (Eastmond and Graham, 2001). Furthermore, this process involves the peroxisome, mitochondrion and cytosol, but not the plastid compartment directly. Nevertheless, peroxisomes do make intimate contact with plastids – whether this is an indirect result of the two organelles sharing a common motility network or a reflection of a more functional relationship remains to be established. Inspection of plastid-peroxisome interactions under different environmental conditions (e.g. photorespiratory stress) and in a wider selection of cell types may address this question.

Previous reports on peroxisome morphology describe that they divide by a budding mechanism and frequently adopt distorted shapes (Jedd and Chua, 2002), corroborating the variability in size and form shown in Figure 4.9. The staccato-like movements of peroxisomes also have been documented previously (Jedd and Chua, 2002; Mathur *et al.*, 2002), and are similar in nature to those of mitochondria and the “stop and go” behaviour of Golgi stacks (Boevink *et al.*, 1998; Nebenführ *et al.*, 1999). That a single actin track can be occupied by several organelles simultaneously provides a mechanism for physical contact between organelles within the cell, without compromising their ability to continue cytoplasmic streaming. The irregular movements of peroxisomes and mitochondria may be due to inconsistent attachment of the (putative) myosin motors to actin microfilaments, or other actin-associated proteins regulating the competency of specific microfilaments to support cytoplasmic streaming. Circumstantial evidence for the latter possibility is from the movements of the stromule and mitochondria in Figure 4.8 G-L: in this series of images, both the stromule and the arrowed mitochondrion are

motile whereas other mitochondria are static. This suggests that both organelles are attached to the same “active” actin microfilament, whereas nearby microfilaments are inactive. The observation of both thick actin bundles and thin actin filaments in the cortex of plant cells (Kandasamy and Meagher, 1999) implies that there may be fundamental differences in the ability of actin microfilaments to support organelle movement, perhaps due to steric inhibition. It is possible, for example, that individual actin microfilaments could transport organelles more smoothly than a thick bundle of several microfilaments that may not lie with identical polarity. Alternatively, organelle movement may be regulated by localised signals: in a model proposed by Nebenführ *et al.* (1999), Golgi movements are regulated in an active manner by so-called “stop” signals from ER export sites. This has yet to be confirmed, for either Golgi movement or that of any other organelle. Whilst we understand reasonably well the mechanisms for organelle movements in plant cells, the factors controlling their movements have yet to be discovered.

### 4.3.3 Can stromules fuse like mitochondria?

To the best of the author’s knowledge, there have been no reports of two separate stromules meeting and fusing to form a single, contiguous stromule. Indeed, the proportion of plastids that are actually interlinked via stromules is very low – this depends on the cell type in question, but it has been reported that even those plastids that appear to be connected prove not to be when subjected to FRAP analysis (Köhler and Hanson, 2000). Two stromules from separate plastids may meet on the same actin microfilament and cross over, but only appear to fuse because they mutually inhibit any further progression along the microfilament. Biological membranes require assistance to fuse with each other, not only because of thermodynamic difficulties derived from repulsive forces between facing phospholipids on the respective membranes (Jahn and Grubmüller, 2002), but also because spontaneous and uncontrolled membrane fusion

would cause breakdown of the structural integrity of cellular compartments. Fusion events within the endomembrane system are mediated by SNARE (soluble *N*-ethylmaleimide-sensitive factor attachment protein receptor) or SNARE-like proteins (Chen and Scheller, 2001). Whilst SNAREs are thought to provide the force, the specificity of membrane fusion instead is largely mediated by the highly diverse group of Rab GTPases (Zerial and McBride, 2001). SNAREs contain coiled-coil domains that mediate extremely stable complexes with similar domains on other cognate SNAREs. Interactions between SNAREs on pre-fusion membranes causes the coiled-coil domains to “zip up” in a multimeric complex, bringing the two membranes into sufficient proximity to fuse (Chen and Scheller, 2001). Thus, the fusion of two membranes is a tightly regulated event, and stromule fusion would require the postulation of a suite of plastid-specific and/or stromule-specific regulatory proteins. Conversely, stromule splitting, which has been observed, may be unavoidable if tension forces act in opposite directions on the same microfilament. In this case, the severed ends of the double membrane presumably re-seal spontaneously. Thus, whilst it is uncertain that stromules never fuse, a more parsimonious explanation for interlinking stromules is that they are the result of incomplete plastid division and the subsequent movement apart of daughter plastids. One prediction of this interpretation is that once plastid division has ceased, any interconnecting stromules should eventually break apart, meaning that cells that have stopped expanding should have a low proportion of interconnected plastids.

Despite the apparent absence of stromule fusion, the observation of megamitochondria under hypoxic conditions implies that double-membrane bound organelles can fuse. A great deal of knowledge regarding mitochondrial dynamics has been gleaned from the budding yeast *Saccharomyces cerevisiae*. In this organism, there are typically 5-10 tubular mitochondria forming a reticulum just below the plasma membrane. Analysis of mutants with altered mitochondrial morphology has revealed that the organelle is in a

dynamic equilibrium between fission and fusion events (Shaw and Nunnari, 2002). In *dnm1* mutant cells, mitochondrial fission is disrupted but fusion continues, resulting in a single continuous mitochondrial network; however, in *fzo1* mutants the fission process is unperturbed whilst fusion does not occur, leading to fragmented mitochondria (Sesaki and Jensen, 1999). In *fzo1 dnm1* double mutants, normal mitochondrial morphology is restored, indicating the two proteins act antagonistically (Sesaki and Jensen, 1999). Dnm1p therefore promotes fission, whereas Fzo1p is necessary for fusion. Notably, Dnm1p localises to distinct punctate structures on the outer mitochondrial membrane, which become sites of mitochondrial fission (Shaw and Nunneri, 2002). Dnm1p is related to the GTPase dynamin, a highly conserved protein that functions in exocytosis by wrapping around the necks of clathrin-coated vesicles and causing them to sever from the parent membrane by constriction (Hinshaw, 2000). Both Fzo1p and Dnm1p are GTPases, and the GTPase domains are essential for their fusion/fission activity (Shaw and Nunnari, 2002). Besides Fzo1p, additional proteins necessary for mitochondrial fusion have recently been described, including Ugo1p and Mgm1p (reviewed by Scott *et al.*, 2003). Mgm1p, another GTPase, resides on the inner mitochondrial membrane and forms complexes with both Ugo1p and Fzo1p, providing a mechanism for the co-ordinated fusion of double membranes (Wong *et al.*, 2003). It is possible that, like SNARE proteins in the secretory pathway, Ugo1p/Fzo1p complexes somehow provide the machinery for mitochondrial fusion. At present, however, it is unclear what regulates the relative contribution of fusion and fission (Scott *et al.*, 2003).

In plants, the dynamic nature of mitochondrial fission and fusion also exists. A recent study showed that plant mitochondria fuse and then split on a rapid and regular basis. Using a photoconvertible fluorescent protein transiently expressed in onion epidermis, Arimura *et al.* (2004) showed that almost complete mixing of mitochondrial contents occurs over two hours, and that mitochondria can fuse and split within 60 seconds. Notably, the authors also showed that there was no similar degree of mixing of contents of

peroxisomes and plastids over the same period; this is further evidence that plastids do not fuse in a related manner. Such rapid dynamics indicate that the machinery for mitochondrial fission and fusion probably can be regulated in response to external stimuli without any change in gene expression, explaining how the hypoxia-induced fusion is so rapid and reversible. Although very little is known about the molecular basis of mitochondrial shape dynamics in plants, *Arabidopsis* homologues of proteins involved in yeast mitochondrial dynamics have recently been identified, along with several mutants with altered morphology (Logan, 2003). Intriguingly, a novel dynamin-related protein, DR3PA, has recently been implicated in regulating the division of both mitochondria and peroxisomes (Mano *et al.*, 2004). A tempting scenario is that the large number of mitochondria in plant cells relative to yeast is due to a shift in the balance between the proteins involved in fission and fusion; it appears that small, numerous mitochondria and peroxisomes are important for metabolic efficiency since *dr3pa* mutants show significant growth retardation (Mano *et al.*, 2004).

In yeast, mitochondrial fusion is necessary for the inheritance of mitochondrial DNA (mtDNA) following mating, and it allows complementation of oxidatively damaged proteins to minimise cellular ageing (Westermann, 2003). Mitochondrial fusion in plants is very poorly studied, with little known about what developmental or environmental stimuli trigger it, with low oxygen levels being the only factor reported so far (Van Gestel and Verbelen, 2002; Ramonell *et al.*, 2001). As a result, it is difficult to speculate on the reasons for such dramatic changes in mitochondrial morphology in plants. One would expect oxidative stress to be low under oxygen limiting conditions, and sharing of mtDNA is unlikely to be necessary. Perhaps enlarged mitochondria use oxygen more steadily, thus prolonging the life of the cell. This may be a direct effect of reduced surface area, or an indirect one of reduced mitochondrial motility, leading to reduced ATP consumption and thus oxygen requirements. Significantly, anoxic or hypoxic condi-

tions are not alien to plants, with waterlogged roots being a prime example. Any such improvement in survival under oxygen-limiting conditions would be highly adaptive.

#### 4.3.4 Protein movement through stromules depends on molecular size

Transport of protein through stromules primarily occurs by diffusion, although a small contribution by an active component has been detected (Köhler *et al.*, 2000). A direct test of this hypothesis is that larger molecules would diffuse more slowly than smaller ones. Recently, it was reported that both Rubisco (550 kDa) and aspartate aminotransferase (90 kDa) could traffic through stromules when fused to GFP (Kwok and Hanson, 2004a). Inspection of the published FRAP curves suggested that stromules containing smaller fluorescent proteins recovered from photobleaching faster (Kwok and Hanson, 2004a), perhaps because of differences in diffusion rates. However, the relative movement of these two proteins could not be compared directly because of possible differences between plants and individual stromules: the proteins were not co-expressed. Although the range of molecular sizes of fluorescent proteins described here is smaller, direct comparisons can be made because of their co-expression in exactly the same place. The differences in photobleaching recovery between DsRED and aadA-GFP were small but consistent (Figure 4.7). Since both proteins are non-endogenous to plastids, it seems unlikely that one would be selected for transport into stromules in preference over another. This is supported by the fact that both proteins show identical distributions in stromules and plastid bodies (Figure 4.6). Significant amounts of active transport would result in similar rates of movement of both proteins through stromules, so diffusion seems to be the dominant mechanism. GFP diffusion in stromules is estimated to be 50-100 times slower than in the cytosol presumably because the stroma is proteinaceous and viscous (Köhler *et al.*, 2000). This implies that stromules might not be the best route for uptake and subsequent transport of metabolites and macromolecules towards the plastid body, or that smaller molecules are more likely to benefit from

stromule transport. However, this may not be important if metabolic processes are as active in stromules as in the rest of the plastid. Currently, there is no evidence for any degree of compartmentalisation within the plastid, with both the stroma and envelope being homogeneous across the plastid body and stromules.

An intriguing observation made from MSK57xDsRED seedlings was that the *aadA*-GFP signal was strongly attenuated in the dark relative to the light. The construct contained in the transplastomic MSK57 (FLARE16-S2) contains the 5' UTR and "downstream box" from the tobacco *rbcl* gene (Kahn and Maliga, 1999). The downstream box (DB) is a 42-nucleotide region encoding the amino terminus of *rbcl*, which enhances translation of artificial constructs 35-fold relative to those in which the DB has been inactivated by mutagenesis (Kuroda and Maliga, 2001). Although light induction of *rbcl* mRNA translation was not reported by Kuroda and Maliga (2001), the 5' UTR of *rbcl* has been implicated in regulating mRNA stability in the light (Shiina *et al.*, 1998). Furthermore, light induction of *rbcl* translation has been accredited to the activation of translation elongation complexes that form in the dark, although the mechanism by which light regulates this is unknown (Kim and Mullet, 2003). Thus, it appears that the upstream regions of FLARE16-S2 confer a light-dependent enhancement and/or dark-dependent repression of expression of the *aadA*-GFP fusion protein.

#### 4.3.5 Intercellular communication via organelles?

The observation of a large mitochondrion being passed from cell to cell is unprecedented. Cytoplasmic continuity is maintained through plasmodesmata (see §6.1.3), and passage of mitochondrial membranes through these structures is the most probable explanation, especially considering the topography of the mitochondrion and cell walls (Figure 4.11). The problem with such observations is reproducibility: the frequency of the event is so low the phenomenon cannot be readily investigated. Strength to the ar-

gument could be added by confirming that plasmodesmata coincide with the point of crossing. This would ideally be achieved by a plasmodesmatal marker, for example one based on a GFP fusion to an endogenous plant protein (Escobar *et al.*, 2003). In addition, cell walls can be highlighted with dyes such as propidium iodide. Intercellular transfer of organellar material has implications for the maintenance of homoplasmy and the transfer of organelle-based signals. However, the low frequency of such an event, coupled with the constrained conditions (low oxygen concentrations) that induced it, suggests that it could be an artefact of little significance. It is therefore important to investigate intercellular sharing of organelles in a system where a more functional basis can be envisaged: this is the topic of Chapter 6.

#### 4.3.6 Conclusions

The revelation of a link between the density of plastids within a cell and the abundance of stromules provides the basis for understanding their function. The important question is whether this truly results from plastids “sensing” their density or whether it is an indirect effect of increased cytoplasmic streaming in larger cells. This may be answered by analysing plastid division mutants to reduce plastid density yet further. The investigations of the morphology and dynamics of three distinct organelles have revealed a common theme – that they are all plastic and variable in shape and motility. Amongst the three, plastids and mitochondria exhibit the greatest variability, which may reflect an underlying requirement for this flexibility in cellular function. Now, our biochemical understandings of organelles must be consolidated with the new findings regarding their complex behaviour in plant cells.

# 5 THE ROLE OF THE ACTIN-BINDING PROTEIN CHUP1 IN STROMULE FORMATION

## 5.1 INTRODUCTION

### 5.1.1 The actin cytoskeleton is responsible for plastid movements

The cytoskeleton has a number of roles in plant cells, including orienting the plane of cell division and expansion (Kost *et al.*, 1999), ensuring segregation of chromosomes during cell division (Baskin and Cande, 1990) and vesicle trafficking (Williamson, 1993). The plant cytoskeleton is composed of two major structural components: microtubules and actin microfilaments, which carry out specific functions within the cell. Microtubules are polymers of  $\alpha$ - and  $\beta$ -tubulin heterodimers, and form tubules of 25 nm in diameter. F-actin microfilaments (filamentous actin) of 10 nm in diameter are formed from the polymerisation of G-actin monomers (globular actin). Formation of both microtubules and actin microfilaments is an energy-dependent process:  $\alpha$ - and  $\beta$ -tubulin heterodimers bind and hydrolyse GTP, whereas actin polymerisation requires ATP. Cellular pools of tubulin heterodimers and actin monomers are dynamically recruited into growing and shrinking microtubules and microfilaments, such that at any one time the majority of a cell's actin or tubulin complement may be incorporated into the cytoskeleton or may exist as free monomers. This dynamic ability to shift between polymerised and monomeric states allows extensive and rapid remodelling of the cytoskeleton, which is necessary for changes in cell growth and differentiation.

The actin cytoskeleton is intimately involved with organelle movements (Williamson, 1993). The motility of organelles allows their spatial repositioning during cell division, thus ensuring the continuity of organellar genomes (Sheahan *et al.*, 2004), and also improves distribution of large macromolecules whose diffusion is restricted by size. For

example, tip growth – the expansion of plant cells from one end, such as in root hairs or pollen tubes – requires the rapid transport of new cell wall and plasma membrane components to the growing tip. This is achieved through the polarised transport of Golgi-derived vesicles moving on actin tracks towards the growing point (Staiger, 2000). Golgi movement itself is also mediated by actin microfilaments (Boevink *et al.*, 1998), as is the movement of mitochondria (Van Gestel *et al.*, 2002) and peroxisomes (Jedd and Chua, 2002; Mathur *et al.*, 2002): the actin cytoskeleton is thus responsible for generalised cytoplasmic streaming movements observed in living plant cells (Williamson *et al.*, 1993). It is not surprising, therefore, that plastid motility is also brought about by interactions with actin. Direct interactions between plastids and actin have been inferred by immunofluorescence of F-actin together with chloroplasts in *Arabidopsis* mesophyll cells, which reveals longitudinal arrays of bundles of actin microfilaments and individual thin microfilaments extending randomly into the cell cortex (Kandasamy and Meagher, 1999). Chloroplasts are closely aligned with both the bundles and the thin microfilaments, whereas there is no alignment with microtubules (Kandasamy and Meagher, 1999). Moreover, actin filaments appear to form a basket-like formation that cradles individual chloroplasts. Treatment with the actin depolymerising drug latrunculin B disrupts this arrangement and causes clumping of chloroplasts, preventing their even distribution throughout the cell (Kandasamy and Meagher, 1999). Besides ensuring the continuity of plastids during cytokinesis, one function of chloroplast movement is to adapt to varying light intensities. Chloroplast movement has been documented in a number of species, and occurs in response to both suboptimal and excess light conditions: chloroplasts move either to maximise light interception, or to minimise it and avoid photodamage (Wada *et al.*, 2003). As expected, these chloroplast movement responses can be inhibited by actin depolymerising drugs (Wada *et al.*, 2003).

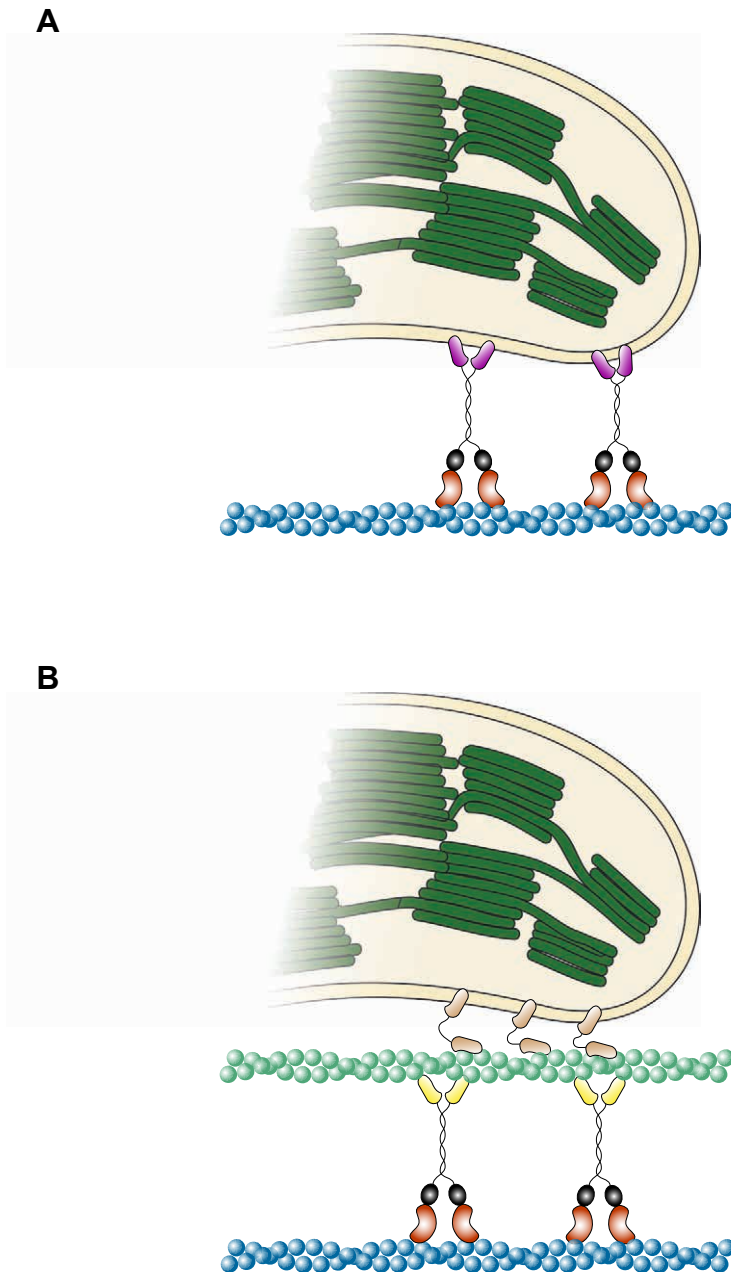


**Figure 5.1 Two types of force generating mechanism for organelle motility**

The motility mechanism depicted is acto-myosin based, using a chloroplast as an example organelle. (A) In the first mechanism, an organelle coated with envelope-bound myosin motor proteins interacts directly with an anchored F-actin track (blue). (B) An organelle is pulled by fixed cytoskeletal elements (green F-actin chains) that are anchored to the organelle envelope by attachment proteins. The attached actin tracks themselves move over a similar anchored track (blue F-actin). The two tracks move relative to one another using forces generated by myosins possessing two sets of actin-interacting heads (brown and yellow). Note that proteins and organelles are not drawn to scale.

## 5.1.2 Chloroplast avoidance movement involves the actin-binding protein

### CHUPI

Intracellular movement is brought about by the action of cytoskeletal binding proteins that generate force, generally termed motor proteins. In the case of actin, the motor protein myosin, or a myosin-like domain on a larger protein, is responsible for movement (Shimmen *et al.*, 2000). There are two conceivable molecular mechanisms for the movement of organelles such as chloroplasts on actin, both of which require a motor protein interacting with the actin and the organelle in some way (Williamson *et al.*, 1993). In the first, an organelle coated in motor proteins moves over an anchored actin track: here, the actin-organelle attachment is direct (Figure 5.1 A). Alternatively, the organelle lacks envelope-attached motor proteins but instead has associated with it further actin filaments, which then slide over a similar, anchored cytoskeletal track: this movement is mediated by motor proteins that do not directly interact with the organelle in question (Figure 5.1 B).

The motor proteins responsible for the movement of chloroplasts have remained elusive until recently, when an *Arabidopsis* mutant defective in the high light avoidance response was identified (Kasahara *et al.*, 2002). This mutant, termed *chup1* (for *chloroplast unusual positioning1*), shows neither avoidance nor accumulation of mesophyll chloroplasts in response to high or low light, and is thus defective in chloroplast movement in general. The cloning of the gene in question revealed *CHUPI* to encode an actin-binding protein, and the deficiency in organelle movement is chloroplast-specific (Oikawa *et al.*, 2003). The *CHUPI* sequence was deposited at GenBank/EBI under accession number AB087408, and is located at locus At3g25690 (TAIR Database). Since *CHUPI* is predicted to encode an actinin-like actin binding domain, it is possible that chloroplast avoidance movement is brought about at least in part by the second

mechanism outlined above, since CHUP1 is not predicted to have myosin-like activity (see §5.2.1).

### 5.1.3 Scope of this Chapter

Stromule movement is promoted by the activity of an acto-myosin-based system, inferred from inhibitor studies and fluorescent labelling of the actin cytoskeleton (Gray *et al.*, 2001; Kwok and Hanson, 2003; 2004a). Actin microfilaments are directly involved in the promotion of stromule movement, but microtubules inhibit it, most probably indirectly through physical blockage of movement by the dense microtubule network (Kwok and Hanson, 2003). The identification of a protein shown to be directly implicated in the general movement of chloroplasts suggests that such a protein may also be important in the pleiomorphic movements of plastids described in §1.3.1, and hence in the formation of stromules. Candidates for mediating the interaction between stromules and the actin cytoskeleton have remained elusive, and CHUP1 represents a subject worthy of investigation. Whilst CHUP1 may be actively involved in stromule formation, it is equally possible that CHUP1 may act as an anchoring protein to secure the chloroplast to actin. In such a scenario, it is plausible that the protein would inhibit plastid envelope motility: a reduction in CHUP1 levels might then increase the degree of stromule formation. This Chapter therefore describes the generation of plants deficient in CHUP1 activity, and the analysis of the resultant stromule phenotype.

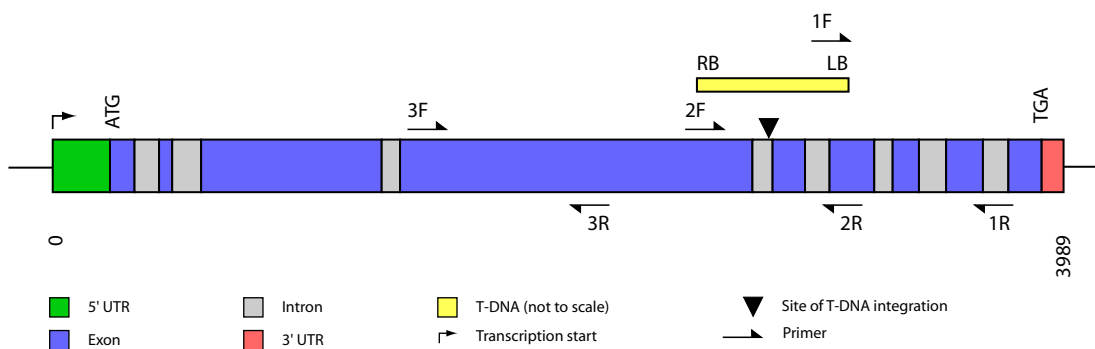
It should be noted that, in the process of carrying out this work, further details on the nature, function and subcellular location of CHUP1 were published by Oikawa *et al.* (2003). Specifically, the authors demonstrated that a truncated version of the protein could bind F-actin *in vitro* by co-immunoprecipitation, and that this protein fragment was targeted to the chloroplast membrane. In addition, they showed that *CHUP1* expression was confined to green tissues of the plant. Thus, certain aspects of the work

described in this Chapter have been reported already; nevertheless, this does not nullify attempts to elucidate a function for CHUP1 in stromule formation and movement.

## 5.2 RESULTS

### 5.2.1 CHUP1 binds actin through an $\alpha$ -actinin domain

*CHUP1* is a 4.0 kb gene (At3g25690; Figure 5.2) encoding a protein of 1044 amino acids. Homology-based analysis of the predicted protein sequence of CHUP1 reveals a number of conserved domains and three other putative gene family members (Table 5.1). However, the protein sequence of one of these (At5g61090) does not exhibit significant homology to CHUP1 in a BLAST-P search, so presumably the assignment of this gene to the same family is spurious and based solely on its proline-rich extensin and proline-rich domains and its chloroplast location (Table 5.1). Of the other two family members, only one (At4g94980) appears to possess features reminiscent of a cytoskeletal-related protein, namely a vinculin/catenin-like domain. Vinculin is a eukaryotic protein whose function is to anchor actin microfilaments to the plasma membrane, and interacts with other structural proteins such as  $\alpha$ -actinin (Niggli, 2001). This membrane-anchoring feature may well be fundamental to this protein's function in either organelle or vesicle movements in plants, but its function and location are presently unknown. Two other proteins with significant homology to CHUP1 are also highlighted in Table 5.1, although they are not classed as family members: these also have domains typical of actin-based cytoskeletal proteins, especially At1g54560 which appears to be a myosin-like motor protein (Table 5.1). Based on these homologies and the data described by Oikawa *et al.* (2003), it is highly likely that CHUP1 mediates an interaction between the chloroplast and the actin cytoskeleton, and so represents a plausible target for investigation in stromule movement and formation.



Primer pair	Forward (F)	Reverse (R)	Product size
1	5'-GCG TGG ACC GCT TGC TGC AAC T-3'	5'-CTC TAA ACG CGA AAC GAA CAC-3'	1114 bp
2	5'-GTT GAG TTT TAT CAA TCA TTG-3'	5'-CT ACA CAA AAC GAT AGA GAT TGA-3'	445 bp
3	5'-TGC ATG TTT ACG GTA TGA GTT-3'	5'-CTT GTT GTT GTG TTC TGA TTC-3'	512 bp

### Figure 5.2 *CHUP1* gene structure and PCR primers

*CHUP1* (At3G25690) consists of nine exons and eight introns, producing a mature transcript of 3.3 kb. SALK\_105043.36.90 contains a T-DNA insert at the 3' end of the fourth intron, with the T-DNA oriented such that the left border (LB) is upstream of the splice site. Also shown are the priming locations, sequences and expected PCR product size of three pairs of primers. Pair 1 and Pair 2 were used to screen SALK\_105043.36.90 for homozygotes. Pair 3 was used to generate a fragment of the largest exon, which was cloned and used to create the inverted repeat in the construct for silencing of *CHUP1* (Figure 5.2 A).

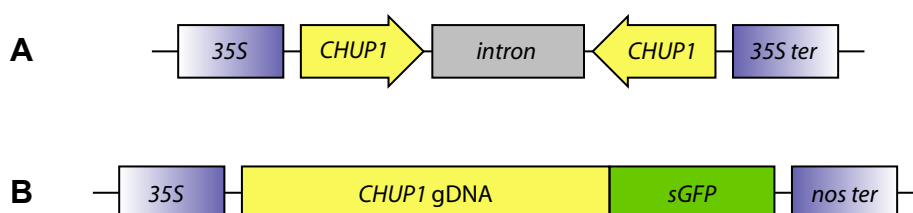


### Figure 5.3 Constructs generated to assess *CHUP1* function

(A) Construct designed to trigger post-transcriptional gene silencing of *CHUP1*, based on an inverted repeat of a 512 bp fragment of *CHUP1*. *35S*: CaMV 35S promoter; *35S ter*: CaMV 35S terminator. (B) Construct designed for subcellular localisation of *CHUP1*, using a full-length genomic DNA clone. *nos ter*: nopaline synthase terminator.

**Table 5.1** Selected results from a BLAST-P search of the CHUP1 amino acid sequence against known and predicted protein sequences in the *Arabidopsis* database

Family member	Domains of interest (number)	Predicted subcellular location	Homology to CHUPI (bit score)
At3g25690 (CHUPI)	Proline-rich extensin (3) Proline-rich (1) Actinin-type actin binding (1)	Chloroplast	N/A
At4g18570	Proline-rich extensin (4) Proline-rich (2)	Chloroplast	311
At4g04980	ATPase/GTPase (2) Proline-rich extensin (8) Proline-rich (1) Vinculin-catenin (4)	Unknown	78
At5g61090	Proline-rich extensin (4) Proline-rich (1)	Chloroplast	<30
At1g52080	Actinin-type actin binding (1)	Endomembrane system	202
At1g54560	ATPase/GTPase (2) Myosin (1) Myosin head (8)	Unknown	44

The bit scores reflect the number of identical amino acid matches between different alignments – a higher bit score indicates more significant homology. The upper four genes are predicted family members; the lower two are non-family genes encoding proteins with significant similarity to CHUP1. Source: The Arabidopsis Information Resource, <http://www.arabidopsis.org/>

## 5.2.2 Generation of lines with reduced *CHUP1* expression

In order to investigate how impaired CHUP1 function might affect stromules, two complementary approaches for reducing CHUP1 activity were employed. It should be noted that attempts to acquire the original *chup1-1* mutant described by Kasahara *et al.* (2002) were unsuccessful so direct analysis of the mutant was not possible. The lines generated were then crossed with transgenic individuals expressing the *recAgfp* transgene described elsewhere in this work (Chapter 3), in order to highlight plastids and stromules.

### 5.2.2.1 Silencing of CHUP1 by gene-specific post-transcriptional gene silencing

Disruption of CHUP1 activity can be achieved by inducing post-transcriptional gene silencing (PTGS). PTGS makes use of an ability conserved amongst eukaryotes to degrade double-stranded RNA (dsRNA) in a gene-specific manner, thus preventing its translation (Yu and Kumar, 2003). PTGS can be triggered by introducing an artificial inverted repeat of part of a target gene for silencing, with each repeat separated by an intron (Smith *et al.*, 2000). When transcribed *in planta*, such a construct will generate complementary dsRNA that will attain a tight hair-pin structure upon splicing of the intron. dsRNA molecules are recognised by the cell as targets for degradation, producing a collection of short RNAs of between 21 and 25 bp in length, termed small interfering RNAs (siRNAs). The siRNAs correspond to both the sense and antisense strands of the target gene, and form part of the degradation system to act as a trigger for the specific degradation of the endogenous, target mRNA (Hamilton and Baulcombe, 1999). In this study, a construct was made which contained two inverted repeats of a 521 bp fragment of *CHUP1* separated by an intron, driven by the CaMV 35S promoter (Figure 5.3 A; based on a binary vector described by Karimi *et al.*, 2002). Construct integrity was verified by PCR, restriction digestion and sequencing, which confirmed that the two repeats were in opposite orientation flanked by 35S promoter and terminator se-

quences (data not shown). The construct was mobilised into *Arabidopsis* (ecotype Columbia) by *Agrobacterium*-mediated transformation, and seven independent lines were identified as positive by PCR (data not shown). Three of these were chosen for expression analysis by northern blotting, all of which exhibited significantly reduced levels of steady-state *CHUP1* transcript accumulation without affecting transcript levels of a control gene (Figure 5.4). These lines were allowed to set seed and homozygous T<sub>2</sub> lines were generated based on resistance to phosphinothricin-containing herbicide, and were termed *CHUP1*\_RNAi/1, *CHUP1*\_RNAi/2 etc. These lines were used as both pollen acceptors and donors in crosses with lines expressing *recAgfp*.

#### 5.2.2.2 Isolation of insertion knock-out mutants of *CHUP1*

As a complement to the gene-silencing route and as a control for verifying the phenotypic effects of *CHUP1* PTGS, databases of T-DNA insertion lines were searched for lines containing a T-DNA insertion within *CHUP1*. One SALK line, SALK\_105043.36.90 (Alonso *et al.*, 2003), was identified where the T-DNA has landed within intron 4 of *CHUP1* (Figure 5.2). Since the insertion is only one base pair from the 3' end of the intron, its position is likely to disrupt the intron splice site and prevent correct splicing. It is expected that this would result in reduced levels, if not complete loss, of *CHUP1* activity in individuals homozygous for the insertion. Homozygotes were identified by PCR using two sets of primers: one pair spanning the putative insertion site, and another pair testing for the presence of the T-DNA insert by using one primer homologous to the left border (LB) of the T-DNA and another that binds downstream of it within *CHUP1* (Figure 5.2). In the case of an azygous or heterozygous individual, the first primer pair should produce a PCR product of 445 bp in size; homozygotes however should produce no band because the intervening T-DNA on both chromosomes greatly increases the necessary amplification distance. In heterozygotes and homozygotes, the second primer pair should produce a band of 1114 bp, which consists of 167 bp from

the LB sequence and the remaining 857 bp from *CHUP1*. Homozygous individuals, therefore, should produce no band with the first primer pair and a band of 1114 bp with the second pair (Figure 5.5). A faint band of approximately 450 bp is formed in all individuals subjected to PCR with the second primer pair (Figure 5.5, lower panel), which is an artefact of the LB primer binding elsewhere in the *Arabidopsis* genome, and which can be produced using this primer alone (data not shown). From these test PCRs, three homozygotes were identified; surprisingly, there were no heterozygotes, which may be due to seed contamination in an otherwise homozygous population. These homozygotes were selfed, and one line, hereafter termed N605043, was chosen for use as a pollen acceptor in crosses with lines expressing *recAgfp*.

### 5.2.3 *CHUP1* is expressed strongly in wild type green tissue but not in roots

As part of determining that *CHUP1* gene expression was reduced in the *CHUP1*\_RNAi lines, gene expression in various tissues of wild type plants was also examined by northern analysis. As shown in Figure 5.4, *CHUP1* expression is highest in both young and mature leaves, and *CHUP1* is expressed to a lesser degree in tissue from the inflorescence axis. Root expression, however, was undetectable. Attempts to isolate RNA from green siliques were repeatedly unsuccessful, but the pattern of expression seems to be limited to green tissues, in keeping with the role of *CHUP1* as a protein involved in the cellular distribution of chloroplasts. However, since stromules are abundant on root plastids, it is clear at least that *CHUP1* cannot be an essential component of stromule movement or formation.

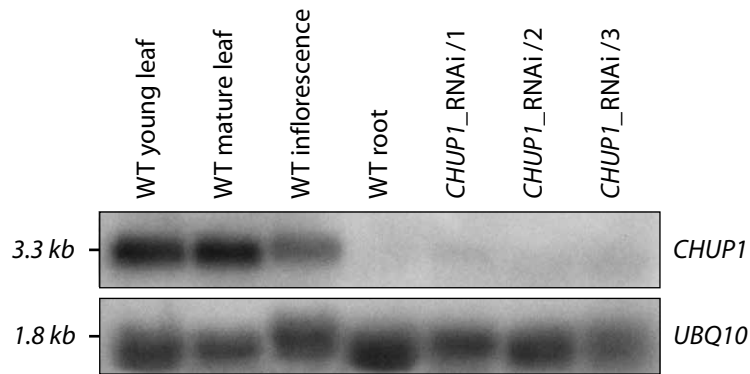


**Figure 5.4 Expression of *CHUP1* in wild type and *CHUP1*\_RNAi lines**

Total RNA was electrophoresed, blotted onto a charged nylon membrane, probed with  $^{32}\text{P}$ -labelled *CHUP1* or *UBQ10* (ubiquitin) fragments and exposed to X-ray film. Upper panel: steady-state levels of *CHUP1* mRNA from various organs of wild type plants and from young leaf tissue of three independent *CHUP1*\_RNAi transformants. The *CHUP1* probe is composed of 600 bp of exon 4 and is distinct from the 521 bp used in the *CHUP1*\_RNAi construct. Lower panel: expression from the *UBQ10* gene as a loading and blotting control.

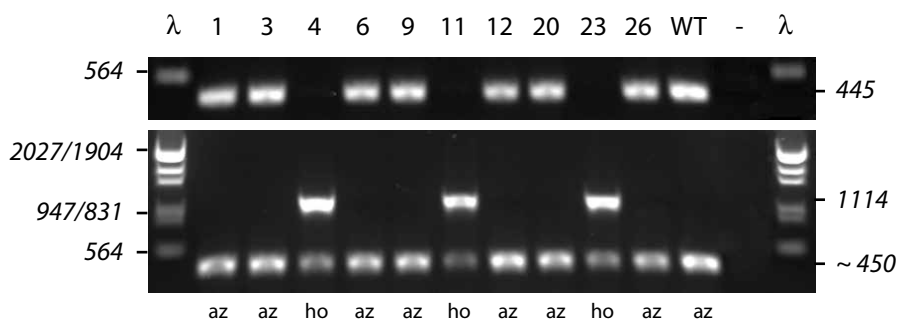


**Figure 5.5 PCR screen for *CHUP1* T-DNA insertion mutants**

Genomic DNA was isolated from ten individuals putatively homozygous for a T-DNA insert within *CHUP1*, and used in PCR with two sets of primers. DNA marker sizes are indicated on the left, product sizes are on the right. Upper panel: Primer Pair 1, spanning the insert location; presence of a band at 445 bp indicates at least one chromosome does not carry the insertion. Lower panel: Primer Pair 2, with one primer homologous to the LB and the other primer hybridising downstream of the insert site within *CHUP1*; a band of 1114 bp indicates at least one chromosome carries the insertion. Lack of a band with Primer Pair 1 and a band of the correct size with Primer Pair 2 indicates the individual is homozygous for the insertion. Note the band of approximately 450 bp in the lower panel - this is due to spurious hybridisation of the LB primer elsewhere in the *Arabidopsis* genome.  $\lambda$ , Lambda DNA digested with *HindIII/EcoRI*; WT, wild type; -, negative control (no template). Numerals correspond to individuals selected at random for DNA extraction. az: azygous for the insertion; ho: homozygous for the insertion.

#### 5.2.4 Subcellular localisation of CHUP1 by fusion with GFP

Since CHUP1 was postulated to act as a chloroplast movement protein, it seemed likely that it should be present on the chloroplast envelope. To determine whether this is the case, an in-frame C-terminal fusion of CHUP1 with sGFP was created (Figure 5.3 B). The construct consisted of the entire genomic coding sequence of *CHUP1* (exons and introns, but excluding any UTRs) and the sGFP coding sequence (Chiu *et al.*, 1996) linked via a 14 amino acid linker to ameliorate protein folding. The entire construct was driven by the 35S promoter, followed by the nopaline synthase terminator at the 3' end. Construct integrity was confirmed at the 5', 3' and linking ends of the construct to ensure that recombination had occurred correctly during construct assembly (see §2.6.1.6). *Arabidopsis* plants were transformed by floral dipping and nine primary transformants survived kanamycin selection and transfer to soil. Despite extensive examination, no GFP fluorescence could be detected in any of these lines. To confirm that the construct was being expressed at the transcriptional level, northern blotting was performed by probing with *sgfp*. A transcript of approximately 4.0kb was detectable in the transgenic lines, which corresponds to the size of the *CHUP1-sgfp* fusion once introns have been processed (Figure 5.6). The northern analysis further indicated that the transgene was expressed strongly in at least two lines with varying degrees of expression in the others. Since no GFP expression could be observed by microscopy, this experiment was abandoned; nevertheless, whilst the presence of frame-shift mutations in the transgene cannot be fully ruled out, it is notable that the same experiment using the full-length *CHUP1* cDNA also produced no GFP expression, probably because of protein mis-folding (Oikawa *et al.*, 2003).

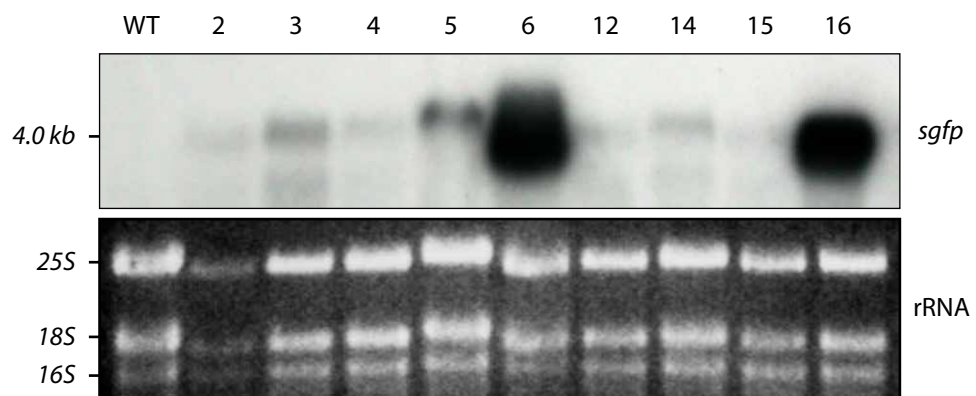


**Figure 5.6 Northern analysis of primary transformants expressing *CHUP1-sgfp***

Total leaf RNA was electrophoresed, blotted onto a charged nylon membrane, probed with a full-length  $^{32}\text{P}$ -labelled fragment of *sgfp* and exposed to X-ray film. Upper panel: a 4.0kb transcript was detected in all samples but was most abundant in individuals 6 and 16. Lower panel: ethidium bromide-stained gel showing the three major rRNA bands, indicating approximately equal loading of total RNA.



**Figure 5.7 Reduction of CHUP1 activity leads to increased propensity to photodamage**

Three-week old wild type (WT Col.), *CHUP1*\_RNAi/2 and N605043 individuals were exposed to strong white light ( $1200 \mu\text{mol m}^{-2} \text{sec}^{-1}$ ) for a total of 48 hours, and photographed every 12 hours. Plants had an adequate supply of water at all times, and temperature was maintained at between 22 and 25 °C. Photodamage was apparent earlier and was more severe in those individuals where CHUP1 activity was compromised.

### 5.2.5 Lines with reduced CHUP1 activity exhibit a *chup1-1* mutant phenotype

To verify that reduced CHUP1 gene expression correlates with reduced function of the protein, a screen was performed that tested the tolerance of the plants to inhibitory levels of light. The ability of chloroplasts to avoid high light fluences is central to avoiding photoinhibition which, if not overcome, would lead to excess levels of active oxygen species, cellular death and leaf necrosis. Over a time course of 48 h, exposure of wild type plants to strong, cool white light ( $1200 \mu\text{mol m}^{-2} \text{sec}^{-1}$ ) led to paling of leaf appearance and some scorching and necrosis of older leaves, but generally the plants tolerated the light levels with minimal damage (Figure 5.7). In contrast, identical treatment of *CHUP1*\_RNAi and N605043 individuals led to relatively more necrotic photodamage. This is evident both in terms of the absolute extent of scorching over the whole 48 h, and in the rate of appearance of such photodamage: even after 12 h of treatment, both lines were suffering appreciably more than wild type (Figure 5.7). Thus, this simple procedure confirmed that reduction of *CHUP1* gene expression phenocopies the *chup1-1* mutant described by Kasahara *et al.* (2002), presumably because of the reduced chloroplast avoidance movement that this mutant exhibits.

### 5.2.6 Crossing of *recAgfp* lines and lines with reduced CHUP1 activity

Plastid-targeted GFP was introduced into genetic backgrounds with reduced CHUP1 activity by crossing. The crossing strategy and screening procedures are depicted in Figure 5.8. Reciprocal crosses were performed between wild type plants expressing *recAgfp* and those expressing the *CHUP1*\_RNAi construct (Figure 5.8 A). In addition, a plant homozygous for the T-DNA insertion in *CHUP1* (N605043) was also crossed with a *recAgfp* line (Figure 5.8 B). Seed from four individual F<sub>1</sub> plants of the crosses with *CHUP1*\_RNAi/2 were kept for the F<sub>2</sub> generation: two individuals from a cross using *CHUP1*\_RNAi/2 as the female parent, termed Cross 1, and two from a cross using *recAgfp*/1 as the female parent, termed Cross 2 (Figure 5.8 A). For crosses with N605043

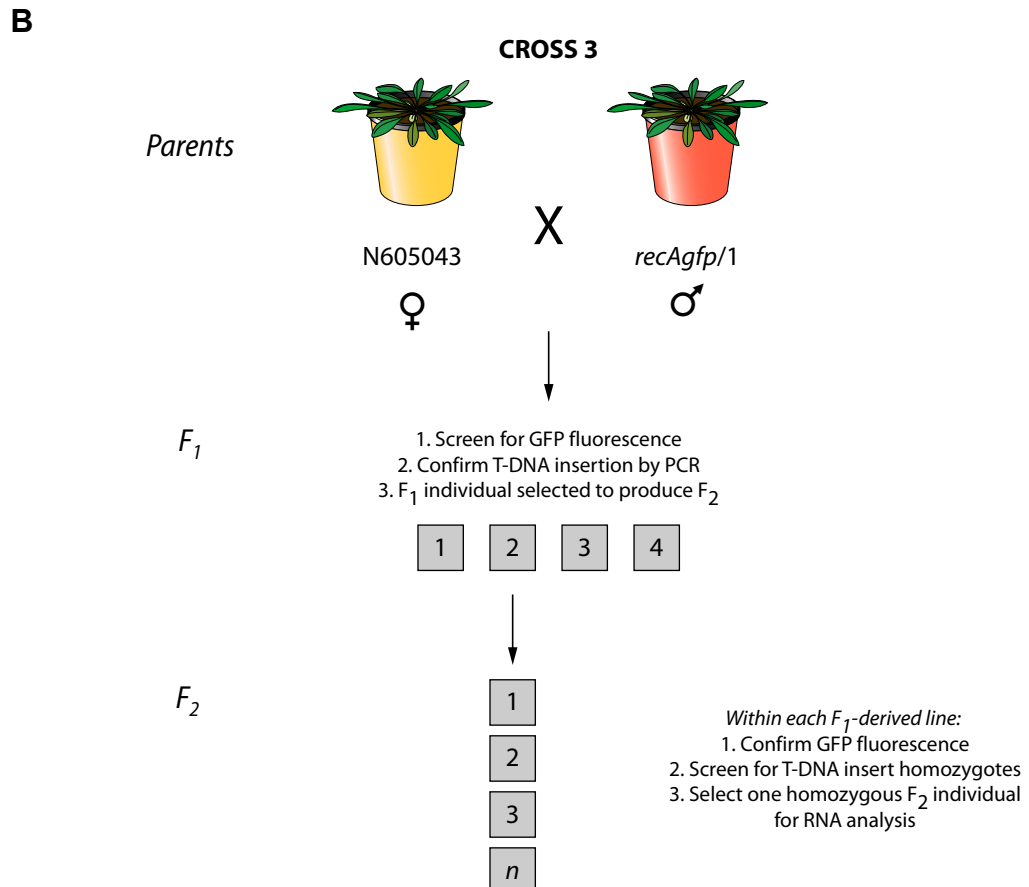
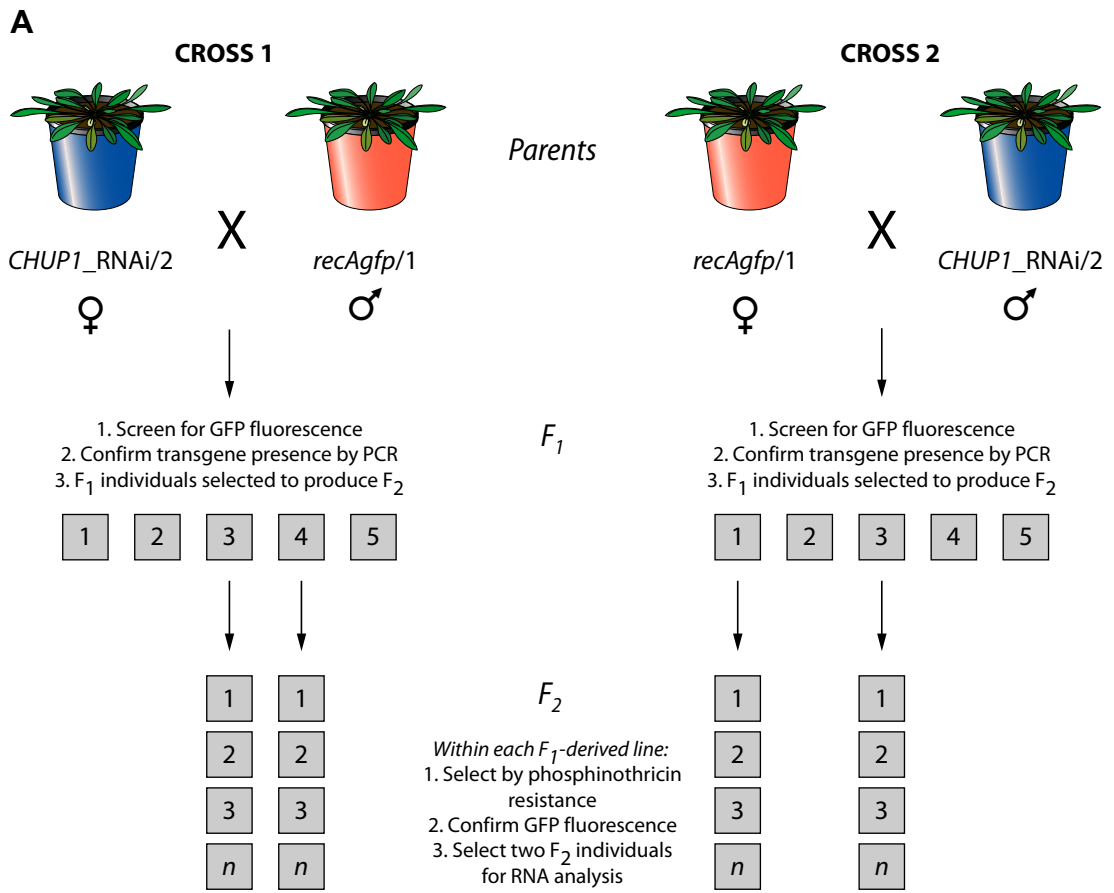
(Cross 3), seed from only one F<sub>1</sub> individual generated by this cross (Cross 3) was taken to the F<sub>2</sub> generation.

Successful crosses were confirmed by screening the F<sub>1</sub> populations by PCR, thus identifying F<sub>1</sub> candidates to be selfed for F<sub>2</sub> seed (Figure 5.9 A). For Crosses 1 and 2, F<sub>2</sub> plants carrying both transgenes were identified first by resistance to phosphinothricin (conferred by the *CHUP1*\_RNAi construct) and then by GFP expression. In the case of Cross 3, F<sub>2</sub> plants were screened for GFP fluorescence and then further identified as homozygotes with respect to the T-DNA insert as outlined in §5.2.2.2 above (Figure 5.9 B). Only one GFP-expressing F<sub>1</sub> individual was obtained from Cross 3, thus yielding only one F<sub>2</sub> family for analysis. In the F<sub>2</sub> generation of this cross, just two homozygotes were identified (Figure 5.9 B).

To confirm that the effect of the *CHUP1*\_RNAi transgene on the endogenous *CHUP1* gene was inherited following crossing, northern blot analysis was carried out using RNA isolated from F<sub>2</sub> individuals of each cross. As depicted in Figure 5.8, two F<sub>2</sub> individuals were analysed per family for Cross 1 and Cross 2, such that a total of four individuals were assessed per cross. This provided an estimate of inter- and intra-family variation in the silencing phenotype. For Cross 3, one F<sub>2</sub> individual homozygous for the T-DNA insert was analysed. *CHUP1* expression was significantly and consistently reduced in all individuals carrying the *CHUP1*\_RNAi transgene, but silencing was incomplete, accumulating perhaps 25% of the transcript levels found in wild type (Figure 5.10). However, the individual from Cross 3 exhibited total loss of *CHUP1* transcript accumulation (Figure 5.10), suggesting that lines homozygous for the T-DNA insertion are effectively null mutants. Thus, the *CHUP1*\_RNAi lines and N605043 homozygotes comprise a spread of *CHUP1* expression levels, which should assist in the characterisation of the role of *CHUP1* in chloroplast morphology.

**Figure 5.8 Crossing of plastid-targeted GFP and *CHUP1*-compromised plants**

(A) Reciprocal crosses between *recAgfp*/1 (red pot) and *CHUP1*\_RNAi/2 (blue pot) lines. The F<sub>1</sub> generation was screened as shown and two randomly chosen, successfully crossed individuals were allowed to set seed and create the F<sub>2</sub> generation. This generation was also screened as shown and analysed as separate lines. (B) Cross between N605043 and *recAgfp*/1. The descendants of this cross were analysed as shown and maintained as separate lines; only one F<sub>1</sub> individual carried the *recAgfp* transgene. Grey boxes with numbers indicate individual plants; *n* depicts an indefinite number of individuals in the F<sub>2</sub> generation.



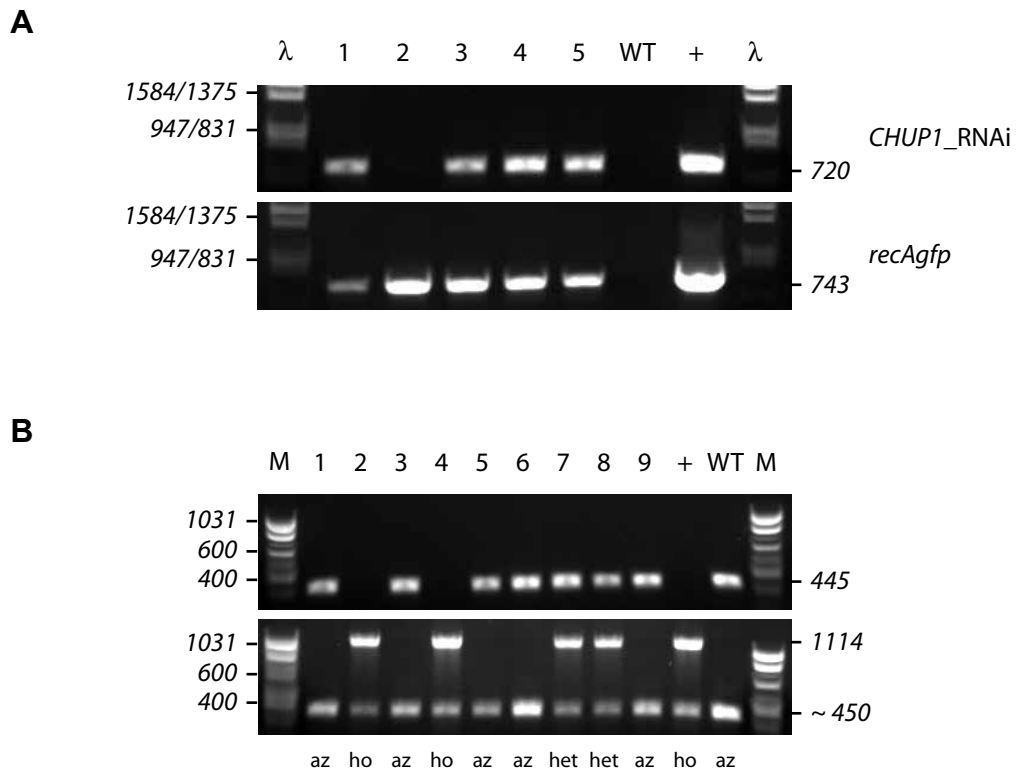


**Figure 5.9 PCR screen for confirmation of crosses and isolation of N605043 homozygotes**

DNA marker sizes are indicated on the left, product sizes are on the right. (A) Example of verification of successful cross between *CHUP1\_RNAi* lines and *recAgfp* lines. Genomic DNA was extracted from various F<sub>1</sub> individuals. Upper panel: detection of *CHUP1\_RNAi* construct; individual 2 did not inherit the transgene. Lower panel: detection of *recAgfp* transgene. PCR conditions, target sequences and primers are described in §2.6.4. Individuals 1 & 2 were F<sub>1</sub> plants from Cross 1, whereas individuals 3, 4 & 5 were from Cross 2. Positive control (+) was either genomic DNA from a parental line (upper panel) or plasmid DNA (lower panel). (B) Analysis of F<sub>2</sub> individuals following a cross between N605043 and *recAgfp/1*. Genomic DNA samples were subjected to PCR using the same primer pairs as described in Figures 5.1 & 5.4. Homozygotes are identified by the lack of band in the upper panel and the presence of a 1114 bp band in the lower panel. Ho: homozygote; het: heterozygote; az: azygote. M: 1000 bp DNA marker; λ, Lambda DNA digested with *HindIII/EcoRI*; WT, wild type.

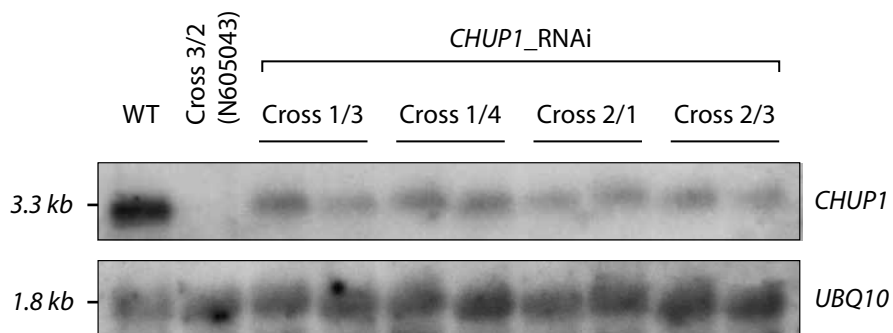


**Figure 5.10 Expression of *CHUP1* in the F<sub>2</sub> generation following crossing**

10 µg of total RNA was electrophoresed, blotted onto a neutral nylon membrane, probed with <sup>32</sup>P-labelled *CHUP1* or *UBQ10* gene fragments and exposed to X-ray film. RNA was isolated from young, emerging leaves. A total of eight F<sub>2</sub> individuals carrying the *CHUP1*\_RNAi transgene were analysed: two per F<sub>1</sub> descendant per cross (refer to Figure 5.7). One F<sub>2</sub> individual from Cross 3, homozygous for the T-DNA insertion, was also analysed. "Wild type" (WT) RNA was isolated from the *recAgfp/1* line as a control. Terminology: Cross Y/Z refers to F<sub>2</sub> descendants of Cross Y, F<sub>1</sub> individual Z (refer to Figure 5.7). Probes used are identical to those described in Figure 5.3.

### 5.2.7 The effects of reduced CHUP1 levels on chloroplast morphology

Using confocal microscopy, whole leaf sections were examined for chloroplast morphology in wild type and CHUP1-deficient lines expressing plastid-targeted GFP. Unfortunately, the level of GFP expression in both N605043 homozygotes identified by PCR (Figure 5.9 B) was insufficient to carry out microscopy. The *recAgfp* lines were particularly prone to silencing, such that seedlings scored as GFP-positive would frequently acquire systemic silencing of the transgene later in development. Time constraints meant that identification of more plants homozygous for the T-DNA insertion could not be performed.

When compared with wild type plants, *CHUP1*\_RNAi plants exhibited no obvious differences in chloroplast morphology. Several leaves from over five F<sub>2</sub> individuals were analysed, paying special attention to the pleiomorphic changes in chloroplast shape. A distinction should be made here between chloroplast movement, which is the locomotion of an entire plastid, and chloroplast motility, which refers to the pleiomorphic changes in shape associated with the chloroplast envelope. Wild type plastids from mesophyll tissues comprise a central chlorophyll-containing region surrounded by a thin periphery of stroma, which contains GFP (Figure 5.11 E). This stromal periphery corresponds to the transparent, motile “jackets of material” (Wildman *et al.*, 1962) that surround the chlorophyll-containing inner structure, and is the basis of chloroplast pleiomorphy and stromule formation. From this region, loops, nodules and occasional tubular stromules of material can be seen (Figure 5.11 E). In *CHUP1*\_RNAi plants, these structures are also visible, and there was no consistent disparity between the two genotypes (Figure 5.11 F). It is, however, noteworthy that in *CHUP1*\_RNAi plants, the palisade mesophyll chloroplasts did not arrange themselves within the cell in the same manner as wild type plants. In order to produce large amounts of young, vigorously growing vegetative tissue for microscopy and molecular analysis, the F<sub>2</sub> generation was

grown under short day conditions. The plants were grown in an artificial growth room, with light supplied by fluorescent tubes at an intensity of approximately  $200 \mu\text{mol m}^{-2} \text{sec}^{-1}$ . In wild type plants grown at this light intensity, chloroplasts are mostly in the periclinal position – i.e. facing perpendicular to the light – as inferred by the relative light transmission of the leaf (Kasahara *et al.*, 2002). This behaviour, known as chloroplast accumulation, maximises light interception (Wada *et al.*, 2003). However, chloroplasts in *CHUP1*\_RNAi plants do not act in this manner, and instead remain more randomly distributed in the cell, with an increased number associated with the anticlinal cell walls. Indeed, Oikawa *et al.* (2003) note that *chup1* chloroplasts accumulate at the bottom and lateral sides of the cell. It is likely that this consistent phenotype of *CHUP1*\_RNAi plants is a result of their impaired ability to respond appropriately to light conditions. This inference is supported by the necrotic phenotype of *CHUP1*\_RNAi plants grown under high light intensity (Figure 5.7). To confirm this, chloroplasts from N605043 plants were also imaged. In such plants, chloroplasts show no ordered accumulation at the upper surface of the cell, and are mostly found at the bottom of the palisade cells instead (Figure 5.12). Therefore, the *CHUP1*\_RNAi plants closely mimic the null mutant phenotype of N605043.

To examine more closely the effects of reduced *CHUP1* gene expression, stromule formation and movement were assessed. The basic machinery for stromule formation was evidently not compromised in *CHUP1*\_RNAi plants, with stromules clearly visible on some mesophyll chloroplasts (Figure 5.13 A-C). Such stromules were rare, in keeping with the plastid and cell type, but were similar in frequency and form to wild type. Stromule movement was also ostensibly unaffected, with rapid movements of the plastid envelope taking place in both epidermal and mesophyll cells (Figure 5.13 D-L). Such time lapse sequences showed stromule movements that were indistinguishable from wild type. On the basis of these results, *CHUP1* does not appear to be substantially involved in regulating chloroplast envelope dynamics. Notwithstanding the issue of in-

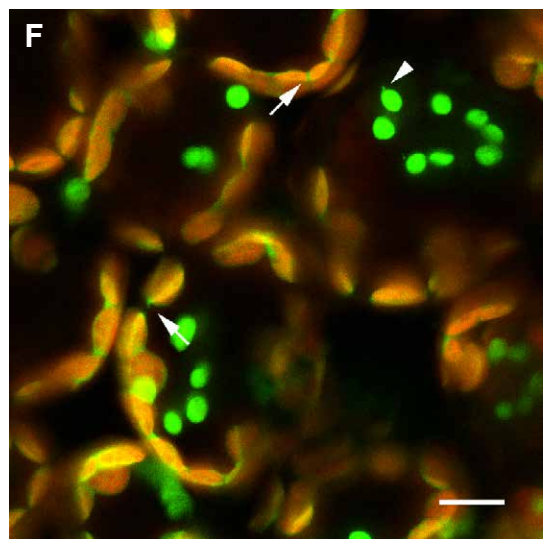
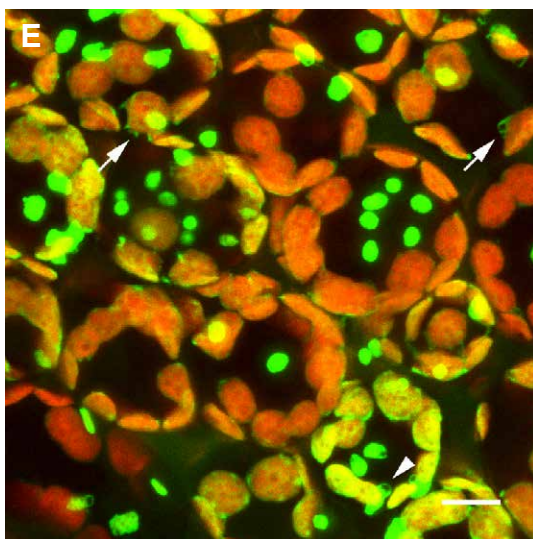
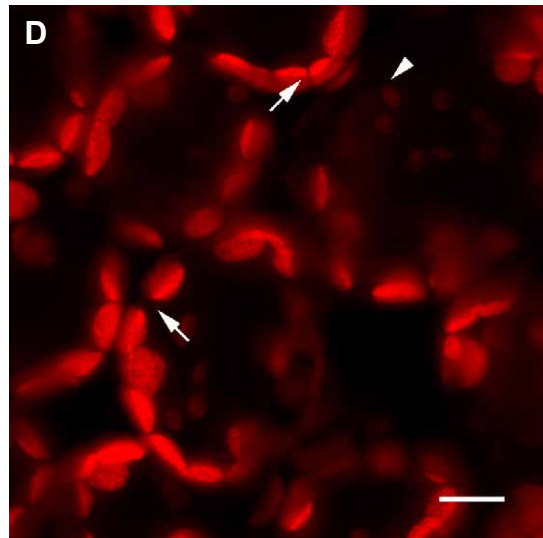
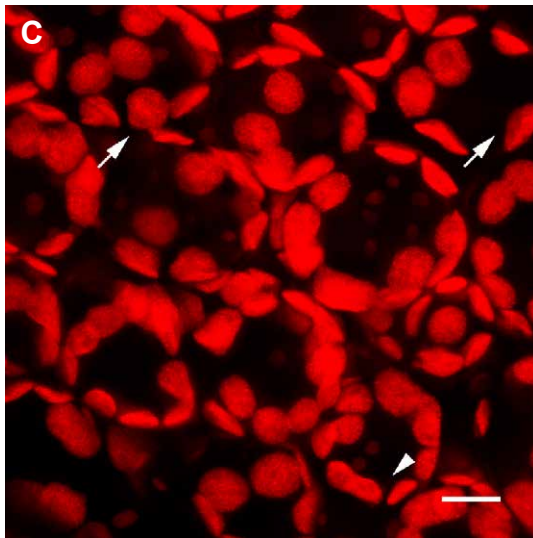
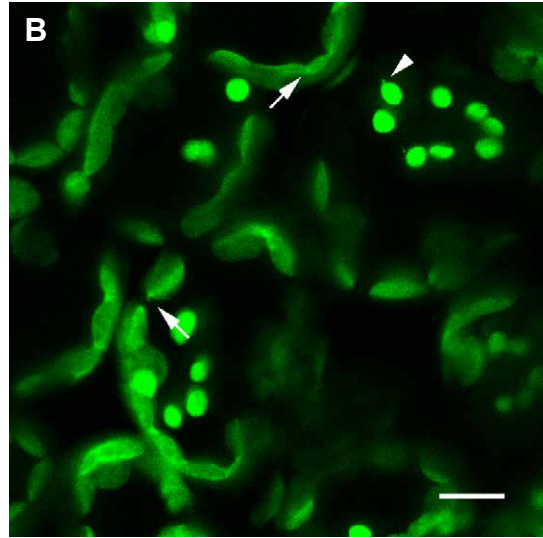
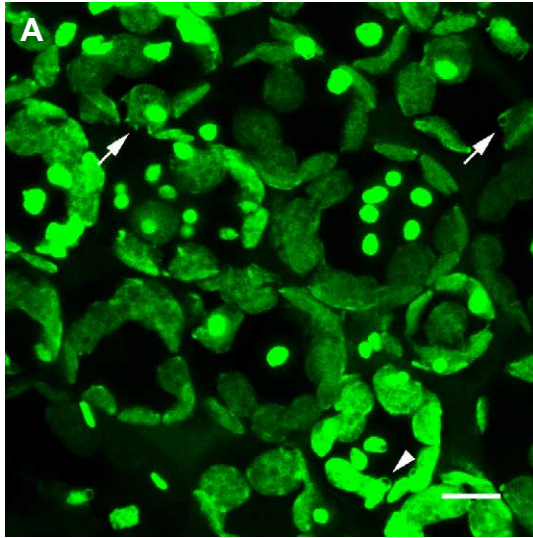
complete CHUP1 disruption by use of RNAi, the effects, if any, of reduced CHUP1 activity on stromules are subtle, and their elucidation would require more extensive examination.

**Figure 5.11 Leaf plastid morphology in wild type and *CHUP1*\_RNAi plants**

Confocal maximum projections through the upper 10-15  $\mu\text{m}$  of the adaxial leaf surface. The GFP signal is shown in green (A, B) and the chlorophyll autofluorescence signal in red (C, D). Merging the two channels (E, F) reveals that the GFP signal largely colocalises with that of chlorophyll, except at the periphery of chloroplasts. Plastid envelope protrusions are present on both epidermal (arrowheads) and palisade mesophyll chloroplasts (arrows). Note that the chlorophyll signal is much weaker, and the GFP signal stronger, from epidermal plastids than from mesophyll chloroplasts. Epidermal plastids are also smaller and are thus easily distinguished from mesophyll chloroplasts. Plastid morphology is similar in both wild type and *CHUP1*\_RNAi leaves, with both genotypes showing a normal "peripheral jacket" of GFP. Likewise, stromule-like protrusions are visible in both genotypes. Note, however, that the mesophyll chloroplasts in *CHUP1*\_RNAi plants are arranged close to the anticlinal cell walls, exposing relatively little plan area to the periclinal cell surface (see text for explanation). Scale bar: 10  $\mu\text{m}$ .

WT

*CHUP1*\_RNAi



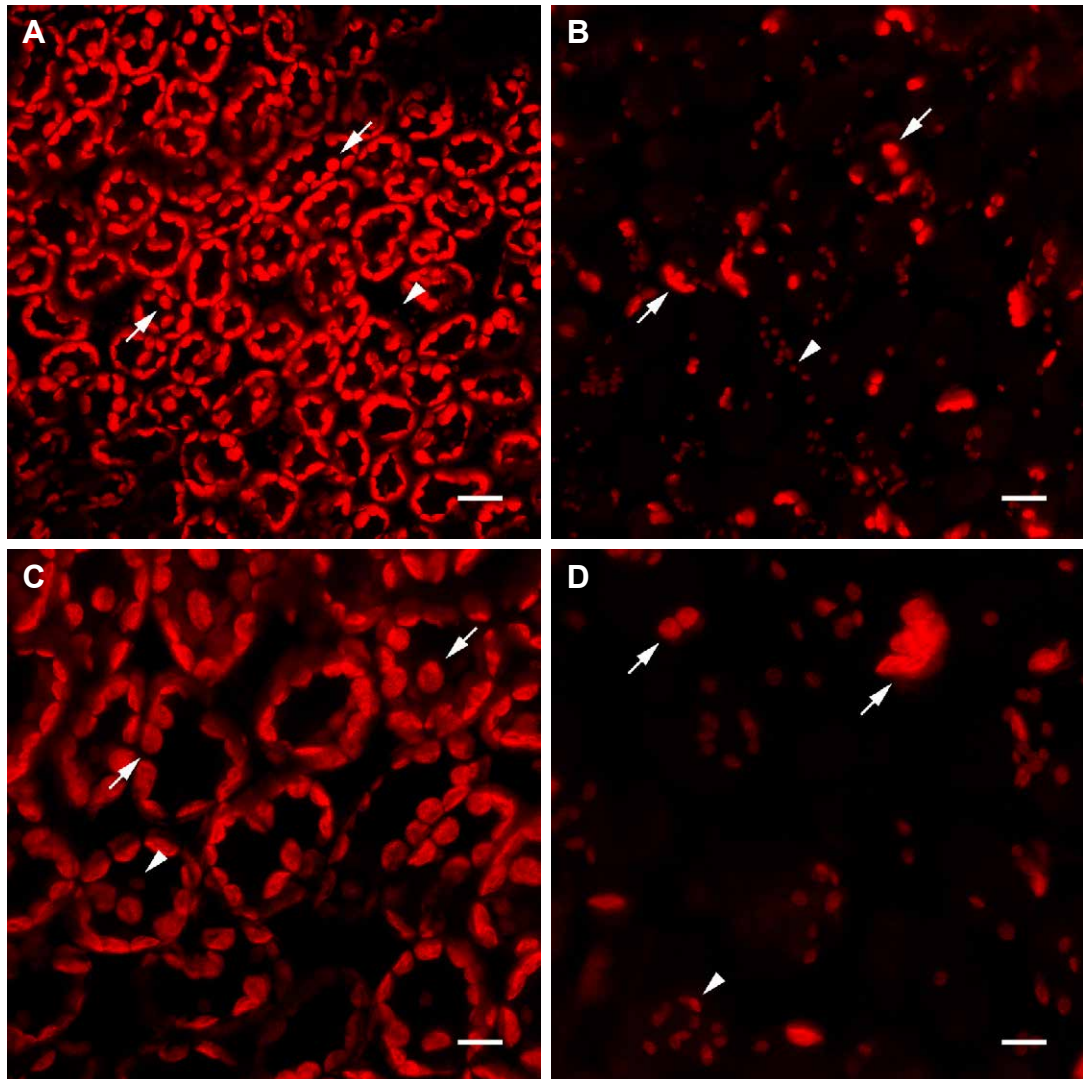
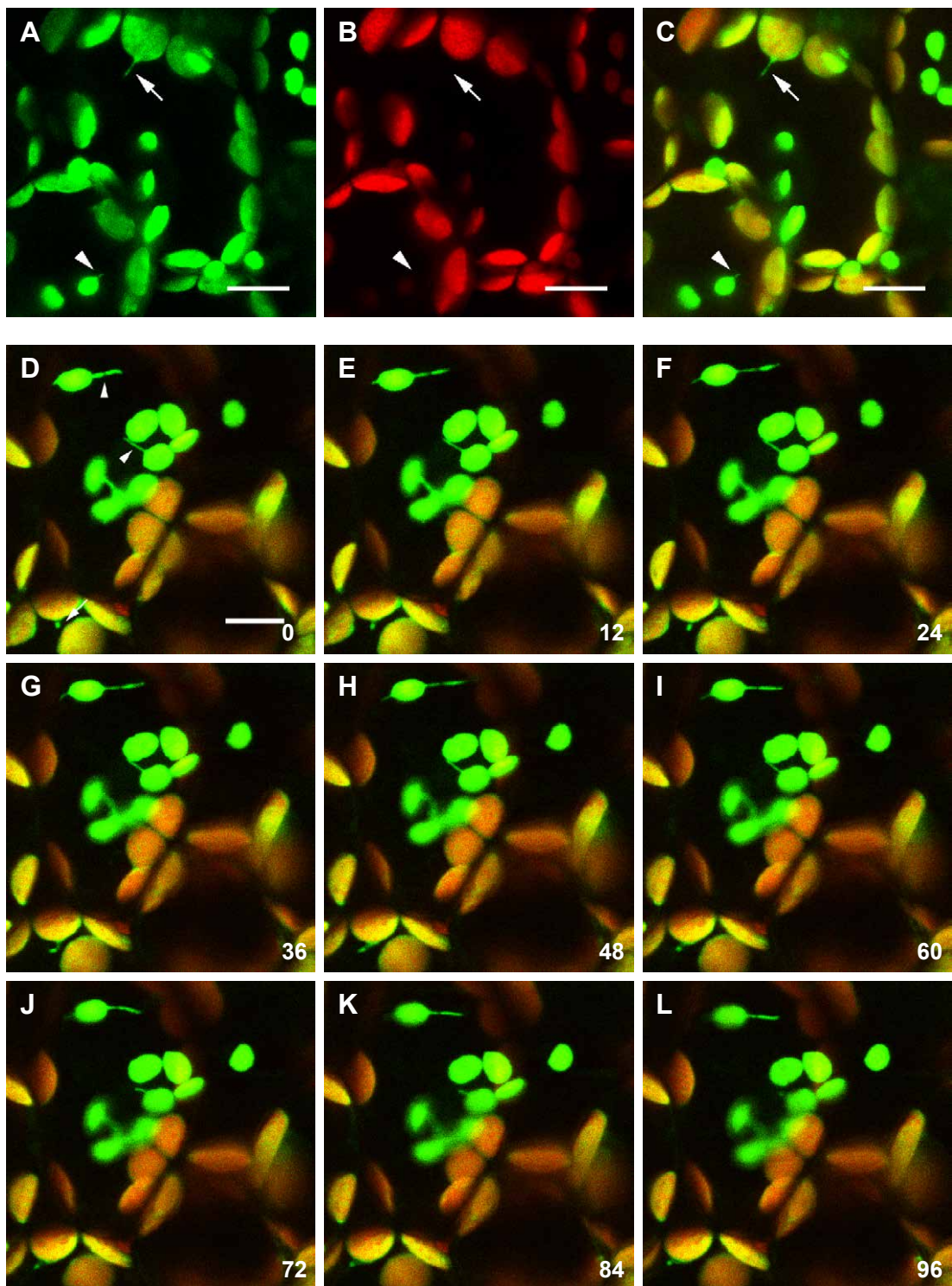


**Figure 5.12 N605043 plants exhibit improper chloroplast accumulation under low light**

Confocal maximum projections of the leaf adaxial surface of plants grown under  $200 \mu\text{mol m}^{-2} \text{s}^{-1}$  of light, using chlorophyll autofluorescence to highlight plastids. Shown are two different magnifications of wild type tissue (A, C) and N605043 tissue (B, D). Under these light conditions, chloroplasts in wild type mesophyll cells (arrows) accumulate in the periclinal position to increase light interception (A, C). Loss of CHUP1 activity in N605043 leads to much less ordered chloroplast positioning, with the mesophyll cell plan area poorly covered by chloroplasts (B, D). Note how the cell outline is readily perceptible in wild type tissue where the chloroplasts are closely aligned with the cell walls. In the mutant, chloroplasts accumulate at the bottom of the cell (only the upper  $25 \mu\text{m}$  is imaged here). Arrowheads indicate poorly fluorescing epidermal plastids which possess relatively little chlorophyll. Scale bar: A, B  $20 \mu\text{m}$ ; C, D  $10 \mu\text{m}$ .

**Figure 5.13 Stromule formation and movement is unaffected in *CHUP1* RNAi plants**

(A-C) Confocal maximum projections through the upper 9  $\mu\text{m}$  of the adaxial leaf surface. GFP (A), chlorophyll (B) and combined (C) channels are shown. Note the prominent stromule emanating from a mesophyll chloroplast (arrow), as well as one from an epidermal plastid (arrowhead). (D-L) Time-lapse series taken from a single confocal plane. Merged GFP and chlorophyll signals are shown. Both epidermal (arrowhead) and mesophyll (arrow) protrusions exhibit substantial motility over the time course, with extensions, re-contractions and changes in direction. Numbers indicate time (in seconds). Scale bar: 10  $\mu\text{m}$ .



## 5.3 DISCUSSION

### 5.3.1 CHUP1\_RNAi phenocopies the *chup1-1* mutant

Chloroplasts of the *chup1-1* mutant do not respond to high or low intensities of light, due to a fault in an association between chloroplasts and the actin cytoskeleton (Kasahara *et al.*, 2002; Oikawa *et al.*, 2003). The primary phenotype of the mutant is disrupted chloroplast arrangement, which leads to photodamage and tissue necrosis under high light intensities. Using RNAi to selectively downregulate *CHUP1*, this phenotype was observed: the plants were super-sensitive to light (Figure 5.7) and exhibited irregular mesophyll chloroplast distributions (Figure 5.11). Whilst northern analysis indicated that the reduction in *CHUP1* gene expression was not complete, it was clearly sufficient to bring about a phenotype. The *chup1-1* mutation was induced by a T-DNA integration into exon 4 but some residual expression remained and may not therefore be a complete knockout (Oikawa *et al.*, 2003), implying that the RNAi lines should mimic the *chup1-1* mutant quite well. The presence of a T-DNA insertion in *CHUP1*, carried by N605043, resulted in total knockout of the gene expression and produced a slightly more severe phenotype. Correspondingly, N605043 represents a sound basis for comparing with the RNAi effects, and confirms that the RNAi approach was reliable.

### 5.3.2 CHUP1 is probably not required for stromule formation and movement

Since N605043 is null with respect to *CHUP1*, it is unfortunate that no microscopic observations of stromules could be made because of problematic GFP expression. Whilst a null mutant would have been the ideal subject for stromule investigation, the RNAi approach, which results in an observable phenotype, still allows a valid assessment of *CHUP1* as a component of the machinery regulating plastid morphology. Since the RNAi lines presumably possessed some residual *CHUP1* activity, one cannot rule out completely the effects of this protein on stromule formation and motility. However,

given the severe effects on plant sensitivity to photodamage, it seems likely that any other roles for CHUP1 also would have been affected. Thus, with some caveats, it appears that the actin-binding protein CHUP1 is not a key player in stromule regulation. This also suggests that chloroplast movement in response to light intensity and chloroplast envelope motility (including stromule formation) are two separate processes with different regulatory systems.

If both chloroplast movement and stromule formation require an intact actin cytoskeleton, how might the mechanics of the two processes differ? The available evidence suggests that stromules move on ready-formed actin microfilaments, although the relative movements of the filaments themselves may also influence stromule morphology (Kwok and Hanson, 2003; Kwok and Hanson, 2004b). In contrast however, chloroplast movement may involve the nucleation and polymerisation of new actin tracks, since a chloroplast will move away in any direction when a bright beam of light a few micrometres in diameter is focused near it (Wada *et al.*, 2003). The implication of the data presented in this Chapter is that the motor proteins involved in stromule formation are distinct from those in chloroplast movement. In a mutant screen, several different alleles of *chup1* were isolated (Oikawa *et al.*, 2003), suggesting a high degree of mutagenesis saturation. Together with the strong *chup1* phenotype, this suggests that only one chloroplast-located protein is required for the locomotion of chloroplasts in response to light. The logical conclusion, therefore, is that other actin-based motor proteins are responsible for producing the force for stromule movement. This leaves the myosin family as strong candidates.

Myosins are classified into 18 subfamilies, termed myosins I – XVIII, of which three, myosins VIII, XI and XIII are found in plants (Hodge and Cope, 2000). Examination of sequence data reveals that *Arabidopsis* contains 17 myosin sequences (Reddy and Day,

2001), of which one, At1g54560, shows significant similarity to CHUP1 (Table 5.1). Thirteen *Arabidopsis* myosins are of the myosin XI subfamily, whilst four are in class VIII (Reddy and Day, 2001); class XIII myosins have so far only been found in the Characean alga *Acetabularia* (Hodge and Cope, 2000). Although the phylogenetic relationships are unclear, class XI myosins structurally resemble non-plant class V myosins, which are involved in vesicle transport in yeast (Bretscher, 2003). The possibility of shared structure reflecting shared function, and their relative abundance in plant genomes, has led to a limited amount of research into myosin XI activities in plants.

Isolation of myosins has been largely hampered by their extreme sensitivity to proteases. Recently, a 175 kDa intact myosin was isolated from cultured tobacco cells and its biochemical activities dissected closely. This protein comprises a globular head domain and an  $\alpha$ -helical coiled-coil tail domain involved in dimer formation (Tominaga *et al.*, 2003). In addition, the protein contains a neck domain of six repeating motifs which bind six calmodulin molecules. Such affinity for calmodulin suggests a regulatory dependence on  $\text{Ca}^{2+}$ , which has been shown to inhibit cytoplasmic streaming in Characean algae (reviewed by Shimmen and Yokota, 1994). Using an optical tweezer arrangement to isolate single beads coated in the tobacco 175 kDa myosin, Tominaga *et al.* (2003) showed that a single molecule moves along actin tracks in a processive manner (i.e. in constant contact with actin) in steps of 35 nm, and at speeds of  $7 \mu\text{m s}^{-1}$ . The velocity decreased with increasing ADP concentration but increased with increasing ATP concentration, typical of ATPase-dependent motor activity. The maximal velocity does not approach that of  $100 \mu\text{m s}^{-1}$  of cytoplasmic streaming in some Characean algae (Shimmen and Yokota, 1994), but multiple myosins per vesicle may improve the speed under optimal, cellular conditions. However,  $7 \mu\text{m s}^{-1}$  is of the correct order of magnitude for estimates of peroxisomal ( $6 \mu\text{m s}^{-1}$ , Jedd and Chua, 2002) and mitochondrial ( $10 \mu\text{m s}^{-1}$ , Van Gestel *et al.*, 2002) movement in higher plants.

Two other reports have implicated myosins of class XI in organelle movement, including that of plastids, in plants. Only one study has investigated the effects of knocking out a specific myosin gene on plant development. The *MYA2* gene of *Arabidopsis* is predicted to encode another 175 kDa polypeptide with domains typical of class XI myosins. Two T-DNA insertions in *MYA2* were reported by Holweg and Nick (2004), one of which was found to be lethal in the homozygous state. The other mutation, *mya2-1*, led to severe defects in plant growth at several stages of development. Mutant plants suffer a generally reduced stature with decreased internodal length, impaired fertility and aberrant trichome branching (Holweg and Nick, 2004). In addition, epidermal cells showed reduced speeds of cytoplasmic streaming. Close inspection of the growth defects revealed that cell elongation was inhibited in *mya2-1* mutants. The authors reasoned that impaired intracellular polar auxin transport within vesicles might be responsible for the reduced cell elongation and thus dwarf growth habit of the mutant, supported by the fact that basipetal transport of auxin in excised stem segments was half that of wild type (Holweg and Nick, 2004). Thus, this particular member of class XI myosins may be associated with a specific membrane-bound cargo, with other members of the class being associated with other organelles. A second report has implicated class XI myosins from maize in mitochondrial and plastid motility. Using a myosin XI-specific antibody, class XI myosins were detected by immunofluorescence in both tissue sections and on isolated organelles (Wang and Pesacreta, 2004). The authors found that myosin XI associated with mitochondria and plastids, but not peroxisomes or nuclei. In addition, myosin XI was present in smaller punctuate structures distributed throughout the cytoplasm, which may represent endomembrane-derived vesicles. Thus, although not specific to any one myosin protein, these data provide good evidence that myosins are prime candidates for mediating organelle motility and, by implication, stromule formation.

### 5.3.3 Conclusions

As a means to establish the role of specific proteins in stromule biogenesis, RNAi and reverse genetics are powerful techniques that, given time, should yield positive results. With a relatively small family of putative myosin motor proteins, high through-put RNAi should be feasible. Future research in this area should now move away from inhibitor studies and towards transient and stable transgenic technologies to target specific genes. It will also be important to confirm that chloroplast movement responses are indeed separate processes to chloroplast envelope motility. In conjunction with mutant analysis, this could be addressed by a more rigorous investigation into the sensitivity of each process to light quality and quantity. In addition, now that actin dynamics can be followed *in vivo* with GFP fusions, it should be possible to determine whether novel actin polymerisation is involved in chloroplast movement, confirming that this is distinct from stromule formation and motility. Speculatively, CHUP1 may act as a site of nucleation for actin polymerisation at the surface of chloroplasts. Alternatively, it may bind actin microfilaments which themselves slide over other actin microfilaments, with the force provided by myosins (Figure 5.1 B). In this way, two chloroplast movement systems are superimposed upon one another: chloroplast avoidance and accumulation movements, mediated by CHUP1, and chloroplast envelope motility, presumably mediated independently by myosins. However, it remains to be established whether the two systems are totally independent, or whether they overlap and share common regulatory signals.

## 6 STROMULE BIOGENESIS IN MAIZE CHLOROPLASTS

### 6.1 INTRODUCTION

#### 6.1.1 C<sub>4</sub> photosynthesis

Within the plant kingdom, there are two primary mechanisms for the photosynthetic fixation of inorganic carbon, termed C<sub>3</sub> and C<sub>4</sub> photosynthesis. The majority of terrestrial plants perform C<sub>3</sub> photosynthesis, where atmospheric carbon dioxide (CO<sub>2</sub>) diffuses into chloroplasts, is fixed directly by Rubisco and is incorporated into the Calvin cycle, a process which can occur entirely within one cell. Tomato is an example of a typical C<sub>3</sub> plant. However, an estimated 8000 species of angiosperms, or about 3% of all terrestrial plant species (Sage *et al.*, 1999), carry out the more complex C<sub>4</sub> photosynthesis. This mode of fixing carbon has been termed “co-operative photosynthesis” (Karpilov, 1970; cited in Leegood, 2000) because of the division of labour between two distinct cell types within the leaf. C<sub>4</sub> plants are widely distributed taxonomically, with both monocot and dicot members (Sage *et al.*, 1999), but all possess common features collectively known as Kranz anatomy (Nelson and Dengler, 1999; Figure 6.1). Firstly, the leaf of a C<sub>4</sub> plant consists of two photosynthetic cell types which are morphologically and biochemically distinct. These are the bundle sheath (BS) cells, which surround the leaf vascular tissue, and the mesophyll cells, distributed in a radial manner around the BS cells. This defines the second feature of Kranz anatomy: that mesophyll cells are arranged toward the exterior of the leaf, directly in contact with the intercellular air spaces, with the BS cells innermost to the mesophyll cells. In addition, because the fixation of carbon is shared between the two cell types, mesophyll and BS cells must be closely juxtaposed in order to minimise the transport distance for metabolites between cells – because of this fact, no mesophyll cell is more than one cell removed from a bundle sheath cell (Hattersley and Watson, 1975). Finally, there is some form of physical mechanism for limiting CO<sub>2</sub> leakage from BS cells; in the case of maize (*Zea mays* L.)

this is achieved through a suberized lamella, which restricts apoplastic movement of solutes (Sowínski *et al.*, 2003).

In  $C_4$  plants,  $CO_2$  is initially fixed in mesophyll cells before being transported to BS cell chloroplasts where the Calvin cycle operates. The process is based upon an auxiliary metabolic cycle, called the  $C_4$  cycle (Figure 6.2). The  $C_4$  cycle acts as a  $CO_2$ -concentrating mechanism in order to improve the efficiency of Rubisco under photo-respiratory conditions (Sage and Pearcy, 2000). Under such conditions, typified by high light fluences and temperatures, the oxygenase activity of Rubisco becomes much more significant relative to its carboxylase activity, leading to the loss of fixed carbon from the Calvin cycle.  $C_4$  plants avoid this metabolic cost by restricting Rubisco to the BS cells, away from molecular oxygen, whilst simultaneously delivering  $CO_2$  by means of the  $C_4$  cycle. In mesophyll cells, atmospheric  $CO_2$  initially reacts with water to form the hydrogen carbonate ion ( $HCO_3^-$ ), which combines with the three-carbon molecule phosphoenolpyruvate (PEP) forming the  $C_4$  acid oxaloacetate. This fixed carbon is imported into mesophyll chloroplasts, and reduced to malate before being shuttled to the BS cells. Once in the BS chloroplasts, the malate is decarboxylated to yield the  $C_3$  acid pyruvate. The resultant  $CO_2$  provides a substrate for Rubisco, and pyruvate is returned to the mesophyll cells to complete the cycle (Figure 6.2). There are three different sub-types of  $C_4$  photosynthesis, defined mainly by the decarboxylating enzyme in BS chloroplasts (Dengler and Nelson, 1999); maize utilises an NADP-dependent malic enzyme (NADP-ME).

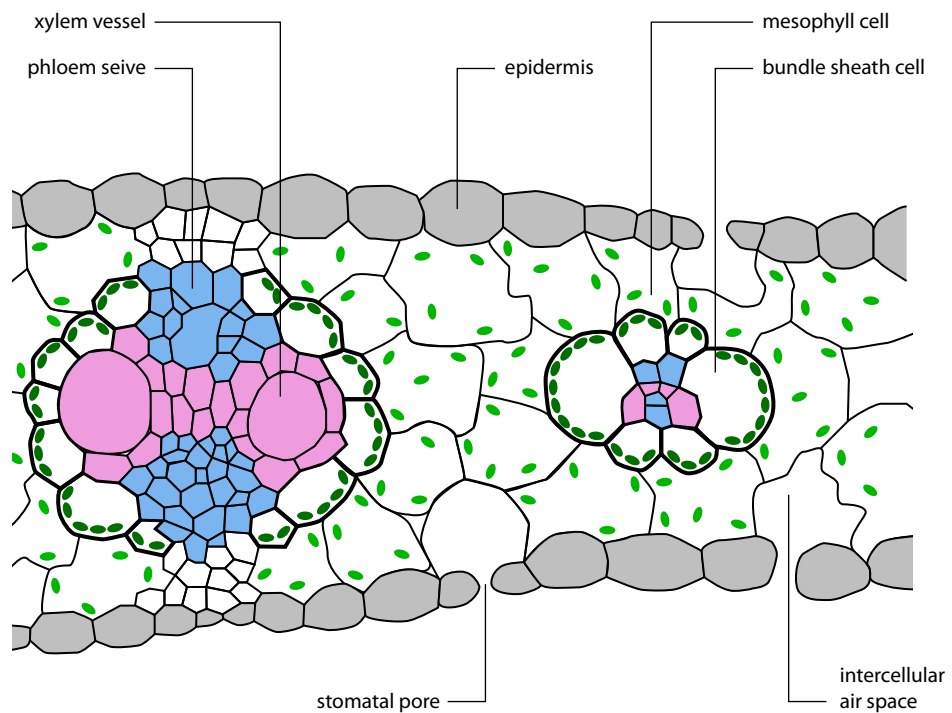


**Figure 6.1 Transverse section of a *Zea mays* leaf**

The maize leaf consists of two photosynthetic cell types. The bundle sheath (BS) cells are distributed in a radial fashion around the vasculature (pink and blue). Mesophyll cells separate adjacent vascular bundles (major vein to the left side of the diagram, minor vein to the right). Gaseous exchange with the atmosphere occurs between the mesophyll cells and intercellular air spaces. Mesophyll cells have evenly distributed chloroplasts (light green) whereas BS cells have centrifugally arranged chloroplasts juxtaposed against the mesophyll-BS boundary. BS cells have a suberized, thickened cell wall at this boundary, here depicted with heavier cell outlines.

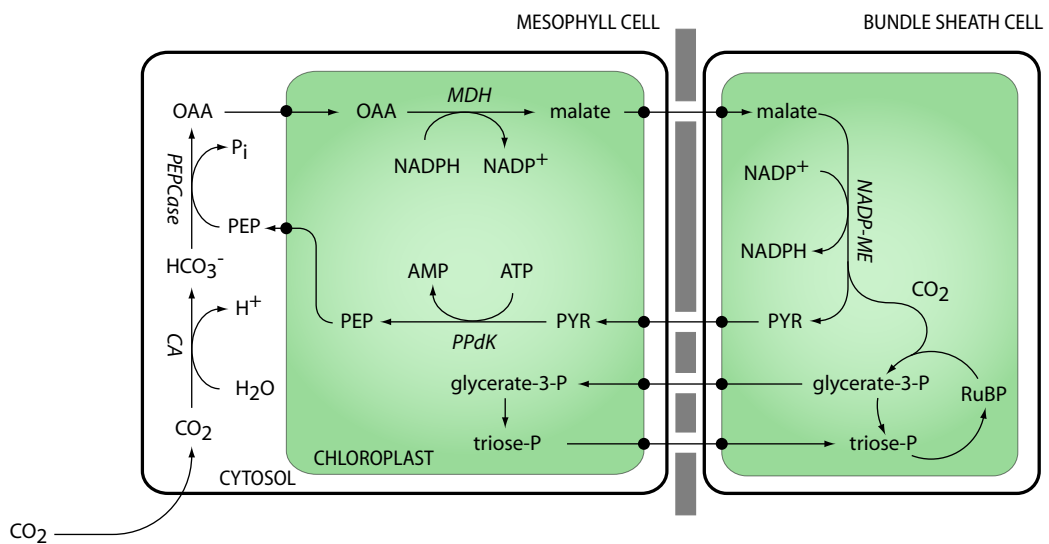


**Figure 6.2 The C<sub>4</sub> cycle requires intercellular metabolite shuttling between two cell types**

Inorganic carbon is fixed in the mesophyll and shuttled in the form of a C<sub>4</sub> acid to the bundle sheath, which is then decarboxylated to provide CO<sub>2</sub> for the Calvin cycle. Simultaneously, reduction of BS-derived glycerate-3-phosphate is performed in the mesophyll chloroplasts, and the resulting triose-phosphates returned to the Calvin cycle in the BS. Solid circles depict putative anion transporters located on the chloroplast envelope; enzymes are labelled in *italics*. CO<sub>2</sub>, carbon dioxide; HCO<sub>3</sub><sup>-</sup>, hydrogen carbonate ion; P<sub>i</sub>, inorganic pyrophosphate; OAA, oxaloacetate; NADPH/NADP<sup>+</sup>, nicotinamide adenine dinucleotide phosphate; PYR, pyruvate; PEP, phosphoeno/pyruvate; RuBP, ribulose bisphosphate; P, phosphate. CA, carbonic anhydrase; *PEPCase*, PEP carboxylase; *MDH*, malate dehydrogenase; *NADP-ME*, NADP-dependent malic enzyme; *PPdK*, pyruvate orthophosphate dikinase.

### 6.1.2 Metabolite movement during C<sub>4</sub> photosynthesis

C<sub>4</sub> photosynthesis depends upon the intercellular transport of metabolites between BS and mesophyll cells. Moreover, there must also be adequate transport between compartments within the cell, because the C<sub>4</sub> cycle is shared between the chloroplast and cytosol. Efficient metabolite transport is fundamentally important not only to ensure the shuttling of compounds from one cell to another, but also to coordinate the rates of CO<sub>2</sub> fixation by the C<sub>4</sub> and Calvin cycles. The Calvin cycle product glycerate-3-phosphate (glycerate-3-P), for example, is exported to the mesophyll chloroplasts for reduction to triose phosphates (triose-P) because of the lack of Photosystem II activity in the bundle sheath (Figure 6.2). The accumulation of triose-P in the mesophyll leads to activation of PEPCase, since high concentrations of triose-P result indirectly from increased Calvin cycle activity in the BS, signalling a need for increased CO<sub>2</sub> fixation by PEPCase in the mesophyll (Leegood, 2000). Such BS-mesophyll metabolic cross-talk ensures photosynthetic efficiency under varying environmental conditions, but is crucially dependent on rapid directional shuttling of the metabolites involved.

Various lines of evidence indicate that extensive communication occurs between the two photosynthetic cell types. Direct attempts to quantify the distribution of C<sub>4</sub> metabolites between the BS and mesophyll tissues of *Z. mays* leaf blades show that certain compounds are highly asymmetrically distributed: some 95% of total leaf blade malate is estimated to be in the mesophyll (Leegood, 1985). This distribution results in a concentration gradient of 87.5 mM, but this is complicated by the fact that much of this malate is photosynthetically inactive (i.e. sequestered in the vacuole), and so precise measurements of C<sub>4</sub> malate gradients are difficult to determine. Leegood (1985) confirmed the presence of a concentration gradient for phosphoenolpyruvate as predicted by the C<sub>4</sub> cycle, and also revealed the unequal distributions of glycerate-3-P (mostly in the BS) and triose-P (mostly in the mesophyll), establishing the operation of the glycer-

ate-3-P/triose-P shuttle as outlined above. These first reports (Leegood, 1985; Stitt and Heldt, 1985) suggested that pyruvate is at higher concentrations in the mesophyll than it is in the BS, leading to a gradient in a direction opposite to that expected. However, this was later shown to be a result of build-up of pyruvate in mesophyll chloroplasts, thus obscuring the true gradient between the cytosols of BS and mesophyll cells (Flügge *et al.*, 1985). Such concentration gradients have led to the view that the intercellular transport of C<sub>4</sub> metabolites occurs by means of simple diffusion alone (Leegood, 2000). This transport certainly occurs very rapidly, as inferred by pulse-chase experiments with <sup>14</sup>C followed by microautoradiography. Within just two seconds of exposure to <sup>14</sup>CO<sub>2</sub>, a significant amount of radiolabel is present in the bundle sheath cells of *Atriplex spongiosa*, despite the fact that the mesophyll is also well labelled (Osmond, 1971).

### 6.1.3 Plasmodesmata in the maize leaf

Rapid fluxes of such metabolites can only be accounted for by means of considerable direct (symplasmic) connections between the two cell types, since plasma membranes and suberized cell walls are relatively resistant to anion transport. Symplasmic connections between adjacent plant cells are mediated by membranous structures called plasmodesmata (PDs). PDs are formed either during cytokinesis of cells within the same layer (i.e. L1, L2, L3), which are termed primary plasmodesmata, or post-cytokinetically, where they are laid down in pre-existing cell walls (secondary plasmodesmata). PDs ensure continuity between cells in three ways: the plasma membrane, cytosol, and endoplasmic reticulum (ER) of adjacent cells are all contiguous, as each is a component of PDs (Kragler *et al.*, 1998). The ER is appressed at the point of passing through PDs, presumably for steric reasons, but significantly this illustrates that PDs permit the passage of membranes other than the plasma membrane.

Besides ions and small metabolites, PDs are capable of transporting macromolecules and their ability to do so changes dynamically *in vivo* (Kragler *et al.*, 1998; Jackson, 2000). Early estimates using dye microinjection techniques indicated that the size exclusion limit (SEL) of PDs is less than 1 kDa, thus excluding the possibility of protein or nucleic acid transport (Jackson, 2000). However, it was later discovered that virus movement proteins (MPs) mediate the transfer of viral nucleic acids from cell to cell through PDs by transiently increasing the SEL of PDs to at least 20 kDa (reviewed in Lucas, 1997). Furthermore, phloem unloading in developing (i.e. sink) leaves is brought about by endogenous changes in the SEL of PDs. By measuring phloem-specific expression and movement of GFP in tobacco, Oparka *et al.* (1999) demonstrated that the sink status of tissues is correlated with increased movement of GFP from cell to cell, both within and between cell layers. Closer investigation with GFP fusion proteins suggested that PDs in sink tissue have a plasmodesmal SEL of between 47 and 61 kDa, whereas source tissues had a dramatically smaller SEL (Oparka *et al.*, 1999). In addition, specific, endogenous proteins also have the ability to modulate the SEL of PDs. The KNOTTED1 (KN1) protein of maize is involved in specifying leaf primordia in the shoot apical meristem (SAM), and acts in a non-cell autonomous manner. Whilst smaller GFP fusion proteins were unable to exhibit intercellular movement, a KN1-GFP fusion moved readily between cell layers both within the leaf and in the SAM of *Arabidopsis* (Kim *et al.*, 2002). Together, these observations imply that PDs are able to regulate actively the intercellular movement of macromolecules and ions, and to increase their SEL under appropriate developmental and, possibly, metabolic conditions.

There exists evidence that regulating plasmodesmatal frequency between BS and mesophyll cells in  $C_4$  plants is important in improving photosynthetic efficiency. In three different  $C_4$  grass species, the frequency of PDs in the BS-mesophyll interface is positively correlated with photosynthetic assimilation rate (Botha, 1992). In other words, the number of PDs, measured per unit length of cell interface in an electron mi-

crograph, is highest in those species with the greatest assimilation rates. Furthermore, of all the cell-cell interfaces considered by Botha (1992), plasmodesmatal frequency is greatest at the BS-mesophyll interface in all three  $C_4$  species, where the greatest flux of symplasmic transport occurs. Botha (1992) also considered a  $C_3$  grass, *Bromus unioloides*, and found that not only were BS-mesophyll PDs considerably less frequent than in the  $C_4$  species, but also that PDs were equally distributed (i.e. equally common) on each of the three cell-cell interfaces examined. A similar relationship between photosynthetic performance and PD frequency has been reported between two inbred varieties of maize which differ in their ability to tolerate cool temperatures (Sowinski *et al.*, 2003). The chill-sensitive variety was shown to be unable to increase the number of PD at the BS-mesophyll interface, whereas the chill-tolerant variety increased the number of PD in response to lower temperatures. At low temperature, the cytosol becomes more viscous and diffusion rates decrease; a  $C_4$  cycle that cannot supply carbon to the Calvin cycle at a sufficient rate may quickly lead to an imbalance of carbohydrate synthesis relative to light harvesting, and photoinhibition will ensue. Increased numbers of PDs may offset the decreased flux through each one. Accordingly, Sowinski *et al.* (2003) speculate that the ability of maize to tolerate sub-optimal temperatures is at least partially related to how readily the plant can regulate PD frequency.

#### 6.1.4 Scope of the Chapter

As discussed above, the chloroplasts in mesophyll and BS cells of maize are biochemically distinct, and are distributed in the cell in a different manner. In addition, they exhibit some degree of structural dimorphism, which is most evident in NADP-ME species. Mesophyll chloroplasts are largely agranal (which correlates with reduced Photosystem II activity), with relatively sparsely distributed thylakoid membranes; they lack starch because the Calvin cycle operates in the BS; and they are distributed evenly throughout the cytoplasm. BS chloroplasts, however, are generally larger than those of

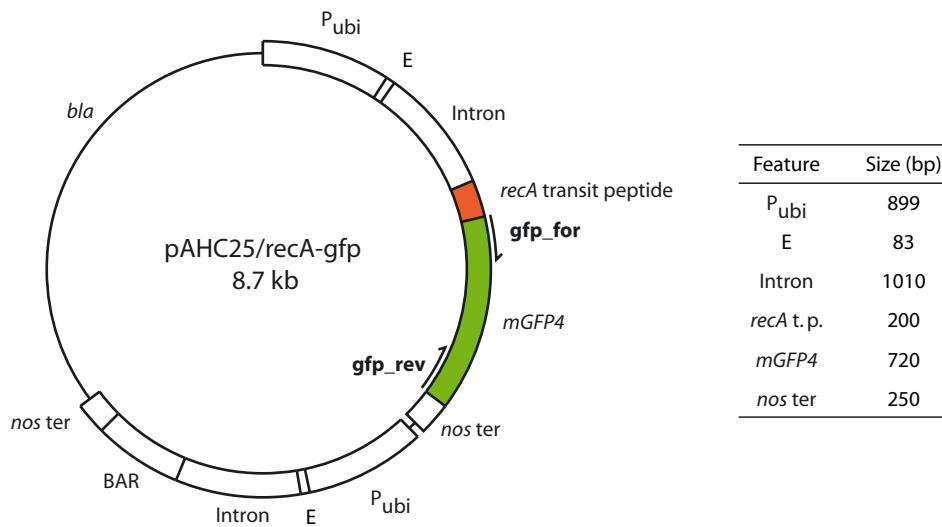
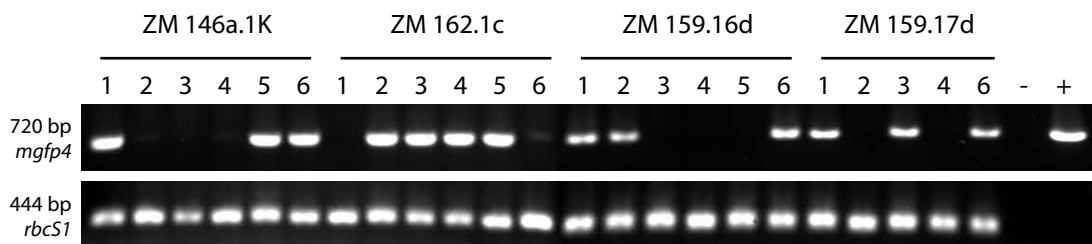
mesophyll cells, are more numerous per cell and are closely appressed towards the mesophyll cells in a centrifugal manner (Dengler and Nelson, 1999). Mesophyll chloroplasts also exhibit a feature known as the peripheral reticulum – a membranous continuity between thylakoid membranes and the inner envelope. The function of this network is unclear, but it has been speculated that they aid the transfer of photosynthetic metabolites across the chloroplast envelope and throughout the plastid (Rosado-Albiero *et al.*, 1968; Dengler and Nelson, 1999). Of particular interest to this work is a proposal made by Slack *et al.* (1969): that the “peripheral reticulum may represent the terminals of tubules connecting the two types [BS and mesophyll] of chloroplast”, a notion that came relatively soon after the documentation by Wildman *et al.* (1962) of the motile phase of chloroplasts.

Given this evidence for plastid dimorphism and the intimate relationship between the metabolisms of the two cell types, the aim of the work presented in this chapter was to investigate stromule formation in the BS and mesophyll cells of maize. The centrifugal arrangement of BS chloroplasts and plasmodesmal frequency between the two cell types present one of the more likely scenarios for the observation of a somewhat elusive phenomenon: the passing of a stromule from one cell to another, presumably through a plasmodesma. Anecdotal evidence (Howells, 2004; this work, Chapter 4; J. C. Gray, pers. comm.) suggests that cell-to-cell stromule connections may occur, but they are very rare events that are difficult to reproduce. The potential biological significance of BS-mesophyll stromules in a  $C_4$  plant is quite clear: the increase in plastid surface area for metabolite transport, and decrease in diffusion distances, could plausibly increase photosynthetic efficiency. This might be particularly relevant under sub-optimal photosynthetic conditions. The discussion of PDs above suggests that a plasmodesma may well accommodate a stromule, especially if a membrane (i.e. the ER) is able to traverse one. In order to address this question, this chapter describes the generation and characterisation of transgenic maize expressing plastid-targeted GFP.

## 6.2 RESULTS

### 6.2.1 Construct design and generation of transgenic plants

In order to express GFP in transgenic maize plants and to target GFP to the plastid, the plasmid DNA construct pAHC25/recA-gfp was engineered (Figure 6.3 A). Derived from pAHC25 (Christensen and Quail, 1996), the plasmid consists of two expression cassettes each driven by the maize ubiquitin-1 (*Ubi-1*) promoter ( $P_{ubi}$ ): one for expression of the desired transgene, the other for selection of transgenic regenerants via phosphinothricin resistance. In pAHC25/recA-gfp, the original  $\beta$ -glucuronidase coding sequence from pAHC25 was excised and replaced with a 1kb fragment consisting of the mGFP4 coding sequence in an N-terminal translational fusion with the *Arabidopsis* recA transit peptide (Köhler *et al.*, 1997). This recA-GFP fusion, which targets GFP to the plastid, is identical to that used in results presented in Chapter 3 and Chapter 5. The recA transit peptide was chosen as the targeting sequence because it was already available, thus avoiding lengthy cloning steps, and because there was no good reason to suppose that it would not function in a monocot as it does in dicots. Strong expression in stably transformed maize plants is achieved by means of  $P_{ubi}$  in conjunction with the 5' UTR (composed of one intron and one short exon) of the maize *Ubi-1* gene, which has been shown to enhance greatly transgene expression levels (Rooke *et al.*, 2000). Construct integrity was confirmed by sequencing outwards from the mGFP4 coding sequence in both directions. Nuclear transformation of maize tissue was performed by means of biolistics, carried out by the University of Missouri-Columbia (see §2.2.4.1). Phosphinothricin-resistant calli were allowed to regenerate into plantlets and designated as primary ( $T_0$ ) transformants. At maturity, these were outcrossed with a non-transgenic maize line in order to improve vigour in the  $T_1$  generation, and  $T_1$  individuals were screened for GFP expression and transgene integration.

**A****B****Figure 6.3 Generation and screening of transgenic maize lines**

(A) Maize transformation vector pAHC25/*recAgfp*. Highlighted in colour is the region encoding plastid-targeted GFP, spliced downstream of the constitutive maize ubiquitin promoter (P<sub>ubi</sub>) and the ubiquitin 5' UTR. Also shown are the positions of the two primers used to amplify the mGFP4 coding region as shown in B. BAR: phosphinothricin selectable marker; E: exon of 5' UTR; nos ter: nopaline synthase terminator sequence; bla: β-lactamase selectable marker for propagation in bacteria. (B) PCR screening of maize T1 lines for presence of *recAgfp* transgene. The screening of only four lines, with 5 or 6 individuals each, is shown here. Upper panel: result of PCR amplification using *mgfp4* primers shown in A. Lower panel: result of PCR amplification using *rbcS1* primers to control for DNA integrity and PCR conditions. Negative control (-) contains no template DNA; positive control (+) contains 10 ng pAHC25/*recAgfp*.

### 6.2.2 PCR screening of transformants

T<sub>1</sub> seeds from a total of ten T<sub>0</sub> transformants were screened for GFP expression by low magnification stereomicroscopy and standard epifluorescence microscopy. Tissue from the third leaf was examined from at least 10 plants per line but no strong GFP expression was evident (data not shown), necessitating molecular characterisation of the lines. Assuming a single transgene integration event in each line, the T<sub>1</sub> lines would be expected to segregate 1:1 hemizygous:azygous (since the T<sub>0</sub> plants were out-crossed). To test that this was the case, five to six seedlings from each of the ten lines were screened for the transgene by PCR using primers specific to the mGFP4 coding sequence (Figure 6.3 B). The probability of selecting six azygotes from a segregating population as assumed above is 0.5<sup>6</sup>, or 0.02. Of the ten lines, eight were found to possess, and be segregating for, the *recA-gfp* transgene.

### 6.2.3 Northern analysis of transgenic lines

Following the initial PCR screen, two transgenic individuals per line were randomly selected for steady-state gene expression levels. Total RNA was extracted from the fifth or sixth leaf, electrophoresed and subjected to northern analysis using the full-length mGFP4 coding sequence as a DNA probe (Figure 6.4). Total RNA isolated from tomato line a17 (which contains the same *recA-gfp* coding sequence) was used as a positive control, and expression of the maize *rbcS1* gene was used as a loading control. Of the eight lines examined, only three (ZM 146a.1K, ZM 159.14c and ZM 159.16d) showed significant levels of transgene expression comparable to the CaMV 35S promoter-driven transgene in tomato. A third, ZM 162.4a, showed weaker expression. Splicing of the intron from the maize polyubiquitin 5' UTR seems to be processed correctly, as the majority of transcripts are of the correct size (1.1 kb) with a faint band of approximately 2.2 kb representing the unprocessed transcript. However, additional transcripts of 5.0 and 4.0 kb in size in ZM 159.14c/2 might indicate transgene rearrangement in this line,

possibly resulting in tandem repeats of the coding sequence. From a total of ten lines, only two (MZ 146a.1K and MZ 159.16d) showed consistently strong transgene expression levels, and hence are putative candidates for strong GFP expression. There was no outward phenotypic difference between plants with differing expression levels, or between azygous and transgenic individuals (Figure 6.4 B).

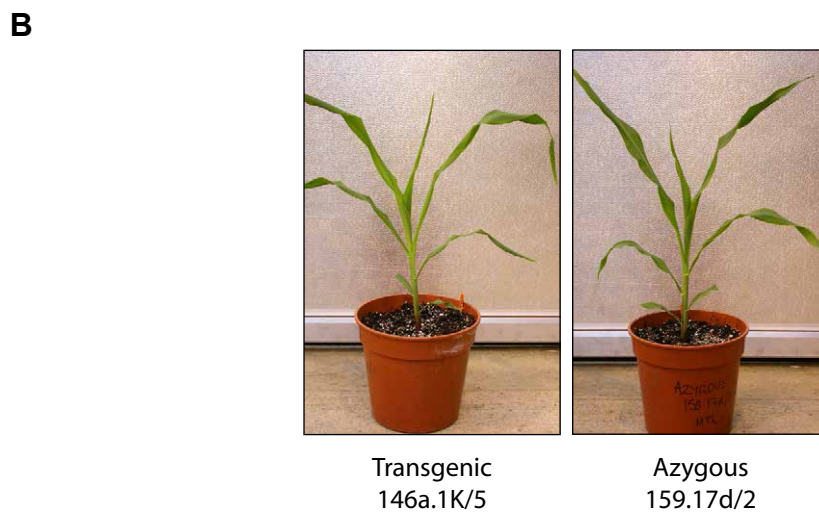
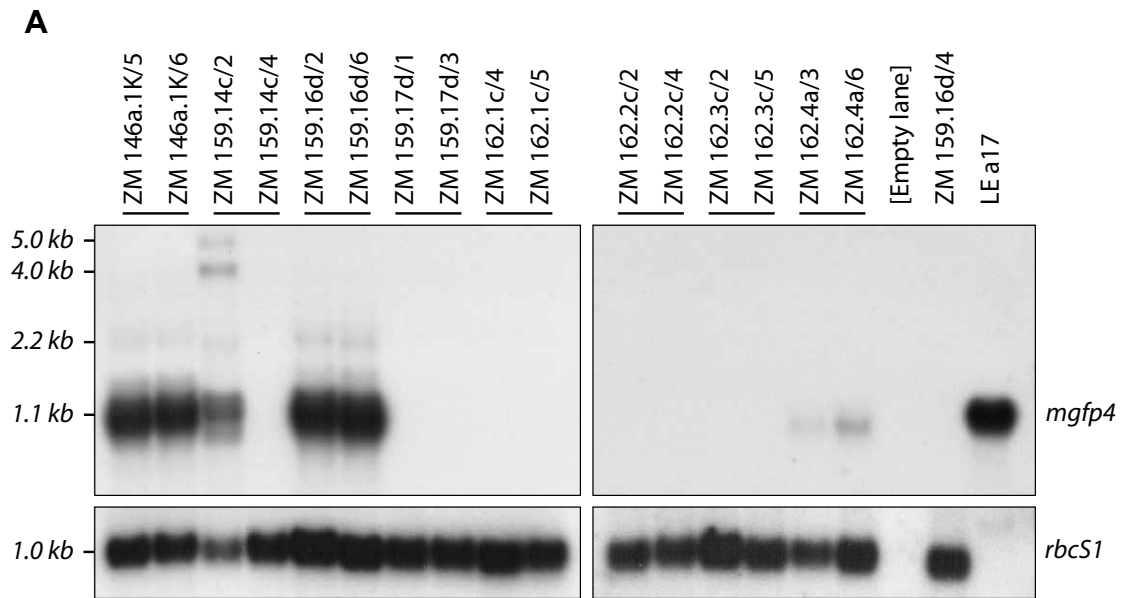


**Figure 6.4 Northern analysis of PCR-positive T<sub>1</sub> lines**

(A) Two individuals per line were assayed. Sizes of RNA standards are shown to the left, and probe used for hybridisation to the right. Upper panels: northern blot probed with the full-length *mgfp4*; note the faint bands at 2.2 kb. Lower panels: the same blot re-probed with a 444 bp fragment of the maize *rbcS1* gene, as a control for RNA loading and blotting. RNA was isolated from azygous individual ZM 159.16d/4 as a negative control; tomato line a17 (LE a17) was used as a positive control. Note that the *rbcS1* probe does not hybridise to RNA isolated from tomato. (B) Transgenic and azygous individuals are morphologically similar. Plants shown are six weeks old.

### 6.2.4 Confocal microscopy of strong transgene expressors

Having identified individual plants exhibiting strong transgene expression, whole leaf segments were examined by confocal microscopy, in order to provide sensitive and specific detection of GFP fluorescence. Using dual-channel imaging (green channel for GFP, red for chlorophyll), some weak GFP fluorescence was detectable in individual MZ 146a.1K/5 in the chloroplast tissue of the leaf mesophyll tissue (Figure 6.5, A-C). However, using the same detection settings (including gain, or electronic signal amplification), a similar weak fluorescence could be detected from the chloroplasts in the green channel in azygous material (Figure 6.5, D). This suggested that there was some bleed-through from chlorophyll autofluorescence into the green channel, which was detectable using such a high level of gain (670 V; for reference, the red channel gain was 510 V, and a strong GFP signal can be imaged using a gain of 400-500 V). Since the fluorescence strength in the green channel was approximately similar between the putative GFP expressor and the azygous individual, it is difficult to verify that the fluorescence seen in the mesophyll chloroplasts of MZ 146a.1K/5 was due to GFP, even though the signal was slightly stronger. Moreover, the signal from stroma-targeted GFP usually extends over a greater area of the chloroplast than chlorophyll autofluorescence, since the former is not restricted to the thylakoids. This would result in a chloroplast with a yellow centre and green periphery in the merged images, which is not observed here (Figure 6.5 C; cf. Köhler *et al.*, 1997). In order to avoid problems of chlorophyll autofluorescence, and therefore to attempt to localise any GFP expression with more certainty, non-chlorophyllous tissues (roots) of transgenic plants were also examined. Unfortunately, similar problems with poor GFP expression were encountered, such that no conclusive data could be collected.

Whilst the expected presence of GFP in the plastid could not be confirmed reliably, two observations suggest that there was at least some detectable GFP in transgenic leaf tis-

sue. Firstly, the green channel of imaged transgenic tissue showed a number of small vesicles, approximately 1  $\mu\text{m}$  in diameter, associated with (but not visibly connected to) chloroplasts in both mesophyll cells and the overlying epidermal tissue (Figure 6.5 A). The vesicles assumed shapes ranging from spheres to sausage-shaped objects resembling large mitochondria or peroxisomes. These vesicles are not detectable in the red channel, and are thus not likely to be artefacts of spurious chlorophyll autofluorescence (Figure 6.5 B). Furthermore, these vesicles were never observed in azygous material (Figure 6.5, D-F), even when the gain was increased beyond a feasible value (data not shown), and were observed in two independent transgenic lines (ZM 146a.1K/5 and ZM 159.14c/2) Secondly, closer inspection of these entities using time-lapse techniques revealed that they are motile, and that they change shape and position slowly within the cell over a period of 90 s (Figure 6.6). These observations thus appear to reflect some form of *in vivo* cytoskeleton-based motility with a pattern similar to leaf peroxisomes. However, this putative identification is not robust and relatively surprising. Even so, the lack of strong GFP fluorescence in chloroplasts suggests that the vesicles are not plastid-derived, and whatever their identity, the visualisation of stromules in these lines is not possible.

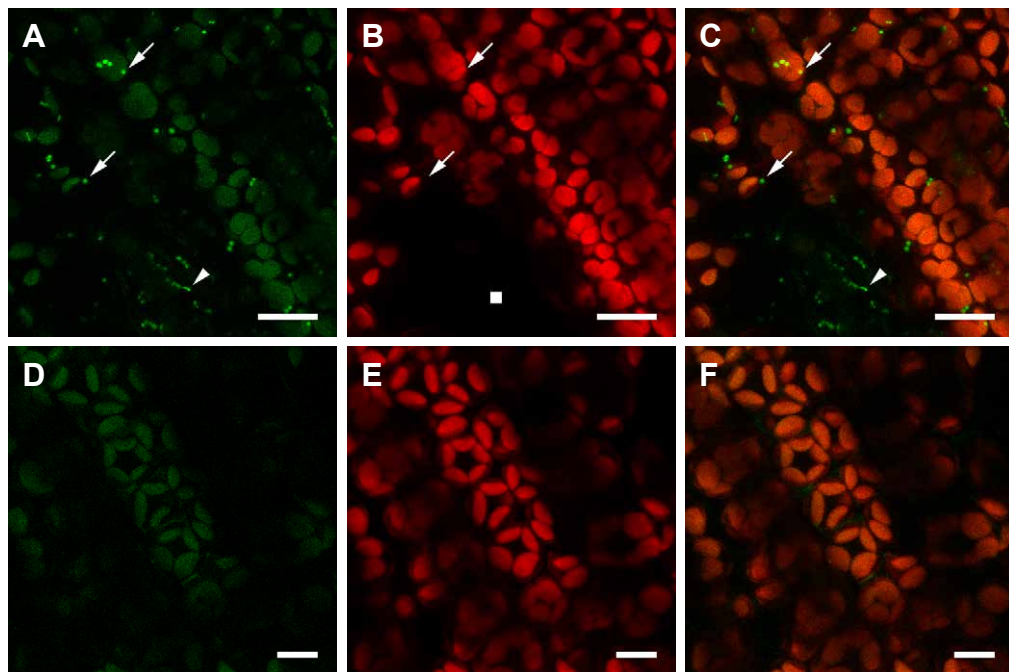


**Figure 6.5 Detection of GFP in transgenic maize leaf tissue by confocal microscopy**

Transgenic (ZM 146a.1K/5, A-C) and azygous (ZM 159.16d/4, D-F) whole leaf segments were imaged, with detection of GFP in the green (A, D) and chlorophyll autofluorescence in the red (B, E) channels. Combined channel images are also shown (C, F). Weak cross-talk of chlorophyll autofluorescence could be detected in the green channel of azygous tissue (D), suggesting that the green signal in mesophyll chloroplasts in transgenic tissue is not truly GFP (A). However, small vesicle-like structures (arrowed in equivalent positions, A-C), which putatively contain GFP, are detectable only in the green channel from imaged transgenic tissue. The dark region lacking chlorophyll autofluorescence in B (lower centre, white square) is an air space directly below a pair of stomatal guard cells that also contain the green vesicles (arrowhead). Images show a maximum projection of 8 images from the upper 10  $\mu\text{m}$  of the leaf, including epidermis and mesophyll cell layers. Scale bars: A-C, 16  $\mu\text{m}$ ; D-E, 8  $\mu\text{m}$ .

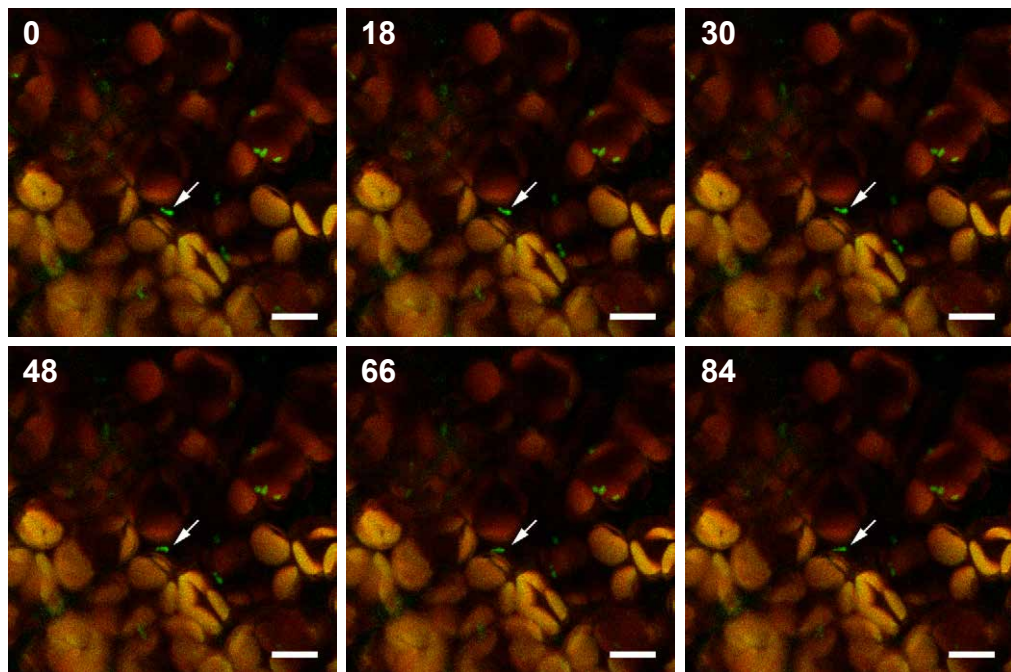


**Figure 6.6 Motility and pleiomorphy of unidentified vesicles in transgenic leaf tissue**

Whole leaf segments from ZM 146a.1K/5 were imaged as in Figure 6.5; merged red and green channel images are shown here. Numbers indicate time (in seconds) of each frame. Note how the arrowed vesicle changes shape and position relative to the arrow (which is fixed in each image). Large orange structures are mesophyll chloroplasts. Images are a time series over a total of 84 seconds in a single confocal plane (a depth of 1  $\mu\text{m}$ ). Scale bar: 8  $\mu\text{m}$ .

### 6.2.5 Immunoblot analysis reveals limited GFP accumulation

To assess further the weak GFP signal detectable by microscopy, and to confirm or otherwise its identification as GFP fluorescence, total soluble leaf proteins were extracted from five strong transgene expressors identified by northern analysis. The proteins were quantified and electrophoresed on a 10% SDS-PAGE gel (Figure 6.7 A), in conjunction with similarly extracted proteins from an azygous individual and from tomato line a17 as negative and positive controls respectively. The proteins were electro-blotted onto a nitrocellulose membrane and the degree of GFP accumulation was determined by immunohybridisation with an anti-GFP polyclonal antibody. Relative to the positive control, only a very weak signal was detectable in any of the strongly expressing individuals, estimated at ~100-fold lower than that of the positive control (Figure 6.7 A). Such a low level of GFP accumulation explains the poor GFP detection *in vivo*, but does confirm that the transgene is capable of directing translation into protein, albeit at limited levels.

For successful visualisation of stromules, GFP must be expressed at high levels and correctly targeted within the cell. In a further attempt to determine whether GFP was present in chloroplasts of leaf tissue, intact chloroplasts were isolated by density-gradient centrifugation from individual MZ 146a.1K/5, which showed the strongest GFP signal on the total leaf protein western blot. Similarly, chloroplasts were isolated from the azygous individual MZ 159.16d/4, and also from tomato line a17 for comparison. Approximately equal quantities of protein were loaded onto the gel as is evident from Coomassie® staining. Notably there is a strong band on the Coomassie®-stained gel at approximately 53 kDa which is present only in LE a17 (Figure 6.7 B), and which is of a size consistent with it being the large subunit of Rubisco. Its absence in the maize samples suggests that the chloroplast extraction method enriched strongly for mesophyll chloroplasts (which do not contain Rubisco), perhaps because the thick-walled bundle

sheath cells are more resistant to lysis. When subjected to immunoblot analysis, there was no detectable GFP signal in MZ 146a.1K/5, despite there being a strong signal in the positive control (Figure 6.7 B). However, assuming the same ~100 fold decrease in GFP accumulation in MZ 146a.1K/5 relative to the positive control as was observed for total leaf protein extracts, the true GFP content of the chloroplasts from MZ 146a.1K/5 may be too low to detect by this method. Consequently, it has not been possible to confirm by this technique whether the limited amounts of GFP present in the transgenic maize lines are correctly localised to the plastid.

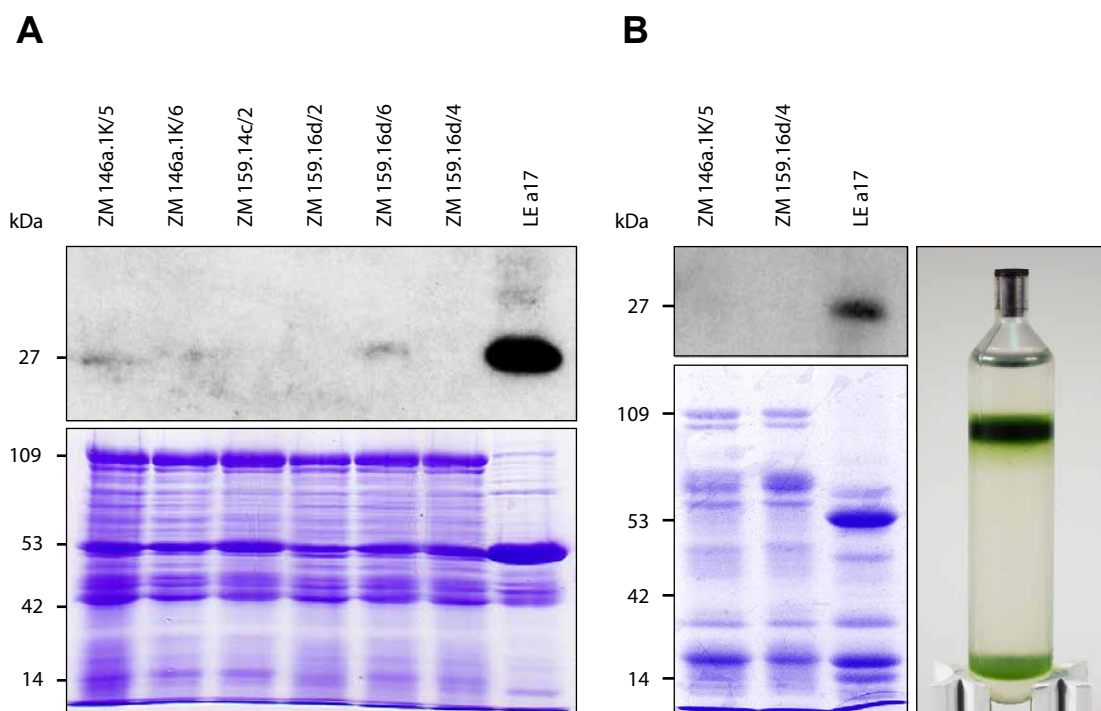


**Figure 6.7 Protein extraction and western analysis from strong mGFP4 expressors**

(A) 15  $\mu$ g of soluble total leaf proteins were loaded per lane on a 10% SDS-PAGE gel and stained with Coomassie® Brilliant Blue (lower panel). Protein size markers are indicated on the left. Note the very different protein profiles of maize and tomato extracts: a greater proportion of Rubisco (at 53 kDa) in  $C_3$  plants compared to  $C_4$  plants means that Rubisco biases the protein quantification method. Upper panel: western analysis of a duplicate gel using an anti-GFP primary antibody. Negative and positive controls as for Figure 6.4. (B) Intact chloroplasts were isolated by centrifugation through a continuous Percoll gradient (right panel) - intact chloroplasts collect at the lower band. Total proteins from these chloroplasts were extracted and run on a 10% SDS-PAGE gel before being stained with Coomassie® Brilliant blue (lower panel) or subjected to western blotting as in (A) (upper panel).

### 6.3 DISCUSSION

The intention of the work presented in this chapter was to investigate the form and function of chloroplast stromules in the C<sub>4</sub> plant maize. To date, stromule formation in a C<sub>4</sub> plant has not been reported in the literature, although stromules have been observed in the mesophyll tissue of other monocot species such as rice (Bourett *et al.*, 1999), suggesting that stromules should exist in maize leaves. As outlined above, the maize C<sub>4</sub> photosynthetic system represents an intriguing scenario for stromule biogenesis, and transgenic plants were generated in order to assess this. Unfortunately, the GFP signal detected by confocal microscopy of leaf tissue from these plants was weak and sporadic, and possibly also mistargeted, rendering the original aim of the study unattainable.

The combination of microscopy and biochemical data described in this chapter leads to two conclusions: a) that the transgenic maize lines did not synthesise and/or accumulate substantial quantities of GFP, and b) that the small amounts of GFP were probably not targeted to the plastid. Considering the low level of GFP accumulation first, there are several steps which could be responsible for the low overall GFP levels in the lines examined, many of which can be dismissed. Starting at the transcriptional level of regulation, the transgene appeared to be transcribed strongly, at a level comparable to the 35S-driven transgene from tomato which produces substantial GFP accumulation and fluorescence. Furthermore, the immature transcript appeared to be spliced correctly, thus removing the 1 kb intron from the *ubi-1* 5' UTR that contains an upstream translation initiation codon, which otherwise may have resulted in an aberrant translation product. Sequence data indicates that the AG splice junction at the 3' end of the intron is intact (data not shown), but the splicing of this intron can occur with varying efficiency (Christensen *et al.*, 1992), explaining why the larger 2.2 kb transcript could be detected. Assuming that transcription at this level was constitutive, then it can be con-

cluded that transcriptional and RNA processing aberrancies were not at fault in producing low amounts of GFP.

That mature transcripts of the correct size accumulated to high levels implied that the problem was probably associated either with the translation stage or with downstream, post-translational events. The presence of low levels of GFP confirms that the construct contains the necessary coding information for the synthesis of protein, and sequence data of the plasmid construct did not reveal any missense mutations. Assuming also that no mutations were present *in planta*, the most parsimonious explanation is that the transgene was translated at low efficiency. However, 5' UTRs, especially those containing introns, improve the expression of protein coding sequences in a number of plant species (Lorkovi *et al.*, 2000), a poorly-understood phenomenon that is particularly prominent in monocots (Bailey-Serres and Dawe, 1996; Clancy and Hannah, 2002). Expression of transgenes driven by the maize ubiquitin promoter together with the 5' UTR of the ubiquitin gene have been reported widely in the literature (Rooke *et al.*, 2000; Taylor *et al.*, 1993), and similarly, a poor rate of translation is unlikely to be an artefact specific to the construct containing GFP (Schenk *et al.*, 1998). It therefore seems unlikely that poor translation rates alone (of abundant mature transcripts) would account for the low levels of GFP.

Therefore, two alternative explanations are plausible, which need not be mutually exclusive. Firstly, increased rates of protein turnover may account for the reduced steady-state levels of GFP, possibly due to misfolding or degradation due to mistargeting. GFP itself is an exceptionally stable protein with a long half-life *in vivo* and *in vitro* (Haseloff, 1999), and GFP has been reported as a functional and stable reporter in a wide variety of subcellular locations (Haseloff and Siemering, 1998; Hanson and Köhler, 2001). Because of this, it would seem improbable that the translation product would be suscepti-

ble to rapid degradation. One possibility, however, is that as a soluble protein GFP would be synthesised in the cytosol prior to putative insertion into the chloroplast. Should the protein not translocate across the plastid envelope efficiently (see below), the protein would be identified as abnormal and be specified for proteolytic destruction, perhaps by the ubiquitin-mediated pathway (Vierstra, 1996).

A second and more favourable explanation is that the transgene promoter activity varied with developmental time, causing discrepancies between mRNA and protein levels, which were isolated at different times. Northern analysis indicated that the transcriptional activity of the transgene was adequate, but this assumes that  $P_{ubi}$ -driven expression was strong and constitutive throughout plant development. Although this promoter is currently the most constitutive available for transgenic studies in monocots, it is generally most active in young, actively-growing tissues such as seedlings and emerging leaves (Rooke *et al.*, 2000) and following heat-shock (Christensen *et al.*, 1992). Whilst RNA and protein were extracted from young leaves, time and space constraints meant that the molecular characterisation had to be performed on single plants of the  $T_1$  generation, and thus variability in gene expression may have occurred between phytomers of different ontological stage. To compound matters, it is possible that some degree of post-transcriptional gene silencing, perhaps induced by strong transgene expression, was initiated at some time between RNA and protein extraction and led to reduced steady-state transcript levels. Closer molecular analyses to discern between these possibilities were beyond the scope of this work, and would require detailed investigations with subsequent generations.

The observations of weak GFP accumulation in unidentified, motile bodies within the cells of leaf tissue were surprising. It is difficult to state categorically that GFP did not accumulate in the plastid since immunoblot analysis was inconclusive, and any weak

GFP fluorescence in living tissue was masked by weak chlorophyll autofluorescence. If these vesicles were plastid-derived, they would represent some form of stromule-like structures that do not resemble anything described previously: they are relatively large and not visibly connected by a stromule to a plastid. Their size, number and motility are reminiscent of peroxisomes (see Chapter 4). Proteins are localised to the peroxisomal compartment by means of a C-terminal peroxisomal target sequence (PTS), typified by the tripeptide S-K-L (Subramani, 1993). There is some plasticity in PTS structure, with a consensus of small, hydrophobic residues at the C-terminus providing targeting specificity (Mullen *et al.*, 1996). The C terminus of mGFP4 is L-Y-K, which does bear superficial similarity to the S-K-L consensus, except that the primary sequence order is not similar. Using site-directed mutagenesis, Mullen *et al.* (1996) tested a wide variety of C-terminal tripeptides for their ability to confer peroxisomal localisation to chloramphenicol acetyltransferase, and found that variation from this consensus led to peroxisomal targeting with differing degrees of efficiency. Although the authors tested a variety of residues at each position, they did not systematically investigate the effect of varying the order of the residues within the S-K-L consensus. Whilst this is highly speculative, it is possible that the vesicles depicted in Figures 6.5 and 6.6 are peroxisomes, which contain GFP because the N-terminal recA transit peptide was not recognised efficiently by the chloroplast and was instead imported by the peroxisome.

Is it plausible that recA is incapable of targeting a protein to the chloroplast in maize? The *Arabidopsis* recA transit peptide (Pang *et al.*, 1992) uniquely targets GFP to chloroplasts in a wide variety of dicotyledonous species (Köhler *et al.*, 1997; this study) but has not been reported as a transit peptide in monocots. Studies on transgenic monocots expressing plastid-targeted proteins have either used endogenous transit peptides (e.g. from the rice *rbcS* gene; Jang *et al.*, 1999) or others derived from dicots, usually the pea *rbcS* transit peptide (Van Breusegem, 1999; Zhong *et al.*, 2003). Recently, a comprehensive analysis of the maize chloroplast proteome failed to detect a recA homologue

(Lonosky *et al.*, 2004). This agrees with Pang *et al.* (1992) who, when using high-stringency hybridisation to search other plant species for homologues to the *Arabidopsis recA* gene, discovered that a *recA* probe hybridised to genomic DNA from two other members of the Brassicaceae, but not to maize DNA. Even so, the lack of evidence for a direct homologue does not suggest one does not exist, or that the *recA* transit peptide should not function in a similar manner in monocots and dicots. Chloroplast transit peptides are highly variable in length and primary sequence, but generally are rich in serine and threonine residues and hydrophobic residues (von Heijne and Nishikawa, 1991). The current view of how transit peptides encode targeting specificity is that a helical tertiary structure is formed upon interaction between the chloroplast envelope lipids, and this conformation is then recognised by parts of the protein import apparatus (Bruce, 2001). Due to the variable nature of the primary sequence and that most protein import studies are performed in dicots, it is difficult to predict whether a given transit peptide sequence will be recognised between species. Little, if any, information is available on differences in peptide recognition between the import apparatus of higher plant taxa. There are examples of maize chloroplast proteins being competent for *in vitro* import into isolated pea chloroplasts (Brutnell *et al.*, 1999), so there is certainly some degree of overlap in transit peptide functionality. Nevertheless, it is possible that this work describes an example of a dicot transit peptide being non-functional in a monocot; unfortunately, the levels of transgene expression are insufficient to be confident in this conclusion. If this is indeed the case, and GFP was in fact targeted elsewhere in these maize lines, then the identity of the vesicles is unclear, meriting further investigation. In addition, any subsequent experiments into chloroplast morphology in maize might be more successful if an alternative transit peptide, such as that from *rbcS*, is employed.

In summary, an attempt was made to target GFP to maize chloroplasts and investigate the possible implications for stromules in a C<sub>4</sub> photosynthetic system. This aim was not

met, due to problematic gene expression and protein accumulation; in addition, further detailed analysis was not possible due to time constraints and the limited use of doing so within the scope of this work. Nevertheless, cell-cell contact through stromules via plasmodesmata is still an interesting possibility which, if addressed in the correct system, may be readily testable.

## 7 GENERAL DISCUSSION

### *7.1 Summary and main conclusions*

By using fluorescent proteins to visualise plastids and other organelles *in vivo*, this work has presented a collection of new insights into stromule biology. As a field of plant research, stromule biology is still in its relative infancy, with plastid shape dynamics only really receiving serious attention since the work of Köhler *et al.* (1997). Thorough investigations into the dynamics of plant cells are now possible with molecular-genetic and pharmacological approaches, coupled with high-resolution microscopy of living cells. One of the most pressing questions regarding stromules is why they vary so substantially in form and frequency, as this is most likely key to their underlying function. This is the main issue that this work set out to address.

The observations made on stromule and plastid morphology in tomato fruit confirmed that the abundance of stromules correlates with plastid type. By following the differentiation of plastids during the development of tomato fruit, it was possible to examine how different plastid types vary with respect to stromules, but without changing other developmental factors such as cell type. Previous studies into the distribution of stromules indicated that they are rare on chloroplasts (Köhler and Hanson, 2000; Gray *et al.*, 2001), and this was supported by manipulating plastid differentiation in tomato fruit. The two distinct populations of plastid in tomato fruit differ dramatically in stromule abundance, which is probably due to a combination of differences in membrane availability and relative plastid density within the cell. Experiments with tobacco hypocotyl epidermis substantiated the notion that stromules elongate with increasing interplastid distance. The underlying mechanism for this may be a specific induction of stromules, or may be an indirect effect of increased cytoplasmic streaming in general when the cell volume increases (see §7.3). Nevertheless, it is important to bear in mind

that stromule formation is doubtless under the influence of a complex interplay between plastid differentiation, plastid density and other unknown factors. This is underlined by the fact that plastids in hypocotyl epidermal cells begin to lose their stromules once chloroplast differentiation is near completion.

By expressing spectrally-distinct fluorescent proteins simultaneously, it was possible to follow the dynamic relationships between plastids, stromules and other organelles. Such associations add weight to the suggestion that stromules improve cellular efficiency by aiding interorganellar communication. However, there arises a difficulty in proving such surmises, or in quantifying the contribution stromules make to processes such as metabolite flux between organelles. Two different plastid-localised fluorescent proteins indicate that molecular distribution within plastids is homogeneous, a conclusion which is also supported by the various GFP fusion proteins reported in the literature (Tirlapur *et al.*, 1999; Kwok and Hanson, 2004a). Given in addition the relatively low rate of diffusion of macromolecules through stromules, it seems reasonable that localised biochemical activities may take place along stromules, rather than a plastid using them as a means to “collect and distribute” metabolites and macromolecules from distant regions of the cytoplasm.

The growth of seedlings under differing light regimes indicates that stromule formation is not responsive to specific light quality. However, the use of continuous light sources may have overplayed the role of chloroplast differentiation, thus ignoring the more short term responses to light quality. When dark-grown seedlings are transferred to red or blue light for short periods of time (up to eight hours), the loss of stromules is more severe for the red light treatment than blue (J. C. Gray, 2004; pers. comm.). This suggests that there exists some receptor that is insensitive to blue light and is capable of directing a rapid change in plastid morphology. Interestingly, it has been shown that

blue light-dependent movement of chloroplasts in the duckweed *Lemna* is dependent on the formation of the carotenoid zeaxanthin, with the xanthophyll pool acting as a possible photoreceptor (Tlalka *et al.*, 1999). Whilst no such response was observed with red light, this is good evidence that there exists a rapid photoreceptor and signal transduction system that is plastid-based. Nonetheless, it is possible that red and blue light differ in their “potency” to bring about differentiation from etioplasts to chloroplasts and that, given time, blue-light transferred seedlings would also lose their stromules to a similar degree as red-light transferred ones. The effect of light intensity that was also inferred in Chapter 4 suggests that this factor should also be considered when interpreting such results. The effects of light on stromules, over and above the influence of plastid differentiation, are still unclear.

Notwithstanding the prospect of a common light perception pathway, the data presented in Chapter 5 indicate that stromule movement is a distinct process that is at least partly independent from chloroplast movements in response to light regimes. Chloroplast movement has been reported in both higher and lower plants (Wada *et al.*, 2003) as well as algae: *Acetabularia*, for example, shows a circadian rhythm in chloroplast positioning (Koop *et al.*, 1978). Likewise, pleiomorphic movements of the chloroplast envelope have also been described in *Acetabularia*, in which stromules are abundant (Menzel, 1994). With cytoplasmic streaming also being an evolutionarily ancient cellular adaptation (Shimmen and Yokota, 1994), determining the evolutionary relationships between these different versions of intercellular movement is complicated. The independence of cytoplasmic streaming, stromule formation and chloroplast movement may become apparent if it can be shown that one process is derived from another. For example, might higher plants have evolved a novel (CHUP1-based) mechanism for chloroplast movement, whilst lower plants and algae make use of an ancestral mechanism based upon chloroplast-localised myosins sharing common elements with stromule movement? Such questions might be answerable once we are aware of pre-

cisely which myosins are responsible for the movement of which organelles, and in which organisms, so that gene sequence phylogenies can be constructed.

It is unfortunate that a proper investigation into the movement of organelles between cells could not be properly conducted. The unprecedented nature of the sharing of organellar material between cells demands repeatability and reproducibility, which can only realistically be achieved in a system where it is commonplace. As such, the C<sub>4</sub> photosynthetic system of maize, based on extensive intercellular continuity, is still a promising framework in which to study this phenomenon.

## **7.2 Likely roles for stromules**

A holistic aim of this work was to gather evidence in favour of stromule function. Whilst the acid test for the importance of stromules to plant growth and development is not yet within our grasp (see §7.3 below), a number of speculations can be made, some stronger than others.

Firstly, and perhaps most convincingly, stromules act to increase the plastid surface area at minimal cost to stromal volume. This notion was substantiated by morphometric analysis in IM cells of tomato fruit and, provided sufficient plastids produce stromules, the benefit to the whole cell is substantial. The advantage to the cell depends rather on the function of the plastid, and the apparent distribution of stromules between plastid types makes empirical sense. In general, plastid types whose primary roles are mostly biosynthetic (e.g. chromoplasts, leucoplasts in etiolated hypocotyl epidermis) would need extensive contact with the rest of the cell. Chloroplasts, which are chiefly the site of photosynthesis, invest most of their membrane complement into internal surface area for light harvesting. Incidentally, chloroplasts differentiating into

chromoplasts lose their thylakoid membranes, and the constituents of which may instead be incorporated into the envelope membrane, leading to longer stromules. Moreover, the generally high density of chloroplasts within the cell leads to an abundance of plastid surface area, negating the requirement for extensive stromules. Since the composition of the envelope membranes and stroma of both the plastid body and stromule are assumed to be the same, plastid import, export and metabolic reactions can occur equally effectively at all locations across the plastid. Given in addition that stromules closely associate with other organelles, it seems unlikely that stromules cannot be functional in certain circumstances. The question, then, is not so much *whether* stromules increase the surface area of the plastid, but “how much effect do they have on the plant?”

Besides assisting in general plastid metabolic activities, stromules may have a more precise role. A great deal of emphasis in the literature has been placed on the ability of stromules to transfer macromolecules between plastids (Köhler *et al.*, 1997; Knoblauch *et al.*, 1999; Köhler *et al.*, 2000; Kwok and Hanson, 2004a) based on the movement of GFP. Encouraged by the fact that plastids are derived from endosymbiotic cyanobacteria, the resemblance of stromules to bacterial pili has given substance to the notion that molecular transfer is a primary role of stromules. Whilst this is an appealing concept, it overlooks three main problems. For one, most plastids are not interconnected, even when they appear to be (Köhler and Hanson, 2000). Secondly, macromolecular transfer between stromules is slow compared to cytoplasmic diffusion (Köhler *et al.*, 2000) and, thirdly, a mechanism for the fusion of plastid membranes needs to be invoked. Consequently, this is not the most parsimonious explanation for the existence of stromules; instead, a surface area argument is more plausible. Nevertheless, it is clear that stromules *can* perform macromolecular transfer – the (perhaps unanswerable) question is how much and why. It is a curious possibility that plastids share DNA and proteins for

much the same reason that mitochondria fuse in yeast; that is, to pass on mitochondrial DNA and complement oxidatively damaged proteins (Westermann, 2003).

At low plastid densities, stromules reduce the mean inter-plastid distance. As an additional and speculative role, stromules take part in some form of signalling between plastids. For example, as the cell expands, plastids divide accordingly. How does a plastid know that it must divide? Rather like bacterial quorum sensing, plastids presumably need to assess their population level within the cell in order to initiate plastid division with appropriate timing. Based on the appearance of lower plants, it is assumed that a high density of chloroplasts is the default state, and the presence of cells with fewer plastids is the derived state. Stromules, by reducing the distance between plastids, could negate the effects of low density, and thus suppress normal plastid division. But, until some insight is made into the regulation of plastid division, possibly by identifying the unknown *arc* genes (Pyke and Leech, 1992), this possibility for stromule function will remain a conjecture.

### **7.3 Future prospects and challenges**

There remains unanswered a fundamental question regarding stromules: do stromules actually increase the adaptive fitness of a plant? In other words, are stromules performing a task that makes the plastid and cell more efficient, ultimately improving the reproductive success of the plant? To address this adequately demands a mutant that lacks stromules. Since we presently are not aware of all the structural and mechanistic proteins, as well as any signalling components, that are involved in stromule biogenesis and movement, we cannot be sure how effective a traditional mutant screen would be. Assuming that relevant mutations would be additive in their impact on stromules, and provided any single mutation had a sufficiently major effect to be detectable, then a mutant screen approach should be feasible. Mutations could then be combined for

physiological and biochemical studies to investigate rates of plant growth, nutrient assimilation and plastid-based biosynthesis. However, stromules exhibit great variability and striking unpredictability, implying that the regulatory frameworks are complex, with multiple developmental and environmental cues influencing stromules to varying degrees. The scope of mutations that might affect stromules is thus large, and many may be too subtle to detect without extensive and laborious work. To overcome this issue, the combination of mutant screens with a more focussed approach might be more productive. Specific, targeted RNAi and reverse genetics on prime candidate genes, such as myosins, would provide clues for further experiments. For example, the regulatory effects of cytosolic  $\text{Ca}^{2+}$  on myosins suggest that microinjection or cage-release experiments could be valuable. Should intriguing results arise, manipulating  $\text{Ca}^{2+}$  ion channels and pumps would be an appropriate logical step. Given the large variability in stromule abundance, it is vital to choose the correct tissue type for experimentation. Hypocotyl epidermis seems an ideal subject, because of the ability to screen rapidly and with accuracy: small effects would be more readily detectable. Whilst experiments with treatments with exogenous substances must be interpreted with care – not least because of the myriad of other effects that increases in  $\text{Ca}^{2+}$  concentrations can have within the cell – they have the potential to provide substantial insights into stromule regulation, and thus function, especially in combination with molecular-genetic methodologies.

Our understanding of stromule function is also tempered by a series of related and often philosophical concerns. Firstly, to what degree are stromules only artefacts of a flexible, membranous “sac” being stretched in different directions by the cytoskeleton? Is plastid shape actively regulated in order to allow stromules to form? This issue is closely related to a second question: what regulates plastid form and shape? Knowing the answer to this will explain why mesophyll chloroplasts are large and of regular shape, whilst leucoplasts are small and possess a highly irregular envelope. As alluded

to in Chapter 3, there are candidate structural proteins located in chloroplasts which may shape plastids in a differentiation status-specific manner, but we know essentially nothing about this phenomenon. Future research should place strong emphasis on this area.

Thirdly, if stromules can be an indirect result of increased membrane flexibility, this implies that stromules may not be specifically and directly regulated. For example, if stromules increase in length when the cell volume increases and cytoplasmic mixing becomes more active, does this merely result from a generalised increase in actomyosin activity that affects all organelles, or are stromules regulated differentially by stromule-specific mechanisms? It has been argued (Kwok and Hanson, 2003) that stromule movement is independent of general cytoplasmic streaming, since cytoplasmic streaming recovers before stromule movement following the removal of myosin inhibitors. It is therefore imperative that the deterministic factors that influence stromules become effectively separated from stochastic and non-specific factors. Indirect and direct regulation may well co-exist, but this does not necessarily have implications for stromule function because the mechanisms are not as important as the outcome. Nevertheless, assigning an accurate role to stromules will be greatly assisted by identifying the specific regulatory factors.

In conclusion, stromules continue to be an enigmatic feature of the plant cell. This work has confirmed that their formation is related specifically to the plastid in question, that they act to increase the plastid surface area when necessary, and that they move independently of light-induced chloroplast movement. Even in the light of these results, a full understanding of these intriguing structures remains a challenge very much for the taking.

## REFERENCES

- Abdallah, F., Salamini, F., and Leister, D.** (2000). A prediction of the size and evolutionary origin of the proteome of chloroplasts of *Arabidopsis*. *Trends Plant Sci.* **5**: 141-142.
- Akhtar, M., Goldschmidt, E., John, I., Rodoni, S., Matile, P., and Grierson, D.** (1999). Altered patterns of senescence and ripening in *gf*, a stay-green mutant of tomato (*Lycopersicon esculentum* Mill.). *J. Exp. Bot.* **50**: 1115-1122.
- Alexander, L., and Grierson, D.** (2002). Ethylene biosynthesis and action in tomato: a model for climacteric fruit ripening. *J. Exp. Bot.* **53**: 2039-2055.
- Alonso, J.M., Stepanova, A.N., Leisse, T.J., Kim, C.J., Chen, H., Shinn, P., Stevenson, D.K., Zimmerman, J., Barajas, P., Cheuk, R., Gadrinab, C., Heller, C., Jeske, A., Koesema, E., Meyers, C.C., Parker, H., Prednis, L., Ansari, Y., Choy, N., Deen, H., Geralt, M., Hazari, N., Hom, E., Karnes, M., Mulholland, C., Ndubaku, R., Schmidt, I., Guzman, P., Aguilar-Henonin, L., Schmid, M., Weigel, D., Carter, D.E., Marchand, T., Risseuw, E., Brogden, D., Zeko, A., Crosby, W.L., Berry, C.C., and Ecker, J.R.** (2003). Genome-wide insertional mutagenesis of *Arabidopsis thaliana*. *Science* **301**: 653-657.
- Ando, R., Hama, H., Yamamoto-Hino, M., Mizuno, H., and Miyawaki, A.** (2002). An optical marker based on the UV-induced green-to-red photoconversion of a fluorescent protein. *PNAS* **99**: 12651-12656.
- Ang, L.-H., and Deng, X.W.** (1994). Regulatory hierarchy of photomorphogenic loci: allele-specific and light-dependent interaction between the *HY5* and *COP1* loci. *Plant Cell* **6**: 613-628.
- Arimura, S.-I., Hirai, A. and Tsutsumi, N.** (2001). Numerous and highly developed tubular projections from plastids observed in tobacco epidermal cells. *Plant Sci.* **169**: 449-454.
- Arimura, S.-I., Yamamoto, J., Aida, G.P., Nakazono, M., and Tsutsumi, N.** (2004). Frequent fusion and fission of plant mitochondria with unequal nucleoid distribution. *PNAS* **101**: 7805-7808.
- Bailey-Serres, J., and Dawe, K. R.** (1996). Both 5' and 3' sequences of maize *adh7* mRNA are required for enhanced translation under low-oxygen conditions. *Plant Physiol.* **112**: 685-695.
- Baird, G.S., Zacharias, D.A. and Tsien, R.Y.** (2000). Biochemistry, mutagenesis and oligomerization of DsRed, a red fluorescent protein from coral. *PNAS* **97**: 11984-11989.
- Baldev, A., Gaikwad, K., Kirti, P.B., Mohapatra, T., Prakash, S., and Chopra, V.L.** (1998). Recombination between chloroplast genomes of *Trachystoma ballii* and *Bassica jucea* following protoplast fusion. *Mol. Gen. Genet.* **260**: 357-361.
- Baskin, T.I., and Cande, W.Z.** (1990). The structure and function of the mitotic spindle in flowering plants. *Annu. Rev. Plant Physiol. Plant Mol. Biol.* **41**: 277-315.
- Bathgate, B., Purton, M.E., Grierson, D., and Goodenough, P.W.** (1985). Plastid changes during the conversion of chloroplasts to chromoplasts in ripening tomatoes. *Planta* **165**: 197-204.
- Batoko, H., Zheng, H.-Q., Hawes, C., and Moore, I.** (2000). A Rab1 GTPase is required for transport between the endoplasmic reticulum and Golgi apparatus and for normal Golgi movement in plants. *Plant Cell* **12**: 2201-2218.
- Bauer, J., Hiltbrunner, A. and Kessler, F.** (2001). Molecular biology of chloroplast biogenesis: gene expression, protein import and intraorganellar sorting. *Cell. Mol. Life Sci.* **58**: 420-433.
- Bauer, D., Viczian, A., Kircher, S., Nobis, T., Nitschke, R., Kunkel, T., Panigrahi, K.C.S., Adam, E., Fejes, E., Schafer, E., and Nagy, F.** (2004). Constitutive photomorphogenesis 1 and multiple photoreceptors control degradation of Phytochrome Interacting Factor 3, a transcription factor required for light signaling in *Arabidopsis*. *Plant Cell* **16**: 1433-1445.
- Baumgartner, B.J., Rapp, J.C. and Mullet, J.E.** (1989). Plastid transcription activity and DNA copy number increase early in barley chloroplast development. *Plant Physiol.* **89**: 1011-1018.

- Beale, S.I.** (1999). Enzymes of chlorophyll biosynthesis. *Photosynth. Res.* **60**: 43-73.
- Bechtel, D.B. and Wilson, J.D.** (2003) Amyloplast formation and starch granule development in hard red winter wheat. *Cereal Chem.* **80**: 175-183.
- Bendich, A.J.** (2004). Circular chloroplast chromosomes: the grand illusion. *Plant Cell* **16**: 1661-1666.
- Bird, C., Smith, C.J.S., Ray, J.A., Moureau, P., Bevan, M.W., Bird, A.S., Hughes, S., Morris, P.C., Grierson, D., and Schuch, W.** (1988). The tomato polygalacturonase gene and ripening-specific expression in transgenic plants. *Plant Mol. Biol.* **11**: 651-662.
- Blanchard, J.L., and Lynch, M.** (2000). Organellar genes: why do they end up in the nucleus? *Trends Genet.* **16**: 315-320.
- Boevink, P., Oparika, K., Santa Cruz, S. Martin, B., Betteridge, A. and Hawes, C.** (1998). Stacks on tracks: the plant Golgi apparatus traffics on an actin/ER network. *Plant J.* **15**: 441-447.
- Boisnard-Lorig, C., Colon-Carmona, A., Bauch, M., Hodge, S., Doerner, P., Bancharel, E., Dumas, C., Haseloff, J., and Berger, F.** (2001). Dynamic analyses of the expression of the HISTONE::YFP fusion protein in *Arabidopsis* show that syncytial endosperm is divided in mitotic domains. *Plant Cell* **13**: 495-509.
- Botha, C.E.J.** (1992). Plasmodesmatal distribution, structure and frequency in relation to assimilation in C<sub>3</sub> and C<sub>4</sub> grasses in southern Africa. *Planta* **187**: 348-358.
- Bourett, T.M., Czymbek, K.J., and Howard, R.J.** (1999). Ultrastructure of chloroplast protuberances in rice leaves preserved by high-pressure freezing. *Planta* **208**: 472-479.
- Bramley, P.M.** (2002). Regulation of carotenoid formation during tomato fruit ripening in development. *J. Exp. Bot.* **53**: 2107-2113.
- Bretscher, A.** (2003). Polarized growth and organelle segregation in yeast: the tracks, motors, and receptors. *J. Cell Biol.* **160**: 811-816.
- Briggs, W.R., and Christie, J.M.** (2002). Phototropins 1 and 2: versatile plant blue-light receptors. *Trends Plant Sci.* **7**: 204-210.
- Bruce, B.D.** (2001). The paradox of plastid transit peptides: conservation of function despite divergence in primary structure. *Biochimica et Biophysica Acta - Molecular Cell Research* **1541**: 2-21.
- Brutnell, T.P., Sawers, R.J.H., Mant, A. and Langdale, J.A.** (1999). BUNDLE SHEATH DEFECTIVE2, a novel protein required for post-translational regulation of the *rbcl* gene of maize. *Plant Cell* **11**: 849-864.
- Bryant, J., Cuming, A.** (1999). Molecular control of development. In: *Plant Biochemistry and Molecular Biology*, P.J. Lea, Leegood, R. C., ed (New York: Wiley).
- Buchanan, B.B., Gruissem, W. and Jones, R.L.** (2000). Biochemistry and molecular biology of plants. (Rockville, Maryland: American Society of Plant Physiologists).
- Büker, M., Schunemann, D., and Borchert, S.** (1998). Enzymic properties and capacities of developing tomato (*Lycopersicon esculentum* L.) fruit plastids. *J. Exp. Bot.* **49**: 681-691.
- Cahoon, A.B., and Timko, M.P.** (2000). *yellow-in-the-dark* mutants of *Chlamydomonas* lack the CHLL subunit of light-independent protochlorophyllide reductase. *Plant Cell* **12**: 559-568.
- Camara, B., Hugueney, P., Bouvier, F., Kuntz, M., and Moneger, R.** (1995). Biochemistry and molecular biology of chromoplast development. *International Review of Cytology* **163**: 175-247.
- Chaley, N., and Possingham, J.V.** (1981). Structure of constricted proplastids in meristematic plant tissues. *Biologie Cellulaire* **41**: 203-210.
- Chen, Y.A., and Scheller, R.H.** (2001). SNARE-mediated membrane fusion. *Nature Rev. Mol. Cell Biol.* **2**: 98-106.

- Cheung, A.Y., McNellis, T. and Piekos, B.** (1993). Maintenance of chloroplast components during chromoplast differentiation in the tomato mutant green flesh. *Plant Physiol.* **101**: 1223-1229.
- Chiter, A., Forbes, J.M., and Blair, G.E.** (2000). DNA stability in plant tissues: implications for the possible transfer of genes from genetically modified food. *FEBS Letts.* **481**: 164-168.
- Chiu, W.-L., Niwa, Y., Zeng, W., Hirano, T., Kobayashi, H. and Sheen, J.** (1996). Engineered GFP as a vital reported in plants. *Curr. Biol.* **6**: 325-330.
- Christensen, A.H. and Quail, P.H.** (1996). Ubiquitin promoter-based vectors for high-level expression of selectable and/or screenable marker genes in monocotyledonous plants. *Transgenic Research* **5**: 213-218.
- Christensen, A. H., Sharrock, R. A., and Quail, P. H.** (1992). Maize polyubiquitin genes: structure, thermal perturbation of expression and transcript splicing, and promoter activity following transfer to protoplasts by electroporation. *Plant Mol. Biol.* **18**: 675-689.
- Clancy, M., and Hannah, L. C.** (2002). Splicing of the maize *Sh1* first intron is essential for enhancement of gene expression, and a T-rich motif increases expression without affecting splicing. *Plant Physiol.* **130**: 918-929.
- Cleary, A.L., Brown, R. C. and Lemmon B. E.** (1992). Microtubule arrays during mitosis in monoplastidic root-tip cells of Isoetes. *Protoplasma* **167**: 123-133.
- Clough, S.J., and Bent, A.F.** (1998). Floral dip: a simplified method for *Agrobacterium*-mediated transformation of *Arabidopsis thaliana*. *Plant J.* **16**: 735-743.
- Cookson, P.J., Kiano, J., Fraser, P.D., Romer S., Shipton, C.A., Schuch, W., Bramley P.M. and Pyke, K.A.** (2003). Increases in cell elongation, plastid compartment size and translational control of carotenoid gene expression underlie the phenotype of the *high pigment-1* mutant of tomato. *Planta* **217**: 896-903.
- Corriveau, J.L., and Coleman, A.W.** (1988). Rapid screening method to detect potential biparental inheritance of plastid DNA and results for over 200 Angiosperm species. *Am. J. Bot.* **75**: 1443-1458.
- Corpas, F.J., Barroso, J.B., and del Rio, L.A.** (2001). Peroxisomes as a source of reactive oxygen species and nitric oxide signal molecules in plant cells. *Trends Plant Sci.* **6**: 145-150.
- Damon, S., Hewitt, J., Nieder, M and Bennett, A. B.** (1988). Sink metabolism in tomato fruit II. Phloem unloading and sugar uptake. *Plant Physiol.* **87**: 631-736.
- Darby, L.A., Ritchie, D.B., and Taylor, I.B.** (1977). Isogenic lines of tomato 'Ailsa Craig'. *The Glasshouse Crops Research Annual Report* 168-184.
- del Río, L.A., Palma, J.M., Sandalio, L.M., Corpas, F.J., Pastori, G.M., Bueno, P., and López-Huertas, E.** (1996). Peroxisomes as a source of superoxide and hydrogen peroxide in stressed plants. *Biochem. Soc. Trans.* **24**: 434-438.
- Dengler, N.G., and Nelson, T.** (1999). Leaf structure and development in C<sub>4</sub> plants. In: *C<sub>4</sub> Plant Biology*, R.F. Sage and R.K. Monson, eds (San Diego: Academic Press), pp. 133-172.
- Deruère, J., Römer, S., d'Harlingue, A., Backhaus, R.A., Kuntz, M., and Camara, B.** (1994). Fibril assembly and carotenoid overaccumulation in chromoplasts: a model for supramolecular lipoprotein structures. *Plant Cell* **6**: 119-133.
- Douce, R., and Neuburger, M.** (1999). Biochemical dissection of photorespiration. *Curr. Opin. Plant Biol.* **2**: 214-222.
- Duffus, C.M.** (1984). Metabolism of reserve starch. In: *Storage Carbohydrates in Vascular Plants*, D.H. Lewis, ed (Cambridge: Cambridge University Press), pp. 231-252.
- Eastmond, P.J., and Graham, I.A.** (2001). Re-examining the role of the glyoxylate cycle in oilseeds. *Trends Plant Sci.* **6**: 72-78.
- Escobar, N.M., Haupt, S., Thow, G., Boevink, P., Chapman, S., and Oparka, K.** (2003). High-throughput viral expression of cDNA-green fluorescent protein fusions reveals novel subcellular addresses and identifies unique proteins that interact with plasmodesmata. *Plant Cell* **15**: 1507-1523.

- Fischer, K., and Weber, A.** (2002). Transport of carbon in non-green plastids. *Trends Plant Sci.* **7**: 345-351.
- Franklin, K.A., Davis, S.J., Stoddart, W.M., Vierstra, R.D., and Whitelam, G.C.** (2003). Mutant analyses define multiple roles for phytochrome C in *Arabidopsis* photomorphogenesis. *Plant Cell* **15**: 1981-1989.
- Fraser, P.D., Truesdale, M. R., Bird, C. R., Schuch, W. and Bramley, P. M.** (1994). Carotenoid biosynthesis during tomato fruit development. *Plant Physiol.* **105**: 405-413.
- Fray, R.G., and Grierson, D.** (1993). Identification and genetic analysis of normal and mutant phytoene synthase genes of tomato by sequencing, complementation and co-suppression. *Plant Mol. Biol.* **22**: 589-602.
- Fujie, M., Kuroiwa, H., Kawano, S. and Kuroiwa, T.** (1994). Behaviour of organelles and their nucleoids in the shoot apical meristem during leaf development in *Arabidopsis thaliana* L. *Planta* **194**: 395-405.
- Gendreau, E., Traas, J., Desnos, T., Grandjean, O., Caboche, M., and Hofte, H.** (1997). Cellular basis of hypocotyl growth in *Arabidopsis thaliana*. *Plant Physiol.* **114**: 295-305.
- Giannelos, P.N., Zannikos, F., Stournas, S., Lois, E., and Anastopoulos, G.** (2002). Tobacco seed oil as an alternative diesel fuel: physical and chemical properties. *Industrial Crops and Products* **16**: 1-9.
- Gilbert, I.R.** (1990). Studies of tropic responses in wild type and mutant plants of tomato (*Lycopersicon esculentum* Mill.). PhD thesis (University of Nottingham).
- Gillaspy, G., Ben-David, H. and Gruissem, W.** (1993). Fruits: a developmental perspective. *Plant Cell* **5**: 1439-1451.
- Gray, J.C., Sullivan, J. A., Hibberd, J. M. and Hansen, M. R.** (2001). Stromules: mobile protrusions and interconnections between plastids. *Plant Biology* **3**: 223-233.
- Grierson, D., Kader, A. A.** (1986). Fruit ripening and quality. In: *The Tomato Crop*, J.G. Atherton, Rudich, J., ed (New York: Chapman and Hall), pp. 241-280.
- Grierson, D., Tucker, G. A. and Robertson, N. G.** (1981). The molecular biology of ripening. In: *Recent Advances in the Biochemistry of Fruit and Vegetables*, J. Friend and M.J.C. Rhodes, eds (London: Academic Press), pp. 149-160.
- Hackett, R.M., Ho, C.-W., Lin, Z., Foote, H.C.C., Fray, R.G., and Grierson, D.** (2000). Antisense inhibition of the *Nr* gene restores normal ripening to the tomato *Never-ripe* mutant, consistent with the ethylene receptor-inhibition model. *Plant Physiol.* **124**: 1079-1086.
- Hamilton, A.J., and Baulcombe, D.C.** (1999). A species of small antisense RNA in posttranscriptional gene silencing in plants. *Science* **286**: 950-952.
- Hammond, J.P., Bennett, M.J., Bowen, H.C., Broadley, M.R., Eastwood, D.C., May, S.T., Rahn, C., Swarup, R., Woolaway, K.E., and White, P.J.** (2003). Changes in gene expression in *Arabidopsis* shoots during phosphate starvation and the potential for developing smart plants. *Plant Physiol.* **132**: 578-596.
- Hanson, M.R., and Kohler, R.H.** (2001). GFP imaging: methodology and application to investigate cellular compartmentation in plants. *J. Exp. Bot.* **52**: 529-539.
- Harrak, H., Lagrange, T., Bisanz-Seyer, C., Lerbs-Mache, S. and Mache, R.** (1995). The expression of nuclear genes encoding plastid ribosomal proteins precedes the expression of chloroplast genes during early phases of chloroplast development. *Plant Physiol.* **108**: 685-692.
- Harris, W.M., and Spurr, A.R.** (1969a). Chromoplasts of tomato fruits I. Ultrastructure of low-pigment and high beta mutants. Carotene analyses. *American Journal of Botany* **56**: 369-379.
- Harris, W.M., and Spurr, A.R.** (1969b). Chromoplasts of tomato fruits. II. The red tomato. *American Journal of Botany* **56**: 380-389.
- Haseloff, J.** (1999). GFP variants for multispectral imaging of living cells. In: *Methods in Cell Biology*, Vol. 58, K. Sullivan and S. Kay, eds. (San Diego: Academic Press), pp. 139-151.

- Haseloff, J., Siemering, K.R., Prasher, D.C., and Hodge, S.** (1997). Removal of a cryptic intron and subcellular localization of green fluorescent protein are required to mark transgenic *Arabidopsis* brightly. *PNAS* **94**: 2122-2127.
- Haseloff, J., and Siemering, K.R.** (1998). The uses of GFP in plants. In *Green Fluorescent Protein: Properties, Applications and Protocols*, M. Chalfie and S. Kain, eds (New York: Wiley-Liss), pp. 191-220.
- Hattersley, P.W. and Watson, L.** (1975) Anatomical parameters for predicting photosynthetic pathways of grass leaves: The 'maximum lateral count' and the 'maximum cells distant count.' *Phytomorphology* **25**: 325-333.
- Heim, R., Prasher, D., and Tsien, R.** (1994). Wavelength mutations and posttranslational autooxidation of green fluorescent protein. *PNAS* **91**: 12501-12504.
- Hellens, R.P., Edwards, E. A., Leyland, N. R., Bean, S. and Mullineaux, P. M.** (2000). pGreen: a versatile and flexible binary Ti vector for *Agrobacterium*-mediated plant transformation. *Plant Mol. Biol.* **42**: 819-832.
- Hibberd, J.M., Linley, P.J., Khan, M.S., and Gray, J.C.** (1998). Transient expression of green fluorescent protein in various plastid types following microprojectile bombardment. *Plant J.* **16**: 627 -632.
- Hibberd, J.M., and Quick, W.P.** (2002). Characteristics of C<sub>4</sub> photosynthesis in stems and petioles of C<sub>3</sub> flowering plants. *Nature* **415**: 451-454.
- Hinshaw, J.E.** (2000). Dynamin and its role in membrane fission. *Ann. Rev. Cell Dev. Biol.* **16**: 483-519.
- Ho, L.C., and Hewitt, J.D.** (1986). Fruit development. In: *The Tomato Crop*, J.G. Atherton, Rudich, J., ed (New York: Chapman and Hall), pp. 201-239.
- Hodge, T., and Cope, M.** (2000). A myosin family tree. *J Cell Sci.* **113**: 3353-3354.
- Holweg, C., and Nick, P.** (2004). Arabidopsis myosin XI mutant is defective in organelle movement and polar auxin transport. *PNAS* **101**: 10488-10493.
- Howells, C.A.** (2004) Investigations into the biology of *Arabidopsis thaliana* plastids. PhD thesis (University of Nottingham).
- Hua, J., and Meyerowitz, E.M.** (1998). Ethylene responses are negatively regulated by a receptor gene family in *Arabidopsis thaliana*. *Cell* **94**: 261-271.
- Huang, C.Y., Ayliffe, M. A. and Timmis, J. N.** (2003). Direct measurement of the transfer rate of chloroplast DNA into the nucleus. *Nature* **422**: 72-76.
- Huguency, P., Bouvier, F., Badillo, A., d'Harlingue, A., Kuntz, M., and Camara, B.** (1995). Identification of a plastid protein involved in vesicle fusion and/or membrane protein translocation. *PNAS* **92**: 5630-5634.
- Jackson, D.** (2000). Opening up the communication channels: recent insights into plasmodesmal function. *Current Opinion in Plant Biology* **3**: 394-399.
- Jahn, R., and Grubmüller, H.** (2002). Membrane fusion. *Curr. Opin. Cell Biol.* **14**: 488-495.
- Jang, I.-C., Nahm, B.H., and Kim, J.-K.** (1999). Subcellular targeting of green fluorescent protein to plastids in transgenic rice plants provides a high-level expression system. *Molecular Breeding* **5**: 453-461.
- Jarvis, P., Chen, L.J., Li, H., Peto, C.A., Fankhauser, C., and Chory, J.** (1998). An *Arabidopsis* mutant defective in the plastid general protein import apparatus. *Science* **282**: 100-103.
- Jarvis, P., and Soll, J.** (2001). Toc, Tic, and chloroplast protein import. *Biochim. Biophys. Acta* **1541**: 64-79.
- Jedd, G., and Chua, N.-H.** (2002). Visualization of peroxisomes in living plant cells reveals acto-myosin-dependent cytoplasmic streaming and peroxisome budding. *Plant Cell Physiol.* **43**: 384-392.
- Jeong, W.J., Park, Y.I., Suh, K., Raven, J.A., Yoo, O.J., and Liu, J.R.** (2002). A large population of small chloroplasts in tobacco leaf cells allows more effective chloroplast movement than a few enlarged chloroplasts. *Plant Physiol.* **129**: 112-121.

- Josse, E.-M., Simkin, A.J., Gaffe, J., Laboure, A.-M., Kuntz, M., and Carol, P.** (2000). A plastid terminal oxidase associated with carotenoid desaturation during chromoplast differentiation. *Plant Physiol.* **123**: 1427-1436.
- Juniper, B.E., and Clowes, F.A.L.** (1965). Cytoplasmic organelles and cell growth in root caps. *Nature* **208**: 864-865.
- Kagawa, T., and Wada, M.** (2002). Blue light-induced chloroplast relocation. *Plant Cell Physiol.* **43**: 367-371.
- Kahn, M.S., and Maliga, P.** (1999). Fluorescent antibiotic resistance marker for tracking plastid transformation in higher plants. *Nature Biotech.* **17**: 910-915.
- Kandasamy, M.K., and Meagher, R.B.** (1999). Actin-organelle interaction: association with chloroplast in *Arabidopsis* leaf mesophyll cells. *Cell Motil. Cytoskeleton* **44**: 110-118.
- Karimi, M., Inze, D., and Depicker, A.** (2002). GATEWAY™ vectors for *Agrobacterium*-mediated plant transformation. *Trends in Plant Science* **7**: 193-195.
- Karol, K.G., McCourt, R.M., Cimino, M.T., and Delwiche, C.F.** (2001). The closest living relatives of land plants. *Science* **294**: 2351-2353.
- Karpilov, Y.S.** (1970). Cooperative photosynthesis in xerophytes. *Proc. Moldavian Inst. Irrigation Agric. Res.* **11**: 3-66.
- Kasahara, M., Kagawa, T., Kazusato, O., Suetsugu, N., Miyao, M. and Wada, M.** (2002). Chloroplast avoidance movement reduces photodamage in plants. *Nature* **420**: 829-832.
- Kasten, B., Buick, F., Nuske, J. and Reski, R.** (1997). Cytokinin affects nuclear-and plastome-encoded energy converting plastid enzymes. *Planta* **201**: 261-272.
- Kay, Q.O.N., Daoud, H.S., and Stirton, C.H.** (1981). Pigment distribution, light reflection and cell structure in petals. *Bot. J. Linn. Soc.* **83**: 57-84.
- Keegstra, K., and Froehlich, J.E.** (1999). Protein import into chloroplasts. *Curr. Opin. Plant Biol.* **2**: 471-476.
- Kelly, A.A., and Dörmann, P.** (2004). Green light for galactolipid trafficking. *Curr. Opin. Plant Biol.* **7**: 262-269.
- Kiessling, J., Kruse, S., Rensing, S. A., Harter, K., Decker, E. L. and Reski, R.** (2000) Visualization of a cytoskeleton-like FtsZ network in chloroplasts. *J. Cell Biol.* **151**: 945-950.
- Kim, J., and Mullet, J.E.** (2003). A mechanism for light-induced translation of the *rbcL* mRNA encoding the large subunit of ribulose-1,5-bisphosphate carboxylase in barley chloroplasts. *Plant Cell Physiol.* **44**: 491-499.
- Kim, J. Y., Yuan, Z., Cilia, M., Khalfan-Jagani, Z., and Jackson, D.** (2002). Intercellular trafficking of a *KNOTTED1* green fluorescent protein fusion in the leaf and shoot meristem of *Arabidopsis*. *PNAS* **99**: 4103-4108.
- Kirk, J.T.O., and Tilney-Bassett, R.A.E.** (1978). The plastids: their chemistry, structure, growth and inheritance. (Amsterdam: Elsevier/North Holland Biomedical Press).
- Kiss, J.Z.** (2000). Mechanism of the early phases of plant gravitropism. *Critical Reviews in Plant Science* **19**: 551-573.
- Kleiner, O., Kircher, S., Harter, K., and Batschauer, A.** (1999). Nuclear localisation of the *Arabidopsis* blue light receptor cryptochrome 2. *Plant J.* **19**: 289-296.
- Knoblauch, M., Hibberd, J., Gray, J. and van Bel, A.** (1999). A galinstan expansion femtosyringe for microinjection of eukaryotic organelles and prokaryotes. *Nature Biotech.* **17**: 906-909.
- Knoll, A.H.** (1992). The early evolution of eukaryotes: a geological perspective. *Science* **256**: 622-627.
- Kobayashi, H., Ngernprasirtsiri, J. and Akazawa, T.** (1990). Transcriptional regulation and DNA methylation in plastids during transitional conversion of chloroplasts to chromoplasts. *EMBO J.* **9**: 307-313.
- Köhler, R.H., Cao, J., Zipfel, W.R., Webb, W.W., and Hanson, M.R.** (1997a). Exchange of protein molecules through connections between higher plant plastids. *Science* **276**: 2039-2042.

- Köhler, R.H., Zipfel, W.R., Webb, W.W., and Hanson, M.R.** (1997b). The green fluorescent protein as a marker to visualize plant mitochondria *in vivo*. *Plant J.* **11**: 613-621.
- Köhler, R.H., and Hanson, M.R.** (2000). Plastid tubules of higher plants are tissue-specific and developmentally regulated. *J. Cell Sci.* **113**: 81-89.
- Köhler, R.H., Schwille, P., Webb, W.W., and Hanson, M.R.** (2000). Active protein transport through plastid tubules: velocity quantified by fluorescence correlation spectroscopy. *J. Cell Sci.* **113**: 3921-3930.
- Koop, H.U., Schmid, R., Heuner, H.H., and Milthaler, B.** (1978). Chloroplast migration: a new circadian rhythm in *Acetabularia*. *Protoplasma* **97**: 301-310.
- Kost, B., Mathur, J. and Chua, N-H.** (1999). Cytoskeleton in plant development. *Curr. Opin. Plant Biol.* **2**: 462-470.
- Kragler, F., Lucas, W. J., and Monzer, J.** (1998). Plasmodesmata: dynamics, domains and patterning. *Annals of Botany* **81**: 1-10.
- Kubis, S., Baldwin, A., Patel, R., Razzaq, A., Dupree, P., Lilley, K., Kurth, J. Leister, D. and Jarvis, P.** (2003). The Arabidopsis *ppi1* mutant is specifically defective in the expression, chloroplast import, and accumulation of photosynthetic proteins. *Plant Cell* **15**: 1859-1871.
- Kuroda, H., and Maliga, P.** (2001). Sequences downstream of the translation initiation codon are important determinants of translation efficiency in chloroplasts. *Plant Physiol.* **125**: 430-436.
- Kwok, E.Y., and Hanson, M.R.** (2003). Microfilaments and microtubules control the morphology and movement of non-green plastids and stromules in *Nicotiana tabacum*. *Plant J.* **35**: 16-26.
- Kwok, E.Y., and Hanson, M.R.** (2004a). GFP-labelled Rubisco and aspartate aminotransferase are present in plastid stromules and traffic between plastids. *J. Exp. Bot.* **55**: 595-604.
- Kwok, E., and Hanson, M.** (2004). *In vivo* analysis of interactions between GFP-labelled microfilaments and plastid stromules. *BMC Plant Biol.* **4**: 2.
- Langeveld, S. M. J., Van Wijk, R., Stuurman, N., Kijne, J. W. and de Pater, S.** (2000) B-type granule containing protrusions and interconnections between amyloplasts in developing wheat endosperm revealed by transmission electron microscopy and GFP expression. *J. Ex. Bot.* **51**: 1357-1361.
- Lawrence, S.D., Cline, K. and Moore, G. A.** (1993). Chromoplast-targeted proteins in tomato (*Lycopersicon esculentum* Mill.) fruit. *Plant Physiol.* **102**: 789-794.
- Lawrence, S.D., Cline, K. and Moore, G. A.** (1997). Chromoplast development in ripening tomato fruit: identification of cDNAs for chromoplast-targeted proteins and characterization of a cDNA encoding a plastid-localised low-molecular-weight heat shock protein. *Plant Mol. Biol.* **33**: 483-492.
- Leegood, R.C.** (1985). The intercellular compartmentation of metabolites in leaves of *Zea mays* L. *Planta* **164**: 163-171.
- Leegood, R.C.** (2000). Transport during C<sub>4</sub> photosynthesis. In: *Photosynthesis: Physiology and Metabolism*, R.C. Leegood, T.D. Sharkey, and S. von Caemmerer, eds (Dordrecht: Kluwer Academic), pp. 459-469.
- León, P., Arroyo, A. and Mackenzie, S.** (1998). Nuclear control of plastid and mitochondrial development in higher plants. *Ann. Rev. Plant Physiol. Plant Mol. Biol.* **49**: 453-480.
- Liebermann, M., Segev, O., Gilboa, N., Lalazar, A., and Levin, I.** (2004). The tomato homolog of the gene encoding UV-damaged DNA binding protein 1 (DDB1) underlined as the gene that causes the *high pigment-1* phenotype. *Theor. Appl. Genet.* **108**: 1574-1561.
- Lin, C.** (2002). Blue Light Receptors and Signal Transduction. *Plant Cell* **14**: S207-225.
- Lincoln, J.E., and Fischer, R.L.** (1988). Regulation of gene expression by ethylene in wild-type and *rin* tomato (*Lycopersicon esculentum*) fruit. *Plant Physiol.* **88**: 370-374.

- Livne, A., and Gepstein, S.** (1988). Abundance of the major chloroplast polypeptides during development and ripening of tomato fruits. *Plant Physiol.* **87**: 239-243.
- Ljubicic, J.M., Wrischer, M. and Ljubicic, N.** (1998). Formation of the photosynthetic apparatus in plastids during greening of potato microtubers. *Plant Physiology and Biochemistry* **36**: 747-752.
- Lloyd, C., and Chan, J.** (2004). Microtubules and the shape of plants to come. *Nature Rev. Mol. Cell Biol.* **5**: 13-22.
- Logan, D.C., and Leaver, C.J.** (2000). Mitochondrial-targeted GFP highlights the heterogeneity of mitochondrial shape, size and movement within living plant cells. *J. Exp. Bot.* **51**: 865-871.
- Logan, D.C.** (2003). Mitochondrial dynamics. *New Phytol.* **160**: 463-478.
- Lois, L.M., Rodriguez-Concepcion, M., Gallego, F., Campos, N., and Boronat, A.** (2000). Carotenoid biosynthesis during tomato fruit development: regulatory role of 1-deoxy-D-xylulose 5-phosphate synthase. *Plant J.* **22**: 503-513.
- Lonosky, P.M., Zhang, X., Honavar, V.G., Dobbs, D.L., Fu, A., and Rodermeil, S.R.** (2004). A proteomic analysis of maize chloroplast biogenesis. *Plant Physiol.* **134**: 560-574.
- Lorkovi, Z.J., Wieczorek Kirk, D.A., Lambermon, M.H.L., and Filipowicz, W.** (2000). Pre-mRNA splicing in higher plants. *Trends Plant Sci.* **5**: 160-167.
- Lucas, W.J.** (1997). Plasmodesmata and the cell-to-cell transport of protein and nucleo-protein complexes. *J. Exp. Bot.* **50**: 979-987.
- Macleery, S.A., and Kiss, J.Z.** (1999). Plastid sedimentation kinetics in roots of wild-type and starch-deficient mutants of *Arabidopsis*. *Plant Physiol.* **120**: 183-192.
- Maliga, P.** (2002). Engineering the plastid genome of higher plants. *Curr. Opin.Plant Biol.* **5**: 164-172.
- Mano, S., Nakamori, C., Kondo, M., Hayashi, M., and Nishimura, M.** (2004). An *Arabidopsis* dynamin-related protein, DRP3A, controls both peroxisomal and mitochondrial division. *Plant J.* **38**: 487-498.
- Marano, M.R., Serra, E.C., Orellano, E.G. and Carrillo, N.** (1993). The path of chromoplast development in fruits and flowers. *Plant Sci.* **94**: 1-17.
- Maroder, H., Prego, I. and Maldonado, S.** (2003). Histochemical and ultrastructural studies on *Salix alba* and *S. matsudana* seeds. *Trees Struct. Funct.* **17**: 193-199.
- Martin, W., and Herrmann, R.G.** (1998). Gene transfer from organelles to the nucleus: how much, what happens, and why? *Plant Physiol.* **118**: 9-17.
- Martin, W., Stoebe, B., Goremykin, V., Hansmann, S., Hasegawa, M., and Kowallik, K.V.** (1998). Gene transfer to the nucleus and the evolution of chloroplasts. *Nature* **393**: 162-165.
- Martin, W., Rujan, T., Richly, E., Hansen, A., Cornelsen, S., Lins, T., Leister, D., Stoebe, B., Hasegawa, M., and Penny, D.** (2002). Evolutionary analysis of *Arabidopsis*, cyanobacterial, and chloroplast genomes reveals plastid phylogeny and thousands of cyanobacterial genes in the nucleus. *PNAS* **99**: 12246-12251.
- Martínez-García, J. F., Huq, E. and Quail, P. H.** (2000) Direct targeting of light signals to a promoter element-bound transcription factor. *Science* **288**: 859-863.
- Más, P., Devlin, P.F., Panda, S., and Kay, S.A.** (2000). Functional interaction of phytochrome B and cryptochrome 2. *Nature* **408**: 207-211.
- Mathur, J., Mathur, N., and Hulskamp, M.** (2002). Simultaneous visualization of peroxisomes and cytoskeletal elements reveals actin and not microtubule-based peroxisome motility in plants. *Plant Physiol.* **128**: 1031-1045.
- Matz, M., Arkady, F., Labas, Y, Savitsky, A., Zaraisky, A., Markelov, M. and Lukyanov, S.** (1999). Fluorescent proteins from nonbioluminescent *Anthozoa* species. *Nature Biotech.* **17**: 969-973.

- Mazzarello, P.** (1999). A unifying concept: the history of cell theory. *Nature Biotech.* **1**: E13-E15.
- McCaskill, D., and Croteau, R.** (1995). Monoterpene and sesquiterpene biosynthesis in glandular trichomes in peppermint (*Mentha x piperita*) rely exclusively on plastid-derived isopentenyl diphosphate. *Planta* **197**: 49-56.
- McFadden, G.I.** (2001). Primary and secondary endosymbiosis and the origin of plastids. *J. Phycol.* **37**: 951-959.
- Menzel, D.** (1994). An interconnected plastidom in *Acetabularia*: implications for the mechanism of chloroplast motility. *Protoplasma* **179**: 166-171.
- Miyamura, S., Kuroiwa, T. and Nagata, T.** (1990). Multiplication and differentiation of plastid nucleoids during development of chloroplasts and etioplasts from proplastids in *Triticum aestivum*. *Plant Cell Physiol.* **31**: 597-602.
- Miyazawa, Y., Sakai, A., Miyagishima, S.-Y., Takano, H., Kawano, S. and Kuroiwa, T.** (1999). Auxin and cytokinin have opposite effects on amyloplast development and the expression of starch synthesis genes in cultured Bright Yellow-2 tobacco cells. *Plant Physiol.* **121**: 461-469.
- Miyazawa, Y., Kutsuna, N., Inada, N., Kuroiwa, H., Kuroiwa, T. and Yoshida, S.** (2002). Dedifferentiation of starch-storing tobacco cells: effects of 2,4-dichlorophenoxy acetic acid on multiplication, starch content, organellar DNA content, and starch synthesis gene expression. *Plant Cell Reprod.* **21**: 289-295.
- Mori, T., Kuroiwa, H., Takahara, M., Miyagishima, S.-Y., and Kuroiwa, T.** (2001). Visualisation of an FtsZ ring in chloroplasts of *Lilium longiflorum* leaves. *Plant Cell Physiol.* **42**: 555-559.
- Morise, H., Shimomura, O., Johnson, F.H., and Winant, J.** (1974). Intermolecular energy transfer in the bioluminescent system of *Aequorea*. *Biochemistry* **13**: 2656-2662.
- Mukherjee, A., and Lutkenhaus, J.** (1998). Dynamic assembly of FtsZ regulated by GTP hydrolysis. *EMBO J.* **17**: 462-469.
- Mullen, R. T., Lee, M. S., Flynn, C. R., and Trelease, R. N.** (1996). Diverse amino acid residues function within the Type 1 peroxisomal targeting signal: Implications for the role of accessory residues upstream of the Type 1 peroxisomal targeting signal. *Plant Physiol.* **115**: 881-889.
- Mustilli, A.C., Fenzi, F., Ciliento, R., Alfano, F., and Bowler, C.** (1999). Phenotype of the tomato *high pigment-2* mutant is caused by a mutation in the tomato homolog of *DEETIOLATED1*. *Plant Cell* **11**: 145-158.
- Nebenführ, A., Gallagher, L.A., Dunahay, T.G., Frohlick, J.A., Mazurkiewicz, A.M., Meehl, J.B., and Staehelin, L.A.** (1999). Stop-and-go movements of plant Golgi stacks are mediated by the acto-myosin system. *Plant Physiol.* **121**: 1127-1141.
- Neff, M.M., and Chory, J.** (1998). Genetic interactions between phytochrome A, phytochrome B, and cryptochrome 1 during *Arabidopsis* development. *Plant Physiol.* **118**: 27-35.
- Nemhauser, J., and Chory, J.** (2002). Photomorphogenesis. In: *The Arabidopsis Book*, C.R. Somerville and E.M. Meyerowitz, eds (Rockville, Maryland: American Society of Plant Biologists), pp. doi/10.1199/tab.0054.
- Neuhaus, H.E., and Emes, M.J.** (2000). Non-photosynthetic metabolism in plastids. *Ann. Rev. Plant Physiol. Plant Mol. Biol.* **51**: 111-140.
- Ni, M., Halliday, K.J., Tepperman, J.M., and Quail, P.H.** (1998). PIF3, a phytochrome-interacting factor necessary for normal photoinduced signal transduction, is a novel basic helix-loop helix protein. *Cell* **95**: 657-667.
- Ni, M., Tepperman, J.M., and Quail, P.H.** (1999). Binding of phytochrome B to its nuclear signalling partner PIF3 is reversibly induced by light. *Nature* **400**: 781-784.
- Niggli, V.** (2001). Structural properties of lipid binding sites in cytoskeletal proteins. *Trends Biochem. Sci.* **26**: 604-611.
- Niklas, K.J.** (1997). *The evolutionary biology of plants.* (Chicago: The University of Chicago Press).

- Oikawa, K., Kasahara, M., Kiyosue, T., Kagawa, T., Suetsugu, N., Takahashi, F., Kanegae, T., Niwa, Y., Kadota, A., and Wada, M.** (2003). CHLOROPLAST UNUSUAL POSITIONING1 is essential for proper chloroplast positioning. *Plant Cell* **15**: 2805-2815.
- Oeller, P.W., Wong, L.-M., Taylor, L. P., Pike, D. A. and Theologis, A.** (1991). Reversible inhibition of tomato fruit senescence by antisense RNA. *Science* **254**: 437-439.
- Ohlrogge, J.B., and Jaworski, J.G.** (1997). Regulation of fatty acid synthesis. *Ann. Rev.Plant Physiol.Plant Mol. Biol.* **48**: 109-136.
- Oparka, K.J., Boevink P. and Santa Cruz, S.** (1996). Studying the movement of plant viruses using green fluorescent protein. *Trends Plant Sci.* **1**: 412-418.
- Oparka, K.J., Roberts, A.G., Boevink, P., Cruz, S.S., Roberts, I., Pradel, K.S., Imlau, A., Kotlizky, G., Sauer, N., and Epel, B.L.** (1999). Simple, but not branched, plasmodesmata allow nonspecific trafficking of proteins in developing tobacco leaves. *Cell* **97**: 743-754.
- Osmond, C.B.** (1971). Metabolite transport in C<sub>4</sub> photosynthesis. *Aust. J. Biol. Sci.* **24**: 159-163.
- Osterlund, M.T., Ang, L.-H., and Deng, X.W.** (1999). The role of COP1 in repression of *Arabidopsis* photomorphogenic development. *Trends Cell Biol.* **9**: 113-118.
- Osterlund, M.T., Hardtke, C.S., Wei, N., and Deng, X.W.** (2000). Targeted destabilisation of HY5 during light-regulated development of *Arabidopsis*. *Nature* **405**: 462-466.
- Osteryoung, K.W., and Pyke, K.A.** (1998). Plastid division: evidence for a prokaryotically derived mechanism. *Curr. Opin. Plant Biol.* **1**: 475-479.
- Osteryoung, K.W., Stokes, K.D., Rutherford, S.M., Percival, A.L., and Lee, W.Y.** (1998). Chloroplast division in higher plants requires members of two functionally divergent gene families with homology to bacterial *ftsZ*. *Plant Cell* **10**: 1991-1994.
- Ottenschläger, I., Wolff, P., Wolverton, C., Bhalerao, R.P., Sandberg, G., Ishikawa, H., Evans, M., and Palme, K.** (2003). Gravity-regulated differential auxin transport from columella to lateral root cap cells. *PNAS* **100**: 2987-2991.
- Öztig, F.** (1962) Sur la forme et l'origine des pigments dans la tomate mûr. *Adv. Front. Plant Sci.* **1**: 153-156.
- Pang, Q., Hays, J., and Rajagopal, I.** (1992). A plant cDNA that partially complements *Escherichia coli* recA mutations predicts a polypeptide not strongly homologous to RecA proteins. *PNAS* **89**: 8073-8077.
- Pecker, I., Gabbay, R., Cunningham, F.X., and Hirschberg, J.** (1996). Cloning and characterisation of the cDNA for lycopene  $\beta$ -cylcase from tomato reveals decrease in its expression during fruit ripening. *Plant Mol. Biol.* **30**: 807-819.
- Peters, J.L., Schreuder, M.E.L., Verduin, S.J.W. and Kendrick, R.E.** (1992). Physiological characterization of a high-pigment mutant of tomato. *Photochemistry and Photobiology* **56**: 75-82.
- Peters, J.L., Szell, M., and Kendrick, R.E.** (1998). The expression of light-regulated genes in the *high-pigment-1* mutant of tomato. *Plant Physiol.* **117**: 797-807.
- Possingham, J.V., and Rose, R.J.** (1967). Chloroplast replication and chloroplast DNA synthesis in spinach leaves. *Proc. Roy. Soc. Lond. B* **193**: 295-305.
- Prasher, D.C., Eckenrode, V.K., Ward, W.W., Prendergast, F.G., and Cormier, M.J.** (1992). Primary structure of the *Aequorea victoria* green-fluorescent protein. *Gene* **111**: 229-233.
- Pyke, K.A.** (1997). The genetic control of plastid division in higher plants. *Amer. J. Bot.* **84**: 1017-1027.
- Pyke, K.A.** (1999). Plastid division and development. *Plant Cell* **11**: 549-556.
- Pyke, K.A., and Howells, C.A.** (2002). Plastid and stromule morphogenesis in tomato. *Annals of Botany* **90**: 559-566.

- Pyke, K.A., and Leech, R.M.** (1992). Chloroplast division and expansion is radically altered by nuclear mutations in *Arabidopsis thaliana*. *Plant Physiol.* **99**: 1005-1008.
- Pyke, K.A., and Leech, R.M.** (1994). A genetic analysis of chloroplast division and expansion *Arabidopsis thaliana*. *Plant Physiol.* **104**: 201-207.
- Quail, P.H.** (2002). Phytochrome photosensory signalling networks. *Nature Rev. Mol. Cell Biol.* **3**: 85-93.
- Ramonell, K.M., Kuang, A., Porterfield, D.M., Crispi, M.L., Xiao, Y., McClure, G., and Musgrave, M.E.** (2001). Influence of atmospheric oxygen on leaf structure and starch deposition in *Arabidopsis thaliana*. *Plant Cell Environ.* **24**: 419-428.
- Reddy, A.S.N., and Day, I.S.** (2001). Analysis of the myosins encoded in the recently completed *Arabidopsis thaliana* genome sequence. *Genome Biology* **2**: 1-17.
- Renzaglia, K.S., Brown, R.C., Lemmon B.E., Duckett, J.G. and Ligrone, R.** (1994). Occurrence and phylogenetic significance of monoplastidic meiosis in liverworts. *Canadian J. Bot.* **72**: 65-72.
- Reski, R.** (2002). Rings and networks: the amazing complexity of FtsZ in chloroplasts. *Trends Plant Sci.* **7**: 103-105.
- Reumann, S.** (2000). The structural properties of plant peroxisomes and their metabolic significance. *Biol. Chem.* **381**: 639-648.
- Robertson, E.J., Pyke K.A. and Leech R.M.** (1995). arc6, a radical chloroplast division mutant of *Arabidopsis* also alters proplastid proliferation and morphology in shoot and root apices. *J. Cell Sci.* **108**: 2937-2944.
- Robinson, N.L., Hewitt, J. D. and Bennett, A. B.** (1988). Sink metabolism in tomato fruit I. Developmental changes in carbohydrate metabolizing enzymes. *Plant Physiol.* **87**: 727-730.
- Rodermel, S.** (2001). Pathways of plastid-to-nucleus signaling. *Trends Plant Sci.* **6**: 471-478.
- Römer, S., d'Harlingue, A., Camara, B., Schantz, R., and Kuntz, M.** (1992). Cysteine synthase from *Capsicum annum* chromoplasts. Characterization and cDNA cloning of an up-regulated enzyme during fruit development. *J. Biol. Chem.* **267**: 17466-17470.
- Rooke, L., Byrne, D., and Salgueiro, S.** (2000). Marker gene expression driven by the maize ubiquitin promoter in transgenic wheat. *Annals of Applied Biology* **136**: 167-172.
- Rosado-Alberio, J., Weier, T. E., and Stocking, C. R.** (1968). Continuity of the chloroplast membrane systems in *Zea mays* L. *Plant Physiol.* **43**: 1325-1331.
- Rosso, S.W.** (1967) An ultrastructural study of the mature chromoplasts of the tangerine tomato (*Lycopersicon esculentum* var. 'Golden Jubilee'). *J. Ultrast. Res.* **20**: 179-189.
- Sage, R.F., and Percy, R.W.** (2000). The physiological ecology of C<sub>4</sub> photosynthesis. In: *Photosynthesis: Physiology and Metabolism*, R.C. Leegood, T.D. Sharkey, and S. von Caemmerer, eds (Dordrecht: Kluwer Academic), pp. 497-532.
- Sage, R.F., Li, M., and Monson, R.K.** (1999). The taxonomic distribution of C<sub>4</sub> photosynthesis. In: *C<sub>4</sub> Plant Biology*, R.F. Sage and R.K. Monson, eds (San Diego: Academic Press), pp. 551-584.
- Sakai, A., Kawano, S., and Kuroiwa, T.** (1992). Conversion of proplastids to amyloplasts in tobacco cultured cells is accompanied by changes in the transcriptional activities of plastid genes. *Plant Physiol.* **100**: 1062-1066.
- Sakai, A., Susuki, T., Miyazawa, Y, Kawano, S., Nagata, T. and Kuroiwa, T.** (1998). Comparative analysis of plastid gene expression in tobacco chloroplasts and proplastids: relationship between transcription and transcript accumulation. *Plant Cell Physiol.* **39**: 581-589.
- Sakai, A., Suzuki, T., Sasaki, N. and Kuroiwa, T.** (1999). Plastid gene expression during amyloplast formation in cultured tobacco cells. *J. Plant Physiol.* **154**: 71-78.
- Sambrook, J., and Russel, D.W.** (2001). *Molecular Cloning: A Laboratory manual*. (New York: Cold Spring Harbor Laboratory Press).

- Schenk, P.M., Elliott, A.R. and Manners, J.M.** (1998). Assessment of transient gene expression in plant tissues using green fluorescent protein as a reference. *Plant Mol. Biol. Report.* **16**: 313-322.
- Schimper, A.F.W.** (1885). Untersuchungen über die Chlorophyllkörper und die ihnen Homologen Gebilde. *Jahrbuecher für Wissenschaftliche Botanik* **16**: 1-247.
- Schnurr, J.A., Shockey, J. M., de Boer, G.-J. and Browse, J. A.** (2002). Fatty acid export from the chloroplast. Molecular characterization of a major plastidial acyl-coenzyme A synthetase from Arabidopsis. *Plant Physiol.* **129**: 1700-1709.
- Schroeder, D.F., Gahrtz, M., Maxwell, B.B., Cook, R.K., Kan, J.M., Alonso, J.M., Ecker, J.R., and Chory, J.** (2002). De-etiolated 1 and damaged DNA binding protein 1 interact to regulate *Arabidopsis* photomorphogenesis. *Curr. Biol.* **12**: 1462-1472.
- Schumacher, K., Vafeados, D., McCarthy, M., Sze, H., Wilkins, T., and Chory, J.** (1999). The Arabidopsis det3 mutant reveals a central role for the vacuolar H<sup>+</sup>-ATPase in plant growth and development. *Genes Dev.* **13**: 3259-3270.
- Scott, S.V., Cassidy-Stone, A., Meeusen, S.L., and Nunnari, J.** (2003). Staying in aerobic shape: how the structural integrity of mitochondria and mitochondrial DNA is maintained. *Curr. Opin. Cell Biol.* **15**: 482-488.
- Sesaki, H., and Jensen, R.E.** (1999). Division versus Fusion: Dnm1p and Fzo1p Antagonistically Regulate Mitochondrial Shape. *J. Cell Biol.* **147**: 699-706.
- Shagin, D.A., Barsova, E.V., Yanushevich, Y.G., Fradkov, A.F., Lukyanov, K.A., Labas, Y.A., Semenova, T.N., Ugalde, J.A., Meyers, A., Nunez, J.M., Widder, E.A., Lukyanov, S.A., and Matz, M.V.** (2004). GFP-like proteins as ubiquitous metazoan superfamily: evolution of functional features and structural complexity. *Mol. Biol. Evol.* **21**: 841-850.
- Shaw, J.M., and Nunnari, J.** (2002). Mitochondrial dynamics and division in budding yeast. *Trends Cell Biol.* **12**: 178-184.
- Sheahan, M.B., Rose, R.J., and McCurdy, D.W.** (2004). Organelle inheritance in plant cell division: the actin cytoskeleton is required for unbiased inheritance of chloroplasts, mitochondria and endoplasmic reticulum in dividing protoplasts. *Plant J.* **37**: 379-390.
- Shiina, T., Allison, L., and Maliga, P.** (1998). *rbcL* transcript levels in tobacco plastids are independent of light: reduced dark transcription rate is compensated by increased mRNA stability. *Plant Cell* **10**: 1713-1722.
- Shiina, T., Hayashi, K., Ishii, N., Morikawa, K., Iwai, K., and Toyoshima, Y.** (2000). Characterisation of stromules visualized in transplastomic plants expressing green fluorescent protein. *Plant Cell Physiol.* **41**: 367-371.
- Shimmen, T., Ridge, R. W., Lambiris, I., Plazinski, J., Yokota, E. and Williamson, R. E.** (2000). Plant myosins. *Protoplasma* **214**: 1-10.
- Shimmen, T., and Yokota, E.** (1994). Physiological and biochemical aspects of cytoplasmic streaming. *Int. Rev. Cytol.* **155**: 97-139.
- Slack, C.R., Hatch, M.D., and Goodchild, D.J.** (1969). Distribution of enzymes in mesophyll and parenchyma-sheath chloroplasts in maize leaves in relation to C<sub>4</sub>-dicarboxylic acid pathway of photosynthesis. *Biochemical J.* **114**: 489-498.
- Smith, A.M., Denyer, K, and Martin, C.** (1997). The synthesis of the starch granule. *Ann. Rev. Plant Physiol. Plant Mol. Biol.* **48**: 67-87.
- Smith, H.** (2000). Phytochromes and light signal perception by plants - an emerging synthesis. *Nature* **407**: 585-591.
- Smith, N.A., Singh, S.P., Wang, M.-B., Stoutjesdijk, P.A., Green, A.G., and Waterhouse, P.M.** (2000). Gene expression: Total silencing by intron-spliced hairpin RNAs. *Nature* **407**: 319-320.
- Sowinski, P., Rudzinska-Langwald, A., and Kobus, P.** (2003). Changes in plasmodesmata frequency in vascular bundles of maize seedling leaf induced by growth at sub-optimal temperatures in relation to photosynthesis and assimilate export. *Environmental and Experimental Botany* **50**: 183-196.

- Staehelein, L.A.** (2003). Chloroplast structure: from chlorophyll granules to supra-molecular architecture of thylakoid membranes. *Photosynth. Res.* **76**: 185-196.
- Staiger, C.J.** (2000). Signalling to the actin cytoskeleton in plants. *Ann. Rev. Plant Physiol. Plant Mol. Biol.* **51**: 257-288.
- Subramani, S.** (1993) Protein import into peroxisomes and biogenesis of the organelle. *Annu. Rev. Cell Biol.* **9**: 445-478.
- Sullivan, J.A., and Deng, X.W.** (2003). From seed to seed: the role of photoreceptors in *Arabidopsis* development. *Developmental Biology* **260**: 289-297.
- Sullivan, J.A., and Gray, J.C.** (2002). Multiple plastid signals regulate the expression of the pea plastocyanin gene in pea and transgenic tobacco plants. *Plant J.* **32**: 763-774.
- Sullivan, J.A., Shirasu, K., and Deng, X.W.** (2003). The diverse roles of ubiquitin and the 26S proteasome in the life of plants. *Nature Rev. Genet.* **4**: 948-958.
- Summer, E.J., and Cline, K.** (1999). Red bell pepper chromoplasts exhibit in vitro import competency and membrane targeting of passenger proteins from the thylakoidal *sec* and  $\Delta$ pH pathways but not the chloroplast signal recognition particle pathway. *Plant Physiol.* **119**: 575-584.
- Sundqvist, C., and Dahlin, C.** (1997). With chlorophyll pigments from prolamellar bodies to light-harvesting complexes. *Physiol. Plant.* **100**: 748-759.
- Swarup, R., Friml, J., Marchant, A., Ljung, K., Sandberg, G., Palme, K., and Bennett, M.** (2001). Localization of the auxin permease AUX1 suggests two functionally distinct hormone transport pathways operate in the *Arabidopsis* root apex. *Genes Dev.* **15**: 2648-2653.
- Taylor, M.G., Vasil, V. and Vasil, I.K.** (1993) Enhanced GUS gene expression in cereal/grass cell suspensions and immature embryos using the maize ubiquitin-based plasmid pAHC25. *Plant Cell Reporter* **12**: 491-495.
- Tepperman, J.M., Zhu, T., Chang, H.-S., Wang, X., and Quail, P.H.** (2001). Multiple transcription-factor genes are early targets of phytochrome A signaling. *PNAS* **98**: 9437-9442.
- The Arabidopsis Genome Initiative** (2000). Analysis of the genome sequence of the flowering plant *Arabidopsis thaliana*. *Nature* **408**: 796-815.
- Theologis, A.** (1992). One rotten apple spoils the whole bushel: the role of ethylene in fruit ripening. *Cell* **70**: 181-184.
- Thompson, A.E., Hepler, R. W. and Kerr, E. A.** (1962). Clarification of the inheritance of high total carotenoid pigments in tomato. *American Society of Horticultural Science* **81**: 434-442.
- Thomson, W.W., Lewis, L.N., and Coggins, C.W.** (1967). The reversion of chromoplasts to chloroplasts in Valencia oranges. *Cytologia* **32**: 117-124.
- Thomson, W.W., and Whatley, J.M.** (1980). Development of non-green plastids. *Ann. Rev. Plant Physiol.* **31**: 375-394.
- Tigchelaar, E.C., McGlasson, W. B. and Buescher, R. W.** (1978). Genetic regulation of fruit ripening. *Horticultural Science* **13**: 508-513.
- Tirlapur, U., Dahse, I., Reiss, B., Meurer, J. and Oelmüller, R.** (1999). Characterization of the activity of a plastid-targeted green fluorescent protein in *Arabidopsis*. *Eur. J. Cell Biol.* **78**: 233-240.
- Tlalka, M., Runquist, M., and Fricker, M.** (1999). Light perception and the role of the xanthophyll cycle in blue-light-dependent chloroplast movements in *Lemna trisulca* L. *Plant J.* **20**: 447-459.
- Tominaga, M., Kojima, H., Yokota, E., Orii, H., Nakamori, R., Katayama, E., Anson, M., Shimmen, T., and Oiwa, K.** (2003). Higher plant myosin XI moves processively on actin with 35 nm steps at high velocity. *EMBO J.* **22**: 1263-1272.
- Turner, G., Gershenzon, J., Nielson, E.E., Froehlich, J.E., and Croteau, R.** (1999). Limonene synthase, the enzyme responsible for monoterpene biosynthesis in peppermint, is localized to leucoplasts of oil gland secretory cells. *Plant Physiol.* **120**: 879-886.

- Van Breusegem, F., Slooten, L., Stassart, J., Botterman, J., Moens, T., Van Montagu, M., and Inze, D.** (1999). Effects of overproduction of tobacco MnSOD in maize chloroplasts on foliar tolerance to cold and oxidative stress. *J. Exp. Bot.* **50**: 71-78.
- Van Gestel, K., Kohler, R.H., and Verbelen, J.-P.** (2002). Plant mitochondria move on F-actin, but their positioning in the cortical cytoplasm depends on both F-actin and microtubules. *J. Exp. Bot.* **53**: 659-667.
- Van Gestel, K., and Verbelen, J.-P.** (2002). Giant mitochondria are a response to low oxygen pressure in cells of tobacco (*Nicotiana tabacum* L.). *J. Exp. Bot.* **53**: 1215-1218.
- Vaughn, K.C., Ligrone, R., Owen, H.A., Hasegawa, J., Campbell, E.O., Renzaglia, K.S., and Mongenajera, J.** (1992). The anthocerot chloroplast - a review. *New Phytol.* **120**: 169-190.
- Vierstra, R. D.** (1996). Proteolysis in plants: mechanisms and functions. *Plant Mol. Biol.* **32**: 275-302.
- Vishnevetsky, M., Ovadis, M., Vainstein, A.** (1999). Carotenoid sequestration in plants: the role of carotenoid associated proteins. *Trends Plant Sci.* **4**: 232-235.
- Vitha, S., McAndrew, R. and Osteryoung, K.** (2001) FtsZ ring formation at chloroplast division site in plants. *J. Cell Biol.* **153**: 111-119.
- Voinnet, O., Vain, P., Angell, S., and Baulcombe, D.C.** (1998). Systemic spread of sequence-specific transgene RNA degradation in plants is initiated by localized introduction of ectopic promoterless DNA. *Cell* **95**: 177-187.
- von Arnim, A.G., and Deng, X.W.** (1994). Light inactivation of *Arabidopsis* photomorphogenic repressor COP1 involves a cell-specific regulation of its nucleocytoplasmic partitioning. *Cell* **79**: 1035-1045.
- von Heijne, G. and Nishikawa, K.** (1991). Chloroplast transit peptides: the perfect random coil? *FEBS Letts.* **278**: 1-3.
- Vothknecht, U.C., and Westhoff, P.** (2001). Biogenesis and origin of thylakoid membranes. *Biochim. Biophys. Acta* **1541**: 91-101.
- Vrebalov, J., Ruezinsky, D., Padmanabhan, V., White, R., Medrano, D., Drake, R., Schuch, W., and Giovannoni, J.** (2002). A MADS-box gene necessary for fruit ripening at the tomato *ripening inhibitor (rin)* locus. *Science* **296**: 343-346.
- Wada, M., Kagawa, T., and Sato, Y.** (2003). Chloroplast movement. *Ann. Rev. Plant Biol.* **54**: 455-468.
- Wada, H., Shintani, D., and Ohlrogge, J.B.** (1997). Why do mitochondria synthesize fatty acids? Evidence for involvement in lipoic acid production. *PNAS* **94**: 1591-1596.
- Wang, H., Ma, L.-G., Li, J.-M., Zhao, H.-Y., and Deng, X.W.** (2001). Direct interaction of *Arabidopsis* cryptochromes with COP1 in light control development. *Science* **294**: 154-158.
- Wang, Y., Jones, B.D., and Brun, Y.V.** (2001). A set of *ftsZ* mutants blocked at different stages of cell division in *Caulobacter*. *Mol. Microbiol.* **40**: 347-360.
- Wang, Z., and Pesacreta, C.** (2004). A subclass of myosin XI is associated with mitochondria, plastids and the molecular chaperone subunit TCP-1 $\alpha$  in maize. *Cell Motil. Cytoskeleton* **57**: 218-232.
- Wei, N., and Deng, X.W.** (1996). The role of the *COP/DET/FUS* genes in light control of *Arabidopsis* seedling development. *Plant Physiol.* **112**: 871-878.
- Wen-jun, S., and Forde, B.G.** (1989). Efficient transformation of *Agrobacterium* spp. by high voltage electroporation. *Nucleic Acids Res.* **17**: 8385.
- Westermann, B.** (2003). Mitochondrial membrane fusion. *Biochim. Biophys. Acta* **1641**: 195-202.
- Weston, E.A., and Pyke, K.A.** (1999). Developmental ultrastructure of cells and plastids in the petals of Wallflower (*Erysimum cheiri*). *Annals of Botany* **84**: 763-769.
- Whatley, J.M., and Whatley, F.R.** (1987). When is a chromoplast? *New Phytol.* **106**: 667-678.

- Wildman, S., Hongladarom, T. and Honda, S. I.** (1962). Chloroplasts and mitochondria in living cells: cinephotomicrographic studies. *Science* **138**, 434-436.
- Wildman, S.G.** (1967). The organization of grana-containing chloroplasts in relation to location of some enzymatic systems concerned with photosynthesis, protein synthesis, and ribonucleic acid synthesis. In: *Biochemistry of Chloroplasts*, T.W. Goodwin, ed (London: Academic Press), pp. 295-319.
- Wilkinson, J.Q.L., M. B., Yen, H.-C., Giovannoni, J. J., and Klee H. J.** (1995). An ethylene-inducible component of signal transduction encoded by *Never-ripe*. *Science* **270**: 1807-1809.
- Williamson, R.E.** (1993). Organelle movements. *Ann. Rev. Plant Physiol. Plant Mol. Biol.* **44**: 181-202.
- Wilson, Z.A., Morroll, S.M., Dawson, J., Swarup, R., and Tighe, P.J.** (2001). The *Arabidopsis* *MALE STERILITY1 (MS1)* gene is a transcriptional regulator of male gametogenesis, with homology to the PHD-finger family of transcription factors. *Plant J.* **28**: 27-39.
- Wong, E.D., Wagner, J.A., Scott, S.V., Okreglak, V., Holewinski, T.J., Cassidy-Stone, A., and Nunnari, J.** (2003). The intramitochondrial dynamin-related GTPase, Mgm1p, is a component of a protein complex that mediates mitochondrial fusion. *J. Cell Biol.* **160**: 303-311.
- Yang, H.-Q., Tang, R.-H., and Cashmore, A.R.** (2001). The signaling mechanism of *Arabidopsis* CRY1 involves direct interaction with COP1. *Plant Cell* **13**: 2573-2587.
- Yen, H.C., Shelton, B. A., Howard, L. R., Lee, S., Vrebalov, J. and Giovannoni, J. J.** (1997). The tomato *high-pigment (hp)* locus maps to chromosome 2 and influences plastome copy number and fruit quality. *Theoretical and Applied Genetics* **95**: 1069-1079.
- Zerial, M., and McBride, H.** (2001). Rab proteins as membrane organizers. *Nature Rev. Mol. Cell Biol.* **2**: 107-119.
- Zhong, H., Teymouri, F., Chapman, B., Maqbool, S. B., Sabzikar, R., El-Maghraby, Y., Dale, B., and Sticklen, M. B.** (2003). The pea (*Pisum sativum* L.) *rbcS* transit peptide directs the *Alcaligenes eutrophus* polyhydroxybutyrate enzymes into the maize (*Zea mays* L.) chloroplasts. *Plant Sci.* **165**: 455-462.

## APPENDIX

### *Calculation of plastid body surface area*

The following assumptions were made for simplicity:

1. A plastid body, pb, is a sphere; and thus
2. The plastid body plan area,  $A_{pb}$ , is a circle, representing one hemisphere;
3. An IM cell contains 250 plastids.

From Table 3.2, mean  $A_{pb}$  of an IM cell, B+7 is  $40.7 \mu\text{m}^2$

Surface area (s.a.) of a sphere is  $4\pi r^2$ , where  $r$  is the radius

$$\begin{aligned}\Rightarrow \text{s.a. of single plastid body} &= 4 \times 40.7 \\ &= 162.8 \mu\text{m}^2 = \alpha\end{aligned}$$

In addition, since  $A = \pi r^2$

it follows that  $r = \sqrt{[A/\pi]}$

$\therefore r_{pb} = 3.599 \mu\text{m}$

### *Calculation of stromule surface area*

Using the above assumptions in addition to:

4. A stromule is a uniform cylinder of  $0.9 \mu\text{m}$  in diameter.

From Table 3.2, mean stromule length in IM cell, B+7 is  $32.6 \mu\text{m}$

s.a. of curved length of a cylinder is  $2\pi rh$ , where  $r$  is the radius and  $h$  the length

$$\begin{aligned}\Rightarrow \text{s.a. of single stromule} &= 2\pi \times 0.45 \times 32.6 \\ &= 92.2 \mu\text{m}^2 = \beta\end{aligned}$$

*Calculation of plastid body volume*

Volume of a sphere is  $\frac{4}{3}\pi r^3$

$$\begin{aligned}\Rightarrow \text{volume of single pb} &= \frac{4}{3}\pi(3.599)^3 \\ &= 195.3 \mu\text{m}^3 = \gamma\end{aligned}$$

*Calculation of stromule volume*

Volume of a cylinder is  $\pi r^2 h$

$$\begin{aligned}\Rightarrow \text{volume of single stromule} &= \pi \times 0.45^2 \times 32.6 \\ &= 20.74 \mu\text{m}^2 = \delta\end{aligned}$$

*Relative contribution of stromules to surface area and volume*

The proportion of *total* plastid surface area given by a stromule is

$$\begin{aligned}&\beta/(\beta + \alpha) \\ \text{i.e.} &= 92.2/(92.2 + 162.8) \\ &= \mathbf{36\%} \text{ (2 s.f.)}\end{aligned}$$

Likewise, the proportion of *total* plastid volume contained within a stromule is

$$\begin{aligned}&\delta/(\delta + \gamma) \\ \text{i.e.} &= 20.74/(20.74 + 195.3) \\ &= \mathbf{9.6\%} \text{ (2 s.f.)}\end{aligned}$$

Since 39% of plastids possess stromules, we can estimate the proportion of total *cellular* plastid surface area and volume occupied by stromules:

	Surface area ( $\mu\text{m}^2$ )	Volume ( $\mu\text{m}^3$ )
Plastid body, <i>pb</i>	$250 \times \alpha = 40,700$	$250 \times \gamma = 48,817$
Stromule, <i>s</i>	$(0.39 \times 250) \times \beta = 8,987$	$(0.39 \times 250) \times \delta = 2,022$
Proportion, $s/(s + pb)$	<b>18 %</b>	<b>4 %</b>

Typeset in:

Utopia Std  
Gill Sans Std  
Myriad Pro

Figures prepared with Adobe Illustrator 10  
Images edited with Adobe Photoshop 7

[www.adobe.com](http://www.adobe.com)



Printed on Evolve Business 100% recycled paper  
with a Hewlett Packard Color LaserJet 2550N

[www.evolve-papers.com](http://www.evolve-papers.com)

